

Early ADMET profiling of anti-inflammatory alkaloids using validated LC-MS/MS methods

Inauguraldissertation

zur

Erlangung der Würde eines Doktors der Philosophie

vorgelegt der

Philosophisch-Naturwissenschaftlichen Fakultät

der Universität Basel

von

Evelyn Andrea Jähne

aus Höri, Zürich

Basel, 2016

Original document stored on the publication server of the University of Basel
edoc.unibas.ch



This work is licenced under the agreement
„Attribution Non-Commercial No Derivatives – 3.0 Switzerland“ (CC BY-NC-ND 3.0 CH)
The complete text may be reviewed here:
creativecommons.org/licenses/by-nc-nd/3.0/ch/deed.en

Genehmigt von der Philosophisch-Naturwissenschaftlichen Fakultät
auf Antrag von

Prof. Dr. Matthias Hamburger

Prof. Dr. Jürgen Drewe

Basel, den 21.06.2016

Prof. Dr. Jörg Schibler
Dekan



Attribution-NonCommercial-NoDerivatives 3.0 Switzerland
(CC BY-NC-ND 3.0 CH)

You are free: to **Share** — to copy, distribute and transmit the work

Under the following conditions:



Attribution — You must attribute the work in the manner specified by the author or licensor (but not in any way that suggests that they endorse you or your use of the work).



Noncommercial — You may not use this work for commercial purposes.



No Derivative Works — You may not alter, transform, or build upon this work.

With the understanding that:

- **Waiver** — Any of the above conditions can be **waived** if you get permission from the copyright holder.
- **Public Domain** — Where the work or any of its elements is in the **public domain** under applicable law, that status is in no way affected by the license.
- **Other Rights** — In no way are any of the following rights affected by the license:
 - Your fair dealing or **fair use** rights, or other applicable copyright exceptions and limitations;
 - The author's **moral** rights;
 - Rights other persons may have either in the work itself or in how the work is used, such as **publicity** or privacy rights.
- **Notice** — For any reuse or distribution, you must make clear to others the license terms of this work. The best way to do this is with a link to this web page.

Für meine Familie und Freunde

Table of contents

List of abbreviations	9
Summary	11
Zusammenfassung	13
1 Aim of work	15
2 Introduction	19
2.1 Natural product based lead discovery	20
2.2 Alkaloids from <i>Isatis tinctoria</i> L. as potential leads for anti-inflammatory drugs	23
2.2.1 Woad (<i>Isatis tinctoria</i> L.).....	24
2.2.2 Tryptanthrin.....	26
2.2.3 Indirubin.....	28
2.2.4 Indolinone derivative.....	31
2.3 Pharmacokinetics and early ADMET profiling in drug discovery	38
2.3.1 Drug discovery and development process.....	39
2.3.2 Pharmacokinetics in drug discovery.....	40
2.3.3 The gastrointestinal tract (GIT) and intestinal epithelium.....	43
2.3.3.1 Rule-based approaches and <i>in silico</i> models.....	44
2.3.3.2 <i>In vitro</i> permeability models.....	45
2.3.3.3 <i>In situ</i> models.....	47
2.3.4 The blood-brain barrier (BBB).....	48
2.3.4.1 Structure BBB permeation relationships and <i>in silico</i> models.....	49
2.3.4.2 <i>In vitro</i> BBB models.....	49
2.3.4.3 <i>In vivo</i> BBB models.....	50
2.3.5 The hERG channel.....	51
2.3.5.1 Structure activity based relationships and <i>in silico</i> approaches.....	52
2.3.5.2 <i>In vitro</i> hERG methods.....	53
2.3.5.3 <i>In vivo</i> hERG methods.....	54

2.4 Bioanalysis	59
2.4.1 Definition and current techniques	59
2.4.2 LC coupled to MS/MS and HR-MS	60
2.4.3 Sample preparation.....	62
2.4.4 Bioanalytical quantification using validated LC-MS/MS methods.....	63
2.4.5 Method development.....	64
2.4.6 Method validation	65
2.4.7 Sample analysis.....	67
3 Results and discussion	69
3.1 Development and validation of a LC-MS/MS method for assessment of an anti-inflammatory indolinone derivative by <i>in vitro</i> blood-brain barrier models.....	70
3.2 Pharmacokinetics and <i>in vitro</i> blood-brain barrier screening of the plant-derived alkaloid tryptanthrin	83
3.3 Development and full validation of an UPLC-MS/MS method for the quantification of the plant-derived alkaloid indirubin in rat plasma	101
3.4 Caco-2 permeability studies and <i>in vitro</i> hERG liability assessment of tryptanthrin and indolinone	115
4 Conclusions and outlook	135
Acknowledgments	145
Curriculum vitae	146

List of abbreviations

ADMET	Absorption, distribution, metabolism, excretion, and toxicity	hERG	Human ether-a-go-go related gene
AUC	Area under the curve	HIV	Human immunodeficiency virus
AhR	Aryl hydrocarbon receptor	HPLC	High performance liquid chromatography
ANVISA	Agência Nacional de Vigilância Sanitária	HR-MS	High resolution mass analyzer
APCI	Atmospheric pressure ionization source	HTS	High-throughput screening
BBB	Blood-brain barrier	IA	Immunoassay
BCRP	Breast cancer resistance protein	IAM	Immobilized artificial membrane
B.w.	Body weight	IC ₅₀	Half maximal inhibitory concentration
C ₀	Initial concentration	ICH	International Conference on Harmonization
Caco-2	Human colon adenocarcinoma cell line	IgE	Immunoglobulin E
C _{max}	Maximum Concentration	I _{Kr}	Delayed rectifier potassium current
CDK	Cyclin dependent kinase	IL-4	Interleukin 4
CerK	Ceramide kinase	I.S.	Internal standard
CFS	Cerebrospinal fluid	IUPAC	International Union of Pure and Applied Chemistry
cGMP	Cyclic guanosine monophosphate	I.v.	Intravenous
CHO	Chinese hamster ovary cells	iNOS	Inducible nitric oxide synthase
CID	Collision induced dissociation	JAK3	Janus kinase 3
CL	Clearance	Kit TK	Kit ligand (stem cell factor)
Cyp P450	Cytochrome P450	k _e	Elimination rate constant
CML	Chronic myelocytic leukemia	5-LOX	5-Lipoxygenase
CNS	Central nervous system	LC-MS	Liquid chromatography coupled to mass spectrometry
COX-2	Cyclooxygenase-2	LC-MS/MS	Liquid chromatography coupled to tandem mass spectrometry
DSS	Dextran sodium sulfate	LC-UV/VIS	Liquid chromatography coupled to ultraviolet/visible absorbance detection
DYRK	Dual specificity tyrosine-phosphorylation-regulated kinases	LLE	Liquid-liquid extraction
ECG	Electrocardiogram	LLOQ	Lower limit of quantification
ELISA	Enzyme-linked immunosorbent assay	LQTS	Long QT syndrome
EMA	European Medicine Agency	LTB4	Leukotriene B4
ESI	Electrospray ionization source	MDCK	Madin-Darby canine kidney cell line
FCεRI	Human high affinity receptor for IgE	MDR1	Multidrug resistant gene 1
FDA	Food and Drug Administration	MHLW	Ministry of Health, Labour and Welfare
GC-MS	Gas chromatography coupled to mass spectrometry	MRI	Magnetic resonance imaging
GIT	Gastrointestinal tract	MRM	Multiple reaction monitoring
GLP	Good laboratory practices	MRP	Multidrug resistance associated protein
GP	Glycogen phosphorylase	MS	Mass spectrometry
GSK-3	Glycogen synthase kinase-3β	NF- κB	Nuclear factor kappa-light-chain-enhancer of activated B cells
GST	Glutathione S-transferases		
HEK 293	Human embryonic kidney cells		
HEL	Human erythroleukemia cell line		

NSAID	Nonsteroidal anti-inflammatory drug	SRM	Selected reaction monitoring
OCT	Organic cation transporter	S-SMEDD	Super-saturated micro-emulsion Drug delivery Systems
PAMPA	Parallel artificial membrane permeability assay	S/N	Signal to noise ratio
P _{app}	Apparent permeability coefficient	SULT	Sulfotransferase
PET	Positron emission tomography	Syk	Spleen tyrosine Kinase
P-gp	P-glycoprotein	t _{1/2}	Half-life
PK	Pharmacokinetic	TCM	Traditional Chinese medicine
PP	Protein precipitation	TdP	Torsades de pointes
PSA	Polar surface area	TEER	Transendothelial electrical resistance
OAT	Organic anion transporter	Th2	T helper type 2 cells
QC	Quality control	TDM	Therapeutic drug monitoring
OCT	Organic cation transporter	t _{max}	Time of maximum drug concentration
Q-TOF	Quadrupole time-of-flight mass spectrometer	TNF- α	Tumor necrosis factor alpha
RAW	Mouse leukemic monocyte macrophage cell line	TQD	Triple quadrupole detector
RE	Relative error	UGT	Uridine 5'-diphospho glucuronosyltransferase
RHB	Ringer HEPES buffer	UHPLC	Ultra-high performance liquid chromatography
RIA	Radio immunoassay	UPLC	Ultra performance liquid chromatography
RTK	Receptor tyrosine kinase	ULOQ	Upper limit of quantification
S.D.	Standard deviation	V _d	Volume of distribution
S.E.M.	Standard error of mean	WS	Working solution
SLE	Supported-liquid extraction		
SOP	Standard operating procedure		
SPE	Solid-phase extraction		

Trivial and systematic IUPAC names:

Trivial name	IUPAC name
Couroupitine A	indolo[1,2- <i>h</i>][1,7]naphthyridine-6,12-dione
Indigo	[2,2'-biindolinylidene]-3,3'-dione
Indirubin	[2,3'-biindolinylidene]-2',3-dione
Indolin-2-one	(<i>E,Z</i>)-3-(4-hydroxy-3,5-dimethoxybenzylidene)indolin-2-one
Tryptanthrin	indolo[2,1- <i>b</i>]quinazoline-6,12-dione

Summary

Natural products provide an important and unique source of new lead compounds for drug discovery. Approximately 50% of all new chemical entities are inspired by nature. In the search of novel anti-inflammatory compounds in the ancient medicinal plant *Isatis tinctoria*, tryptanthrin, indirubin, and (*E,Z*)-3-(4-hydroxy-3,5-dimethoxybenzylidene)indolin-2-one (indolinone) were identified as pharmacologically active constituents. They inhibit, at low μM to nM concentrations, cyclooxygenase-2 (COX-2), 5-lipoxygenase (5-LOX) catalyzed leukotriene synthesis, cyclin-dependent kinase (CDK), glycogensynthase kinase-3 β (GSK), and mast cell degranulation. While the molecular modes of action of these alkaloids are not yet fully understood, their unique pharmacological profiles, structural drug-like properties, and low cytotoxicity render these molecules promising anti-inflammatory leads. To further evaluate the potential of these alkaloids as novel anti-inflammatory and anti-allergic leads, an assessment of their ADMET properties was warranted. For exact quantification of the compounds, LC-MS/MS methods were developed and validated according to current regulatory guidelines.

To get a first prognostic picture for the *in vivo* performance of our compounds, a pilot PK study was performed in male Sprague Dawley rats after intravenous administration at a concentration of 2 mg/kg b.w.. Tryptanthrin and indirubin showed a half-life ($t_{1/2}$) of around 40 min, while indolinone was quickly eliminated ($t_{1/2} = 4$ min).

As most of the drugs are preferentially administered orally, the gastrointestinal tract (GIT) represents the major site of drug absorption. Human colon carcinoma cells (Caco-2 cells) serve as the method of choice to predict human drug absorption across the intestinal wall *in vitro*. To study the permeability of the three compounds across the epithelial monolayer, the alkaloids were screened at concentrations of 5-10 μM in the Caco-2 assay. As efflux transporters can greatly impact the *in vivo* absorption and, thus, the bioavailability of a drug candidate, the compounds were tested for possible P-glycoprotein (P-gp) interaction. Therefore, the alkaloids were co-incubated with the P-gp inhibitor verapamil (50 μM). Active efflux was assessed by calculating the efflux ratio (ER) from bidirectional assays. Due to high lipophilicity of indirubin, the compound precipitated in the transporter buffer and was thus excluded for further investigations in aqueous solutions. Tryptanthrin displayed a high permeability ($P_{\text{app}} > 32.0 \times 10^{-6}$ cm/s) across the cell monolayer. The efflux ratio below 2 (< 1.12) and the unchanged P_{app} values in presence of the P-glycoprotein (P-gp) inhibitor verapamil indicated that tryptanthrin was not involved in P-gp mediated efflux. In the Caco-2 assay, the recovery of indolinone was low, pointing to possibly extensive phase II metabolism. Further investigation by a high-resolution mass spectrometry (HR-MS) system revealed the formation of two sulfate and two glucuronide conjugates for indolinone.

Another well-known biological barrier in the human body is the blood-brain barrier (BBB). To evaluate the BBB permeation potential of tryptanthrin and indolinone, the compounds were tested in three cell-based human and animal BBB models. Data obtained with the human and animal BBB models showed good correlation and were indicative of a high BBB permeation potential of tryptanthrin and indolinone. Furthermore, active-mediated efflux was evaluated by calculating the ER from bidirectional assays. The ERs below 2 suggested that both compounds were not involved in active-mediated efflux.

Besides P-gp, another critical anti-target in drug development is the human ether-a-go-go (hERG) potassium channel. In the late 1990s, an increasing number of non-cardiovascular drugs have been withdrawn from the market due to cardiotoxic side-effects linked to hERG blocking. Since then, regulatory agencies insist on acquiring experimental hERG data of drug candidates before moving into clinical trials. Possible cardiotoxic liability of the compounds was assessed *in vitro*, by measurement of an inhibitory effect on hERG tail currents in stably transfected HEK 293 cells using the patch-clamp technique. Slight hERG inhibition was found for tryptanthrin (IC₅₀ of 22 μM) and indolinone (IC₅₀ of 25 μM).

Data obtained from the *in vitro* assays were corroborated by *in silico* predictions. For tryptanthrin and indolinone, all criteria for high human oral absorption and passive BBB penetration were met. In addition, the slight hERG inhibition found for tryptanthrin and indolinone *in vitro* could be confirmed by *in silico* predictions.

Zusammenfassung

Naturstoffe sind eine wichtige und einzigartige Quelle von neuen Leitstrukturen in der Wirkstoffentdeckung. Schätzungsweise 50% aller neuen chemischen Wirkstoffe sind von Naturstoffen inspiriert worden. Auf der Suche nach entzündungshemmenden Substanzen in der traditionellen Medizinalpflanze *Isatis tinctoria* konnten die drei Substanzen Tryptantrin, Indirubin und (*E,Z*)-3-(4-Hydroxy-3,5-dimethoxybenzyliden)indolin-2-on (Indolinon) als pharmakologisch wirksame Inhaltsstoffe identifiziert werden. Es konnte gezeigt werden, dass sie die Cyclooxygenase-2 (COX-2), die 5-Lipoxygenase (5-LOX) katalysierte Leukotriensynthese, die Cyclin-abhängige Kinase (CDK), die Glycogensynthase Kinase-3 β (GSK) und die Mastzelldegranulation im tiefen micro bis nanomolekularen Bereich inhibieren. Während die exakten molekularen Wirkmechanismen dieser Alkaloide noch nicht vollständig entschlüsselt werden konnten, machen ihre einzigartigen pharmakologischen Profile, ihre wirkstoffartigen Strukturen, und die geringe Zytotoxizität sie zu vielversprechenden anti-inflammatorischen Leitstrukturen. Um ihr Potential als Leitstrukturen weiter bewerten zu können, war eine erste Abschätzung ihrer ADMET Eigenschaften gefragt. Dabei wurden für die exakte Quantifizierung der Substanzen Methoden mittels Flüssigchromatographie mit Massenspektrometrie-Kopplung (LC-MS/MS, engl. liquid chromatography-mass spectrometry) entwickelt und gemäss regulatorischen Richtlinien validiert.

Um ein erstes prognostisches Bild zum Verhalten unserer Substanzen *in vivo* zu erhalten, führten wir eine Pilotstudie an männlichen Sprague Dawley Ratten durch. Hierzu wurden die Substanzen intravenös bei einer Konzentration von 2 mg/kg Körpergewicht appliziert. Tryptanthrin und Indirubin zeigten eine Halbwertszeit von rund 40 Minuten, während Indolinon bereits nach 4 Minuten eliminiert wurde.

Da die meisten Medikamente oral eingenommen werden, stellt der gastrointestinal Trakt (GIT) den Hauptabsorptionsort für Arzneimittel dar. Dabei sind die humanen Kolonkarzinom-Zellen (Caco-2 Zellen) die Methode erster Wahl, um *in vitro* Abschätzungen zur oralen Absorption einer Substanz machen zu können. Um die Permeabilität der drei Substanzen über den epithelialen Monolayer beurteilen zu können, wurden die Alkaloide in Konzentrationen von 5-10 μM im Caco-2 Modell getestet. Da Effluxtransporter einen grossen Einfluss auf die Absorption und damit auch auf die Bioverfügbarkeit eines Medikaments haben können, wurden die Substanzen zudem auf P-Glycoprotein (P-gp) Interaktionen untersucht. Dazu wurden die Alkaloide gemeinsam mit dem P-gp Inhibitor Verapamil (50 μM) inkubiert. Zudem wurde der aktive Efflux über die Berechnung des Efflux Verhältnisses (ER, engl. efflux ratio) aus den bi-direktionellen Experimenten ermittelt. Aufgrund der hohen Lipophilie von Indirubin fiel die Substanz in der wässrigen Transportlösung aus und wurde für weitere Studien in wässrigen Medien ausgeschlossen. Tryptanthrin zeigte hingegen eine hohe Permeabilität (P_{app} Werte $> 32.0 \times 10^{-6}$ cm/s) über den Caco-2 Zellmonolayer. Das Efflux

Verhältnis unter 2 (1.12) sowie die unveränderte Permeabilität der Substanz in Anwesenheit des P-gp Inhibitors Verapamil liessen darauf schliessen, dass Tryptanthrin nicht in einen P-gp vermittelten Efflux involviert ist. Indolinon zeigte in den Caco-2 Untersuchungen eine tiefe Massenbilanz. Die Ergebnisse deuteten auf eine extensive Phase II Metabolisierung hin. Weitere Untersuchungen mittels hochauflösender Massenspektrometrie (HR-MS, engl. high-resolution mass spectrometry) ergaben, dass Indolinon in zwei Sulfat- und zwei Glukuronid-Konjugate umgewandelt wurde.

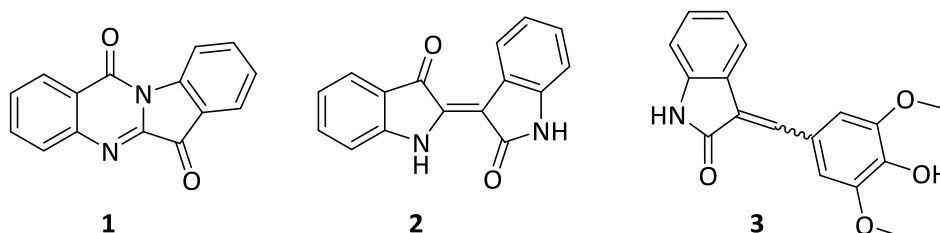
Eine weitere bedeutende biologische Barriere im menschlichen Körper ist die Blut-Hirn-Schranke. Um das Permeationspotential von Tryptanthrin und Indolinon zu untersuchen, wurden die Substanzen in drei verschiedenen Zell-basierten menschlichen und tierischen Blut-Hirn-Schranken Modellen getestet. Daten aus den menschlichen und den zwei tierischen Modellen zeigten eine gute Übereinstimmung und wiesen auf eine hohe Blut-Hirn-Schranken-Gängigkeit von Tryptanthrin und Indolinon hin. Des Weiteren wurden das Efflux-Verhältnis aus bidirektionellen Experimenten ermittelt. Da der Quotient kleiner als 2 war, konnte gezeigt werden, dass keine der beiden Substanzen in einen aktiven Efflux involviert war.

Neben dem P-gp, stellt der hERG Kalium-Kanal ein weiteres kritisches Anti-Target im Medikamentenentwicklungsprozess dar. In den späten 1990er Jahren wurden zahlreiche nicht-kardiovaskuläre Medikamente aufgrund ihrer kardiotoxischen Nebenwirkungen vom Markt genommen. Später konnten diese Nebenwirkungen mit der Blockade des hERG Kanals in Verbindung gebracht werden. Seit dem schreiben regulatorische Behörden vor, dass alle neuen Wirkstoffe auf ihre hERG Aktivität hin getestet werden müssen, bevor sie für klinische Studien zugelassen werden. Um ein mögliches kardiotoxisches Potential unserer Substanzen ausschliessen zu können, wurde Tryptanthrin und Indolinon auf hERG-Strom-hemmenden Eigenschaften an stabil transfizierten HEK 293 Zellen mittels der Patch-Clamp Methode getestet. Dabei konnte festgestellt werden, dass Tryptanthrin ($IC_{50} = 22 \mu M$) und Indolinon ($IC_{50} = 25 \mu M$) eine leichte hERG Inhibition auslösten.

Insgesamt zeigten unsere *in vitro* Daten eine gute Übereinstimmung mit den *in silico* Berechnungen. Für Tryptanthrin und Indolinon konnten alle Parameter für eine hohe orale Absorption sowie passive Blut-Hirn-Schranken-Gängigkeit erfüllt werden. Die leichte hERG Blockade der beiden Substanzen *in vitro* wurde mit Hilfe von *in silico* Daten bestätigt.

1 Aim of work

In previous studies, the alkaloids tryptanthrin (**1**), indirubin (**2**), and indolinone (**3**) were identified as pharmacologically active compounds in the ancient medicinal plant *Isatis tinctoria* L. (Brassicaceae). They inhibit COX-2, 5-LOX catalyzed leukotriene synthesis, cyclin-dependent kinase (CDK), glycogen synthase kinase-3 β (GSK), and mast cell degranulation, at low μ M to nM concentrations¹⁻⁴. While the molecular mode of action is not fully clarified yet, their unique structure and pharmacological profile, the lack of cytotoxicity and their structural drug-like properties, earmarked these compounds as interesting anti-inflammatory leads for further development.



In the early 1970s, selectivity and potency were considered as the key parameters for successful drug discovery⁵. However, therapeutic efficacy of a bioactive compound can be greatly influenced by its absorption, distribution, metabolism, excretion and toxicity (ADMET) parameters. Therefore, it has been widely recognized that ADMET properties need to be addressed early in the drug discovery process.

The overall aim of this work was to assess first *in vivo* key pharmacokinetic (PK) parameters and the *in vitro* permeation potential across biological barriers (gastrointestinal tract [GIT] and blood-brain barrier [BBB]) of tryptanthrin, indirubin and indolinone by means of validated UPLC-MS/MS quantification methods.

In a first step, we aimed to develop quantitative UPLC-MS/MS methods in lithium heparinized rat plasma, Hank's Balanced Salt Solution (HBSS), and Ringer HEPES buffer (RHB), and validate them according to current international guidelines for industry⁶⁻⁸. To demonstrate that our quantitative measurements in the given matrix are reliable and reproducible, we aimed at validating the methods with respect to accuracy, precision, selectivity, sensitivity, and short and long-term stability.

The objective of the second part of the PhD thesis was to apply the quantification methods in lithium heparinized rat plasma to a pilot pharmacokinetic (PK) study in Sprague Dawley rats. To obtain first PK parameters of tryptanthrin, indolinone, and indirubin, we aimed at testing the compounds in male Sprague Dawley rats after intravenous application (2 mg/kg b.w.)⁹.

In the third part of the thesis, we aimed at using the validated methods in the two buffers HBSS and RHB to study the *in vitro* permeability of the three compounds across the GIT and the BBB.

The most convenient route for systemic application is oral administration. However, to reach satisfactory bioavailability, various requirements need to be met. For instance, the compounds have to

be sufficiently soluble, withstand high enzymatic activity (degradation and metabolism), and permeate through the intestinal epithelium in a sufficiently high amount. Thus, to assess the suitability of our three compounds for oral administration, we aimed at determining the absorptive/secretory permeability coefficients of our compounds across the Caco-2 cell monolayer. In addition, to investigate P-glycoprotein (P-gp) interaction and active mediated efflux, we aimed at evaluating the permeability of the compounds in presence of a P-gp inhibitor (verapamil) and by calculating the efflux ratios from bidirectional assays.

The BBB is a highly restrictive barrier and thus protects the brain from harmful substances, such as toxins and bacteria. However, the BBB is so restrictive that it often prevents the penetration of potentially life-saving drugs. On the other hand, drugs intended for the periphery might enter the brain, where they could cause undesired central effects, such as dizziness, headache, or drowsiness^{10,11}. Hence, independent of the therapeutic purpose, BBB permeability assessments of drug candidates are warranted. To evaluate the brain penetration of our compounds, we aimed at screening the substances in a cell-based *in vitro* monoculture BBB model, which we previously established by using an immortalized human brain microvascular endothelial cell line (hBMEC)^{12,13}. Immortalized cells are easy to culture, maintain their phenotype even after extensive passaging, and are thus highly suitable for a standardized screening. However, using immortalized cells faces numerous limitations such as poor barrier properties, insufficient tight junction formation, and low expression of key transporters¹⁴. For this reason, we aimed at comparing the results obtained from the human immortalized BBB model with widely accepted and validated animal primary co-culture BBB models¹⁵⁻¹⁷.

Drug-induced hERG inhibition is the most important risk factor leading to fatal cardiac complications, including arrhythmia. Due to these severe side effects, numerous cardiac and non-cardiac drugs have been withdrawn from the market, or their use has been restricted. For this reason, hERG blocking is considered as the primary anti-target regarding drug-induced cardiotoxicity. To identify potential hERG liabilities of our three anti-inflammatory alkaloids, we aimed at evaluating the effect of tryptanthrin, indirubin, and indolinone on the hERG potassium channel by means of the patch-clamp technique.

References

1. Danz, H., Stoyanova, S., Wippich, P., Brattström, A. & Hamburger, M. Identification and isolation of the cyclooxygenase-2 inhibitory principle in *Isatis tinctoria*. *Planta Med.* **67**, 411–416 (2001).
2. Ishihara, T. *et al.* Tryptanthrin inhibits nitric oxide and prostaglandin E2 synthesis by murine macrophages. *Eur. J. Pharmacol.* **407**, 197–204 (2000).
3. Kiefer, S., Mertz, A. C., Koryakina, A., Hamburger, M. & Küenzi, P. (E,Z)-3-(3',5'-Dimethoxy-4'-hydroxy-benzylidene)-2-indolinone blocks mast cell degranulation. *Eur. J. Pharm. Sci.* **40**, 143–147 (2010).
4. Hoessel, R. *et al.* Indirubin, the active constituent of a Chinese antileukemia medicine. *Nat. Cell Biol.* **1**, 60–7. (1999).
5. Gardner, C. R., Walsh, C. T. & Almarsson, Ö. Drugs as materials: valuing physical form in drug discovery. *Nat. Rev. Drug Discov.* **3**, 926–934 (2004).
6. FDA, U. Guidance for industry: bioanalytical method validation (draft guidance). *US FDA* (2013).
7. Guideline on bioanalytical method validation. European Medicines Agency (EMA/CHMP/EWP/192217/2009). London, 21 July 2011.
8. Administration, F. and D. Guidance for industry: bioanalytical method validation (2001). *Md. USA* (2007).
9. Oufir, M., Sampath, C., Butterweck, V. & Hamburger, M. Development and full validation of an UPLC-MS/MS method for the determination of an anti-allergic indolinone derivative in rat plasma, and application to a preliminary pharmacokinetic study. *J. Chromatogr. B* **902**, 27–34 (2012).
10. Novakova, I. *et al.* Transport rankings of non-steroidal antiinflammatory drugs across blood-brain barrier *in vitro* models. *PLoS One* **9**, e86806 (2014).
11. Mutschler, E., Geisslinger, G., Kroemer, H. K., Menzel, S. & Ruth, P. *Mutschler Arzneimittelwirkungen: Pharmakologie - Klinische Pharmakologie - Toxikologie*. 143-369 (Wissenschaftliche Verlagsgesellschaft Stuttgart, 2012).
12. Eigenmann, D. E. *et al.* Comparative study of four immortalized human brain capillary endothelial cell lines, hCMEC/D3, hBMEC, TY10, and BB19, and optimization of culture conditions, for an *in vitro* blood-brain barrier model for drug permeability studies. *Fluids Barriers CNS* **10**, 33 (2013).
13. Eigenmann, D. E., Jähne, E. A., Smieško, M., Hamburger, M. & Oufir, M. Validation of an immortalized human (hBMEC) *in vitro* blood-brain barrier model. *Anal. Bioanal. Chem.* 1–13 (2016).
14. Eigenmann D.E., Dissertation: Establishment and validation of an immortalized *in vitro* human blood-brain barrier (BBB) model for drug permeability studies, and application to natural product derived leads. Available at: https://forschdb2.unibas.ch/inf2/rm_projects/object_view.php?r=3343775. (Accessed: 12th April 2016)
15. Jähne, E. A. *et al.* Development and validation of a LC-MS/MS method for assessment of an anti-inflammatory indolinone derivative by *in vitro* blood-brain barrier models. *J. Pharm. Biomed. Anal.* (2014).
16. Culot, M. *et al.* An *in vitro* blood-brain barrier model for high throughput (HTS) toxicological screening. *Toxicol. In Vitro* **22**, 799–811 (2008).
17. Nakagawa, S. *et al.* A new blood-brain barrier model using primary rat brain endothelial cells, pericytes and astrocytes. *Neurochem. Int.* **54**, 253–263 (2009).

2 Introduction

2.1 Natural product based lead discovery

For thousands of years, plants, animals, and microorganisms were the source of all medicinal preparations¹. Before the 19th century, only crude and semi-crude extracts from natural origin were available to treat human diseases². However, with the growing understanding in enzymology and receptor pharmacology in the early 20th century, the concept about remedies was revolutionized³: pure isolated compounds instead of extracts became the standard of pharmacotherapy. The isolation of the narcotic morphine from Opium by the German pharmacist Sertüner in 1805 is often considered as the starting point of natural product research. Shortly thereafter, the isolation of numerous important natural products such as emetine (1817), atropine (1819), quinidine (1820), caffeine (1820), and digoxin (1841) followed⁴. In this compound series, quinidine and morphine were the first commercially available pure natural products, marketed by Caventou in 1826 and Merck in 1827, respectively. In the late 19th century, structural modifications of morphine into diacetylmorphine (heroin, 1898) and salicylic acid into acetylsalicylic acid (Aspirin[®], 1899)⁵ led to the first semisynthetic drugs, developed by Hoffman at the pharmaceutical company Bayer⁶. Other prominent examples of drugs derived from traditional medicinal plants include the first local anesthetic cocaine (1869), the muscle relaxant tubocurarine (1935), and the antihypertensive reserpine (1951)⁴.

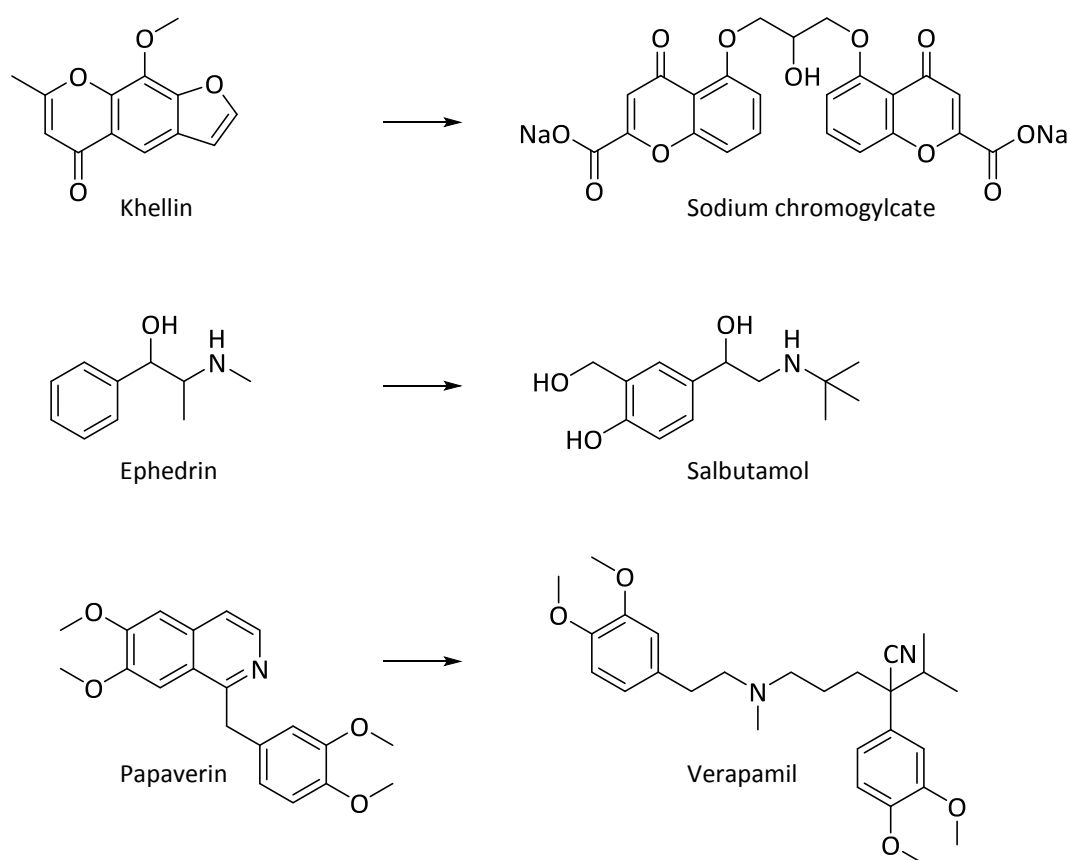


Figure 1: Drugs derived from traditional medicinal plants⁹

Various studies demonstrated that there is a positive correlation between the therapeutic indication of plant-derived drugs and their ethnomedicinal uses^{7,8}. For instance, khellin from *Ammi visnaga* (traditionally used to treat asthma) served as scaffold for the bronchodilator chromolyn (sodium chromoglycate); papaverin from *Papaver somniferum* (used as sedative) led to the development of the antiarrhythmic verapamil; and ephedrine from the traditional Chinese medicine (TCM) plant *Ephedra sinica*, served as a starting point for the development of beta agonists such as salbutamol (**Fig. 1**)^{9,10}. More recent examples of natural-derived compounds serving as an inspirational source for new drugs include the antitumor drug paclitaxel (Taxol[®]) and derivatives of the antimalarial artemisinin (Artemotil[®]). Discovery of the latter compound was awarded with the Nobel Prize of Medicine in 2015.

Up to the present, the contribution of natural products to modern pharmacotherapy has been remarkable. According to Newman and Cragg, approximately 50% of all approved new drug entities (NDE) in the last 30 years are linked to natural products (**Fig. 2**)¹¹. Moreover, it was proposed that 60 out of 243 lead structures derive solely from plant origin^{4,12}. Nevertheless, despite this success over the past decades, pharmaceutical companies have scaled down the number of natural products research projects and a drop of 30% in natural product based projects could be recorded between 2001 and 2008¹³. The introduction of molecular modelling, combinatorial chemistry and high-throughput screening (HTS) of synthetic libraries in the early 1990s mainly contributed to the declining interest in natural product research¹⁴.

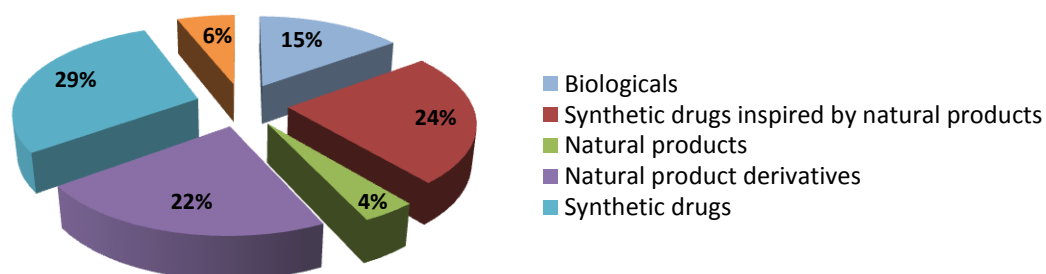


Figure 2: Origin of all approved new drug entities (NDE) from 1981 - 2010¹¹. In total 50% of all NDE are directly or indirectly linked to natural products. Modified from D.J. Newman, G.M. Cragg J. Nat. Prod. 2012

Historically, natural product research has been confronted with several challenges, such as unsecured access and supply of source material, and issues concerning intellectual property (IP) rights¹³. Further difficulties in natural product research include the (1) characterization of complex mixtures, (2) high probability of hit duplication, (3) solubility and stability issues, (4) synergistic/antagonistic activities, (5) complex structures rendering structural modifications highly challenging, (6) extremely low amounts of active constituents, and (7) cost-intensive development of synthetic strategies¹³. All these issues made natural product isolation a relatively slow and time-consuming process. Interestingly, despite the alleged disadvantages of natural products HTS over synthetic HTS, the success rate of

finding new synthetic lead compounds, particularly in certain key therapeutic areas such as anti-infective, immunosuppression, oncology and metabolic diseases, remained relatively low^{1,14}. This could be explained by the fact that natural products are chemically and structurally much more diverse than synthetic molecules. In fact, more than 40% of natural product scaffolds are absent in chemical compound libraries². Moreover, natural products contain a wide range of pharmacophores and a high number of stereocenters rendering them an ideal starting point for chemical modifications. Above all, natural products are natural metabolites, which mean that they are not only biologically active, but also favorable substrates of carrier proteins that can deliver the molecule to the intracellular target¹⁴. These circumstances, along with the introduction of powerful novel technologies and innovative strategies, led to the re-discovery of natural product research¹⁵. Moreover, it should be noted that only 6% of higher plants (of the approximately 30`000 known species), less than 1% of microbial species, and very few marine sources have been pharmacologically investigated so far⁹. Consequently, nature still retains a high unexplored potential and will remain an essential source for future lead discovery.

References

1. Lahlou, M. Screening of natural products for drug discovery. *Expert Opin. Drug Discov.* **2**, 697–705 (2007).
2. Lahlou, M. The success of natural products in drug discovery. *J. Pharm. Pharmacol.* **4**, 17–31 (2013).
3. Rishton, G. M. Natural products as a robust source of new drugs and drug leads: past successes and present day issues. *Am. J. Cardiol.* **101**, 43–49 (2008).
4. Potterat, O. & Hamburger, M. in *Natural compounds as drugs, Volume 65*, 45–118 (Springer, 2008).
5. Sneader, W. The discovery of aspirin: a reappraisal. *Br. Med. J.* **321**, 1591 (2000).
6. Schmidt, B. *et al.* A natural history of botanical therapeutics. *Metabolism* **57**, 3–9 (2008).
7. Hamburger, M., Marston, A. & Hostettmann, K. Search for new drugs of plant origin. in *Adv. Drug Res.* **20**, 167–215 (Academic Press, 1991).
8. Farnsworth, N. R., Akerele, O., Bingel, A. S., Soejarto, D. D. & Guo, Z. Medicinal plants in therapy. *Bull. World Health Organ.* **63**, 965 (1985).
9. Cragg, G. M. & Newman, D. J. Natural products: a continuing source of novel drug leads. *Biochim. Biophys. Acta BBA-Gen. Subj.* **1830**, 3670–3695 (2013).
10. Fabricant, D. S. & Farnsworth, N. R. The value of plants used in traditional medicine for drug discovery. *Environ. Health Perspect.* **109**, 69 (2001).
11. Newman, D. J. & Cragg, G. M. Natural products as sources of new drugs over the 30 years from 1981 to 2010. *J. Nat. Prod.* **75**, 311–335 (2012).
12. Sneader, W. Drug Prototypes and their Exploitation. *Eur. J. Med. Chem.* **1**, 91 (1997).
13. Li, J. W.-H. & Vederas, J. C. Drug discovery and natural products: end of an era or an endless frontier? *Science* **325**, 161–165 (2009).
14. Harvey, A. L., Edrada-Ebel, R. & Quinn, R. J. The re-emergence of natural products for drug discovery in the genomics era. *Nat. Rev. Drug Discov.* **14**, 111–129 (2015).
15. Wang, Y. Needs for new plant-derived pharmaceuticals in the post-genome era: an industrial view in drug research and development. *Phytochem. Rev.* **7**, 395–406 (2008).

2.2 Alkaloids from *Isatis tinctoria* L. as potential leads for anti-inflammatory drugs

Inflammation is a non-specific immune response of the body tissue to harmful biological, chemical or physical stimuli¹. The process is typically characterized by redness, heat, pain, swelling and loss of function. Under normal conditions inflammation is a self-limiting process. However, persistent inflammatory processes can lead to chronic disorders such as asthma², inflammatory bowel disease³, and rheumatoid arthritis⁴. In the last decades, chronic inflammation has also been linked to cancer⁵, diabetes mellitus, cardiovascular disorders⁶, and even Alzheimer's disease⁷. The most common anti-inflammatory drugs include nonsteroidal anti-inflammatory drugs (NSAIDs) and corticosteroids. However, long-term use is often associated with numerous side effects such as gastric ulcers, bronchospasm (NSAIDs), or osteoporosis, truncal obesity, and hyperglycemia (corticosteroids)⁸. Thus, there is a clear unmet medical need for better tolerated anti-inflammatory drugs, which could possibly be filled by natural products with a favorable risk/benefit ratio. It is known that plant-derived secondary metabolites are able to (directly or indirectly) interact with various key mediators in the inflammation cascade such as^{9,10}:

- (1) pro-inflammatory molecules such as cyclooxygenase (COX-2), inducible NO synthase (iNOS), and cytokines (interleukins, TNF- α),
- (2) various inflammatory mediators (e.g. arachidonic acid metabolites, cytokines),
- (3) second messengers (e.g. protein kinases, cGMP), and
- (4) transcription factors such as NF- κ B or proto-oncogenes, among many others.

In the search of anti-inflammatory compounds in the traditional medicinal plant *Isatis tinctoria*, tryptanthrin, indirubin and (*E,Z*)-3-(4-hydroxy-3,5-dimethoxybenzylidene)indolin-2-one (indolinone) were identified as pharmacologically active compounds in our research group. Their mode of action is not yet completely understood, but their pharmacological profile seems to be different from already known anti-inflammatory compounds. The following section provides an overview of the history, occurrence, and pharmacological activities of the traditional medicinal plant *Isatis tinctoria* L. and its three isolated constituents tryptanthrin, indirubin and indolinone.

2.2.1 Woad (*Isatis tinctoria* L.)

Historical background of an ancient dye plant



Figure 3: *Isatis tinctoria* L..

Source : Carl Axel Magnus Lindman,
Bilder ur Nordens Flora (1901-05)

Since antiquity, woad (*Isatis tinctoria* L., Brassicaceae, **Fig. 3**) has been used as a medicinal herb and dye plant. Although the original habitat of *Isatis tinctoria* is in the grasslands of southeastern Russia, the plant spread widely to Europe and Asia by cultivation. From medieval times up to the 18th century, woad was extensively cultivated in certain parts of Germany (Thuringia, Jülich), France (Languedoc, Somme, Normandy), Great Britain (Somerset, Lincolnshire) and Italy (Tuscany). The commerce with the highly prized indigo brought economic prosperity to these countries. However, in the late 17th century, the woad trade declined with the import of brighter and cheaper indigo from Asia, produced from *Indigofera* species. In the late 19th century, both woad and natural indigo were completely replaced by synthetic indigo^{11,12}.

Traditional medicinal uses

The medicinal properties of *Isatis tinctoria* have been known for centuries in Europe and China. In Europe, first written records on the medicinal effect of the plant were given by Hippocrates (5th B.C.), Pliny, the Elder (1st century A.D.), and Galen (2nd century A.D.)¹². Furthermore, in a number of mediaeval herbals, the medicinal use of the plant was described for the treatment of fever, wounds and various other inflammatory ailments^{11,12}. In China, the taxonomically closely related *Isatis indigotica* is still one of the most important and popular herbals in the TCM, indicated for the treatment of inflammatory ailments. Moreover, *Isatis indigotica* leaves (Daqingye) and roots (Banlangen), and natural indigo (Qingdai) are official listed drugs in the Chinese Pharmacopoeia, used as anti-inflammatory, hemostatic, antipyretic, antibacterial and antiviral agents¹³.

Phytochemical and pharmacological profiling of an anti-inflammatory medicinal plant

In the last 40 years, numerous phytochemical, biological, and pharmacological investigations have been performed on woad. In phytochemical characterizations of *Isatis tinctoria* and *Isatis indigotica*, more than 100 secondary metabolites were found¹¹. Both species are rich in glucosinolates¹⁴⁻¹⁶, which is characteristic for the family Brassicaceae. Moreover, they contain numerous indole derivatives such as tryptanthrin (**1**)¹⁷, the blue dye indigo^{18,19} and its red isomer indirubin (**2**)¹⁹, indolinone (**3**)²⁰,

deoxyvasicinone²¹, and the indigo precursors' isatan A and isatan B²² (**Fig. 4**). Also, other compounds such as aromatic and aliphatic carboxylic acids²³, various glucosides²⁴, isoprenoids^{24,25}, amino acids²⁵, sphingolipids²⁶, nitriles, furans^{27,28}, lignans²⁹, flavonoids, and anthranoids²¹ have been isolated.

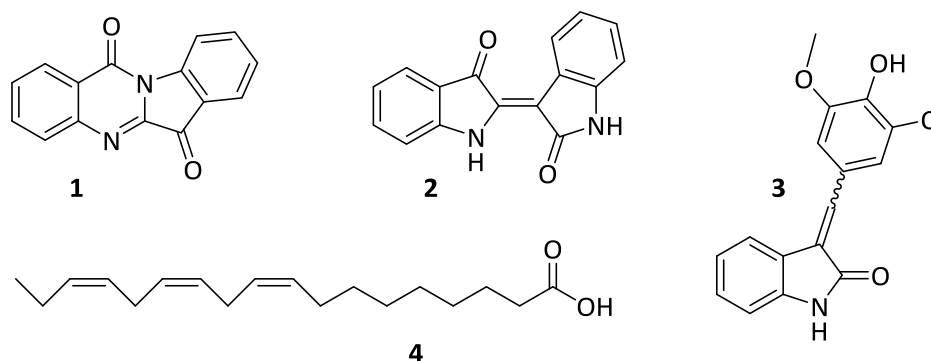


Figure 4: Structures of the main pharmacologically active constituents (1-4) of *Isatis tinctoria*

In various pharmacological studies, the antiviral, antifungal, antibacterial, cytoinhibitory and insecticidal properties of *Isatis tinctoria* and its constituents have been analyzed.

However, the anti-inflammatory potential of *Isatis tinctoria* and its active principles remained uncharacterized at that time. For this purpose, a broad-based pharmacological screening against 20 clinically relevant targets was initiated in our research group some years ago. The lipophilic woad extract displayed a promising *in vitro* profile against numerous inflammation-related targets including inhibition of cyclooxygenase-2 (COX-2), 5-lipoxygenase (5-LOX), inducible nitric oxide synthase (iNOS), histamine and serotonin release, and of leucocyte elastase³⁰. Subsequent HPLC-based activity profiling enabled the identification of tryptanthrin (**1**) as a potent inhibitor of COX-2³⁰ and 5-LOX³¹ catalyzed eicosanoid synthesis, and indolin-2-one (**3**) as an inhibitor of histamine release from mast cells³². γ -Linolenic acid (**4**), an unsaturated fatty acid, was identified as the major 5-LOX inhibitor³¹. Fractions containing α -linolenic, linoleic, *cis*-11-octadecenoic acid, oleic and palmitic acids showed a significant activity against the human neutrophil elastase³³. For indirubin (**2**) only marginal COX-2 inhibition was found¹¹. However, other groups reported anti-inflammatory^{34,35} and antiproliferative³⁶ properties of the compound.

In vivo studies in models of acute and chronic inflammation³⁷, contact allergy, and rheumatoid arthritis³⁸, and a clinical pilot study in experimentally induced skin erythema in human volunteers³⁹, showed the anti-inflammatory activity of the lipophilic woad extract in oral and/or topical applications. However, comparisons of the topical application of woad extract and pure tryptanthrin revealed that the extract is clinically more effective than the compound alone. Further investigations in an *ex vivo* cutaneous microdialysis model demonstrated that the skin penetration of tryptanthrin from the extract was substantially higher than for the compound alone⁴⁰. These observations supported the notion that also other compounds synergistically contribute to the clinical efficacy of the extract and may enhance the aqueous solubility of the otherwise poorly soluble alkaloids such as tryptanthrin¹¹.

2.2.2 Trypanthrin (Couroupitine A)

Discovery and occurrence

The history of trypanthrin dates back to 1878 when Sommaruga observed that by sublimation of indigo, golden-yellow needles were formed⁴¹. In 1915, Friedlander and Roschdestwensky first proposed the molecular structure of this alkaloid⁴², which was confirmed 60 years later by X-ray analysis^{43,44}. Since it was observed in 1971 that this molecule is synthesized by the yeast *Candida lipolytica* when cultured in L-tryptophan-enriched medium, the compound was named trypanthrin⁴⁵. Moreover, it should be noted that in 1974 Sen et al.⁴⁶ isolated a yellow compound from dried and powdered fruits of *Couroupita guaianensis* and elucidated structure **6** with the trivial name couroupitine A (**Fig. 5**). However, Bergman et al.⁴⁷ corrected this erroneous formula of the structure **6** later to the originally proposed structure **1**⁴⁷. In addition, trypanthrin was isolated from various other natural sources such as fungi (*Schizophyllum commune*⁴⁸, *Leucopaxillus cerealis*⁴⁹), cold water marine bacteria (*Oceanibulbus indolifex*⁵⁰) and numerous higher plants (*Strobilanthes cusia*⁵¹, *Isatis tinctoria*¹⁷, *Isatis indigotica*⁵², *Polygonum tinctorium*¹⁷, two *Calanthe* species⁵³ including *C. discolor* and *C. liukiensis*, *Wrightia tinctoria*⁵⁴, and many others^{46,55-57}). Moreover, it was reported that the compound is also present in mammals, particularly in the urine of Asian elephants (*Elephas maximus*⁵⁸) and in the wing-sac liquids of bats (*Saccopteryx bilineata*⁵⁹).

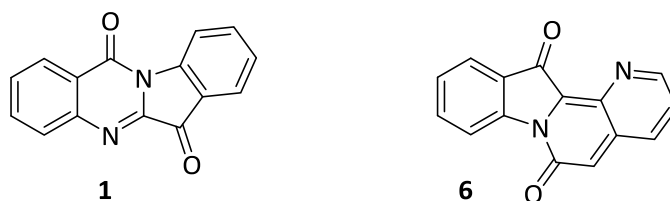


Figure 5: Trypanthrin (**1**) and the original proposed structure of couroupitine A (**6**)

Biological activities

In various pharmacological studies the antibacterial, antifungal, antiprotozoal, antiparasitic, and cytotoxic activity of trypanthrin was investigated. Trypanthrin exhibited growth inhibition in the μM range against pathogenic bacteria such as *Bacillus subtilis*⁶⁰, *Escherichia coli*⁶¹, *Mycobacterium tuberculosis*⁶², *Helicobacter pylori*⁶³, methicillin-resistant *Staphylococcus aureus*⁶⁴, as well as dermatophytic fungi such as *Trichophyton*, *Microsporum*, and *Epidermophyton* species⁵¹. The compound was also evaluated for its antiprotozoal potential and was considered active against *Leishmania donovani*⁶⁵, *Plasmodium falciparum*⁶⁶, *Toxoplasma gondii*⁶⁷, and *Trypanosoma brucei*⁶⁸. In addition, the compound showed cytotoxic^{55,69} activities against various mammalian cancer cell lines^{55,69}, and inhibited hepatocyte growth factor in human fibroblasts⁷⁰, as well as overexpression of the multidrug resistance gene MDR1 in breast cancer cells^{71,72}. Recently, trypanthrin was also reported

to activate the aryl hydrocarbon receptor (AhR), a ligand-activated transcriptional factor that controls the expression of xenobiotic-metabolizing enzymes such as cytochrome P450⁷³.

Although, tryptanthrin was originally isolated from *Isatis tinctoria* as an anti-dermatophytic compound by Honda et al. in 1980⁷⁴, the anti-inflammatory activity of the alkaloid was not explored at that time. Based on the promising results obtained by the HPLC-based activity profiling, further investigations on tryptanthrin in cell- and mechanism-based assays were initiated in our research group. In these studies, tryptanthrin inhibited COX-2 in two cell lines (Mono Mac and RAW 264.7) with a potency (IC₅₀ 37 nM and IC₅₀ 250 nM), that was comparable to the preferential COX-2 inhibitor nimesulide (IC₅₀ 27 nM and IC₅₀ 270 nM)^{30,75}. In HEL cells, the compound (IC₅₀ 0.36 μM) inhibited COX-1 catalyzed thromboxane B2 (TXB2) formation 100 times less potently than two non-selective COX inhibitors (diclofenac and indomethacin)¹¹. These findings were in agreement with the results obtained from enzyme-based assays with isolated COX enzymes, where tryptanthrin displayed a strong COX-2 (IC₅₀ 0.83 μM), but no significant COX-1 (IC₅₀ 50 μM) inhibition⁷⁵. Additionally, in a cell-based assay with calcium-ionophore-stimulated human granulocytes (neutrophils) the ability of tryptanthrin to inhibit 5-LOX was evaluated by measuring the leukotriene B4 (LTB4) formation as an indirect indicator of the 5-LOX activity. The results indicated that the inhibition of LTB4 release from neutrophils for tryptanthrin (IC₅₀ 0.15 μM) was in the same range as for the clinically used anti-asthmatic 5-LOX inhibitor zileuton (IC₅₀ 0.35 μM)⁷⁵. Recent data revealed that tryptanthrin does not directly interfere with the 5-LOX activity, but modifies the subcellular localization of 5-LOX via a not yet fully understood mechanism⁷⁶.

Moreover, Ishihara et al. demonstrated that tryptanthrin inhibits the expression of iNOS and prostaglandine E⁷⁷. Further immune-modulatory activities of tryptanthrin were reported by other groups such as the inhibition of T helper type 2 cells (Th2) development, immunoglobulin E (IgE) mediated degranulation, IL-4⁷⁸ and interferon-γ⁷⁹ production, and NF-κB⁷⁶.

Despite the potent and selective COX-2 inhibition of tryptanthrin, it is remarkable that there is no synthetic COX-2 inhibitor, neither on the market nor under development^{11,80}, which shows a structural similarity to tryptanthrin. Only the plant-derived rutaecarpine, a COX-2 inhibitor isolated from *Evodia rutaecarpa*⁸¹, bears certain resemblance to tryptanthrin¹¹. Moreover, it is assumed that dual inhibition of COX and 5-LOX could enhance the anti-inflammatory potency and reduce the undesired side effects with NSAIDs⁸². On the basis of this idea, numerous COX-2/5-LOX inhibitors have been synthesized and among these, licofelone⁸³ has currently reached phase III clinical trials. But also in this case, tryptanthrin showed no structural similarities to any COX-2/5-LOX inhibitor, neither to the anti-asthmatic 5-LOX inhibitor zileuton nor to the dual COX-2/5-LOX inhibitor¹¹ (**Fig. 6**).

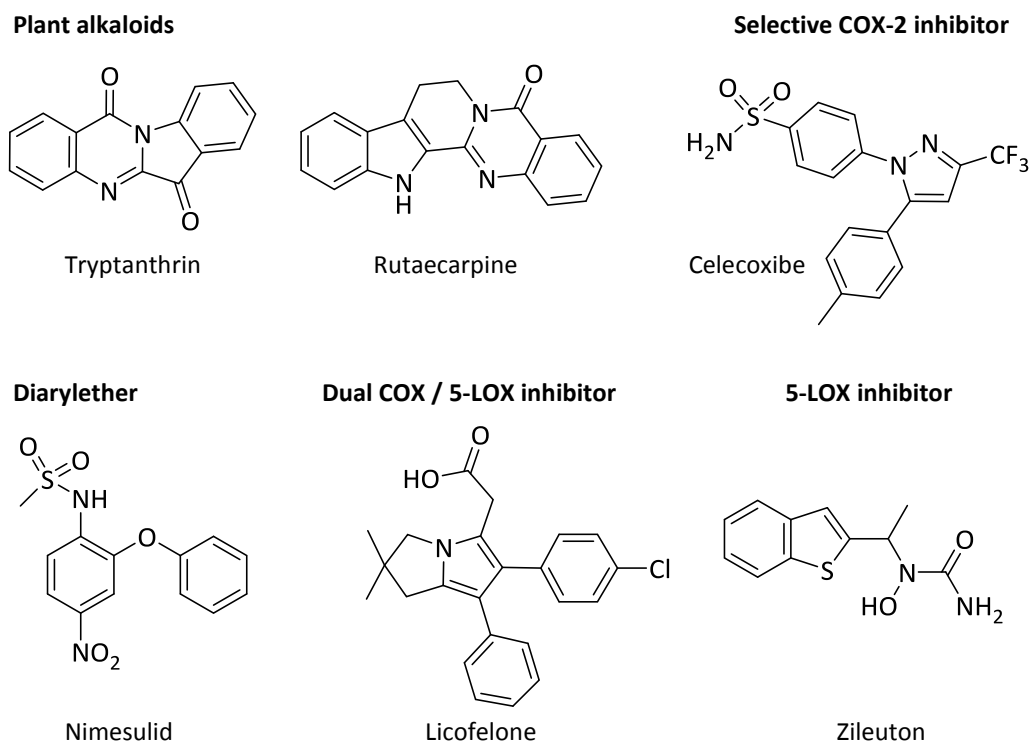


Figure 6: Structure of tryptanthrin, rutaecarpine, and synthetic compounds including COX-2, 5-LOX and dual COX/5-LOX inhibitors. Modified from Hamburger, *Phytochemistry Reviews*, 2002¹¹

Even though the mode of action of tryptanthrin is not yet fully understood, its structural uniqueness, the broad pharmacological spectrum of activities, and the structural drug-like properties render the compound as a promising lead for the further development of novel anti-inflammatory agents. Also, tryptanthrin is easily accessible by synthesis, and its scaffold provides numerous possibilities for structural modification for lead optimization¹¹.

2.2.3 Indirubin

Discovery and occurrence

The second constituent of *Isatis tinctoria* that raised our particular interest due to its promising pharmacological profile was the bis-indole, indirubin (**2**). The compound was first isolated from *Isatis tinctoria* by Schunck in 1855⁸⁴. Later he discovered that indirubin (**7**) (also known as isoindigotin or indigo red) is the red isomer of the blue dye indigo (indigotin)⁸⁵ (**Fig. 7**). In the late 1890s, Adolf von Bayer achieved the first chemical synthesis of indirubin along with indigo and laid therefore the starting point for chemical dye industry⁸⁶. In plants both indigoids derive from spontaneous dimerization of the colorless precursors indoxyl and isatin, which themselves are liberated during the fermentation process from the precursors indican or isatan B^{12,36}.

Indirubin and its precursors occur in various indigo-producing plants including *Baphicacanthus cusia* (Acanthaceae), *Polygonum tinctorium* (Polygonaceae), *Indigofera tinctoria* (Fabaceae), *Indigofera suffruticosa* (Fabaceae), *Isatis tinctoria* (Brassicaceae)³⁶, and two *Calanthe* species (*C. discolor* and *C. liukiensis*, Orchidaceae)⁵³, and in some marine mollusks (*Muricidae*)⁸⁷. Interestingly, indirubin was also found in mammals, especially in human urine from patients suffering from the purple urine bag syndrome^{88,89}. Additionally, indirubin was obtained from various recombinant bacteria expressing human cytochrome P450⁹⁰, and diverse enzymes such as naphthalene dioxygenase^{91,92}, and toluene dioxygenase⁹² among many others^{93–95}.

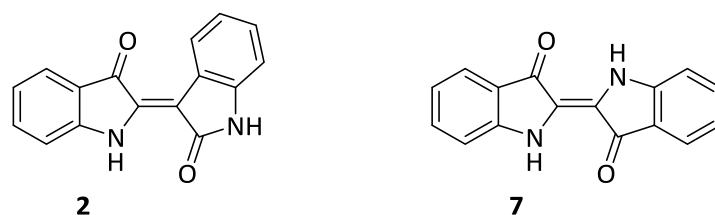


Figure 7: The blue dye indigo (7) and its red isomer indirubin (2)

Biological and pharmacological profile

The clinical interest in indirubin was triggered in the early 1980s when indirubin was identified as the active principle of Danggui Longhui Wan, a mixture of 11 herbals used in TCM to treat chronic myelocytic leukemia (CML)^{86,36}. The antiproliferative activity of indirubin was extensively confirmed in various human cancer cell lines^{96,97}, as well as in *in vivo* studies using human tumor xenograft models⁹⁸. Further investigations in the late 1990s revealed at least partially its molecular mode of action: indirubin strongly inhibited the cyclin-dependent kinases (CDK-1, CDK-2, CDK-4, and CDK-5) by binding to the ATP-binding pocket of CDKs³⁶. Moreover, the compound induced a cell cycle arrest mainly in G2 and/or G2/M phase leading to apoptosis of the cell^{36,99}. Besides CDK inhibition, indirubin was shown to block other kinases such as glycogen synthase kinase-3 β (GSK-3)^{100,101} and c-Src kinase¹⁰². In the last decade, indirubin was also found to block the cell cycle via the activation of the aryl hydrocarbon receptor (AhR)^{100,103,104}. Additionally, indirubin was shown to possess anti-inflammatory properties by inhibiting the production of various cytokines such as interferon γ , interleukin 6^{34,35}, and RANTES¹⁰⁵. Further studies revealed its ability to suppress the NF- κ B signaling pathway and the expression of NF- κ B target genes involved in tumorigenesis³⁵. In the last years, a large number of other targets such as Stat3 transcription factor¹⁰², glycogen phosphorylase (GP)¹⁰⁶, c-Jun NH₂-terminal kinase¹⁰⁷, dual specificity tyrosine-phosphorylation-regulated kinases (DYRK)¹⁰⁸, casein kinase¹⁰⁹, and caspases¹¹⁰, among many others⁹³ have been identified for indirubin and its derivatives.

***In vivo* toxicity studies and clinical trials**

In six-month toxicity studies in dogs given a dose of indirubin that was 25 times higher than those used for human therapy, reversible diarrhea and some liver damages were observed³⁶. Hematopoiesis, electroencephalogram activity, and renal function remained unaffected under indirubin treatment^{97,111}. Further *in vivo* long-term studies in animals showed that indirubin neither exhibited bone marrow toxicity nor hematotoxicity⁹⁷. In clinical trials with 314 patients suffering from CML, indirubin was given orally at a daily dosage of 150 - 450 mg¹¹². In 26% complete recovery and in 33% partial remission was observed in response to indirubin treatment. Overall, the toxicity of the compound was low and only mild to moderate side effects such as nausea, vomiting, abdominal pain and diarrhea were reported¹¹¹.

Aqueous solubility of indirubin

One of the major drawbacks of indirubin is its low aqueous solubility leading to poor bioavailability. These circumstances triggered the search for novel indirubin derivatives with improved selectivity, solubility and efficacy against tumor cells. Based on crystallographic data of CDK2, CDK5 and GSK3 in complex with indirubin derivatives, and on molecular modelling, a variety of different indirubin structure analogs were synthesized^{86,113}. The newly synthesized analogs (e.g. **Fig. 8**) showed enhanced solubility, selectivity against CDK2, and were almost colorless, which are all favorable prerequisites for drugs entering preclinical studies¹¹⁴.

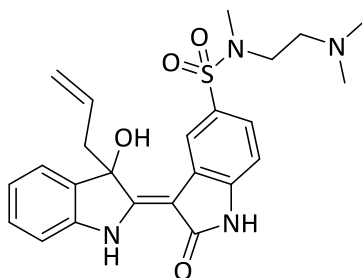


Figure 8: (Z)-3-allyl-N-(2-(dimethylamino)ethyl)-3-hydroxy-N-methyl-2'-oxo-[2,3'-biindolinylidene]-5'-sulfonamide, C₂₄H₂₈N₄O₄S, MW = 469 g/mol

In addition to these medicinal efforts, galenic approaches were described to overcome the low solubility of indirubin. Some of these approaches included the development of Super-Saturated Micro-Emulsion Drug Delivery Systems (S-SMEDDs)^{115,116}, a Self-Nano-Emulsing DDS¹¹⁷, and an indirubin nanoparticle formulation¹¹⁸ to enhance the oral bioavailability of the compound.

In summary, despite the low aqueous solubility of indirubin, the potent anti-proliferative and anti-inflammatory activities as well as its low toxicity, render the compound as a promising lead for further drug development.

2.2.4 Indolinone derivative

Biological activities of indolinone and pharmacology of mast cell stabilizers

Another *Isatis* compound that attracted attention in the HPLC-activity based profiling was the indolinone derivate (*E,Z*)-3-(4-hydroxy-3,5-dimethoxybenzylidene)indolin-2-one (indolinone).

The clinical use of indolinone derivatives was already known since the 1950s. Methisazone, a thiosemicarbazone, was one of the first antiviral drugs used for the treatment of smallpox¹¹⁹ (**Fig. 9**). Nowadays, the medicinal use of Methisazone is obsolete, but the development of synthetic indolinone derivatives as novel drug candidates is still ongoing. In the last decade a large number of indolinone analogs were screened for activities against Multiple Sclerosis¹²⁰, HIV¹²¹, various infectious diseases¹²², and cancer¹²³. In 2006, the indolinone-based drug Sunitinib (Sutent[®], Pfizer, **Fig. 9**) was approved by the Food and Drug Administration (FDA) as multiple receptor tyrosine kinase (RTK) inhibitor for the treatment of renal cell carcinoma and advanced gastrointestinal stromal tumors¹²⁴. Some years later, toceranib (Palladia[®], Pfizer), a structural analog of sunitinib, entered the market as RTK inhibitor for the treatment of canine mast cell tumors¹²⁵ (**Fig. 9**).

RTKs are key regulators in cellular processes and their increased activities have been linked to various diseases such as cancer, atherosclerosis, angiogenesis, inflammatory diseases, and other immune-mediated disorders¹²⁶. Previous crystallographic data with 3-substituted indolin-2-ones, suggested that the indolinone scaffold bears a kinase inhibitory activity by binding to the ATP-binding pocket of RTKs¹²⁷. This connection led to the assumption that the anti-allergic *Isatis* constituent, indolinone, possibly possesses some kinase-inhibitory activity³².

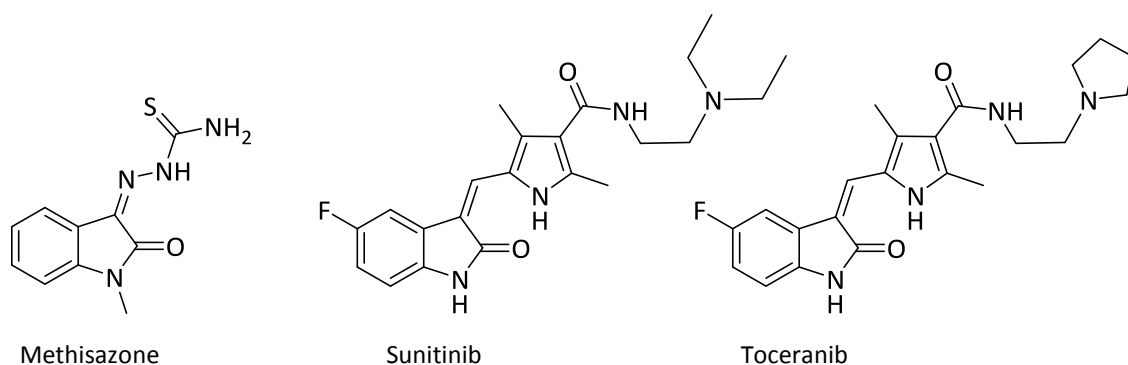


Figure 9: Indolinone-based drugs in market

In studies, which aimed at identifying the active principles of *Isatis tinctoria*, indolinone was found to inhibit the compound 48/80-induced histamine release from rat peritoneal mast cells with an IC₅₀ of 15 μ M. Strikingly, the suppression of histamine release was 100 fold higher than that of the clinically used mast cell stabilizer disodium chromoglycate (IC₅₀ 1.5 mM). Based on these promising results, a series of structurally related benzylidene-2-indolinones were synthesized and tested for their inhibitory activity against histamine release. However, none of them inhibited mast cell granulation at

concentrations up to 40 μM ¹²⁸. As the synthesized indolinone derivatives were all inhibitors of various kinases, the missing activity in the screening indicated that kinase inhibition is most probably not the underlying mechanism of the suppressed histamine release of indolinone (even though the compound itself was not tested in the kinase panel)¹²⁸. More recent data revealed that indolinone blocks the IgE mediated degranulation of sensitized mast cells (murine bone marrow derived mast cells) at nM concentrations ($\text{IC}_{50} = 54 \text{ nM}$) without directly interfering with the targets upstream of the histamine containing granules. Hence, it is thought that indolinone inhibits the granule exocytosis by possibly binding to surface fusion proteins such as SNAREs that play a central role in mast degranulation^{32,129}.

From a therapeutic point of view, mast cell stabilization can be a useful approach for the treatment of asthma. The most common direct mast cell stabilizers in clinical use are disodium cromoglycate (**Fig. 1**) and its derivative nedocromil¹³⁰. However, major drawbacks of these drugs are the frequent dosing (up to four times daily), as well as the unpleasant taste¹³¹. More recent approaches to stabilize mast cells include the development of Syk, JAK3, phosphodiesterases inhibitors and anti-IgE antibodies¹³⁰. In 2006, one of these anti-IgE antibodies, omalizumab (Xolair[®], Novartis), was approved by the FDA for the treatment of persistent allergic asthma and chronic idiopathic urticarial¹³². Major deficiencies of omalizumab are, however, the subcutaneous administration, the increased risk for anaphylaxis, and the relatively high therapy costs¹³². Consequently, there still remains an urgent need for the development of novel anti-allergic agents with improved pharmacological properties.

While the exact molecular mode of action of indolinone remains to be identified, the apparent selectivity, the remarkable potency to block mast cell degranulation¹²⁸, the lack of cytotoxicity³², and the structural drug-like properties render the molecule as an interesting lead for the further development of new anti-allergic drugs.

References

1. Ferrero-Miliani, L., Nielsen, O. H., Andersen, P. S. & Girardin, S. E. Chronic inflammation: importance of NOD2 and NALP3 in interleukin-1 β generation. *Clin. Exp. Immunol.* **147**, 227–235 (2007).
2. Murdoch, J. R. & Lloyd, C. M. Chronic inflammation and asthma. *Mutat. Res.* **690**, 24–39 (2010).
3. Hanauer, S. B. Inflammatory bowel disease: Epidemiology, pathogenesis, and therapeutic opportunities. *Inflamm. Bowel Dis.* **12**, S3–S9 (2006).
4. Epstein, F. H., Choy, E. H. & Panayi, G. S. Cytokine pathways and joint inflammation in rheumatoid arthritis. *N. Engl. J. Med.* **344**, 907–916 (2001).
5. Coussens, L. M. & Werb, Z. Inflammation and cancer. *Nature* **420**, 860–867 (2002).
6. Haffner, S. M. The Metabolic Syndrome: Inflammation, diabetes mellitus, and cardiovascular disease. *Am. J. Cardiol.* **97**, 3–11 (2006).
7. Akiyama, H. *et al.* Inflammation and Alzheimer's disease. *Neurobiol. Aging* **21**, 383–421 (2000).
8. Mutschler, E., Geisslinger, G., Kroemer, H. K., Menzel, S. & Ruth, P. *Mutschler Arzneimittelwirkungen: Pharmakologie - Klinische Pharmakologie - Toxikologie*. 211-279 (Wissenschaftliche Verlagsgesellschaft Stuttgart, 2012).
9. Santos, A. R. Anti-inflammatory compounds of plant origin. Part I. Action on arachidonic acid pathway, nitric oxide and nuclear factor κ B (NF- κ B). *Planta Med.* **69**, 973–983 (2003).
10. Santos, A. R. Anti-inflammatory compounds of plant origin. Part II. Modulation of pro-inflammatory cytokines, chemokines and adhesion molecules. *Planta Med.* **70**, 93–103 (2004).
11. Hamburger, M. *Isatis tinctoria*—From the rediscovery of an ancient medicinal plant towards a novel anti-inflammatory phytopharmaceutical. *Phytochem. Rev.* **1**, 333–344 (2002).
12. Hurry, J. B. *The woad plant and its dye*. (AM Kelley, 1973).
13. Tang, P. D. W. & Eisenbrand, P. D. G. in *Chinese Drugs of Plant Origin* 805–812 (Springer Berlin Heidelberg, 1992).
14. Elliott, M. C. & Stowe, B. B. Distribution and variation of indole glucosinolates in woad (*Isatis tinctoria* L.). *Plant. Physiol.* **48**, 498–503 (1971).
15. Fréchar, A. *et al.* Novel indole-type glucosinolates from woad (*Isatis tinctoria* L.). *Tetrahedron Lett.* **42**, 9015–9017 (2001).
16. Goetz, J. K. & Schraudolf, H. Two natural indole glucosinolates from Brassicaceae. *Phytochemistry* **22**, 905–907 (1983).
17. Honda, G., Tosirisuk, V. & Tabata, M. Isolation of an antidermatophytic, tryptanthrin, from indigo plants, *Polygonum tinctorium* and *Isatis tinctoria*. *Planta Med.* **38**, 275–276 (1980).
18. Perkin, A. G. XLIII.—Constituents of natural indigo. Part II. *J. Chem. Soc., Transactions* **91**, 435–440 (1907).
19. Perkin, A. G. & Bloxam, W. P. XXX.—Some constituents of natural indigo. Part I. *J. Chem. Soc., Transactions* **91**, 279–288 (1907).
20. Wu, X., Liu, Y., Sheng, W., Sun, J. & Qin, G. Chemical constituents of *Isatis indigotica*. *Planta Med.* **63**, 55–57 (1997).
21. Wu, X., Qin, G., Cheung, K. K. & Cheng, K. F. New alkaloids from *Isatis indigotica*. *Tetrahedron* **53**, 13323–13328 (1997).
22. Oberthür, C., Schneider, B., Graf, H. & Hamburger, M. The elusive indigo precursors in woad (*Isatis tinctoria* L.)—Identification of the major indigo precursor, isatan A, and a structure revision of isatan B. *Chem. Biodivers.* **1**, 174–182 (2004).
23. Hartleb, I. & Seifert, K. Acid constituents from *Isatis tinctoria*. *Planta Med.* **61**, 95–96 (1995).
24. HATLEB, I. & Seifert, K. A novel anthranilic acid derivative from *Isatis tinctoria*. *Planta Med.* **60**, 578–579 (1994).
25. Zhu, Y.-P. *Chinese materia medica: chemistry, pharmacology and applications*. (CRC Press, 1998).
26. Li, X. *et al.* New sphingolipids from the root of *Isatis indigotica* and their cytotoxic activity. *Fitoterapia* **78**, 490–495 (2007).
27. Conurso, C. *et al.* The leaf volatile constituents of *Isatis tinctoria* by solid-phase microextraction and gas chromatography/mass spectrometry. *Planta Med.* **72**, 924 (2006).
28. Miyazawa, M. & Kawata, J. Identification of the key aroma compounds in dried roots of *Isatis tinctoria*. *J. Essent. Oil Res.* **18**, 508–510 (2006).
29. Peng, J., Fan, G. & Wu, Y. Isolation and purification of clemastanin B and indigoticoiside A from *Radix Isatidis* by high-speed counter-current chromatography. *J. Chrom. A* **1091**, 89–93 (2005).
30. Danz, H., Stoyanova, S., Wippich, P., Brattström, A. & Hamburger, M. Identification and isolation of the cyclooxygenase-2 inhibitory principle in *Isatis tinctoria*. *Planta Med.* **67**, 411–416 (2001).

31. Oberthür, C., Jäggi, R. & Hamburger, M. HPLC based activity profiling for 5-lipoxygenase inhibitory activity in *Isatis tinctoria* leaf extracts. *Fitoterapia* **76**, 324–32. (2005).
32. Kiefer, S., Mertz, A. C., Koryakina, A., Hamburger, M. & Küenzi, P. (E,Z)-3-(3',5'-Dimethoxy-4'-hydroxy-benzylidene)-2-indolinone blocks mast cell degranulation. *Eur. J. Pharm. Sci.* **40**, 143–147 (2010).
33. Hamburger, M., Rüster, G. U. & Melzig, M. F. HPLC based activity profiling for inhibitors of human neutrophil elastase in *Isatis tinctoria* leaf extracts. *Nat. Prod. Commun.* **1**, 1107–10. (2006).
34. Kunikata, T. *et al.* Indirubin inhibits inflammatory reactions in delayed-type hypersensitivity. *Eur. J. Pharmacol.* **410**, 93–100 (2000).
35. Sethi, G. *et al.* Indirubin enhances tumor necrosis factor-induced apoptosis through Modulation of Nuclear Factor- κ B Signaling Pathway. *J. Biol. Chem.* **281**, 23425–23435 (2006).
36. Hoessel, R. *et al.* Indirubin, the active constituent of a Chinese antileukemia medicine. *Nat. Cell Biol.* **1**, 60–7. (1999).
37. Recio, M. C., Cerda-Nicolas, M., Potterat, O., Hamburger, M. & Rios, L. Anti-inflammatory and antiallergic activity in vivo of lipophilic *Isatis tinctoria* extracts and tryptanthrin. *Planta Med.* **72**, 539–46. (2006).
38. Recio, M. C., Cerda-Nicolas, M., Hamburger, M. & Rios, L. Anti-arthritic activity of a lipophilic woad (*Isatis tinctoria*) extract. *Planta Med.* **72**, 715–20. (2006).
39. Heinemann, C., Schliemann-Willers, S., Oberthür, C., Hamburger, M. & Elsner, P. Prevention of experimentally induced irritant contact dermatitis by extracts of *Isatis tinctoria* compared to pure tryptanthrin and its impact on UVB-induced erythema. *Planta Med.* **70**, 385–90. (2004).
40. Oberthür, C., Heinemann, C., Elsner, P., Benfeldt, E. & Hamburger, M. A comparative study on the skin penetration of pure tryptanthrin and tryptanthrin in *Isatis tinctoria* extract by dermal microdialysis coupled with isotope dilution ESI-LC-MS. *Planta Med.* **69**, 385–9. (2003).
41. Sommaruga, E. V. Ueber die Molekulargröße des Indigos. *Berichte der deutschen chemischen Gesellschaft* **11**, 1355–1356 (1878).
42. Friedländer, P. & Roschdestwenski, N. Über ein Oxidationsprodukt des Indigoblaus. *Ber. Dtsch. Chem. Ges.* **48**, 1841–7. (1915).
43. Brufani, M., Fedeli, W., Mazza, F., Gerhard, A. & Keller-Schierlein, W. The structure of tryptanthrin. *Cell Mol Life Sci* **27**, 1249–1250 (1971).
44. Fedeli, W. & Mazza, F. Crystal structure of tryptanthrin (indolo[2,1-b]quinazoline-6,12-dione). *J. Chem. Soc., Perkin Trans. 2* 1621–1623 (1974).
45. Schindler, F. & Zähler, H. Stoffwechselprodukte von Mikroorganismen. *Archiv für Mikrobiologie* **79**, 187–203 (1971).
46. Sen, A. K., Mahato, S. B. & Dutta, N. L. Courouputine A, a new alkaloid from *Couroupita guianensis*. *Tetrahedron Lett.* **15**, 609–610 (1974).
47. Bergman, J., Egestad, B. & Lindström, J.-O. The structure of some indolic constituents in *Couroupita Guaianensis* Aubl. *Tetrahedron Lett.* **18**, 2625–2626 (1977).
48. Hosoe, T. *et al.* Isolation of a new potent cytotoxic pigment along with indigotin from the pathogenic basidiomycetous fungus *Schizophyllum commune*. *Mycopathologia* **146**, 9–12 (1999).
49. Jahng, Y. Progress in the studies on tryptanthrin, an alkaloid of history. *Arch. Pharm. Res.* **36**, 517–535 (2013).
50. Wagner-Döbler, I. *et al.* *Oceanibulbus indolifex* gen. nov., sp. nov., a North Sea alphaproteobacterium that produces bioactive metabolites. *Int. J. Syst. Evol. Microbiol.* **54**, 1177–1184 (2004).
51. Honda, G. & Tabata, M. Isolation of Antifungal Principle Tryptanthrin, from *Strobilanthes cusia* O. Kuntze. *Planta Med.* **36**, 85–86 (1979).
52. Li, Q., Jin, J., Chong, M. & Song, Z. Studies on the antifungal constituent of Qing Dai (*Isatis indigotica*). *Zhongcaoyao* **14**, 440–441 (1983).
53. Yoshikawa, M. *et al.* Novel indole S,O-bisdesmoside, calanthoside, the precursor glycoside of tryptanthrin, indirubin, and isatin, with increasing skin blood flow promoting effects, from two *Calanthe* species (Orchidaceae). *Chem. Pharm. Bull.* **46**, 886–888 (1998).
54. George, V., Koshy, A. S., Singh, O. V., Nayar, M. N. S. & Pushpangadan, P. Tryptanthrin from *Wrightia tinctoria*. *Fitoterapia* **67**, 553–554 (1996).
55. Jao, C.-W., Lin, W.-C., Wu, Y.-T. & Wu, P.-L. Isolation, structure elucidation, and synthesis of cytotoxic tryptanthrin analogues from *Phaius mishmensis*. *J. Nat. Prod.* **71**, 1275–1279 (2008).
56. Xu, F. *et al.* Structures of new flavonoids and benzofuran-type stilbene and degranulation inhibitors of rat basophilic leukemia cells from the Brazilian herbal medicine *Cissus sicyoides*. *Chem. Pharm. Bull.* **57**, 1089–1095 (2009).
57. Liu, Y., Ou, Y. F. & Yao, X. S. Chemical constituents in the leaves of *Baphicacanthus cusia* (Nees) Bremek. *Chin. J. Med. Chem.* **19**, 273–275 (2009).

58. Rasmussen, L. E. L., Lee, T. D., Daves Jr, G. D. & Schmidt, M. J. Female-to-male sex pheromones of low volatility in the Asian elephant, *Elephas maximus*. *J. Chem. Ecol.* **19**, 2115–2128 (1993).
59. Caspers, B., Franke, S. & Voigt, C. C. in *Chem. Signal Vertebrates 11* 151–160 (Springer, 2008).
60. Honda, G., Tabata, M. & Tsuda, M. The antimicrobial specificity of tryptanthrin. *Planta Med.* **37**, 172–174 (1979).
61. Bandekar, P. P. *et al.* Antimicrobial Activity of Tryptanthrins in *Escherichia coli*. *J. Med. Chem.* **53**, 3558–3565 (2010).
62. Mitscher, L. A. & Baker, W. Tuberculosis: A search for novel therapy starting with natural products. *Med. Res. Rev.* **18**, 363–374 (1998).
63. Kataoka, M. *et al.* Antibacterial action of tryptanthrin and kaempferol, isolated from the indigo plant (*Polygonum tinctorium* Lour.), against *Helicobacter pylori*-infected Mongolian gerbils. *J. Gastroenterol.* **36**, 5–9 (2001).
64. Kawakami, J. *et al.* Antibacterial and antifungal activities of tryptanthrin derivatives. *Transactions of the Materials Research Society of Japan* **36**, 603–606 (2011).
65. Bhattacharjee, A. K. *et al.* Analysis of stereoelectronic properties, mechanism of action and pharmacophore of synthetic indolo[2,1-b]quinazoline-6,12-dione derivatives in relation to antileishmanial activity using quantum chemical, cyclic voltammetry and 3-D-QSAR CATALYST procedures. *Bioorg. Med. Chem.* **10**, 1979–1989 (2002).
66. Bhattacharjee, A. K. *et al.* Structure-activity relationship study of antimalarial indolo [2,1-b]quinazoline-6,12-diones (tryptanthrins). Three dimensional pharmacophore modeling and identification of new antimalarial candidates. *Eur. J. Med. Chem.* **39**, 59–67 (2004).
67. Krivogorsky, B., Grundt, P., Yolken, R. & Jones-Brando, L. Inhibition of *Toxoplasma gondii* by indirubin and tryptanthrin analogs. *Antimicrob. Agents Chemother.* **52**, 4466–4469 (2008).
68. Scovill, J., Blank, E., Konnick, M., Nenortas, E. & Shapiro, T. Antitrypanosomal activities of tryptanthrins. *Antimicrob. Agents Chemother.* **46**, 882–883 (2002).
69. Kimoto, T. *et al.* Cytotoxic effects of substances in indigo plant (*Polygonum tinctorium* Lour.) on malignant tumour cells. *Nat. Med.* **53**, 72–9 (1999).
70. Motoki, T. *et al.* Inhibition of hepatocyte growth factor induction in human dermal fibroblasts by tryptanthrin. *Biol. Pharm. Bull.* **28**, 260–266 (2005).
71. Yu, S.-T., Chen, T.-M., Chern, J.-W., Tseng, S.-Y. & Chen, Y.-H. Downregulation of GSTpi expression by tryptanthrin contributing to sensitization of doxorubicin-resistant MCF-7 cells through c-jun NH2-terminal kinase-mediated apoptosis. *Anticancer Drugs* **20**, 382–388 (2009).
72. Yu, S.-T., Chen, T.-M., Tseng, S.-Y. & Chen, Y.-H. Tryptanthrin inhibits MDR1 and reverses doxorubicin resistance in breast cancer cells. *Biochem. Biophys. Res. Commun.* **358**, 79–84 (2007).
73. Schrenk, D., Riebinger, D., Till, M., Vetter, S. & Fiedler, H.-P. Tryptanthrins: A novel class of agonists of the aryl hydrocarbon receptor. *Biochem. Pharmacol.* **54**, 165–171 (1997).
74. Honda, G., Tosirisuk, V. & Tabata, M. Isolation of an antidermatophytic, tryptanthrin, from indigo plants, *Polygonum tinctorium* and *Isatis tinctoria*. *Planta Med.* **38**, 275–276 (1980).
75. Danz, H. *et al.* Inhibitory activity of tryptanthrin on prostaglandin and leukotriene synthesis. *Planta Med.* **68**, 875–880 (2002).
76. Pergola, C. *et al.* On the inhibition of 5-lipoxygenase product formation by tryptanthrin: mechanistic studies and efficacy in vivo. *Br. J. Pharmacol.* **165**, 765–776 (2012).
77. Ishihara, T. *et al.* Tryptanthrin inhibits nitric oxide and prostaglandin E2 synthesis by murine macrophages. *Eur. J. Pharmacol.* **407**, 197–204 (2000).
78. Iwaki, K. *et al.* Tryptanthrin inhibits Th2 development, and IgE-mediated degranulation and IL-4 production by rat basophilic leukemia RBL-2H3 cells. *J. Ethnopharmacol.* **134**, 450–459 (2011).
79. Takei, Y. *et al.* Tryptanthrin inhibits interferon-gamma production by Peyer's patch lymphocytes derived from mice that had been orally administered staphylococcal enterotoxin. *Biol. Pharm. Bull.* **26**, 365–367 (2003).
80. Dannhardt, G. & Kiefer, W. Cyclooxygenase inhibitors--current status and future prospects. *Eur. J. Med. Chem.* **36**, 109–126 (2001).
81. Moon, T. C. *et al.* A new class of COX-2 inhibitor, rutaecarpine from *Evodia rutaecarpa*. *Inflamm. Res.* **48**, 621–625 (1999).
82. Fiorucci, S., Meli, R., Bucci, M. & Cirino, G. Dual inhibitors of cyclooxygenase and 5-lipoxygenase. A new avenue in anti-inflammatory therapy? *Biochem. Pharmacol.* **62**, 1433–1438 (2001).
83. Boileau, C. *et al.* Licofelone (ML-3000), a dual inhibitor of 5-lipoxygenase and cyclooxygenase, reduces the level of cartilage chondrocyte death in vivo in experimental dog osteoarthritis: inhibition of pro-apoptotic factors. *J. Rheumatol.* **29**, 1446–1453 (2002).

84. Schunck, E. *On the formation of indigo-blue*. (1855).
85. Sumpter, W. C. & Miller, F. M. *The Chemistry of Heterocyclic Compounds, Indole and Carbazole Systems*. (John Wiley & Sons, 2009).
86. Jautelat, R. *et al.* From the Insoluble Dye Indirubin towards Highly Active, Soluble CDK2-Inhibitors. *Chem. Bio. Chem.* **6**, 531–540 (2005).
87. Cooksey, C. J. Tyrian Purple: 6,6'-Dibromoindigo and Related Compounds. *Molecules* **6**, 736–769 (2001).
88. Allegri, G., Bertazzo, A., Comai, S. & Costa, C. V. Production of indirubin and indigoids in humans. *Indirubin, the red shade of indigo*, L. Meijer, N. Guyard, LA Skaltsounis and G. Eisenbrand (Eds.), Editions 'Life in Progress', Station Biologique de Roscoff 89–101 (2006).
89. Tan, C.-K., Wu, Y.-P., Wu, H.-Y. & Lai, C.-C. Purple urine bag syndrome. *CMAJ* **179**, 491 (2008).
90. Guengerich, P. F. & Wu, Z.-L. Biosynthesis of novel indirubins by recombinant cytochrome P450 systems. *Indirubin, the red shade of indigo*, L. Meijer, N. Guyard, LA Skaltsounis and G. Eisenbrand (Eds.), Editions 'Life in Progress', Station Biologique de Roscoff 79–87 (2006).
91. Ensley, B. D. *et al.* Expression of naphthalene oxidation genes in Escherichia coli results in the biosynthesis of indigo. *Science* **222**, 167–169 (1983).
92. Kim, J. Y., Lee, K., Kim, Y. & Kim, C.-K. Production of dyestuffs from indole derivatives by naphthalene dioxygenase and toluene dioxygenase. *Lett. Appl. Microbiol.* **36**, 343–348 (2003).
93. Meijer, L., Shearer, J., Bettayeb, K. & Ferandin, Y. Diversity of the intracellular mechanisms underlying the anti-tumor properties of indirubins. *Int. Congress Series* **1304**, 60–74 (2007).
94. Kim, I.-C., Chang, H.-C. & Oriel, P. Production of indigo and indirubin by Escherichia coli containing phenol hydroxylase gene of Bacillus stearothermophilus. *J. Microbiol. Biotechnol. (Korea Republic)* (1997).
95. Rui, L., Reardon, K. F. & Wood, T. K. Protein engineering of toluene ortho-monooxygenase of Burkholderia cepacia G4 for regiospecific hydroxylation of indole to form various indigoid compounds. *Appl. Microbiol. Biotechnol.* **66**, 422–429 (2005).
96. Niederberger, E. Mechanismusorientierte Untersuchungen zur antineoplastischen Wirkung von Naturstoffen und Naturstoffderivaten. (Dissertation, Universität Kaiserslautern, 1998).
97. Eisenbrand, G., Hippe, F., Jakobs, S. & Muehlbeyer, S. Molecular mechanisms of indirubin and its derivatives: novel anticancer molecules with their origin in traditional Chinese phytomedicine. *J. Cancer Res. Clin. Oncol.* **130**, 627–635 (2004).
98. Kim, S.-A. *et al.* Antitumor activity of novel indirubin derivatives in rat tumor model. *Clin. Cancer Res.* **13**, 253–259 (2007).
99. Merz, K. H. *et al.* Novel indirubin derivatives, promising anti-tumor agents inhibiting cyclin-dependent kinases. *Int. J. Clin. Pharmacol. Ther.* **42**, 656–658 (2004).
100. Leclerc, S. *et al.* Indirubins inhibit glycogen synthase kinase-3 β and CDK5/P25, two protein kinases involved in abnormal tau phosphorylation in Alzheimer's disease. *J. Biol. Chem.* **276**, 251–60. (2001).
101. Meijer, L. *et al.* GSK-3-selective inhibitors derived from Tyrian purple indirubins. *Chem. Biol.* **10**, 1255–1266 (2003).
102. Nam, S. *et al.* Indirubin derivatives inhibit Stat3 signaling and induce apoptosis in human cancer cells. *Proceedings of the National Academy of Sciences of the United States of America* **102**, 5998–6003 (2005).
103. Adachi, J. *et al.* Indirubin and indigo are potent aryl hydrocarbon receptor ligands present in human urine. *J. Biol. Chem.* **276**, 31475–31478 (2001).
104. Knockaert, M. *et al.* Independent actions on cyclin-dependent kinases and aryl hydrocarbon receptor mediate the antiproliferative effects of indirubins. *Oncogene* **23**, 4400–4412 (2004).
105. Mak, N.-K. *et al.* Inhibition of RANTES expression by indirubin in influenza virus-infected human bronchial epithelial cells. *Biochem. Pharmacol.* **67**, 167–174 (2004).
106. Kosmopoulou, M. N. *et al.* Binding of the potential antitumour agent indirubin-5-sulphonate at the inhibitor site of rabbit muscle glycogen phosphorylase b. *Eur. J. Biochem.* **271**, 2280–2290 (2004).
107. Xie, Y. *et al.* Indirubin-3'-oxime inhibits c-Jun NH 2-terminal kinase: Anti-apoptotic effect in cerebellar granule neurons. *Neurosci. Lett.* **367**, 355–359 (2004).
108. Myrianthopoulos, V. *et al.* Novel inverse binding mode of indirubin derivatives yields improved selectivity for DYRK kinases. *ACS Med. Chem. Lett.* **4**, 22–26 (2012).
109. Cheng, X. *et al.* 7, 7'-Diazaindirubin—A small molecule inhibitor of casein kinase 2 in vitro and in cells. *Bioorg. Med. Chem.* **22**, 247–255 (2014).
110. Ribas, J. *et al.* 7-Bromoindirubin-3'-oxime induces caspase-independent cell death. *Oncogene* **25**, 6304–6318 (2006).
111. Hössel, R. Synthese von Derivaten des Indirubins und Untersuchungen zur Mechanismusaufklärung ihrer antineoplastischen Wirkung. (Dissertation Universität Kaiserslautern, 1999).

112. Maruta, H. Indirubin in *Tumor suppressing viruses, genes, and drugs: innovative Cancer Therapy Approaches*. 157-168 (Academic Press, 2001).
113. Polychronopoulos, P. *et al.* Structural basis for the synthesis of indirubins as potent and selective inhibitors of glycogen synthase kinase-3 and cyclin-dependent kinases. *J. Med. Chem.* **47**, 935–946 (2004).
114. Potterat, O. & Hamburger, M. in *Natural Compounds as Drugs Volume I* 45–118 (Springer, 2008).
115. Gaboriaud-Kolar, N., Vougianniopoulou, K. & Skaltsounis, A.-L. Indirubin derivatives: a patent review (2010-present). *Expert Opin. Ther. Pat.* **25**, 583–593 (2015).
116. Chen, Z.-Q., Liu, Y., Zhao, J.-H., Wang, L. & Feng, N.-P. Improved oral bioavailability of poorly water-soluble indirubin by a supersaturatable self-microemulsifying drug delivery system. *Int. J. Nanomed.* **7**, 1115 (2012).
117. Heshmati, N., Cheng, X., Eisenbrand, G. & Fricker, G. Enhancement of oral bioavailability of E804 by self-nanoemulsifying drug delivery system (SNEDDS) in Rats. *J. Pharm. Sci.* **102**, 3792–3799 (2013).
118. Wu, B. Nanoparticles of indirubin, derivatives thereof and methods of making and using same. (2015).
119. McLean, D. M. Methisazone therapy in pediatric vaccinia complications. *Ann. N.Y. Acad. Sci.* **284**, 118–121 (1977).
120. Bouérat, L. *et al.* Indolin-2-ones with high in vivo efficacy in a model for Multiple Sclerosis. *J. Med. Chem.* **48**, 5412–5414 (2005).
121. Boechat, N. *et al.* Design, synthesis and pharmacological evaluation of HIV-1 reverse transcriptase inhibition of new indolin-2-ones. *Med. Chem.* **3**, 533–542 (2007).
122. Bouchikhi, F. *et al.* Synthesis and biological evaluation of diversely substituted indolin-2-ones. *Eur. J. Med. Chem.* **43**, 2316–2322 (2008).
123. Kaur, K. & Talele, T. T. 3D QSAR studies of 1, 3, 4-benzotriazepine derivatives as CCK 2 receptor antagonists. *J. Mol. Graph. Model.* **27**, 409–420 (2008).
124. Atkins, M., Jones, C. A. & Kirkpatrick, P. Sunitinib maleate. *Nat. Rev. Drug Discov.* **5**, 279–280 (2006).
125. London, C. A. *et al.* Multi-center, placebo-controlled, double-blind, randomized study of oral toceranib phosphate (SU11654), a receptor tyrosine kinase inhibitor, for the treatment of dogs with recurrent (either local or distant) mast cell tumor following surgical excision. *Clin. Cancer Res.* **15**, 3856–3865 (2009).
126. Lemmon, M. A. & Schlessinger, J. Cell signaling by receptor tyrosine kinases. *Cell* **141**, 1117–1134 (2010).
127. Sun, L. *et al.* Synthesis and biological evaluations of 3-substituted indolin-2-ones: a novel class of tyrosine kinase inhibitors that exhibit selectivity toward particular receptor tyrosine kinases. *J. Med. Chem.* **41**, 2588–2603 (1998).
128. Rüster, G. U., Hoffmann, B. & Hamburger, M. Inhibitory activity of indolin-2-one derivatives on compound 48/80-induced histamine release from mast cells. *Pharmazie* **59**, 236–7. (2004).
129. Puri, N., Kruhlak, M. J., Whiteheart, S. W. & Roche, P. A. Mast cell degranulation requires N-ethylmaleimide-sensitive factor-mediated SNARE disassembly. *J. Immunol.* **171**, 5345–5352 (2003).
130. Finn, D. F. & Walsh, J. J. Twenty-first century mast cell stabilizers. *Br. J. Pharmacol.* **170**, 23–37 (2013).
131. Rubin, J. S., Sataloff, R. T. & Korovin, G. S. *Diagnosis and Treatment of Voice Disorders*. Mast cell stabilizers 620-622 (Plural Publishing, 2014).
132. Strunk, R. C. & Bloomberg, G. R. Omalizumab for asthma. *N. Engl. J. Med.* **354**, 2689–2695 (2006).

2.3 Pharmacokinetics and early ADMET profiling in drug discovery

In the early 1970s, scientists mainly focused on finding the most active and selective drug candidate. Issues concerning pharmacokinetics (PK), stability, and ADMET properties of a compound were addressed later during the drug development phase. In the late 1980s, a landmark study, however, revealed that the main reasons for drug failure in the development phase were poor PK and biopharmaceutical properties (39.4%), rather than unsatisfactory efficacy (29.3%)¹. As a consequence of this, companies started to implement compound property assessments using high-throughput methods (*in silico*, *in vitro*, *in vivo*) already during early drug discovery².

In a first approach, higher throughput *in vitro* assays were implemented, which efficiently provide information about the physicochemical properties of a compound such as solubility, permeability, and metabolic stability. In an additional approach, higher throughput animal studies were incorporated in order to screen more test compounds. Moreover, these preliminary PK studies provided important key PK parameters that allowed prediction of the *in vivo* ADMET success in humans.

Most companies introduced a combination of various approaches for compound assessment in early drug discovery. As a consequence of these strategy changes, failure due to insufficient compound properties dropped from 39% in 1988 to 10% in 2000. A study in 2002, however, revealed that toxicity and formulation still remained major challenges in drug discovery^{2,3}.

Considering this, we aimed at evaluating preliminary PK and early ADMET properties of the three anti-inflammatory compounds, tryptanthrin, indirubin and indolinone. The focus of the following chapter is on the drug development process, followed by an introduction to pharmacokinetics (PK), the gastrointestinal tract (GIT) and the blood-brain barrier (BBB) as biological barriers, and the human ether-a-go-go related gene (hERG) potassium channel.

2.3.1 Drug discovery and development process

Drug discovery and development is a costly and time-consuming process (**Fig. 10**). On average, drug discovery and development takes 14.2 years and costs up to \$2.5 billion for a single marketed drug^{4,5}. The complete process can be divided into three phases: drug discovery, development, and registration. Typically, the discovery phase requires 3 - 5 years and involves biological target identification and validation, hit identification, and lead finding and optimization⁴. During drug discovery, ADMET (absorption, distribution, metabolism, excretion, and toxicity) properties are also assessed by a series of *in silico*, *in vitro*, and *in vivo* tools^{4,6,7}. Based on these data, lead structures are optimized, before they enter the drug development phase. At this stage, the compound is subjected to preclinical testing in animals (~ 2 years), first-in-man studies (also known as phase I), and full clinical trials (phase II and III, ~ 6 years), before the compound finally enters the registration phase (~ 1.8 years)⁴. According to the US Food and Drug Administration (FDA), only 8% of phase I trial drugs become a marketed product, and 4% of the approved drugs are withdrawn from the market (e.g. Vioxx)⁸. As drug discovery and development is a highly risky and expensive activity, many companies are following the “fail fast, fail cheap” strategy⁴.

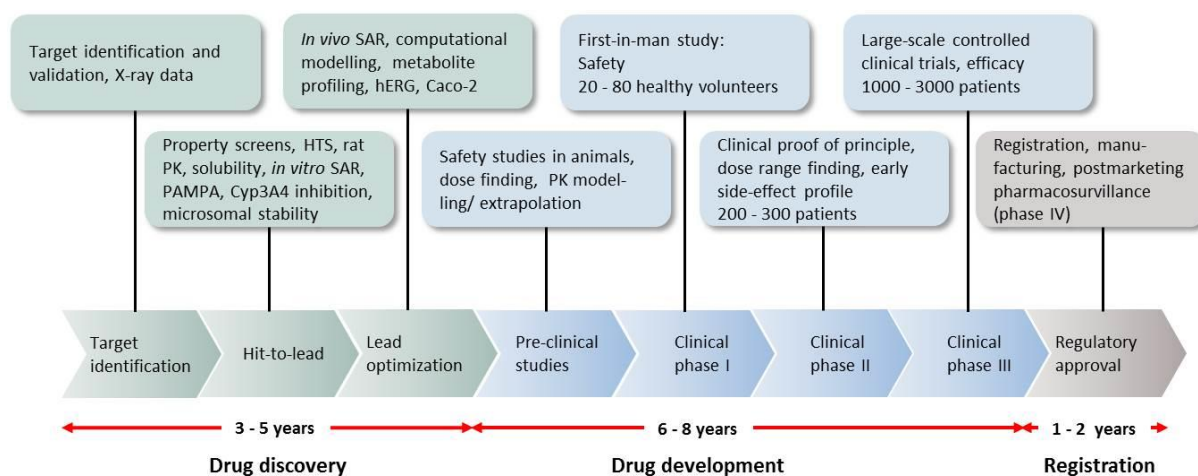


Figure 10: Drug discovery and development stages, average time span and their major activities. HTS: High-throughput screening, PK: Pharmacokinetics. SAR: structure-activity relationship. Adapted from^{3,9-12}.

2.3.2 Pharmacokinetics in drug discovery

Key PK parameters

PK describes the concentration time course of a compound *in vivo*² (**Table 1**). The concentration time course of a drug changes depending on a number of factors, including the route of administration. An intravenously (i.v.) administered compound immediately *distributes* from the bloodstream into the tissues, before it is *eliminated* from the body by the liver and kidneys. Orally administered drugs first have to dissolve (*liberation*), penetrate through the gastrointestinal tract (*absorption*), and pass through the liver (*metabolism*), before they enter the systemic circulation. As a consequence, the time (t_{max}) to reach the maximal plasma peak concentration (C_{max}) in the bloodstream is delayed². The area under the curve (AUC) reflects the total drug exposure over time. The bioavailability (F) is linked to the AUC and describes the fraction of an administered dose that reaches the systemic blood circulation unchanged³. By definition, drugs given i.v. have a bioavailability of 100%. Bioavailability of other administration routes is determined by comparison with i.v. dosing (“absolute bioavailability”). A bioavailability of less than 100% is usually the result of incomplete absorption (low solubility, low permeability, high efflux, and/or enzymatic or pH hydrolysis) and/or high first pass metabolism (phase I and II). Moreover, it should be noted that a compound with low bioavailability bears the risk of high patient-to-patient variability, particularly when its drug-metabolizing enzymes (cytochrome P450) are polymorphic in a population (slow vs fast metabolizer)³. Another elementary PK parameter is the clearance (CL), which is defined as the ratio of the administered dose to the AUC. The volume of distribution (V_d) is an apparent volume and reflects the drug extent of localization outside the plasma. Thus, the higher the V_d ($= \text{dose}/C_0$), the lower the initial drug concentration C_0 in the plasma.

Table 1: Descriptions, typical units and calculations of key PK parameters³

PK parameter	Description	Typical units	Calculation
Area under the curve (AUC)	Integral of the concentration-time curve	h*ng/mL	$AUC_{0-\infty} = \int_0^{\infty} C dt$ $AUC_{0-last} = \int_0^{last} C dt$
Initial concentration (C_0)	Initial blood concentration after i.v. dosing	ng/mL	Direct measurement
Volume of distribution (V_d)	The apparent volume in which the compound is dissolved	L/kg or mL/kg/b.w.	$V_d = \frac{\text{dose}}{C_0}$
Clearance (CL)	Describes how fast a compound is extracted from systemic circulation	L/h/kg or mL/min/kg	$CL = \frac{\text{dose}}{AUC_{i.v.}}$
Elimination rate constant (k_e)	Elimination rate of first order kinetics	h^{-1}	$k_e = \frac{\ln(2)}{t_{1/2}} = \frac{CL}{V_d}$
Half-life ($t_{1/2}$)	Time required to reach half of the initial concentration	min or h	$t_{1/2} = \frac{\ln(2)}{k_e}$
Bioavailability (%F)	Fraction that reaches systemic circulation	%	$\%F = \frac{AUC_{p.o.}}{AUC_{i.v.}} * \frac{\text{dose}_{i.v.}}{\text{dose}_{p.o.}} * 100$
Maximum Concentration (C_{max})	Peak plasma concentration following dose	ng/mL	Direct measurement
Time of maximum drug concentration (t_{max})	Time to reach C_{max}	min or h	Direct measurement

The half-life ($t_{1/2}$) is the time required to reach half of the initial drug concentration in the body. This parameter is inversely proportional to the elimination constant (k_e) and linked to the CL and V_d . Thus, a high k_e leads to a short half-life and a rapid decline of plasma concentration¹³. Furthermore, $t_{1/2}$ allows estimation on how frequent a dose has to be administered to maintain the drug concentration in a therapeutic range². It should be noted that PK parameters are highly dependent on the structural properties of a compound (molecular weight, hydrogen bonds, lipophilicity, polar surface area, and pK_a) and the exposed physical/biochemical environment (e.g. blood flow, pH, transporters, protein binding, and enzymes)³. A highly active compound *in vitro* is thus not necessarily an efficient drug *in vivo*, if e.g. the bioavailability is poor. On the other hand, drug candidates with lower bioactivity but favorable physicochemical properties may result in more efficacious *in vivo* drugs. Therefore, it is an important prerequisite to assess PK parameters along with physicochemical properties in early drug discovery, in order to improve *in vivo* performance of a compound by structural modifications. Common goals for PK parameters in drug discovery are summarized in **Table 2**.

Table 2: Categorization of the main PK parameters in drug discovery².

PK parameters	High	Low
Volume of distribution (V_d)	>10 L/kg	<1 L/kg
Plasma clearance (CL)	Rat: >45 mL/min/kg Human: >15 mL/min/kg	Rat: <10 mL/min/kg Human: <5 mL/min/kg
Half-life ($t_{1/2}$)	Rat: >3h Human: >8h	Rat: <1h Human: <3h
Oral bioavailability ¹⁴ (%F)	Rat: >50%	Rat: <20%
Oral exposure ¹⁴ (AUC)	Rat: >2000 h*ng/mL	Rat: <500 h*ng/mL
Time of maximum drug concentration (t_{max})	>3h	<1h

Plasma protein binding (PPB)

Drug molecules can bind to a wide variety of blood components such as red blood cells, leukocytes and platelets, proteins (albumin, α_1 -acid glycoprotein, lipoproteins, erythrocytes), and α -, β -, and γ -globulins². The most prominent plasma proteins involved in drug binding in humans are human serum albumin (HSA; representing 60% of total plasma proteins), α_1 -acid glycoprotein (AGP) and lipoproteins^{2,15}.

Plasma is the liquid fraction of whole blood (without cells) and is produced when blood is collected in the presence of an anticoagulant (e.g. heparin). Blood cells are removed by centrifugation and the resulting supernatant represents the plasma. In contrast, serum is obtained without an anticoagulant. Clotting factors (e.g. fibrinogen) are removed by centrifugation to produce the serum. In PK studies, the plasma is used for analysis. Plasma contains both the protein-bound and unbound fraction of drugs, while the cell-bound drug fraction is discarded².

Plasma proteins can adsorb high amounts of drug molecules. As only the unbound drug fraction can reach the target tissue, protein binding impacts the exposure to the therapeutic target and the ADMET

properties of a molecule. However, it should be noted that not only the extent of drug binding, but also the rate of association/dissociation influences the drug disposition in the body². Moreover, plasma protein binding (PPB) can vary among species, different disease states, or with age¹⁶⁻¹⁸.

PK dosing and sampling

In early drug discovery, a compound is typically screened in 2 - 4 animals (e.g. rats)². Common concentrations used in PK studies are around 10 mg/kg for oral and 1 mg/kg for i.v. administration². Administration of a single test compound is often called *discrete dosing*. An alternative approach (so-called *cassette dosing*) consists of the co-administration of several compounds (typically 4 - 10) as a one dose solution to animals¹⁹. The advantage of this strategy is that fewer animals are needed, and that PK parameters of several compounds can be assessed in parallel. However, the major drawback of this method is the risk of drug-drug interactions (e.g. competition for same transporter/enzymes, solubility issues) possibly resulting in misinterpretation of PK properties²⁰.

Ideally, drug concentrations in plasma samples are quantified by LC-MS/MS. Data analysis is performed using computational software programs (e.g. WinNonlin, PKsolver), which rapidly fit the data to mathematical PK models and calculate standard PK parameters².

2.3.3 The gastrointestinal tract (GIT) and intestinal epithelium

The main function of the gastrointestinal tract (GIT) is the digestion of food and the absorption of nutrients²¹. As most of the drugs are delivered via the oral route, the GIT also presents the major site of drug absorption²². The first obstacle for oral drugs is the acidic environment (pH 1.4 - 7)² of the stomach, which not only breaks down food but also drug molecules. The small intestine connects the stomach to the large intestine (colon). Absorption occurs mainly in the three sections of the small intestine (duodenum, jejunum, and ileum). The surface area of the intestinal lumen is greatly amplified (600-fold) by macroscopic valve-like folds (circular folds), the villi, and the microvilli²² (**Fig. 11**). The microvilli and the glycocalyx form the brush border, a highly active enzymatic barrier. Moreover, the epithelial surface is coated by mucus containing large glycoproteins (mucin), enzymes, bacteria (gut microbes) and electrolytes. The pH of the three intestinal sections varies from slightly acid (pH 4.4) in the duodenum in a fasting state to slightly basic (pH 8) at the end of the ileum²³.

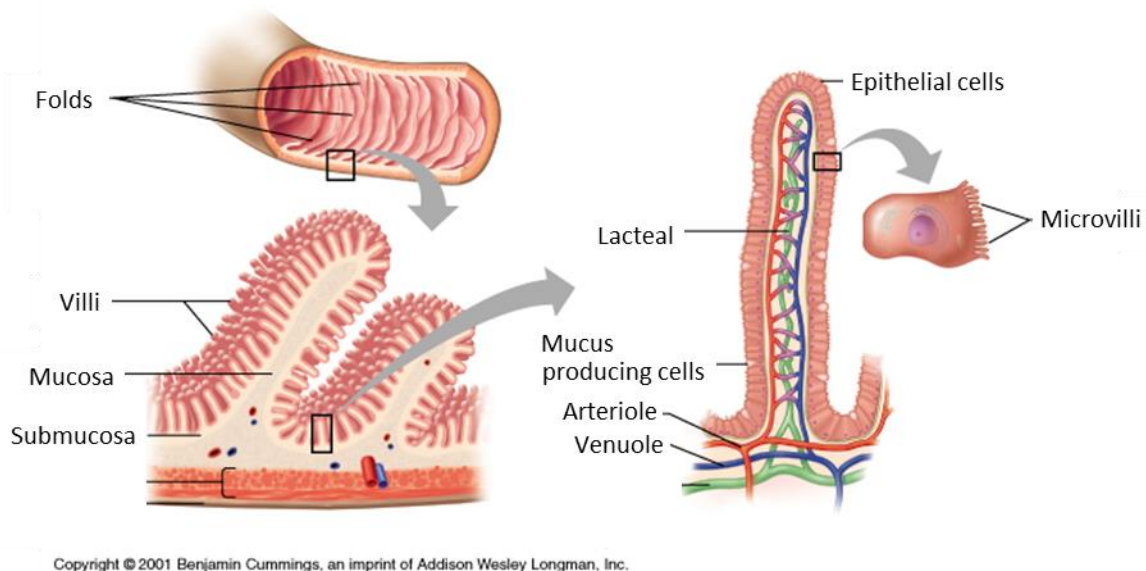


Figure 11: Schematic representation of the small intestine.

Permeation mechanisms

Approximately 96% of all commercial drugs penetrate through the GIT by passive diffusion². Passive diffusion is driven by the concentration gradient across the phospholipid bilayer membrane. Diffusion can occur either through the epithelial cells (transcellular) or between the cell junctions (paracellular)²⁴. Due to the lipophilic nature of the membrane, hydrophobic compounds (e.g. testosterone) can easily cross the cell membrane and are, therefore, primarily transported transcellularly²⁴. Hydrophilic molecules, such as mannitol, are almost impermeable across the cell membrane and cross, therefore, the membrane predominantly via cell junctions (paracellular transport)²⁴. These cell junction (pores/channels) in the epithelium are size-selective and usually exclude macromolecules with a molecular diameter of $> \sim 8 \text{ \AA}$ ^{25,26}. Compared to other barriers, such as the blood-brain barrier (BBB), the junctions of the GIT are rather loose and allow molecules to slip

between². Another major mechanism of permeability is the carrier-mediated influx. Carrier-mediated influx often occurs against a concentration gradient and requires energy. Examples for uptake transporters (solute carrier family [SLC]) involved in drug absorption include the human di/tri-peptide transporter (hPEPT1, at the apical side)²⁷, members of the human organic anion transporting polypeptide (OATP) family (at the apical side), and the organic cation transporter 1 (OCT1, SLC22A1, expressed at the basolateral side)²⁸. In carrier-mediated efflux, molecules are actively transported by efflux pumps from the inside of a cell back into the intestinal lumen. The body is thus protected from potentially harmful substances (drugs, toxins). The apically expressed efflux pumps (ABC transporter family), include the P-glycoprotein (P-gp, also known as multidrug resistance protein 1 [MDR1] or ATP-binding cassette sub-family B member 1 [ABCB1]), the breast cancer resistance protein (BCRP, ABCG2), and the multidrug resistance associated protein 2 (MRP2, ABCC2)^{29,30}. Among them, P-gp is the most prominent efflux transporter, as it can greatly impact the ADME process of a compound and consequently the success of a drug discovery project².

Intestinal metabolism

Besides the liver, drug molecules can also be metabolized in the intestine before they enter the systemic circulation. Metabolism is divided into phase I and phase II. Phase I reactions are modifications (e.g. oxidation, dealkylation) of the parent drug catalyzed by monooxygenases such as the cytochrome P450 (CYP) family². In the subsequent phase II metabolism, polar moieties such as glucuronic acid, sulfate, or glutathione are added to the molecule. Various cytochromes (e.g. CYP2D6, CYP3A4) are also present in the epithelial cells of the small intestine. The major metabolic enzyme in the small intestine is CYP3A4 present at approximately 50% of the hepatic level²². Besides phase I, also various phase II enzymes such as uridine 5'-diphospho-glucuronosyl transferases (UDP-UGTs), sulfotransferases (SULTs), and glutathione S-transferases (GSTs) are expressed in the small intestine^{31,32}.

2.3.3.1 Rule-based approaches and *in silico* models

The fastest method to predict oral absorption of a compound is to apply “rules”. Even though many scientists have evaluated structural properties of drug candidates for optimal oral absorption, the most prominent rule became the “rule of 5”³³. This set of rules was elaborated by the chemist Christopher A. Lipinski and predicts that oral absorption of a compound is more likely when 1) the number of H-bond donors is < 5 , 2) the number of H-bond acceptors < 10 , 3) the molecular weight (MW) < 500 , and 4) the LogP < 5 . The “rule of 5” can only be applied to compounds transported by passive diffusion; molecules that are involved in active transport are excluded from this rule³⁴. Subsequent studies by Veber et al.³⁵ suggested that oral absorption of a molecule is favored if the sum of rotatable bonds is ≤ 10 , and the polar surface area (PSA) $\leq 140 \text{ \AA}^2$ or the total H-bonds (acceptor plus donor) ≤ 12 .

In the past years, numerous computational models for the prediction of intestinal drug absorption have been developed (e.g. QikProp, Schrodinger or ACD/Labs Percepta Drug Profiler)³⁶. Compared to the labor-intensive *in vitro* and *in vivo* methods, *in silico* models offer a fast, high-throughput, and cost-efficient approach. However, *in silico* data should be considered with caution, as oral absorption is a complex and dynamic process which is affected by various factors (gastrointestinal physiology, formulation, food, etc.) that complicate the development of correct computational models³⁷.

2.3.3.2 *In vitro* permeability models

In vitro approaches can be divided into physicochemical and cell-based methods. While the physicochemical assays allow predictions about the passive diffusion of a compound, cell-based assays also allow estimations about transporter-mediated routes.

Physicochemical models

A well-known physicochemical assay is the parallel artificial membrane permeability assay (PAMPA). This model was first established in 1998 by Kansy et al.³⁸. Instead of a cell-based barrier, the model is made of phospholipids dissolved in long-chain hydrocarbons (e.g. dodecane)². The phospholipid compositions can be modified in order to mimic different biological barriers (e.g. GIT, BBB).

The immobilized artificial membrane high performance liquid chromatography (IAM-HPLC) represents an additional approach to evaluate passive diffusion². The IAM methodology consists of an IAM column (packed with a stationary phase consisting of phospholipids bonded to the solid support) and a HPLC. Retention time is measured for a test compound and a standard drug. By comparing retention times of the test compound with the standard, permeability of the test compound can be predicted³⁹. The IAM-HPLC methodology can also be used to investigate brain uptake or skin permeability²¹.

The advantages of such physicochemical methods are the high-throughput capability, the low costs, and the relatively high reproducibility. However, they only provide information on passive diffusion, and the absence of cells expressing relevant transporters limits their predictive capability⁴⁰.

Cell-based models

The most popular *in vitro* model to assess intestinal drug permeability is the Caco-2 (human colon adenocarcinoma cell line) assay^{41,42}. Caco-2 cells are grown over a period of 21 days on semipermeable filter inserts until they form a monolayer of entero-like cells (**Fig. 12**). Despite its colon origin, a number of transporters of enterocytes of the small intestine are expressed in this cell line (e.g. P-gp, MRP2, OCT1, BCRP, and PEPT1)². Similar to the small intestine, Caco-2 cells develop microvilli structures and a well-differentiated brush border on the apical side³¹ (**Fig. 12**).

The permeability assay is usually carried out in a bidirectional way (from apical to the basolateral compartment, and from the basolateral to the apical compartment, **Fig. 12**) to assess the permeability (expressed by the apparent permeability coefficient P_{app} , **Table 3**) and the contribution of active transporters in the permeability process (e.g. by calculation of the efflux ratio, **Table 3**)^{2,4}. A complementary approach to test whether a compound is a transporter substrate (e.g. P-gp) is the co-incubation with inhibitors (e.g. verapamil)². However, Caco-2 cells are not genetically identical and expression levels of transporters can vary among laboratories⁴³. Therefore, it is recommendable that each laboratory establishes its own Caco-2 model.

Table 3: Permeability ranges typically used in the Caco-2 assay as benchmarks².

Observed permeability	Explanation
$P_{app} < 2 \times 10^{-6}$ cm/s	Low permeability
$2 \times 10^{-6} < P_{app} < 20 \times 10^{-6}$ cm/s	Moderate permeability
$P_{app} > 20 \times 10^{-6}$ cm/s	High permeability
Uptake ratio: $P_{A \rightarrow B} / P_{B \rightarrow A} \geq 2$	The compound is most probably involved in active uptake
Efflux ratio: $P_{B \rightarrow A} / P_{A \rightarrow B} \geq 2$	The compound is most probably subjected to efflux
If $P_{A \rightarrow B} \approx P_{B \rightarrow A}$	The compound most probably permeates through the GIT by passive diffusion ²

In a typical Caco-2 assay, aliquots are taken from both compartments after different time points over a 1-2 hours incubation period⁴⁴. Test concentrations commonly range from 5 - 10 μ M. Some laboratories argue that the oral drug concentration is closer to 50 - 100 μ M, and thus recommend using higher concentrations in this assay². But it should be noted that at such high concentrations, most transporters are probably saturated². The Caco-2 assay is often performed at two pH conditions. In the apical compartment (representing the intestinal lumen), an acidic pH (e.g. pH 5 - 6.5) and in the basolateral compartment (blood) a neutral pH is used². However, one major drawback of using a pH gradient is that passive diffusion is enhanced, for acids in the direction of lower pH, and for bases in the direction of the higher pH. Therefore, it is also common to use a pH of 7.4 in both compartments².

Caco-2 cells express phase II enzymes such as UDP-glucuronosyltransferases, sulfotransferases, and glutathione-S-transferases³¹. Unfortunately, they express only insignificant levels of the drug metabolizing CYP P450 enzymes^{45,46}. An additional weakness of the Caco-2 model is the poor representation of the paracellular route, which might be explained by the tight junctions between the cells: compared to the human intestine, the Caco-2 assay has a significantly higher transepithelial resistance (TEER) (about 60 – 120 Ω cm² compared to 400 Ω cm²)^{47,48}. Moreover, Caco-2 cells are not able to produce mucus⁴⁹. Despite these apparent disadvantages, the Caco-2 assay shows a good correlation to human oral absorption and therefore, provides a valuable tool to assess both active and passive routes of an oral administered drug⁴.

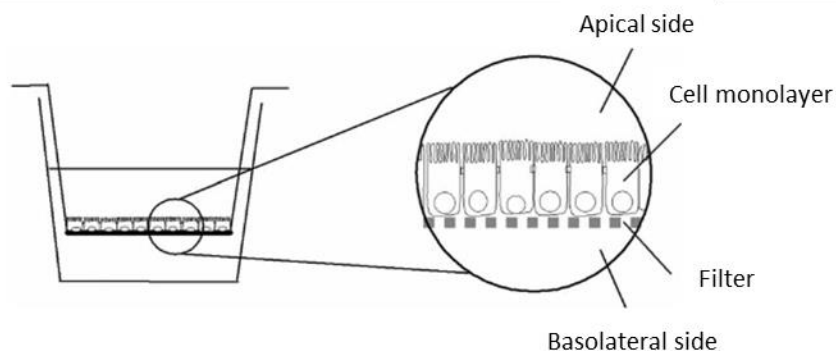


Figure 12: Caco-2 monolayer grown on a semipermeable filter insert³⁷

An alternative cell line for estimating oral absorption is the Madin-Darby canine kidney cell line (MDCK)²¹. An advantage of this assay is that this cell line only requires 3 days of cultivation to reach similar integrity as Caco-2 cell monolayers (21 days)²¹. However, MDCK cells originate from dog kidneys, and their expression pattern of transporters differs from that of the human intestine²¹. To circumvent this drawback, stable transfected MDCKs that express specific transporters have been implemented as a permeability screening tool⁴⁰.

2.3.3.3 *In situ* models

Permeability of drugs can also be studied by *in situ* perfusion of intestinal segments of rodents (e.g. rats, rabbits). An enormous advantage of *in situ* methods compared to *in vitro* assays is the presence of intact blood and nerve supply²¹. However, in order to obtain statistically significant data, a large number of animals are required. Moreover, the high costs and the relatively high amount of test compounds needed, render the model not feasible in early phases of drug discovery²¹.

2.3.4 The blood-brain barrier (BBB)

The blood-brain barrier (BBB) is a restrictive barrier that separates the brain from the systemic blood circulation⁵⁰. The main function of the BBB is the protection of the central nervous system (CNS) from potentially harmful substances such as xenobiotics, toxic metabolites, viruses, and bacteria⁴⁰. It has been estimated that more than 98% of small drug molecules are unable to cross the BBB⁵¹. BBB penetration is, however, a prerequisite for drugs acting on the CNS. On the other hand, BBB penetration might cause unwanted side effects for drugs not intended for the CNS. Therefore, regardless of the therapeutic area, it is important to assess BBB permeation of a drug candidate in early drug discovery³⁹.

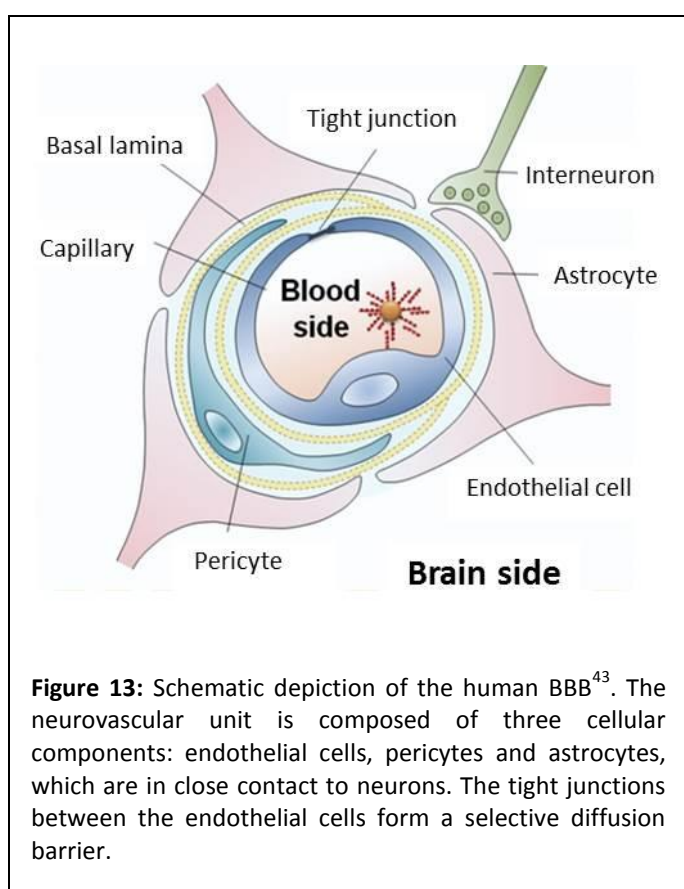


Figure 13: Schematic depiction of the human BBB⁴³. The neurovascular unit is composed of three cellular components: endothelial cells, pericytes and astrocytes, which are in close contact to neurons. The tight junctions between the endothelial cells form a selective diffusion barrier.

The BBB is composed of endothelial cells covering the inner surface of the brain capillaries⁵². The capillary network⁵³ in the human brain is more than 600 km long and has a surface area of 12 - 20 m². The capillary endothelial cells are connected through tight junctions and adherens junctions (**Fig. 13**)⁵⁴. Tight junctions (composed of the proteins occludin, claudins, and junctional adhesion molecules) seal the intercellular space resulting in extremely high TEER values⁵⁵. Pericytes surround the endothelial cells. Both pericytes and endothelial cells are embedded in the basal lamina⁵². Due to their close contact, it is believed that pericytes stabilize the integrity of endothelial cells and conserve the barrier function^{50,56}. The perivascular endfeet of astrocytes are attached to the basal lamina and cover a significant surface part of the endothelial cells⁵⁷ (**Fig. 13**). By releasing growth factors and signaling molecules, astrocytes mainly contribute to the development and maintenance of the BBB characteristics⁵⁰. Unlike the capillaries in the rest of the body, the BBB capillaries are characterized by high efflux activity, lack of fenestrations, limited pinocytosis, tight intracellular junctions, high metabolic activity (CYP P450 are expressed), and thus limited BBB penetration⁵⁸.

Passive diffusion is the dominant permeability mechanism across the BBB. Factors that favor this mechanism are low MW and high lipophilicity of a molecule⁵⁹. Most of the compounds are transported out of the brain back into the blood via efflux pumps. Besides the efflux transporters BCRP and MRP1, MDR1 (P-gp) is highly expressed in the BBB⁶⁰. Compared to other (cellular)

tissues, the paracellular permeation is drastically reduced in the BBB due to the presence of the tight junctions. Only a few transporter substrates such as nutrients (e.g. amino acids, peptides, glucose) and other endogenous molecules are actively taken up^{2,60}. Importantly, it should be noted that BBB permeability can be altered in CNS pathologies (e.g. epilepsy, stroke, infectious processes, Alzheimer's disease)⁵⁹.

2.3.4.1 Structure BBB permeation relationships and *in silico* models

BBB-permeation of a compound depends on various physicochemical properties such as lipophilicity, PSA, MW, H-bonding, and ionization state. In 1995, Pardridge⁶¹ first introduced a set of rules. He suggested that compounds more likely pass the BBB, if the total sum of H-bonds is $< 8-10$, $MW < 400-500$, and if the compound is not acidic. Other researchers proposed that BBB penetration is favored if the sum of nitrogen and oxygen is < 6 , $PSA < 60-70 \text{ \AA}$, $MW < 450$, and the LogD (at pH 7.4) is between 1 and 3^{62,63}. Moreover, various *in silico* tools have been established as pre-screening tools to test large chemical datasets (e.g. B₃PP by Martins et al. 2012)⁶⁴. But again, the absence of physiological conditions renders *in silico* tools vulnerable to false positive/negative results.

2.3.4.2 *In vitro* BBB models

The first potentially useful *in vitro* BBB model was introduced in the early 1980s by using freshly isolated primary bovine brain capillary endothelial cells⁶⁵. Shortly thereafter, various mono-cultures BBB models using primary endothelial cells from rat, murine, porcine, and bovine origin were established³⁹ (**Fig. 14**). It soon turned out that endothelial cells cultured alone rapidly de-differentiate and lose their phenotype⁶⁶. Numerous studies have shown that brain-derived cellular components (particularly astrocytes) are able to induce BBB properties⁶⁷. Therefore, various co-culture or triple co-cultures *in vitro* BBB models using astrocytes, pericytes and/or neurons have been implemented to mimic the *in vivo* anatomy of the neurovascular unit⁶⁸ (**Fig. 14**).

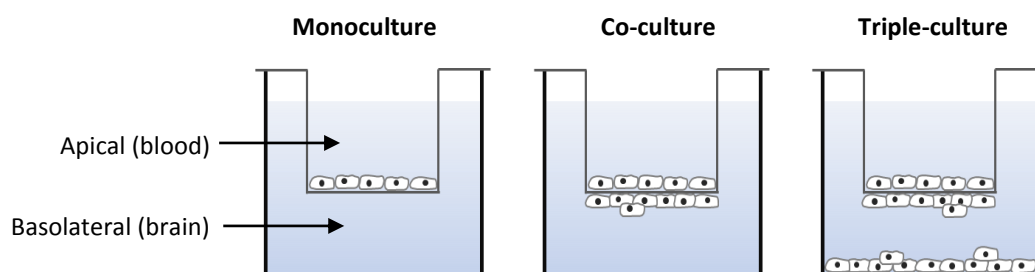


Figure 14: *In vitro* BBB models cultured as monoculture, or in co- and triple-culture⁶⁸.

However, using primary cells faces numerous challenges. The cell isolation and purification is time-consuming, expensive, and needs experience⁶⁸. Besides this, the yield of cells is relatively low, the

lifespan is limited, and the expression pattern of uptake proteins and efflux pumps from animals differs from endothelial cells of human origin^{69,70}. To avoid species differences, the use of human-derived primary cells would be ideal³⁹. However, brain tissue derived from surgical material often cannot be considered as “healthy”⁶⁸. Additionally, difficulties in access, ethical reasons, patient-related heterogeneity, and poor TEER values restrict the use of human primary endothelial cells⁶⁶.

To circumvent these shortcomings, a number of immortalized brain endothelial cell lines of human (e.g. hCMEC/ D3) and animal (e.g. RBE4 from rats) origin have been generated in the last years⁶⁷. Immortalized cell lines are easy to culture and maintain their differentiated properties even after extensive passaging³⁹. However, compared to the *in vivo* situation, immortalized cell lines show various deficits, such as poor barrier properties including relatively low TEER values, insufficient tight junctions, and reduced expression of key transporters^{53,71}. In the last decades, also cells lines of non-cerebral origin (e.g. Caco-2 or MDCK, stably transfected with specific transporters) have been widely established in the pharmaceutical industry as screening tools in early drug discovery⁵³. These cell lines are easy to culture and show tight and reproducible barrier properties. However, epithelial cells differ in their morphology and transporter expression from BBB endothelial cells⁵³. Recently, BBB models using endothelial cells derived from human pluripotent and hematopoietic stem cells have been implemented^{55,72}. Unlike primary cell cultures, stem cells exhibit (unlimited) self-renewal while maintaining their homogenous gene expression profile⁶⁶. Even though further benchmarking studies against established BBB models are required, the self-renewing potency and the fully human origin render such *in vitro* BBB models highly promising^{39,66}.

2.3.4.3 *In vivo* BBB models

In vivo BBB permeability studies provide the most reliable data regarding BBB permeation⁴⁰. A number of invasive techniques in animals, including *in situ* brain perfusion with radiolabeled compounds, HPLC analysis of brain homogenates, and intracerebral microdialysis have been implemented to assess BBB permeability and brain distribution⁵⁸. One of the few techniques applicable to humans is the cerebrospinal fluid (CSF) sampling⁵⁸. In this method, the drug concentration in the CSF is used to predict the unbound drug concentration in the brain⁷³. More recent approaches to monitor the brain-uptake of compounds include various non-invasive imaging techniques, such as magnetic resonance imaging (MRI) and positron emission tomography (PET). However, these methods are not able to distinguish between parent compound and metabolites (for labeled compounds)⁵⁸. Several reviews and books have discussed further *in vivo* methods in more detail^{40,74,75}. But as *in vivo* approaches are low-throughput, costly and labor-intensive, they are mainly applied at later stages of the drug development process³⁹.

2.3.5 The hERG channel

In the late 1990s a number of non-cardiovascular drugs had to be withdrawn from the market due to unexpected post-marketing reports of sudden cardiac death⁷⁶. Later it was found that this fatal side-effect was associated with hERG channel inhibition in the heart. Since then, regulatory agencies carefully review new drug applications for potential hERG liabilities. Cardiac arrest due to hERG channel inhibition is a rare event, and in clinical trials a large number of patients are required to prove cardiac safety for a drug candidate. Hence, costs are tremendously increased if a compound shows hERG liability at an advanced stage of drug development. Therefore, it has become routine in practice to screen for hERG channel activity in an early lead optimization stage².

The *hERG* gene (KCNH2, K_v11.1) is fully named *human ether-a-go-go related gene* and encodes the pore-forming subunit of a potassium ion channel that is primarily expressed in the heart⁷⁷. The hERG channel consists of a tetramer of four identical subunits. Each subunit has six transmembrane regions. Being a typical voltage-gated ion channel, the membrane potential controls the opening and closing transition of the ion pore. The flow of K⁺ ions out of the cells generates the rapidly activating delayed rectifier K⁺ current called I_{Kr}^{2,78}.

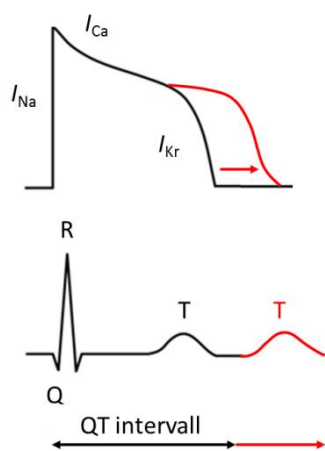


Figure 15: Correlation between ventricular action potential duration and QT interval^{79,80}.

I_{Kr} plays a pivotal role in the ensemble of ion channels that generates the cardiac action potential. The cardiac action potential is initiated with the opening of sodium channels² (**Fig. 15**). The rapid influx of Na⁺ ions into the cell causes a depolarization from about -90mV (resting state) to about +20mV. The subsequent opening of calcium ion channels maintains the depolarization and allows Ca²⁺ to move into the cells. By opening of the potassium channels, K⁺ flows out of the cells leading to a repolarization of -90mV. The hERG ion channel is thus mainly involved in the repolarization of the cardiac action potential^{2,78}.

If a compound binds within the inner cavity of hERG, it can prevent K⁺ ions from moving out of the cell, leading to a longer repolarization time (**Fig. 15**). On the electrocardiogram (ECG), this event can be monitored as a delay of the T wave (QT prolongation, also called long QT syndrome [LQTS], **Fig. 15**)². Excessive LQT can induce the potentially life-threatening arrhythmia called torsades de pointes (TdP)⁸¹. But hERG blocking alone is often not the only trigger that causes TdP. Additional risk factors include genetic factors, electrolyte disorders (e.g. hypokalemia, hypomagnesemia), female gender, impaired hepatic/renal function, pre-existing cardiac diseases (e.g. bradycardia), and co-administration of a drug that either also blocks the hERG channel or inhibits the metabolism of a potential hERG inhibitor⁸².

Many class III antiarrhythmic drugs induce QT prolongation based on their pharmacological action. Ironically, antiarrhythmic agents also have a proarrhythmic potential, and the induction of TdP is a frequent side effect (e.g. 1–5% of patients treated with sotalol are affected)^{83,84}.

Not all antiarrhythmic drugs bear the same risk for generating arrhythmia. As many overlapping ion currents contribute to the cardiac action potential, other ion channels may also counteract the reduced potassium current. The most prominent example for this observation is verapamil. Although verapamil shows high hERG channel affinity, it also acts as a calcium channel antagonist⁸².

Unlike class III antiarrhythmic agents, the incidence of drug-induced LQTS by non-cardiac drugs (such as antihistamines, antibiotics, or prokinetics, **Fig. 16**) is relatively low (less than one in 100'000)^{82,85}. Nevertheless, even a low level of risk is unacceptable for drugs used for the treatment of non-life threatening diseases, particularly if the risk outweighs the benefits and safer alternatives are available. For this reason, several non-cardiac drugs (e.g. terfenadine⁸⁶, cisapride⁸⁷, **Fig. 16**) have been withdrawn from the market or their use has been restricted (e.g. chloroquine⁸⁸, moxifloxacin⁸⁹, **Fig. 16**).

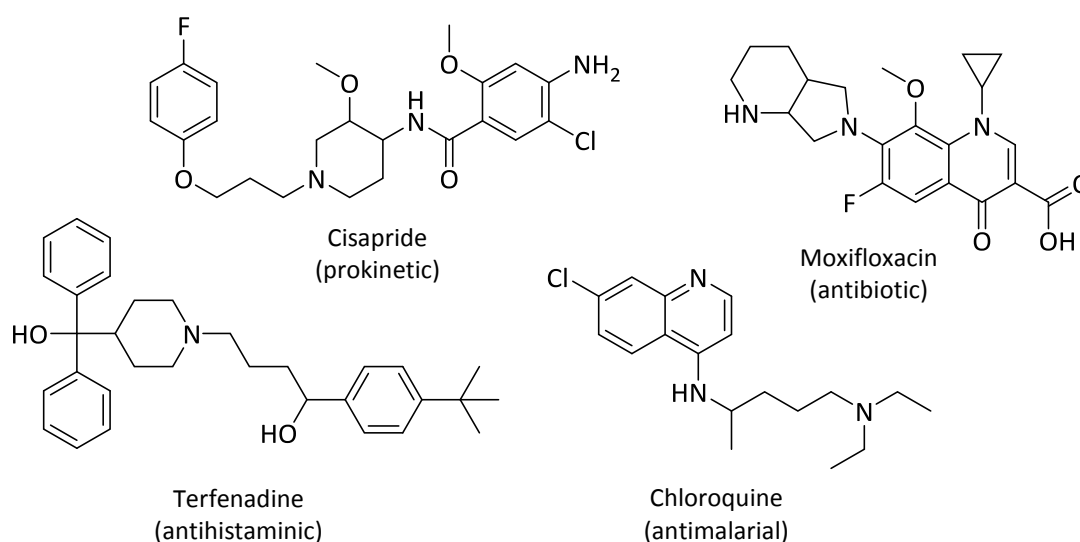


Figure 16: Commercial drugs that were withdrawn or carry warning labels due to hERG channel inhibition⁸².

Most of the drugs that cause TdP or LQTS are hERG inhibitors. But not all hERG inhibitors induce arrhythmia, which makes cardiac safety assessment a challenging task. Therefore, a three-step approach (including *in silico* assessments, *in vitro* screenings by electrophysiological tools, and *in vivo* electrocardiograms) is often used to facilitate decision-making².

2.3.5.1 Structure-activity relationships and *in silico* approaches

Site-specific mutation studies have identified the amino acids Try652 and Phe656 of the hERG channel protein as the most important residues for drug binding⁹⁰. Aromatic compounds seem to interfere with Try652 via either π -stacking or cation- π interactions⁹¹. Phe656 appears to interact with

the non-aromatic hydrophobic substructures of a compound⁸⁰. The main binding site lies within the inner cavity of hERG and can only be reached in the opened state. Compared to other ion channels, hERG can trap a compound within its central cavity. This observation might be explained by certain amino acid sequences⁹² (Pro-X-Pro) that enlarge the inner volume of the hERG channel, even in a closed state⁹³.

Although structurally diverse compounds block the hERG channel, several studies have repetitively shown common structural features that are associated with hERG inhibition. Most of the compounds that favor hERG blocking (1) are basic amines ($pK_a > 7.3$), (2) have hydrophobic/lipophilic substructures (calculated $\log P \geq 3.7$), (3) lack negatively ionizable groups, and (4) are absent of oxygen H-bond acceptors⁹⁴. Even though hERG structure-activity relationship is a highly active research field in academia/industry, the large chemical diversity of hERG blockers makes accurate *in silico* predictions difficult. Yet, due to the growing availability of databases, *in silico* models for hERG blocking predictions became commercially available in the last years (e.g. ACD/Labs Percepta Drug Profiler)².

2.3.5.2 *In vitro* hERG methods

Various *in vitro* hERG assays have been implemented to assess cardiac safety of a drug candidate. *In vitro* hERG methods are typically cell-based assays and use stable (*hERG*) transfected cells lines such as human embryonic kidney cells (HEK293) or Chinese hamster ovary cells (CHO). In general, two types of *in vitro* assays can be distinguished².

(I) Indirect methods usually monitor effects that are linked to the K^+ flux across the hERG channel and include fluorescence-based assays⁹⁵ (measure the intracellular amount of a voltage dependent dye), binding competition assays⁹⁶ (which detect the displacement of a radiolabeled ligand by the test compound) and rubidium efflux methods⁷⁸ (where the intracellular amount of Rb^+ is determined, based on the ability of Rb^+ to cross potassium channels). Although these assays are all favorable for high-throughput screenings, they often show low correlation to *in vivo* electrophysiology².

(II) In contrast to these “indirect methods”, electrophysiological techniques measure the potassium current directly and are thus often considered as “gold standard” (e.g. patch-clamp, two electrode voltage-clamp)⁹⁷. The most widely used electrophysiological tool in ion channel research is the “patch-clamp” method. In this technique, a glass pipette with an open diameter of about 1 μm is filled with a cytoplasm-compatible buffer and an electrode is inserted. This pipette is attached to a micromanipulator, which facilitates under the microscope placing of the tip in close contact to a hERG expressing cell (e.g. genetically modified HEK 293, CHO cells). In this position a negative pressure is applied and a piece of the membrane is “patched” on the tip of the patch-pipette. The electrode is used to “clamp” the membrane potential at a certain voltage, while the current needed to maintain this

voltage is recorded (**Fig. 17**). The K^+ ion efflux across the cell membrane can thus be measured directly. By changing the membrane potential from -80mV to +20mV, the hERG channel opens and an outward current can be observed (positive current amplitude). A decrease of the membrane potential to -40mV leads to a transient peak of the ion current (based on a fast transition of inactivated hERG channels to the open state) before the channel goes back to its closed state. If a test compound is a hERG inhibitor (e.g. E-4031) the channel gets blocked and the potassium outward current is reduced (**Fig. 17**)².

Although electrophysiological measurements provide valuable information regarding the hERG activity of a compound, *in vitro* hERG data are not sufficient for a full assessment of cardiac risk in humans. According to the ICH (International Conference on Harmonization) safety guideline S7B, the following nonclinical data are required^{79,98}: (1) effects mediated through other ion channels (e.g. sodium channel), (2) action potential parameters in isolated cardiac preparations (e.g. Purkinje fibers, papillary muscles, or intact hearts from dogs, guinea pigs, rabbits or sheeps), (3) ECG parameters measured in animals (e.g. dog), and (4) data evaluating the proarrhythmic effect in isolated cardiac preparations or animals.

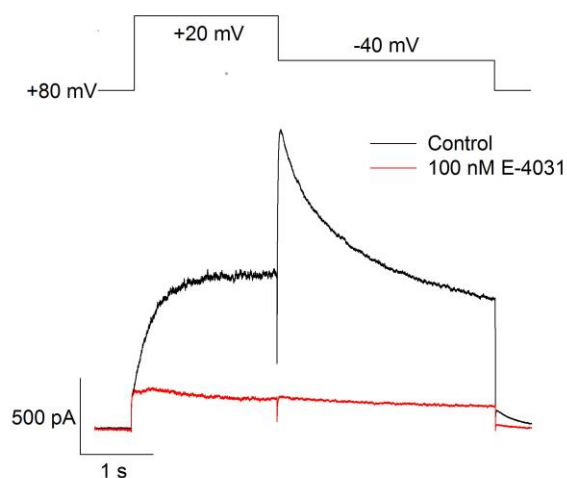


Figure 17: Typical ion current profile from patch-clamp for hERG blockers. Source: B'SYS GmbH

2.3.5.3 *In vivo* hERG methods

The most conclusive data regarding hERG inhibition are provided by *in vivo* studies. In this technique, electrodes are attached to the surface of the heart. If a compound is a hERG blocker, the QT prolongation can be directly seen on the ECG^{2,99}. The major advantage of this method is that additional safety parameters (e.g. heart rate, blood pressure) can be assessed in parallel⁹⁹.

A safety margin that is frequently used is the ratio between the hERG IC_{50} and the $C_{max, unbound}$ ¹⁰⁰. To reach an acceptable degree of safety, a value >30 is aimed for. This value has been set based on experimental observations: a ratio >30, showed in 15% generation of TdP, while 85% remained unaffected. For values <30, 95% developed TdP and only 5% were not affected¹⁰⁰. Besides C_{max} , also other PK parameters (e.g. metabolism) and plasma protein binding have to be considered as they can greatly impact the amount of compound reaching the heart tissue. An additional safety margin refers to the QT prolongation. According to ICH-E14 guideline for clinical studies major concerns are expressed about a drug candidate when the LQT exceeds 5 ms compared to normal^{2,101}.

References

1. Prentis, R. A., Lis, Y. & Walker, S. R. Pharmaceutical innovation by the seven UK-owned pharmaceutical companies (1964–1985). *Br. J. Clin. Pharmacol.* **25**, 387–396 (1988).
2. Kerns, E. & Di, L. *Drug-like properties: concepts, structure design and methods: from ADME to toxicity optimization*. 6-414 (Academic Press, 2008).
3. Di, L. & Kerns, E. H. Profiling drug-like properties in discovery research. *Curr. Opin. Chem. Biol.* **7**, 402–408 (2003).
4. Wang, J. & Urban, L. The impact of early ADME profiling on drug discovery and development strategy. *Drug Discov. World* **5**, 73–86 (2004).
5. Mullard, A. New drugs cost US[dollar]2.6 billion to develop. *Nat. Rev. Drug Discov.* **13**, 877–877 (2014).
6. Balunas, M. J. & Kinghorn, A. D. Drug discovery from medicinal plants. *Life Sci.* **78**, 431–441 (2005).
7. Kramer, J. A., Sagartz, J. E. & Morris, D. L. The application of discovery toxicology and pathology towards the design of safer pharmaceutical lead candidates. *Nat. Rev. Drug Discov.* **6**, 636–649 (2007).
8. Caskey, C. T. The drug development crisis: efficiency and safety. *Annu. Rev. Med.* **58**, 1–16 (2007).
9. Nwaka, S. & Ridley, R. G. Virtual drug discovery and development for neglected diseases through public–private partnerships. *Nat. Rev. Drug Discov.* **2**, 919–928 (2003).
10. Ashburn, T. T. & Thor, K. B. Drug repositioning: identifying and developing new uses for existing drugs. *Nat. Rev. Drug Discov.* **3**, 673–683 (2004).
11. Royle, K. E., del Val, I. J. & Kontoravdi, C. Integration of models and experimentation to optimise the production of potential biotherapeutics. *Drug Discov. Today* **18**, 1250–1255 (2013).
12. Hata-Uribe Y.A. Dissertation: Discovery of antiprotozoal compounds. Available at: <http://edoc.unibas.ch/33421/1/PhD%20Final%20Document%20Yoshie%20Hata-Uribe.pdf> (Accessed: 15th April 2016)
13. Ratain, M. J. & William K. Plunkett, J. Principles of Pharmacokinetics. In: Kufe D.W., Pollock R.E., Weichselbaum R.R., Bast R.C., Gansler T.S., Holland J.F., Frei E. (eds). *Holland- Frei Cancer Medicine*, 6th ed. Hamilton (ON) (BC Decker, 2003).
14. Mei, H., Korfmacher, W. & Morrison, R. Rapid *in vivo* oral screening in rats: reliability, acceptance criteria, and filtering efficiency. *AAPS J.* **8**, E493–E500 (2006).
15. Kratochwil, N. A., Huber, W., Müller, F., Kansy, M. & Gerber, P. R. Predicting plasma protein binding of drugs: a new approach. *Biochem. Pharmacol.* **64**, 1355–1374 (2002).
16. Grandison, M. K. & Boudinot, F. D. Age-related changes in protein binding of drugs. *Clin. Pharmacokinet.* **38**, 271–290 (2000).
17. Kosa, T., Maruyama, T. & Otagiri, M. Species differences of serum albumins: I. Drug binding sites. *Pharm. Res.* **14**, 1607–1612 (1997).
18. Kosa, T., Maruyama, T. & Otagiri, M. Species differences of serum albumins: II. Chemical and thermal stability. *Pharm. Res.* **15**, 449–454 (1998).
19. Bayliss, M. K. & Frick, L. W. High-throughput pharmacokinetics: cassette dosing. *Curr. Opin. Drug Discov. Devel.* **2**, 20–25 (1999).
20. White, R. E. & Manitpisitkul, P. Pharmacokinetic theory of cassette dosing in drug discovery screening. *Drug Metab. Dispos.* **29**, 957–966 (2001).
21. Balimane, P. V., Chong, S. & Morrison, R. A. Current methodologies used for evaluation of intestinal permeability and absorption. *J. Pharmacol. Toxicol. Methods* **44**, 301–312 (2000).
22. Van De Waterbeemd, H., Smith, D. A., Beaumont, K. & Walker, D. K. Property-based design: optimization of drug absorption and pharmacokinetics. *J. Med. Chem.* **44**, 1313–1333 (2001).
23. Daugherty, A. L. & Mersny, R. J. Transcellular uptake mechanisms of the intestinal epithelial barrier Part one. *Pharm. Sci. Technol. Today* **2**, 144–151 (1999).
24. Li, A. P. Screening for human ADME/Tox drug properties in drug discovery. *Drug Discov. Today* **6**, 357–366 (2001).
25. Menard, S., Cerf-Bensussan, N. & Heyman, M. Multiple facets of intestinal permeability and epithelial handling of dietary antigens. *Mucosal Immunol.* **3**, 247–259 (2010).
26. Chediack, J. G., Caviedes-Vidal, E., Fasulo, V., Yamin, L. J. & Karasov, W. H. Intestinal passive absorption of water-soluble compounds by sparrows: effect of molecular size and luminal nutrients. *J. Comp. Physiol. B* **173**, 187–197 (2003).
27. Daniel, H. Molecular and integrative physiology of intestinal peptide transport. *Annu. Rev. Physiol.* **66**, 361–384 (2004).

28. Sai, Y. & Tsuji, A. Transporter-mediated drug delivery: recent progress and experimental approaches. *Drug Discov. Today* **9**, 712–720 (2004).
29. Chan, L. M., Lowes, S. & Hirst, B. H. The ABCs of drug transport in intestine and liver: efflux proteins limiting drug absorption and bioavailability. *Eur. J. Pharm. Sci.* **21**, 25–51 (2004).
30. Takano, M., Yumoto, R. & Murakami, T. Expression and function of efflux drug transporters in the intestine. *Pharmacol. Ther.* **109**, 137–161 (2006).
31. Meunier, V., Bourrie, M., Berger, Y. & Fabre, G. The human intestinal epithelial cell line Caco-2; pharmacological and pharmacokinetic applications. *Cell Biol. Toxicol.* **11**, 187–194 (1995).
32. Lin, J. H., Chiba, M. & Baillie, T. A. Is the role of the small intestine in first-pass metabolism overemphasized? *Pharmacol. Rev.* **51**, 135–158 (1999).
33. Lipinski, C. A., Lombardo, F., Dominy, B. W. & Feeney, P. J. Experimental and computational approaches to estimate solubility and permeability in drug discovery and development settings. *Adv. Drug Deliv. Rev.* **64**, 4–17 (2012).
34. Leeson, P. Drug discovery: Chemical beauty contest. *Nature* **481**, 455–456 (2012).
35. Veber, D. F. *et al.* Molecular properties that influence the oral bioavailability of drug candidates. *J. Med. Chem.* **45**, 2615–2623 (2002).
36. Ioakimidis, L., Thoukydidis, L., Mirza, A., Naeem, S. & Reynisson, J. Benchmarking the reliability of QikProp. Correlation between experimental and predicted values. *QSAR Comb. Sci.* **27**, 445–456 (2008).
37. Dokoumetzidis, A., Kalantzi, L. & Fotaki, N. Predictive models for oral drug absorption: from *in silico* methods to integrated dynamical models. *Expert Opin. Drug Metab. Toxicol.* **3**, 491–505 (2007).
38. Kansy, M., Senner, F. & Gubernator, K. Physicochemical high throughput screening: parallel artificial membrane permeation assay in the description of passive absorption processes. *J. Med. Chem.* **41**, 1007–1010 (1998).
39. Eigenmann D.E. Dissertation: Establishment and validation of an immortalized *in vitro* human blood-brain barrier (BBB) model for drug permeability studies, and application to natural product derived leads. Available at: https://forschdb2.unibas.ch/inf2/rm_projects/object_view.php?r=3343775. (Accessed: 12th April 2016)
40. Mensch, J., Oyarzabal, J., Mackie, C. & Augustijns, P. *In vivo*, *in vitro* and *in silico* methods for small molecule transfer across the BBB. *J. Pharm. Sci.* **98**, 4429–4468 (2009).
41. Yee, S. *In vitro* permeability across Caco-2 cells (colonic) can predict *in vivo* (small intestinal) absorption in man—fact or myth. *Pharm. Res.* **14**, 763–766 (1997).
42. Artursson, P. & Karlsson, J. Correlation between oral drug absorption in humans and apparent drug permeability coefficients in human intestinal epithelial (Caco-2) cells. *Biochem. Biophys. Res. Commun.* **175**, 880–885 (1991).
43. Hayashi, R. *et al.* Comparison of drug transporter gene expression and functionality in Caco-2 cells from 10 different laboratories. *Eur. J. Pharm. Sci.* **35**, 383–396 (2008).
44. Hubatsch, I., Ragnarsson, E. G. & Artursson, P. Determination of drug permeability and prediction of drug absorption in Caco-2 monolayers. *Nat. Protoc.* **2**, 2111–2119 (2007).
45. Thummel, K. E., Kunze, K. L. & Shen, D. D. Enzyme-catalyzed processes of first-pass hepatic and intestinal drug extraction. *Adv. Drug Deliv. Rev.* **27**, 99–127 (1997).
46. Crespi, C. L., Penman, B. W. & Hu, M. Development of Caco-2 cells expressing high levels of cDNA-derived cytochrome P4503A4. *Pharm. Res.* **13**, 1635–1641 (1996).
47. Grasset, E., Pinto, M., Dussaulx, E., Zweibaum, A. & Desjeux, J.-F. Epithelial properties of human colonic carcinoma cell line Caco-2: electrical parameters. *Am. J. Physiol.-Cell Physiol.* **247**, C260–C267 (1984).
48. Artursson, P., Ungell, A.-L. & Löfroth, J.-E. Selective paracellular permeability in two models of intestinal absorption: cultured monolayers of human intestinal epithelial cells and rat intestinal segments. *Pharm. Res.* **10**, 1123–1129 (1993).
49. Karlsson, J., Wikman, A. & Artursson, P. The mucus layer as a barrier to drug absorption in monolayers of human intestinal epithelial HT29-H goblet cells. *Int. J. Pharm.* **99**, 209–218 (1993).
50. Vries, H. E. de, Kuiper, J., Boer, A. G. de, Berkel, T. J. C. V. & Breimer, D. D. The blood-brain barrier in neuroinflammatory diseases. *Pharmacol. Rev.* **49**, 143–156 (1997).
51. Pardridge, W. M. The blood-brain barrier and neurotherapeutics. *Neurotherapeutics* **2**, 1–2 (2005).
52. Abbott, N. J., Patabendige, A. A., Dolman, D. E., Yusof, S. R. & Begley, D. J. Structure and function of the blood–brain barrier. *Neurobiol. Dis.* **37**, 13–25 (2010).
53. Cecchelli, R. *et al.* Modelling of the blood–brain barrier in drug discovery and development. *Nat. Rev. Drug Discov.* **6**, 650–661 (2007).
54. Ballabh, P., Braun, A. & Nedergaard, M. The blood–brain barrier: an overview: structure, regulation, and clinical implications. *Neurobiol. Dis.* **16**, 1–13 (2004).

55. Lippmann, E. S. *et al.* Derivation of blood-brain barrier endothelial cells from human pluripotent stem cells. *Nat. Biotechnol.* **30**, 783–791 (2012).
56. Tajés, M. *et al.* The blood-brain barrier: structure, function and therapeutic approaches to cross it. *Mol. Membr. Biol.* **31**, 152–167 (2014).
57. Wilhelm, I., Fazakas, C. & Krizbai, I. A. *In vitro* models of the blood-brain barrier. *Acta Neurobiol. Exp. Wars* **71**, 113–28 (2011).
58. Nicolazzo, J. A., Charman, S. A. & Charman, W. N. Methods to assess drug permeability across the blood-brain barrier. *J. Pharm. Pharmacol.* **58**, 281–293 (2006).
59. Banks, W. A. Characteristics of compounds that cross the blood-brain barrier. *BMC Neurol.* **9**, S3 (2009).
60. Giacomini, K. M. *et al.* Membrane transporters in drug development. *Nat. Rev. Drug Discov.* **9**, 215–236 (2010).
61. Pardridge, W. M. Transport of small molecules through the blood-brain barrier: biology and methodology. *Adv. Drug Deliv. Rev.* **15**, 5–36 (1995).
62. Clark, D. E. *In silico* prediction of blood–brain barrier permeation. *Drug Discov. Today* **8**, 927–933 (2003).
63. Krämer, S. D. Absorption prediction from physicochemical parameters. *Pharm. Sci. Technol. Today* **2**, 373–380 (1999).
64. Martins, I. F., Teixeira, A. L., Pinheiro, L. & Falcao, A. O. A Bayesian approach to *in silico* blood-brain barrier penetration modeling. *J. Chem. Inf. Model.* **52**, 1686–1697 (2012).
65. Bowman, P. D., Ennis, S. R., Rarey, K. E., Lorrin Betz, A. & Goldstein, G. W. Brain microvessel endothelial cells in tissue culture: a model for study of blood-brain barrier permeability. (1983).
66. Stanimirovic, D. B., Bani-Yaghoub, M., Perkins, M. & Haqqani, A. S. Blood-brain barrier models: *in vitro* to *in vivo* translation in preclinical development of CNS-targeting biotherapeutics. *Expert Opin. Drug Discov.* **10**, 141–155 (2015).
67. Fabulas-Da Costa, A. *et al.* in *In Vitro Toxicology Systems* 147–166 (Springer, 2014).
68. Deli, M. A., Ábrahám, C. S., Kataoka, Y. & Niwa, M. Permeability studies on *in vitro* blood–brain barrier models: physiology, pathology, and pharmacology. *Cell. Mol. Neurobiol.* **25**, 59–127 (2005).
69. Syvänen, S. *et al.* Species differences in blood-brain barrier transport of three positron emission tomography radioligands with emphasis on P-glycoprotein transport. *Drug Metab. Dispos.* **37**, 635–643 (2009).
70. Warren, M. S. *et al.* Comparative gene expression profiles of ABC transporters in brain microvessel endothelial cells and brain in five species including human. *Pharmacol. Res.* **59**, 404–413 (2009).
71. Jonathan C.H. Choi Research Group. Available at: http://www.bme.cuhk.edu.hk/jchchoi/r_SHIAE14-16.php. (Accessed: 18th January 2016)
72. Cecchelli, R. *et al.* A stable and reproducible human blood-brain barrier model derived from hematopoietic stem cells. *PLoS ONE* **6**, e99733 (2014).
73. Redzic, Z. Molecular biology of the blood-brain and the blood-cerebrospinal fluid barriers: similarities and differences. *Fluids Barriers CNS* **8**, 3 (2011).
74. Shityakov, S., Salvador, E. & Förster, C. *In silico*, *in vitro*, and *in vivo* methods to analyse drug permeation across the blood–brain barrier: a critical review. *OA Anaesth.* **1**, 13 (2013).
75. Hammarlund-Udenaes, M. in *The Blood Brain Barrier (BBB)* 21–48 (Springer, 2014).
76. Sanguinetti, M. C. & Tristani-Firouzi, M. hERG potassium channels and cardiac arrhythmia. *Nature* **440**, 463–469 (2006).
77. Warmke, J. W. & Ganetzky, B. A family of potassium channel genes related to eag in *Drosophila* and mammals. *Proc. Natl. Acad. Sci.* **91**, 3438–3442 (1994).
78. Priest, B., Bell, I. M. & Garcia, M. Role of hERG potassium channel assays in drug development. *Channels* **2**, 87–93 (2008).
79. Schramm, A. Dissertation: Modulation of ion channels by natural products-identification of hERG channel inhibitors and GABA_A receptor ligands from plant extracts. (University of Basel, 2014).
80. Stansfeld, P. J., Sutcliffe, M. J. & Mitcheson, J. S. Molecular mechanisms for drug interactions with hERG that cause long QT syndrome. *Exp. Opin. Drug Metab. Toxicol.* **2**, 81-94 (2006)
81. Sanguinetti, M. C. & Mitcheson, J. S. Predicting drug–hERG channel interactions that cause acquired long QT syndrome. *Trends Pharmacol. Sci.* **26**, 119–124 (2005).
82. De Ponti, F., Poluzzi, E., Cavalli, A., Recanatini, M. & Montanaro, N. Safety of non-antiarrhythmic drugs that prolong the QT interval or induce torsade de pointes. *Drug Saf.* **25**, 263–286 (2002).
83. Vandenberg, J. I., Walker, B. D. & Campbell, T. J. hERG K⁺ channels: friend and foe. *Trends Pharmacol. Sci.* **22**, 240–246 (2001).
84. Hohnloser, S. H. & Woosley, R. L. Sotalol. *N. Engl. J. Med.* **331**, 31–38 (1994).

85. Haverkamp, W. *et al.* The potential for QT prolongation and pro-arrhythmia by non-anti-arrhythmic drugs: clinical and regulatory implications. *Cardiovasc. Res.* **47**, 219–233 (2000).
86. Woosley, R. L., Chen, Y., Freiman, J. P. & Gillis, R. A. Mechanism of the Cardiotoxic Actions of Terfenadine. *JAMA J. Am. Med. Assoc.* **269**, 1532–1536 (1993).
87. Bran S, Murray WA, Hirsch IB & Palmer JP. Long QT syndrome during high-dose cisapride. *Arch. Intern. Med.* **155**, 765–768 (1995).
88. Traebert, M. *et al.* Inhibition of hERG K⁺ currents by antimalarial drugs in stably transfected HEK293 cells. *Eur. J. Pharmacol.* **484**, 41–48 (2004).
89. Alexandrou, A. J. *et al.* Mechanism of hERG K⁺ channel blockade by the fluoroquinolone antibiotic moxifloxacin. *Br. J. Pharmacol.* **147**, 905–916 (2006).
90. Vandenberg, J. I. *et al.* hERG K⁺ Channels: Structure, Function, and Clinical Significance. *Physiol. Rev.* **92**, 1393–1478 (2012).
91. Fernandez, D., Ghanta, A., Kauffman, G. W. & Sanguinetti, M. C. Physicochemical features of the HERG channel drug binding site. *J. Biol. Chem.* **279**, 10120–10127 (2004).
92. Del Camino, D., Holmgren, M., Liu, Y. & Yellen, G. Blocker protection in the pore of a voltage-gated K⁺ channel and its structural implications. *Nature* **403**, 321–325 (2000).
93. Mitcheson, J. S., Chen, J. & Sanguinetti, M. C. Trapping of a methanesulfonanilide by closure of the HERG potassium channel activation gate. *J. Gen. Physiol.* **115**, 229–240 (2000).
94. Aronov, A. M. Predictive in silico modeling for hERG channel blockers. *Drug Discov. Today* **10**, 149–155 (2005).
95. Dorn, A. *et al.* Evaluation of a high-throughput fluorescence assay method for HERG potassium channel inhibition. *J. Biomol. Screen.* **10**, 339–347 (2005).
96. Murphy, S. M. *et al.* Evaluation of functional and binding assays in cells expressing either recombinant or endogenous hERG channel. *J. Pharmacol. Toxicol. Methods* **54**, 42–55 (2006).
97. Wood, C., Williams, C. & Waldron, G. J. Patch clamping by numbers. *Drug Discov. Today* **9**, 434–441 (2004).
98. FDA. *Guidance for industry: S7B nonclinical evaluation of the potential for delayed ventricular repolarization (QT interval prolongation) by human pharmaceuticals, 2005.* (2006).
99. Thomsen, M. B., Matz, J., Volders, P. G. & Vos, M. A. Assessing the proarrhythmic potential of drugs: current status of models and surrogate parameters of torsades de pointes arrhythmias. *Pharmacol. Ther.* **112**, 150–170 (2006).
100. Redfern, W. S. *et al.* Relationships between preclinical cardiac electrophysiology, clinical QT interval prolongation and torsade de pointes for a broad range of drugs: evidence for a provisional safety margin in drug development. *Cardiovasc. Res.* **58**, 32–45 (2003).
101. FDA. *Guidance for industry: E14 clinical evaluation of QT/QTc interval prolongation and proarrhythmic potential for non-antiarrhythmic drugs.* *Food Drug Adm.* (2005).

2.4 Bioanalysis

2.4.1 Definition and current techniques

Bioanalysis is a sub-discipline of analytical chemistry that focuses on the analysis of xenobiotics (drugs, metabolites and biomarkers) and biotics (DNA, macromolecules, proteins) in biological matrices (e.g. blood, plasma, serum, urine, CSF and saliva)¹. Quantitative and qualitative analysis of molecules in biological systems play an important role in various areas including drug discovery and development, pharmacokinetics and metabolic studies, therapeutic drug monitoring (TDM), and clinical and forensic toxicology²⁻⁵.

For the detection and quantification of analytes in biological matrices, different bioanalytical techniques have been established. Immunoassays (IAs) are one of the most frequently used techniques in routine analysis. They are sensitive, easy to use, time efficient and can be automated (**Table 4**)⁶. However, the major disadvantages of all IAs are the requirement of analyte-specific antibodies and the risk of cross-reactions that may lead to false positive results^{6,7}. Gas chromatography coupled to mass spectrometry (GC-MS) is considered as a more selective and sensitive technique⁶. Moreover, reference libraries of mass spectra are available which facilitates the detection of known compounds. Nevertheless, GC-MS requires a time-consuming sample preparation (derivatization), as the samples need to be volatile and thermostable for the analysis⁸. Over many years, liquid chromatography (LC) hyphenated with spectrometric detection such as ultraviolet/visible (UV/VIS) absorbance or occasionally fluorescence was often used in bioanalytics⁹. Even though both detection systems are highly robust, the techniques are limited to compounds possessing a chromophore (UV/VIS) or fluorophore (fluorescence)¹⁰. In the last decades liquid chromatography- mass spectrometry (LC-MS) has undergone tremendous technological improvements with the introduction of new interfaces, ionization and detection techniques¹¹. These advancements allowed the application of LC-MS/(MS) to

Table 4: Comparison of some available bioanalytical techniques⁶

Method	Comments	Advantage	Disadvantage
IA	e.g. enzyme-linked immunosorbent assay (ELISA) ¹² Radio-IA (RIA) ¹³	Highly sensitive Relatively easy Automated High-throughput ¹³	High price of reagents (analyte-specific-antibodies) Cross-reactions Health hazards (RIA) ¹³
GC-MS	Well suited for apolar, thermostable and low molecular weight analytes	Sensitive and selective Reference databases of spectra available ⁶	Not compatible with polar, thermolabile, or high-molecular weight compounds Derivatization sometimes required
LC- UV/Vis	Useful for aromatic compounds/unsaturated systems Fixed or programmable wavelength detector available	Moderately sensitive Robust	UV/VIS absorbance of compounds required
LC- MS/(MS)	Compatible with non-volatile and thermolabile molecules Gold standard for small molecules (MW < 800) ¹⁴	Sensitive and selective Applicable to a wide range of analytes	Matrix effect ⁶

the qualitative and/or quantitative analysis of endogenous components (e.g. proteins, peptides, carbohydrates, DNA), drugs, or metabolites^{5,15,16}. Up to the present, LC-MS/(MS) is considered as the gold standard for small molecules due to its unsurpassed selectivity and sensitivity¹⁴. But also high-resolution mass spectrometry (HR-MS)(either time-of-flight or orbitrap mass analyzer) has been on rise, as these instruments can simultaneously provide qualitative and quantitative analysis of compounds and their metabolites¹⁴.

2.4.2 LC coupled to MS/MS and HR-MS

Liquid chromatography (LC)

LC can be classified into high performance liquid chromatography (HPLC) and ultra-high performance liquid chromatography (UHPLC), or as one vendor calls it ultraperformance liquid chromatography (UPLC)⁹. While conventional HPLC instruments are designed for pressures of approximately 400-600 bar (5800-8700 psi), UHPLC systems generate back-pressures of around 1000-1300 bar (14500-18900 psi)⁹. The capability of operating at such high pressures allows the use of shorter columns with a smaller particle size of the packing material (below 2 μm)¹⁷, which in turn results in higher resolving power and reduced analysis time⁹.

Mass spectrometer (MS)

A mass spectrometer consists of an ion source, a mass analyzer and a detector¹⁸. Before the analyte can enter the mass analyzer, the sample introduced into the source has to be transferred from the liquid or solid phase to the gas phase and needs to be ionized⁹. The most common ion source is the atmospheric pressure ionization (API) source to which the electrospray ionization (ESI)¹⁹ and the atmospheric pressure chemical ionization (APCI)⁹ source belong. In both ionization techniques, molecules eluting from the column, are ionized to either positively ($\text{M}+\text{H}^+$) or negatively ($\text{M}-\text{H}^-$) charged ions. Both ESI and APCI are considered as “soft” ionization techniques as they induce only little fragmentation to the analyte^{8,9}. While APCI is used to analyze small, thermostable and non-polar compounds, ESI is preferentially applied to investigate labile and more polar molecules^{8,18}. After ionization of the analyte, the mass analyzer separates the ions according to their mass-to-charge ratio (m/z). The most popular mass analyzer in drug quantification is the triple quadrupole detector (TQD or QqQ)⁸. The TQD system is a tandem mass spectrometer (MS/MS) that consists of three quadrupole mass analyzers connected in series (**Fig. 18**). The first (Q1) and the third (Q3) quadrupoles consist of four parallel conducting rods that permit the passage of only a single m/z value, whereas the middle quadrupole (Q2) acts as a (non-mass-resolving) collision cell²⁰. The arrangement of the TQD allows the performance of different scan types⁹. Selected reaction monitoring (SRM) is the most common scan type in quantitative analysis. In this mode, Q1 selects a specific m/z (parent ion) to be fragmented in Q2 in the presence of an inert gas (argon or nitrogen). After this so-called collision induced

dissociation (CID), the second mass analyzer (Q3), filters a specific m/z fragment (daughter ion) to be detected by an electron- or photo- multiplier²¹. This procedure offers high selectivity and sensitivity, and ensures that only the molecule of interest is quantified, whereas unwanted molecules (e.g. matrix constituents) do not reach the detector¹⁰. When more than one specific m/z is selected for Q1 and Q3, the scan type is denoted as multiple reactions monitoring (MRM).

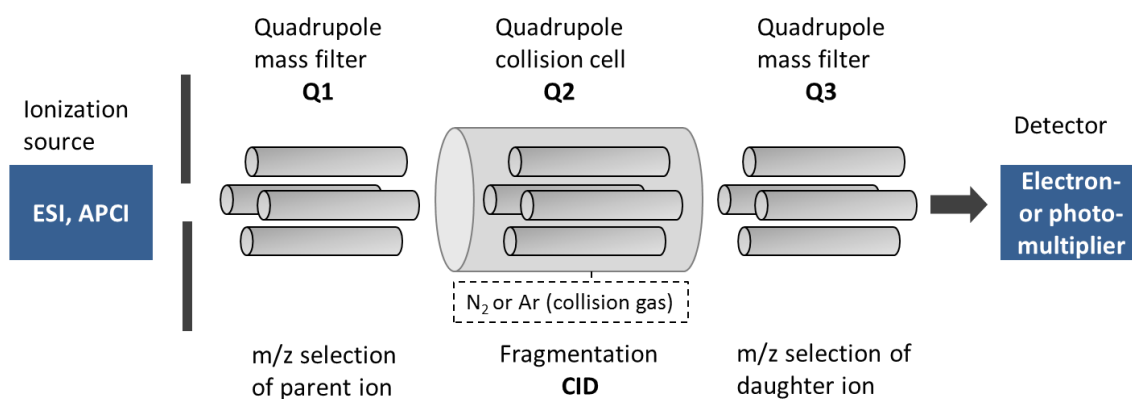


Figure 18: Schematic presentation of a triple quadrupole detector (QqQ) instrument

High resolution mass analyzer (HR-MS) systems are preferentially used to obtain more accurate mass data (< 5 ppm)²², which is particularly desirable for metabolite identification and structural elucidation. One instrument working at such high resolving power is the time-of-flight (TOF) mass analyzer. The Q-TOF system can be considered as a modified TQD system, where the third quadrupole (Q3) is replaced by a orthogonal reflectron-TOF mass analyzer²² (**Fig. 19**). This TOF mass analyzer measures the mass-dependent time that ions need to move from the pusher electrode to the detector. Low m/z ions fly at a higher velocity and reach the detector within a shorter time than higher m/z ions⁹. Calibration of the accelerating field with reference substances (“lock masses”) permits the exact mass analysis of unknown compounds⁹.

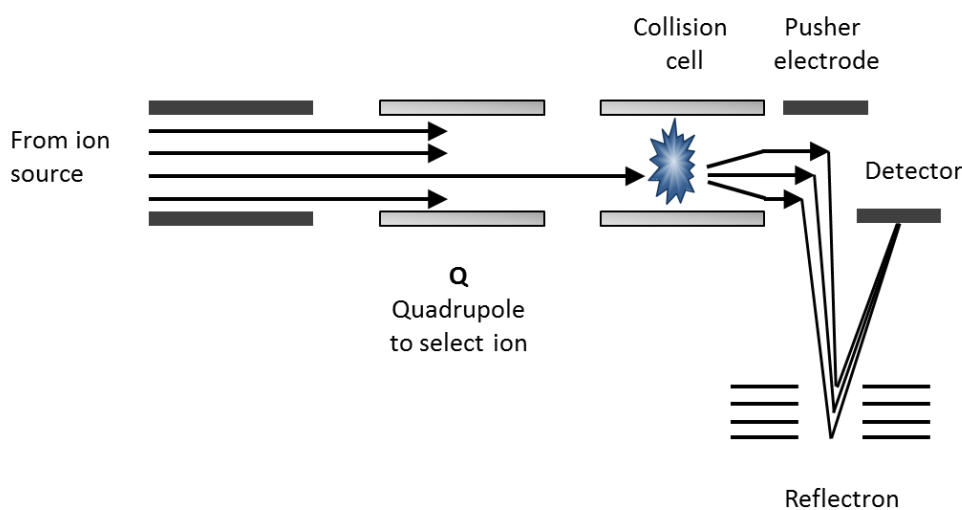


Figure 19: Schematic presentation of the Q-TOF instrument²³

2.4.3 Sample preparation

Biological matrices are highly complex mixtures, usually containing a high content of proteins, salts, phospholipids, and other endogenous material⁹. Most of these biological samples are not suitable for direct LC-MS/MS analysis, but need to be cleaned-up prior to injection. If done properly, sample extraction enhances selectivity and sensitivity, and additionally increases column and instrumentation lifetime¹⁰. Sample extraction techniques currently used to clean up biological samples include sample dilution (“dilute-and-shoot”), protein precipitation (PP), liquid-liquid extraction (LLE), and solid phase extraction (SPE)⁶. In recent years, the supported-liquid extraction (SLE) has become increasingly popular²⁴ (**Table 5**). But also newer phospholipid removal techniques such as the OstroTM (Waters) pass-through sample preparation plates (combination of filtration and sorbent interaction) have emerged.

Dilution: In this clean-up technique, samples (e.g. urine) are diluted with water or mobile phase, and directly injected into the LC-MS/MS system. This “dilute-and-shoot” process is a fast and easy procedure. Samples are usually diluted in a ratio of 1:10 or higher to reduce the matrix effect. However, this process also dilutes out the compound of interest⁶.

Protein precipitation (PP): The purpose of the protein precipitation is to remove endogenous proteins and cellular components that would interfere with the LC-MS/MS system. Protein denaturation can be achieved through exposure to strong acids/bases (leading to a pH change), organic solvents (methanol, acetonitrile), or heat¹. As denaturation changes the secondary and tertiary structure of the protein, the analyte bound to these proteins becomes freely soluble in the reagent solvent¹. After centrifugation, the supernatant is evaporated to dryness and reconstituted in an injection solvent/mobile phase prior to injection into the LC-MS/MS system²⁵.

Liquid-liquid extraction (LLE): The liquid-liquid extraction involves the transfer of a compound in aqueous solution into an immiscible organic phase (e.g. ethyl acetate, methylene chloride, and hexane)²⁶. To facilitate the equilibrium partitioning of the analyte between the phases, samples are vortexed. After phase separation by centrifugation, the organic phase containing the extracted analyte is evaporated to dryness and reconstituted in injection solvent before analysis²⁷.

Supported-liquid extraction (SLE): The supported-liquid extraction (SLE) is an analogous technique to the traditional LLE and uses the same organic solvents for sample extraction²⁸. Instead of shaking the two immiscible phases together, in SLE, the aqueous sample is immobilized on an inert support, while the organic phase flows through the packing material²⁴. In this way, problems such as emulsion formation and low analyte recoveries can be circumvented²⁸.

Solid phase extraction (SPE): The separation is based on the affinity of the analyte towards the stationary phase²⁵. After loading the analyte onto a pre-conditioned SPE cartridge, the compound

retains on the stationary phase, until it is eluted with an appropriate solvent. Commercial SPE cartridges (e.g. Oasis SPE, Waters)²⁹ are inert plastic tubes packed with an adsorbent. Package materials (reversed or normal phase) are similar as in LC columns. However, the particle size of the package in SPE cartridges is often considerably larger than in LC columns, to ensure a reasonable permeability of the analyte²⁵.

Table 5: Currently most used sample preparation techniques⁶.

Method	Comments	Advantages	Disadvantages
Dilute and shoot	Matrix interferences are not removed No pre-concentration of analyte	Easy and simple Time-efficient	Possible interferences Lack of sensitivity Instrument and column contamination
Protein precipitation (PP)	Most widely used extraction method ²⁴	Simple and fast Inexpensive	Numerous co-extracted compounds Less clean compared to LLE
Liquid-liquid extraction (LLE)	Based on the relative solubility of a compound in two different immiscible liquids	Suitable for numerous compounds Good selectivity Few matrix effects; provides cleaner extracts than PP ²⁴	Limited extraction of large hydrophilic compounds Variable recoveries Large volumes of costly solvents needed
Supported-liquid extraction (SLE)	Commercial available 96-well plates (e.g. Isolute® SLE+ from Biotage) ²⁸	Highly clean samples High recovery and reproducibility ²⁴	Expensive Limited sample aliquot volume (< 400 µL) due to the 96-well format ²⁴
Solid-phase extraction (SPE)	Numerous types of supports: reversed phase silica material (e.g. C18), cation or anion exchanger, organic polymer (e.g. N-vinylpyrrolidone) ⁶	Highly clean extracts Good selectivity Suitable for numerous compounds	High cost of cartridge More expensive than PP and LLE

2.4.4 Bioanalytical quantification using validated LC-MS/MS methods

The aim of bioanalytical quantification methods is to provide accurate and reliable results. Particularly, in the field of forensic and clinical toxicology, correct data interpretation plays a significant role³⁰. Unreliable analytical findings might result in fatal outcomes such as unjustified legal consequences for the defendant, or incorrect dosing of patients³⁰. Thus, method validation is a prerequisite for correct quantification. Method development builds the basis of method validation. Once a method is validated, it can be applied to the study (**Fig. 20**).

To standardize bioanalytical method validation procedures, the US Food and Drug Administration (FDA)^{31,32} and the European Medicine Agency (EMA)³³ have released bioanalytical guidance documents which are in compliance with the good laboratory practices (GLP)³⁰. But also other regulatory authorities, such as the Japanese Ministry of Health, Labour and Welfare (MHLW)³⁴, or the Agência Nacional de Vigilância Sanitária (ANVISA) Resolution from Brazil³⁵ have issued guidelines for the design and conduction of bioanalytical quantification studies. Unfortunately, each guideline is slightly different, and at present no harmonized global guideline has been established³⁶.

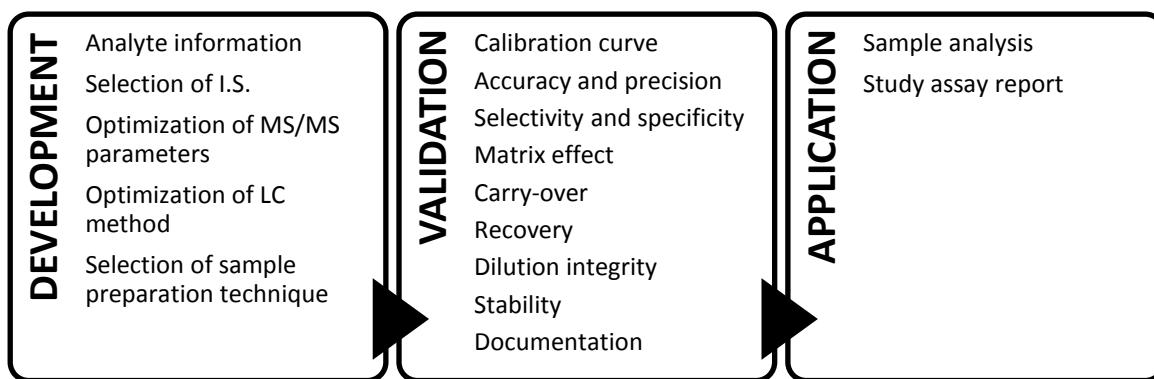


Figure 20: Major steps in method development, validation, and application to a study⁸

2.4.5 Method development

LC-MS/MS method development includes the following steps³⁷:

1. **Physicochemical properties:** For developing a reliable quantification method, information about the physicochemical properties of the analyte such as chemical structure, functional group(s), molecular weight, solubility, and stability are crucial. Based on these properties, suitable solvents can be selected and handling precautions can be taken (such as temperature storage, light protection of photosensitive compounds, etc.)³⁷.
2. **Selection of the best internal standard (I.S.):** I.S. is a compound added in a constant amount to the quantitative sample to correct variations during sample preparation and analysis³⁸. A stable isotopic-labeled version of analyte is the ideal I.S. due to its similar physicochemical characteristics. However, D (²H), ¹³C, and ¹⁵N-labeled compounds are very expensive and mostly not available for natural products³⁹. Therefore, synthetic structural analogs are often used as alternatives.
3. **Optimization of MS/MS parameters:** To reach high selectivity and sensitivity for the analyte, a suitable ion source needs to be selected (e.g. ESI, or APCI). Moreover, MS/MS parameters such as SRM transition, cone voltage, collision energy, etc. have to be generated and optimized for analyte and I.S..
4. **Optimization of the LC method:** To obtain an optimal chromatographic separation the following variables needs to be modified: (1) column type (e.g. reversed phase [RP-LC], normal phase LC [NP-LC], or hydrophilic interaction [HILIC]) (2) mobile-phase composition/gradient (3) temperature (column, autosampler), and (4) eluent additives and pH³⁷.
5. **Selection of sample preparation technique:** Sample preparation is the most critical step in method development, as it can highly impact the quality of the data. PP is the most common extraction technique. But for highly complex mixtures (e.g. plasma) more sophisticated techniques are sometimes required (e.g. SPE)¹⁰.

2.4.6 Method validation

After a method has been developed, it needs to be demonstrated that the quantification assay is reliable and reproducible for the intended use². For analytes in a different matrix (e.g. plasma, aqueous buffer) a new method has to be validated⁹. Partial validations are required, when modifications in e.g. sample preparation technique, detection system, or changes within the matrix are made for a validated method⁹. Cross-validations are necessary, when one study is performed in different laboratories or when different analytical techniques (e.g. ELISA vs. LC-MS/MS) are used for data generation³⁰. According to the FDA and EMA guidelines a method should be validated with respect to calibration curve, accuracy, precision, selectivity, specificity, matrix effect, carry-over, recovery (= extraction yield), dilution integrity, and stability³¹⁻³³.

A **Calibration curve** should include six to eight calibrators that cover the total experimental concentration range. The calibration curve is generated by plotting the peak response against the retention time. The peak response is usually defined as the ratio of the peak area of the analyte to the I.S. Data are fitted either by linear or quadratic regression. But also other models (e.g. power fit) are used⁹. Weighting factors such as 1/concentration (also known as 1/X or 1/X²) are often applied to improve the fit of the regression to the data⁹. The response of the lowest calibrator (LLOQ = lowest limit of quantification) should be at least 5 times higher than the response of the analyte in the blank and the signal to noise ratio (S/N) should be higher than 10^{31,33}. To check the reliability of the calibration curve, quality controls (QCs) should be incorporated into each analytical run. These QC samples should cover the low (3x LLOQ), the medium (50% of ULOQ, ULOQ = upper limit of quantification), and the high (70-85% of ULOQ) concentration range of the calibration curve^{31,33}.

Accuracy is an assessment of the differences between the determined concentration and the nominal concentration and is expressed by the relative error RE%. **Precision** evaluates the closeness of an individual measurement to multiple measurements on an homogenous set of sample and is defined by the coefficient of variation (CV%)^{31,33}.

$$RE (\%) = \frac{\text{Determined conc.} - \text{Nominal conc.}}{\text{Nominal conc.}} \times 100$$

$$CV (\%) = \frac{\text{Standard deviation (S.D.)}}{\text{Mean conc.}} \times 100$$

To fulfill the acceptance criteria of the FDA and EMA guidelines, imprecision (CV%) should be below 15% for all levels (20% for the LLOQ as exception) and inaccuracy (RE%) should be within $\pm 15\%$ of the nominal value for all levels ($\pm 20\%$ of the nominal value for the LLOQ).

Intra-run accuracy and precision of a method are assessed within one analytical run on the same day, whereas inter-run accuracy and precision are determined within different analytical runs over at least three days^{31,33}.

Selectivity refers to the ability to distinguish the analyte and I.S. from other interfering endogenous or exogenous components in the sample. Selectivity of the method is assessed by analyzing at least six individual sources of blank matrix^{31,33}. However, for rare matrices the use of fewer sources is also acceptable (e.g. three different batches for rat plasma)³³. **Specificity** is defined as the lowest concentration that can be measured with precision and accuracy^{31,33}. While specificity is considered as an absolute term, selectivity can be graded⁴⁰.

The **matrix effect** is a signal suppression or enhancement of the analyte due to the presence of endogenous substances, phospholipids, salts, impurities etc.⁹. This effect can result in a shift in retention time, poor peak shapes or even inaccurate measurements⁹. Therefore, the matrix effect should be assessed to ensure the reliability of the method^{31,33}.

Carry-over is the transfer of analyte or I.S. (amount) to the following sample injected. Carry-over typically occurs within the LC-MS/MS system (e.g. syringe, switching valve) or within the column⁹. But it can also be the result of inaccurate pipetting during the sample preparation process. To assess the carry-over with an analytical run, a blank sample is injected after the ULOQ. The EMA guideline requests a carry-over below 20% for the analyte and 5% for the I.S.:³³.

According to the FDA and EMA guidelines the **extraction yield** does not need to be close to 100%. However, to avoid under/overestimation of data, the recovery has to be consistent, reproducible and precise over the validated range^{31,33}.

Sample dilution should not impact accuracy and precision of a method. To demonstrate the **dilution integrity**, a QC sample prepared at higher concentrations than the ULOQ should be diluted with blank matrix and analyzed.

Stability tests are performed to mimic the experimental conditions such as sample collection, processing, and storage. Typical short-term stability tests include three freeze-and-thaw cycles, 4 hours storage at benchtop, and autosampler stability. For the assessment of the long-term stability of the analyte, unprocessed samples are kept for days, month or even years under storage conditions (e.g. -20°C or -80°C). Stability data on the stock solution of analyte and I.S. should be generated to ensure the stock solution stability^{31,33}. A degradation of less than 5% is typically tolerated.

Finally, a standard operating procedure (SOP) should be written and generated data for the establishment of the method should be **documented** in a validation report.

2.4.7 Sample analysis

After a method has been validated, it can be applied to a study. Gained experience regarding sample handling during the validation has to be taken into consideration for the study. For sample quantification, like for validation tests, two sets of calibrators along with six QCs (low, medium, high QCs in duplicates) are injected into the LC-MS/MS system. The analytical run is considered to be valid, if 75% of the calibrators and 67% (e.g. at least four out of six) of the QCs of the measured concentration are within 15% of their respective nominal values (20% for the LLOQ as exception)^{31,33}. In addition, if samples are diluted, diluted QCs should be included in the analysis.

References

1. Kole, P. L., Venkatesh, G., Kotecha, J. & Sheshala, R. Recent advances in sample preparation techniques for effective bioanalytical methods. *Biomed. Chromatogr.* **25**, 199–217 (2011).
2. González, O. *et al.* Bioanalytical chromatographic method validation according to current regulations, with a special focus on the non-well defined parameters limit of quantification, robustness and matrix effect. *J. Chromatogr. A* **1353**, 10–27 (2014).
3. Hill, H. Development of bioanalysis: a short history. *Bioanalysis* **1**, 3–7 (2009).
4. Booth, B. P. Welcome to bioanalysis. *Bioanalysis* **1**, 1–2 (2009).
5. Viswanathan, C. T. *et al.* Workshop/conference report—quantitative bioanalytical methods validation and implementation: best practices for chromatographic and ligand binding assays. *AAPS J.* **9**, E30–E42 (2007).
6. Viette, V., Fathi, M., Rudaz, S., Hochstrasser, D. & Veuthey, J.-L. Current role of liquid chromatography coupled to mass spectrometry in clinical toxicology screening methods. *Clin. Chem. Lab. Med.* **49**, 1091–1103 (2011).
7. Šmisterová, J., Ensing, K. & De Zeeuw, R. A. Methodological aspects of quantitative receptor assays. *J. Pharm. Biomed. Anal.* **12**, 723–745 (1994).
8. Hacker, M., Il, W. S. M. & Bachmann, K. A. *Pharmacology: principles and practice*. (Academic Press, 2009).
9. Ramanathan, R. *Mass spectrometry in drug metabolism and pharmacokinetics*. (John Wiley & Sons, 2011).
10. Establishment and validation of an immortalized *in vitro* human blood-brain barrier (BBB) model for drug permeability studies, and application to natural product derived leads. Available at: https://forschdb2.unibas.ch/inf2/rm_projects/object_view.php?r=3343775. (Accessed: 12th April 2016)
11. Shah, V. P. *et al.* Bioanalytical method validation—a revisit with a decade of progress. *Pharm. Res.* **17**, 1551–1557 (2000).
12. Engvall, E. The ELISA, enzyme-linked immunosorbent assay. *Clin. Chem.* **56**, 319–320 (2010).
13. Darwish, I. A. Immunoassay methods and their applications in pharmaceutical analysis: basic methodology and recent advances. *Int. J. Biomed. Sci. IJBS* **2**, 217–235 (2006).
14. van Dongen, W. D. & Niessen, W. M. LC-MS systems for quantitative bioanalysis. *Bioanalysis* **4**, 2391–2399 (2012).
15. Bronsema, K. J., Bischoff, R. & van de Merbel, N. C. Internal standards in the quantitative determination of protein biopharmaceuticals using liquid chromatography coupled to mass spectrometry. *J. Chromatogr. B* **893**, 1–14 (2012).
16. Kang, J.-S. Principles and applications of LC-MS/MS for the quantitative bioanalysis of analytes in various biological samples. *Tandem Mass Spectrom. Princ.* 441–492 (2012).
17. Xu, R. N., Fan, L., Rieser, M. J. & El-Shourbagy, T. A. Recent advances in high-throughput quantitative bioanalysis by LC-MS/MS. *J. Pharm. Biomed. Anal.* **44**, 342–355 (2007).
18. Gross, J. H. *Mass spectrometry: a textbook*. (Springer Science & Business Media, 2006).
19. Whitehouse, C. M., Dreyer, R. N., Yamashita, M. & Fenn, J. B. Electrospray interface for liquid chromatographs and mass spectrometers. *Anal. Chem.* **57**, 675–679 (1985).

20. Johnson, J. V., Yost, R. A., Kelley, P. E. & Bradford, D. C. Tandem-in-space and tandem-in-time mass spectrometry: triple quadrupoles and quadrupole ion traps. *Anal. Chem.* **62**, 2162–2172 (1990).
21. Yost, R. A. & Enke, C. G. Selected ion fragmentation with a tandem quadrupole mass spectrometer. *J. Am. Chem. Soc.* **100**, 2274–2275 (1978).
22. Fujii, T. *Ion/Molecule Attachment Reactions: Mass Spectrometry*. 87-101 (Springer, 2015).
23. Mass spectrometry (Proteomics). Available at: <http://what-when-how.com/proteomics/mass-spectrometry-proteomics/>. (Accessed: 17th April 2016)
24. Meng, M. & Bennett, P. K. in *LC-MS in Drug Bioanalysis* 33–66 (Springer, 2012).
25. Devanshu, S., Rahul, M., Annu, G., Kishan, S. & Anroop, N. Quantitative Bioanalysis by LC-MS/MS: A Review. *J. Pharm. Biomed. Sci. JPBMS* **7**, (2010).
26. Mazzeo, J. R., D. Neue, U., Kele, M. & Plumb, R. S. Advancing LC performance with smaller particles and higher pressure. *Anal. Chem.* **77**, 460 A–467 A (2005).
27. Henion, J., Brewer, E. & Rule, G. Peer Reviewed: Sample Preparation for LC/MS/MS: Analyzing Biological and Environmental Samples. *Anal. Chem.* **70**, 650A–656A (1998).
28. Biotage - ISOLUTE® SLE+ Supported Liquid Extraction Products. Available at: <http://www.biotage.com/product-page/isolute-sle-supported-liquid-extraction-products>. (Accessed: 31st March 2016)
29. Oasis SPE : Waters. Available at: http://www.waters.com/waters/de_DE/Oasis-Sample-Extraction-Products/nav.htm?locale=de_DE&cid=513209. (Accessed: 14th April 2016)
30. Tiwari, G. & Tiwari, R. Bioanalytical method validation: An updated review. *Pharm. Methods* **1**, 25–38 (2010).
31. Guidance for Industry: Bioanalytical Method Validation, US Food and Drug Administration (FDA), Center for Drug Evaluation and Research, May 2001.
32. FDA, U. Guidance for industry: bioanalytical method validation (draft guidance). *US FDA* (2013).
33. Guideline on bioanalytical method validation. European Medicines Agency (EMA/CHMP/EWP/192217/2009). London, 21 July 2011.
34. Guideline on Bioanalytical Method Validation in Pharmaceutical Development, Ministry of Health, Labour and Welfare (MHLW), Japan, 2013.
35. BRASIL, R.-R. n° 899, de 29 de maio de 2003, Guia para a validação de métodos analíticos e bioanalíticos. *Diário Of. União*
36. Whitmire, M. *et al.* LC-MS/MS bioanalysis method development, validation, and sample analysis: points to consider when conducting nonclinical and clinical studies in accordance with current regulatory guidances. *J. Anal. Bioanal. Tech.* **2011**, (2013).
37. Bioanalytical Method Development. Available at: http://www.pharmacelsus.de/bioanalytical_method_development/. (Accessed: 1st April 2016)
38. LeLacheur, R. M. Evolving role of mass spectrometry in drug discovery and development. (2009).
39. Wang, S., Cyronak, M. & Yang, E. Does a stable isotopically labeled internal standard always correct analyte response?: A matrix effect study on a LC/MS/MS method for the determination of carvedilol enantiomers in human plasma. *J. Pharm. Biomed. Anal.* **43**, 701–707 (2007).
40. Vessman, J. *et al.* Selectivity in analytical chemistry (IUPAC Recommendations 2001). *Pure Appl. Chem.* **73**, 1381–1386 (2001).

3 Results and discussion

3.1 Development and validation of a LC-MS/MS method for assessment of an anti-inflammatory indolinone derivative by *in vitro* blood-brain barrier models

Evelyn A. Jähne, Daniela E. Eigenmann, Maxime Culot, Roméo Cecchelli, Fruzsina R. Walter, Mária A. Deli, Robin Tremmel, Gert Fricker, Martin Smieško, Matthias Hamburger, and Mouhssin Oufir

Journal of Pharmaceutical and Biomedical Analysis 98 (2014) 235–246

DOI: 10.1016/j.jpba.2014.05.026

The anti-inflammatory and anti-allergic compound (*E,Z*)-3-(4-hydroxy-3,5-dimethoxybenzylidene)-indolin-2-one (indolinone, **Fig. 1**) from woad (*Isatis tinctoria* L., Brassicaceae) was screened in our recently validated immortalized human *in vitro* blood-brain barrier (BBB) model and in two well-characterized primary animal *in vitro* BBB models. For the exact quantification of indolinone, we developed and validated an ultra-performance liquid chromatography tandem mass-spectrometry (UPLC-MS/MS) quantification method in Ringer HEPES buffer (RHB) according to current international guidelines. Data obtained in the three different models showed good correlation and were indicative of a high BBB permeation potential of indolinone. P-glycoprotein (P-gp) interaction of indolinone was studied with the aid of a calcein-acetoxymethyl (AM) uptake assay using porcine brain capillary endothelial cells, and by calculation of the efflux ratio (ER) from the bidirectional permeability assays. The ER below 2 indicated that the compound was not involved in active mediated efflux. The calcein-AM uptake assay demonstrated that indolinone was neither a P-gp substrate nor a P-gp inhibitor.

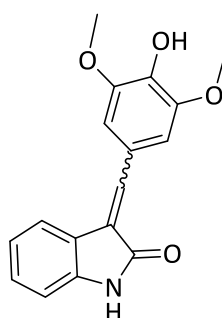


Fig.1: *E,Z*-3-(4-hydroxy-3,5-dimethoxybenzylidene)indolin-2-one (indolinone)

My contributions to this publication: validation of the UPLC-MS/MS method in RHB, cultivation of human cells (hBMEC cell line), sample preparation and analysis, recording and analyzing data, writing the manuscript draft, and preparation of figures and tables.

Evelyn Andrea Jähne



Contents lists available at ScienceDirect

Journal of Pharmaceutical and Biomedical Analysis

journal homepage: www.elsevier.com/locate/jpba

Development and validation of a LC–MS/MS method for assessment of an anti-inflammatory indolinone derivative by *in vitro* blood–brain barrier models



Evelyn A. Jähne^a, Daniela E. Eigenmann^a, Maxime Culot^b, Roméo Cecchelli^b, Fruzsina R. Walter^c, Mária A. Deli^c, Robin Tremmel^d, Gert Fricker^d, Martin Smiesko^e, Matthias Hamburger^a, Mouhssin Oufir^{a,*}

^a Institute of Pharmaceutical Biology, Department of Pharmaceutical Sciences, University of Basel, Klingelbergstrasse 50, CH-4056 Basel, Switzerland

^b Université Lille Nord de France, UArtois, BBB Laboratory EA 2465, IMPRT: IFR114, 62307 Lens Cedex, France

^c Institute of Biophysics, Biological Research Centre, Hungarian Academy of Sciences, Temesvári krt. 62, H-6726 Szeged, Hungary

^d Institute of Pharmacy and Molecular Biotechnology, Im Neuenheimer Feld 329, D-69120 Heidelberg, Germany

^e Molecular Modeling, Department of Pharmaceutical Sciences, University of Basel, Klingelbergstrasse 50, CH-4056 Basel, Switzerland

ARTICLE INFO

Article history:

Received 29 March 2014

Received in revised form 15 May 2014

Accepted 16 May 2014

Available online 27 May 2014

Keywords:

*Isatis tinctoria**(E,Z)*-3-(4-Hydroxy-3,5-dimethoxybenzylidene)indolin-2-one

Anti-inflammatory

LC–MS/MS

Blood–brain barrier (BBB)

ABSTRACT

The compound *(E,Z)*-3-(4-hydroxy-3,5-dimethoxybenzylidene)indolin-2-one (indolinone) was identified from lipophilic woad extracts (*Isatis tinctoria* L., Brassicaceae) as a compound possessing potent histamine release inhibitory and anti-inflammatory properties [1]. To further evaluate the potential of indolinone in terms of crossing the blood–brain barrier (BBB), we screened the compound in several *in vitro* cell-based human and animal BBB models. Therefore, we developed a quantitative LC–MS/MS method for the compound in modified Ringer HEPES buffer (RHB) and validated it according to FDA and EMA guidelines [2,3]. The calibration curve of indolinone in the range between 30.0 and 3000 ng/ml was quadratic, and the limit of quantification was 30.0 ng/ml. Dilution of samples up to 100-fold did not affect precision and accuracy. The carry-over was within acceptance criteria. Indolinone proved to be stable in RHB for 3 h at room temperature (RT), and for three successive freeze/thaw cycles. The processed samples could be stored in the autosampler at 10 °C for at least 28 h. Moreover, indolinone was stable for at least 16 days in RHB when stored below –65 °C. This validation study demonstrates that our method is specific, selective, precise, accurate, and capable to produce reliable results.

In the immortalized human BBB mono-culture model, the apparent permeability coefficient from apical to basolateral ($P_{app\ A\rightarrow B}$), and the P_{app} from basolateral to apical ($P_{app\ B\rightarrow A}$) were $19.2 \pm 0.485 \times 10^{-6}$ cm/s and $21.7 \pm 0.326 \times 10^{-6}$ cm/s, respectively. For the primary rat/bovine BBB co-culture model a $P_{app\ A\rightarrow B}$ of $27.1 \pm 1.67 \times 10^{-6}$ cm/s was determined. In the primary rat BBB triple co-culture model, the $P_{app\ A\rightarrow B}$ and the $P_{app\ B\rightarrow A}$ were $56.2 \pm 3.63 \times 10^{-6}$ cm/s and $34.6 \pm 1.41 \times 10^{-6}$ cm/s, respectively. The data obtained with the different models showed good correlation and were indicative of a high BBB permeation potential of indolinone confirmed by *in silico* prediction calculations. P-glycoprotein (P-gp) interaction for indolinone was studied with the aid of a calcein-AM uptake assay, and by calculation of the efflux ratio (ER) from the bidirectional permeability assays. For both bidirectional BBB models an ER below 2 was calculated, indicating that no active mediated transport mechanism is involved for indolinone. In porcine

Abbreviations: BBB, blood–brain barrier; BSA, bovine serum albumin; BBEC, primary bovine brain capillary endothelial cells; Cal, calibrator; cLogP, calculated logarithm of partitioning coefficient; Calcein-AM, calcein-acetoxymethylester; C_{cl} , cell layer capacitance; Conc., concentration; CNS, central nervous system; CV%, coefficient of variation; CPT-cAMP, 8-(4-chlorophenylthio)-adenosine-3',5'-cyclic monophosphate, sodium salt; DMEM, Dulbecco's modified Eagle's medium; DMSO, dimethyl sulfoxide; DNase I, deoxyribonuclease type I; 96-DWP, 96-deep well plate; EMA, European Medicines Agency; ER, efflux ratio; ESI, electrospray ionization; FBS, fetal bovine serum; FDA, Food and Drug Administration; hBMEC, immortalized human brain microvascular endothelial cell line; HEPES, 4-(2-hydroxyethyl)-1-piperazineethanesulfonic acid; HPLC, high-performance liquid chromatography; I.S., internal standard; KRB, Krebs–Ringer buffer; LLOQ, lower limit of quantification; LTS, long-term stability; MRM, multiple reaction monitoring; MW, molecular weight; Na-F, sodium fluorescein; NMR, nuclear magnetic resonance; PBCEC, porcine brain capillary endothelial cells; PBS, phosphate buffered saline; P_{app} , apparent permeability coefficient; P-gp, P-glycoprotein; PSA, polar surface area; QC, quality control; QCH, quality control high; QCL, quality control low; QCM, quality control medium; RBEC, primary rat brain capillary endothelial cell; RE%, relative error; RHB, Ringer HEPES buffer; Rpm, revolutions per minute; RT, room temperature; SD, standard deviation; S.E.M., standard error of the mean; SS, stock solution; TEER, transendothelial electrical resistance; TFA, trifluoroacetic acid; TQD, tandem quadrupole detector; ULOQ, upper limit of quantification; UPLC–MS/MS, ultra performance liquid chromatography with tandem mass spectrometric detection; v/v, volume per volume; WS, working solution.

* Corresponding author. Tel.: +41 61 267 1425; fax: +41 61 267 1474.

E-mail address: mouhssin.oufir@unibas.ch (M. Oufir).

<http://dx.doi.org/10.1016/j.jpba.2014.05.026>

0731-7085/© 2014 Elsevier B.V. All rights reserved.

brain capillary endothelial cells (PBCECs), the calcein-AM uptake assay demonstrated that indolinone is neither a P-gp substrate nor a P-gp inhibitor and is accumulated into cells at high extent.

© 2014 Elsevier B.V. All rights reserved.

1. Introduction

In the course of an investigation of anti-inflammatory and anti-allergic compounds in the ancient anti-inflammatory plant *Isatis tinctoria* [1,4–20] we identified (*E,Z*)-3-(4-hydroxy-3,5-dimethoxybenzylidene)indolin-2-one (indolinone) as the compound responsible for the inhibition of histamine release from activated mast cells [1]. The compound was a potent inhibitor of antigen-induced histamine release by stabilizing mast cells [1] by a molecular mode of action that is not yet fully understood but different from known compounds. The compound was shown not to act *via* targets upstream of the histamine containing granules and, hence, is thought to interact with the membrane of histamine-containing granules [1]. Given the new mechanism of action, low cytotoxicity, anti-allergic potency, and drug-like physicochemical properties [21], indolinone is a promising lead for the development of new anti-allergic drugs. For further assessment of the potential of indolinone we recently developed and validated an UPLC–MS/MS method for quantification of indolinone in lithium heparinized rat plasma for a preliminary pharmacokinetic study in Sprague-Dawley male rats [22]. To further evaluate the potential of indolinone in terms of blood–brain barrier (BBB) permeability, we screened the compound in several *in vitro* cell-based human and animal BBB models.

Blood–brain barrier (BBB) penetration is necessary for drugs acting on the central nervous system (CNS). High passive membrane permeability and low P-glycoprotein (P-gp) interaction favor CNS exposure [23]. On the other hand, low BBB penetration is desirable for drugs aimed at peripheral targets to minimize CNS-related side effects. Hence, regardless of the therapeutic area, assessment of BBB penetration is required at an early phase of the drug discovery process [24]. For this purpose, we developed a quantitative LC–MS/MS assay for indolinone in Ringer HEPES buffer (RHB) and validated it according to international guidelines [2,3]. Indolinone was screened in several cell-based *in vitro* human and animal BBB models [25–27], and the permeability of indolinone was assessed by LC–MS/MS. P-gp interaction was studied with the aid of a calcein-AM uptake assay in porcine brain capillary endothelial cells (PBCECs), and by calculation of the efflux ratio (ER) from the bidirectional permeability assays [25,27]. To further explore the transporter mechanism of indolinone, an uptake assay was performed in PBCECs.

2. Materials and methods

2.1. *In silico* prediction of blood–brain barrier permeability

Three-dimensional computer models of both (*E*)- and (*Z*)-3-(4-hydroxy-3,5-dimethoxybenzylidene)indolin-2-one (indolinone) were built in Maestro modeling environment (Maestro, version 9.3, Schrödinger, LLC, New York, NY, 2012), and the most favorable conformers were identified by the conformational search in MacroModel (MacroModel, version 9.9, Schrödinger, LLC, New York, NY, 2012) using the OPLS-2005 force-field, implicit solvent conditions (water), and 1000 iterations of the mixed serial/low mode sampling method. For each isomer, the conformers within 5 kcal/mol from the corresponding global minimum were used as input for the QikProp application (QikProp, version 3.5, Schrödinger, LLC, New York, NY, 2012), to

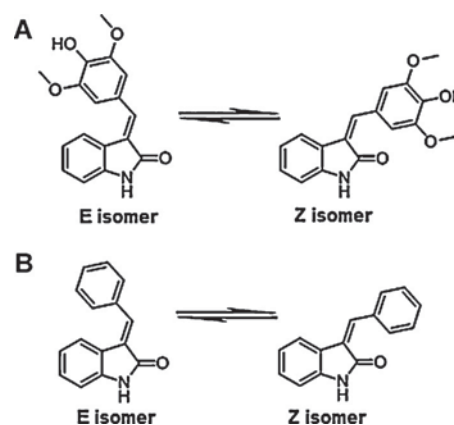


Fig. 1. Chemical structures of (*E,Z*)-3-(4-hydroxy-3,5-dimethoxybenzylidene)indolin-2-one (indolinone) (A) and internal standard, (*E,Z*)-3-(benzylidene)indolin-2-one (B) [22].

evaluate various descriptors relevant for drug permeability. For comparison, the polar surface area (PSA) and the logarithm of partition coefficient (cLogP) descriptors were calculated also using the Calculator plugin of Chemaxon Marvin web-application (<http://www.chemaxon.com/marvin/sketch/index.php>, accessed on February 12, 2014) requiring only the 2D structural formula as input.

2.2. LC–MS/MS analysis

2.2.1. Chemicals and reagents

(*E,Z*)-3-(4-Hydroxy-3,5-dimethoxybenzylidene)indolin-2-one (indolinone) (Fig. 1A) and the internal standard (I.S.) (*E,Z*)-3-(benzylidene)indolin-2-one (Fig. 1B) were synthesized according to a general protocol for indolinones [28]. Both compounds showed a purity of $\geq 99\%$ as determined by HPLC–UV–ESI–MS and ^1H and ^{13}C NMR [29]. The ratio of *E* to *Z* isomers for indolinone and I.S. was assessed by ^1H NMR and HPLC as 71:29 and 75:25, respectively [22]. Preparative separation of isomers failed because of slow spontaneous isomerization at RT [9,28]. All used solvents were of HPLC grade. Acetonitrile and dimethyl sulfoxide (DMSO) were supplied by Scharlau (Barcelona, Spain). Methanol was from Lab-Scan (Gliwice, Poland). Formic acid and trifluoroacetic acid (TFA) were purchased from BioSolve (Valkenswaard, Netherlands), and albumin from bovine serum (BSA) was supplied by Sigma–Aldrich (Steinheim, Germany). HPLC grade water was obtained by an EASYpure II (Barnstead, Dubuque, IA, USA) water purification system. Ringer HEPES buffer (RHB) (150 mM NaCl, 2.2 mM CaCl_2 , 0.2 mM MgCl_2 , 5.2 mM KCl, 2.8 mM glucose, 5 mM HEPES, 6 mM NaHCO_3 , 0.2% BSA) was prepared in-house, adjusted to pH 7.4, and stored at 4 °C.

2.2.2. LC–MS/MS instrument and chromatographic conditions

Method validation was performed on an Acquity UPLC system consisting of a binary pump, an autosampler set at 10 °C, and a column heater set at 45 °C, which was coupled to an Acquity TQD (all Waters Corp., Milford, MA, USA). Separation of analyte (indolinone) and I.S. ((*E,Z*)-3-(benzylidene)indolin-2-one) was achieved with a UPLC HSS T3 column (100 mm \times 2.1 mm; 1.8 μm

particle size) (Waters Corp., Milford, MA, USA). The mobile phase consisted of water containing 0.1% formic acid (Eluent A) and acetonitrile containing 0.1% formic acid (Eluent B). Chromatographic separation was performed at a flow rate of 0.5 ml/min with the following gradient: 0–0.5 min, B 2%; 0.5–2 min, B 2–100%; 2–2.5 min, B 100%; 2.5–2.6 min, B 100–2%; 2.6–4 min, B 2%. The total run time was 4 min. As injection solvent a mixture of 35% water containing 0.1% formic acid and 65% methanol containing 0.1% formic acid was used (35:65, v/v). Weak and strong wash solvents were water–acetonitrile (50:50, v/v) containing 0.2% TFA, and acetonitrile–isopropanol–acetone (40:40:30, v/v/v) containing 0.2% TFA, respectively. The seal wash solvent consisted of a water–acetonitrile mixture (90:10, v/v).

MS detection was performed with electrospray ionization in positive ion mode (ESI+). Nitrogen, generated by a nitrogen generator N2-Mistral (Schmidlin AG, Neuheim, Switzerland), was used both as desolvation and nebulization gas. Argon was used as collision gas. MS/MS parameters were generated using Waters IntelliStart software followed by manual optimization.

MRM transitions were 297.7 > 265.0 for indolinone, and 221.8 > 194.0 for I.S. ((*E,Z*)-3-(benzylidene)-indolin-2-one). The capillary voltage was 3.5 kV. Cone voltage was 46 V, and collision energy was 21 eV for both indolinone and I.S. Source temperature was set at 150 °C, and the desolvation temperature was 400 °C. The flow rates for desolvation gas and cone gas were 900 l/h and 10 l/h, respectively. The dwell time was automatically set at 69 ms. Data were acquired with MassLynx V4.1 software and quantified by means of QuanLynx software (Waters Corp., Milford, MA, USA).

2.2.3. Standards and stock solutions

Stock solutions (SS) of analyte and I.S. were prepared by weighing pure compounds on an analytical balance (Mettler-Toledo, Switzerland) and dissolving them in DMSO. The working solutions (WS1) of analyte and I.S. were freshly prepared in methanol by further diluting the corresponding SS to obtain a concentration of 100 µg/ml for indolinone, and 10 µg/ml for the I.S. For the I.S., a daily second working solution (WS2) at a concentration of 1000 ng/ml was freshly prepared by diluting WS1 (10 µg/ml) with methanol. All SS and WS (except WS2, which was discarded after use) were stored below –65 °C until analysis.

2.2.4. Preparation of calibration and quality control samples

Seven calibration samples (calibrators) in the range of 30.0–3000 ng/ml and quality controls (QCs) at low, middle and high levels (QCL = 90.0 ng/ml, QCM = 1500 ng/ml, QCH = 2400 ng/ml) were prepared in RHB by serial dilution of the WS of indolinone (100 µg/ml). After dilution, all samples were vortexed, aliquoted into polypropylene tubes, and stored below –65 °C until analysis.

2.2.5. Sample extraction in Ringer HEPES buffer

To 200 µl of RHB containing indolinone, 100 µl of I.S. at 1000 ng/ml, 200 µl of BSA solution (60 g/l), and 1000 µl of ice cold acetonitrile were added. The mixture was briefly vortexed, mixed for 10 min at room temperature (RT) in an Eppendorf Thermomixer (1400 rpm), and centrifuged for 20 min at 13 200 rpm at 10 °C (Centrifuge 5415R, Eppendorf, Schoenenbuch, Switzerland). The supernatant (1300 µl) was transferred into a 96-deep well plate (DWP), dried under nitrogen gas flow (Evaporex EVX-96, Apricot Designs, Monovia, CA, USA), and reconstituted with 200 µl of injection solvent (35% solvent A + 65% solvent B, A: water + 0.1% formic acid, B: methanol + 0.1% formic acid). Afterwards, the 96-DWP was shaken for 45 min at RT in an Eppendorf Mixmate and centrifuged for 2 min at 3000 rpm (Megafuge, Heraeus Instruments AG, Switzerland). Due to nonspecific adsorption of I.S. onto the 96-DWP, each sample was transferred into a 300 µl glass insert of a

HPLC vial before injection into the UPLC–MS/MS system in full loop mode (5 µl).

2.3. Method validation

The method was validated according to the guidelines of the US Food and Drug Administration (FDA) [2] and the European Medicines Agency (EMA) [3].

2.3.1. Chromatographic performance

The calibration curve was generated by seven calibrators ranging from 30.0 to 3000 ng/ml. To meet requirements of the FDA guidance, the coefficient of determination (R^2) has to be higher than 0.96 and at least 75% of all calibrators should be valid. Furthermore, for both levels: LLOQ and ULOQ, only one value could be omitted.

2.3.2. Regression parameters

Two sets of seven calibrators (ranging from 30.0 to 3000 ng/ml) were injected at the beginning and at the end of each analytical run, starting from the lower limit of quantification (LLOQ = 30.0 ng/ml) to the upper limit of quantification (ULOQ = 3000 ng/ml). The calibration curve was validated by six QCs (duplicates of QCL, QCM and QCH), which were inserted randomly into the analytical run.

2.3.3. Carry-over

To evaluate the carry-over of analyte and I.S. in each analytical run, an extracted RHB blank was injected immediately after the ULOQ (3000 ng/ml) of both sets of calibrators. Mean carry-over ($n = 2$) in the blank sample following the ULOQ should not exceed 20% of the signal of the LLOQ (30.0 ng/ml) for indolinone and 5% for I.S.

2.3.4. Selectivity

Six QC samples of indolinone at the LLOQ (duplicates, three different batches of RHB) were extracted and injected within a validation run into the UPLC–MS/MS system. Selectivity imprecision (CV%) had to be below 20% and inaccuracy (RE%) had to be within $\pm 20\%$ of the nominal values. Moreover, only one QC sample of each RHB batch was allowed to have an inaccuracy of more than $\pm 20\%$.

2.3.5. Specificity

A total of six blank samples (duplicates, three different batches of RHB) without the addition of indolinone and I.S. were injected into the UPLC–MS/MS within an analytical run and quantified by means of a valid calibration curve. For all three batches of RHB, the peak areas evaluated in the blank samples were not allowed to exceed 20% of the mean LLOQ peak area.

2.3.6. Intra-run and inter-run repeatability

Six replicates of QCs at five concentration levels (30.0, 90.0, 1500, 2400, 3000 ng/ml) were processed and injected into the UPLC–MS/MS. To ensure the reproducibility, these sets of QCs were tested within three validation runs on three different days. In each run, intra-run imprecision (CV%) of each QC series had to be below 15% (20% at the LLOQ) and intra-run inaccuracy (RE%) had to be within $\pm 15\%$ of the nominal values ($\pm 20\%$ at the LLOQ). At the end of the three series, inter-run imprecision and inaccuracy were assessed by calculating the overall mean and standard deviation (SD) for each QC level. The acceptance criteria for imprecision (CV%) and inaccuracy (RE%) were the same as described above.

2.3.7. Extraction yield

The absolute recovery of the analyte was calculated using six replicates of indolinone at low (90.0 ng/ml), medium (1500 ng/ml), and high concentration (2400 ng/ml) which were spiked with I.S. after extraction compared to six blank RHB samples which were

spiked with indolinone at three concentration levels (90.0, 1500, and 2400 ng/ml) and I.S. after extraction.

The extraction yield of I.S. was calculated by comparison of six processed samples containing I.S. which were spiked with indolinone at medium level (1500 ng/ml) after extraction versus six replicates of blank RHB samples which were spiked with I.S. and indolinone (1500 ng/ml) after extraction.

2.3.8. Dilution test

In order to demonstrate that the dilution of samples at higher concentration levels than the ULOQ (3000 ng/ml) did not affect the reliability of the method, a dilution test was performed. For this purpose, the matrix was spiked with the WS of indolinone (100 µg/ml) to obtain a final concentration of 15 000 ng/ml (*i.e.* 5 × ULOQ). This solution was further serially diluted to give six replicates at a concentration of 1500 ng/ml (10-fold dilution) and six replicates at a concentration of 150 ng/ml (100-fold dilution). Concentrations of the replicates of each dilution level were calculated using a valid calibration curve. Furthermore, the resulting mean concentration, imprecision, and inaccuracy were calculated. According to guidelines [2,3], the imprecision (CV%) had to be below 15% and the inaccuracy had to be within ±15% of the nominal value.

2.3.9. Short-term stabilities of indolinone in Ringer HEPES buffer

2.3.9.1. Freeze and thaw cycles below –65 °C. Six replicates of QCL (90.0 ng/ml) and QCH (2400 ng/ml) were exposed to three freeze (below –65 °C, storage time > 24 h) and thaw (at RT) cycles before they were processed and quantified using a valid calibration curve. At both concentration levels, the imprecision (CV%) had to be below 15% and the inaccuracy (RE%) had to be within ±15% of the nominal value.

2.3.9.2. Biological sample stability on benchtop at RT. Six replicates of QCL (90.0 ng/ml) and QCH (2400 ng/ml) were stored at RT for 4 h and quantified using a valid calibration curve. At both concentration levels, the imprecision (CV%) had to be below 15% and the inaccuracy (RE%) had to be within ±15% of the nominal value.

2.3.9.3. Processed sample stability in the autosampler at 10 °C. Six replicates of QCL (90.0 ng/ml) and QCH (2400 ng/ml) were processed and quantified using a valid calibration curve. All QCs were stored for 28 h in the autosampler (set at 10 °C, protected from light) before they were re-injected and re-analyzed with freshly prepared calibrators and QCs. At both concentration levels, the imprecision (CV%) had to be below 15% and the inaccuracy (RE%) had to be within ±15% of the nominal value.

2.3.10. Long-term stability below –65 °C

Three replicates of RHB samples freshly prepared at low, medium and high concentration (90.0, 1500, 2400 ng/ml) were quantified at time zero ($t=0$). Three other replicates at the same concentration levels (90.0, 1500, 2400 ng/ml) were stored below –65 °C. After 16 days of storage, the samples were processed and quantified by means of a valid calibration curve which consisted of two sets of freshly prepared calibrators and QCs. The mean values of each concentration level at 16 days were calculated and compared to the mean values of the appropriate concentration from the first day ($t=0$) of the long-term stability test. The results of $t=16$ days were plotted in function of $t=0$ and a linear regression, forced through zero, was performed. To confirm the stability of the samples, the slope had to be within 1 ± 0.15 .

2.3.11. Stock solutions stability test

According to the FDA guideline, the eventual degradation should not exceed the threshold of 5% for both compounds [2].

2.4. Blood–brain barrier permeability screening

2.4.1. Immortalized mono-culture human *in vitro* BBB model

Indolinone was screened in a human *in vitro* BBB model which we previously established using immortalized human brain microvascular endothelial cells (hBMEC cell line) [25,30]. Culture medium for hBMEC cells was EBM-2 supplemented with hydrocortisone, ascorbic acid, heparin, antibiotic-antimycotic solution, and 20% fetal bovine serum (FBS).

For the *in vitro* BBB model, hBMEC cells were seeded at a density of 6.0×10^4 cells/cm² on the apical side of collagen-coated filter membranes of 24-well tissue culture inserts from Greiner Bio-one® (transparent PET membrane, 3.0 µm pore size, 0.6×10^6 pores/cm²). The tissue culture inserts were transferred into a 24-well cell module of a CellZscope system (NanoAnalytics, Münster, Germany) [31], incubated at 37 °C (5% CO₂), and transendothelial electrical resistance (TEER) values were recorded in real-time every hour. After 50 h, at a TEER value of $40.8 \pm 0.884 \Omega \text{ cm}^2$ (Fig. 4), the permeability assay for indolinone was carried out as follows. The tissue culture inserts were transferred into a 24-well plate containing 1200 µl of pre-warmed (37 °C) RHB in each well (basolateral compartment). Medium in inserts (apical compartment) was subsequently replaced with 300 µl of a pre-warmed (37 °C) WS containing indolinone (5 µM) and sodium fluorescein (Na-F) as integrity control marker (10 µg/ml) in RHB. The 24-well plate was incubated at 37 °C on an orbital shaker (ELMI DTS-2, Riga, Latvia) with moderate speed (100 rpm) and aliquots of 250 µl of both apical and basolateral compartments were collected after 1 hour. Quantification of Na-F fluorescence was carried out using a Chameleon microplate reader (Hidex, Turku, Finland). Quantification of indolinone was done by LC–MS/MS. All experiments were performed bidirectionally and in triplicate.

2.4.2. Animal *in vitro* BBB models

2.4.2.1. Primary co-culture rat/bovine *in vitro* BBB model. The method of Dehouck et al. [32] was used with minor modifications. Bovine brain capillary endothelial cells (BBECs) isolated from capillary fragments were co-cultured with primary mixed glial cells from newborn Sprague-Dawley rats. The glial cells were isolated according to the method of Booher and Sensenbrenner [33] and cultured for 3 weeks, plated on the bottom of cell culture clusters containing six wells each. The BBECs were seeded onto collagen-coated 6-well tissue culture inserts which were placed in the wells containing glial cells. The medium used for the co-culture was Dulbecco's modified Eagle's medium (DMEM, Life technologies, Saint Aubin, France) supplemented with 10% (v/v) newborn calf serum (Integro b.v., Zaandam, Netherlands), 10% (v/v) horse serum (Life technologies), 2 mM glutamine (Sigma Aldrich), 50 µg/ml gentamycin, and 1 ng/ml of basic fibroblast growth factor (bFGF, Sigma Aldrich). The medium was changed every second day. Under these conditions, BBECs formed a confluent monolayer after 5 days. The permeability assay for indolinone was carried out 7 days after confluency by transferring BBEC monolayers to six-well plates containing 2.5 ml of RHB per well. The solution containing 5 µM indolinone and 1 µM Na-F, used as integrity control marker, in RHB was added to the cell monolayer (1.5 ml for 6-well plate filters), and the plates were placed on an orbital shaker. After 1 hour, aliquots were taken from both compartments. Quantification of Na-F fluorescence was carried out using a Synergy H1 multiplates reader (BioTek Instruments, Winooski, USA). Quantification of indolinone was done by LC–MS/MS. All experiments were performed in triplicate. The mean TEER value after 7 days in co-culture with rat primary glial cells was in the range of 350–400 Ω cm² [34].

2.4.2.2. Primary triple co-culture rat *in vitro* BBB model. Primary rat brain capillary endothelial cells (RBECs) were isolated from 3-week-old Wistar rats, similarly as described earlier [35,36]. Fore-brains were collected in sterile phosphate buffered saline (PBS) on ice, and meninges were removed using heat sterilized filter paper. Gray matter was cut by scalpels into 1 mm³ pieces which were digested in Dulbecco's modified Eagle's medium (DMEM, Life Technologies, Gibco, USA) with 1 mg/ml collagenase (Worthington, USA) and deoxyribonuclease type I (DNase I, Roche, USA) for 50 min at 37 °C. Microvessels were separated by a gradient centrifugation in 20% BSA–DMEM (1000 × g, 20 min) from myelin, and this step was repeated three times. The isolated and pooled fraction was further digested with 1 mg/ml collagenase–dispase (Roche, USA) and DNase I in DMEM for 30 min. From the digested cell suspension, brain endothelial cell clusters were separated on a 33% Percoll gradient (Sigma Aldrich, USA) (1000 × g, 10 min), collected and washed twice in cell culture medium before plating on 60 mm Petri dishes (Orange, Belgium) coated with collagen type IV and fibronectin (Sigma Aldrich, USA). RBECs were cultured in DMEM/F12 supplemented with 15% plasma-derived bovine serum (First Link, UK), 1 ng/ml basic fibroblast growth factor (bFGF, Roche, USA), insulin (5 μg/ml), transferrin (5 μg/ml), sodium selenite (5 ng/ml) (insulin-transferrin-sodium selenite media supplement, Sigma Aldrich, USA), 100 μg/ml heparin (Sigma Aldrich, USA) and 50 μg/ml gentamicin (Sigma Aldrich, USA). In the first 4 days, cell culture medium contained puromycin (3 μg/ml, Sigma Aldrich, USA) to selectively eliminate P-gp negative contaminating cell types [37]. When cultures reached 90% confluency (fourth day in dish), the puromycin treated RBECs were passaged to the apical side of the collagen type IV and fibronectin coated filter membranes of 24-well tissue culture inserts from Greiner Bio-one® (transparent PET membrane, 3.0 μm pore size) at a cell number of 2.5 × 10⁴ cells/insert and used for the permeability experiments. To induce BBB characteristics, RBECs were co-cultured with rat cerebral glial cells and rat pericytes [27].

Primary cultures of rat mixed glial cells were obtained from 1-day-old Wistar rats [35,36]. Meninges were removed by forceps on a small drop of PBS, then cortical pieces were mechanically dissociated by pressing the tissue through a nylon mesh (40 μm, Millipore, USA) in DMEM containing 10% FBS (Lonza, Switzerland) and 50 μg/ml gentamicin. Dissociated cell clusters were plated on 5 μg/ml poly-L-lysine (Sigma Aldrich, USA) coated 24-well plates from Greiner Bio-One® and cultured for at least 2 weeks before use. In confluent glia cultures 89% of cells were positively stained for the astroglia cell marker glial fibrillary acidic protein (GFAP), while the remaining 11% were positive for CD11b, a microglia marker.

Cultures of rat brain microvessel pericytes were prepared by a 3-week long culture of isolated rat brain capillary fragments which contained a high number of pericytes besides endothelial cells. The same microvessel isolation yielded RBECs, and pericytes if puromycin-treatment was omitted. Cell survival and proliferation were helped by selective culture conditions using uncoated dishes and DMEM (Life Technologies, Gibco, low glucose) supplemented with 10% FBS and antibiotics. Culture medium was changed every 3 days. Rat brain microvessel pericyte cultures were positive for α-smooth muscle actin, NG2 and PDGFRβ immunostaining, and negative for von Willebrand factor and GFAP markers [38].

To assemble the BBB model from the three cell-types, Greiner Bio-one® tissue culture inserts were put into 24-well plates containing glia at the bottom of the wells. Pericytes at passage number 3 were seeded on the bottom side of the inserts (basolateral) and RBECs were passaged to the upper side of the coated inserts (apical) with endothelial culture medium in both compartments [27]. After 2 days of co-culturing, 550 nM hydrocortisone (Sigma Aldrich, USA) was added to the culture medium [39]. Before experiments, cells were treated with 8-(4-chlorophenylthio)-adenosine-3',5'-cyclic monophosphate (CPT-cAMP, 250 μM, Sigma Aldrich, USA) and RO

20-1724 (17.5 μM, Roche) for 24 h to tighten junctions and elevate resistance [37,39].

At a TEER value of 427.8 ± 62.9 Ω cm² (day 4 of co-culture), the permeability assay for indolinone was performed. Before the experiment, working solutions consisting of indolinone (5 μM) and Na-F (10 μg/ml) for layer integrity control were prepared in pre-warmed (37 °C) RHB. To protect cell layer integrity, RHB contained 0.1% BSA. Tissue culture inserts with RBECs and pericytes were transferred into a new 24-well plate containing 700 μl of RHB for apical to basolateral (A to B) permeability measurements or 700 μl working solution for basolateral to apical (B to A) transport assays. Medium in inserts (apical compartment) was subsequently replaced with 300 μl working solution for A to B or 300 μl RHB for B to A transport tests. The 24-well plate was incubated at 37 °C on a horizontal shaker (100 rpm, Biosan, Latvia) for 1 h. Aliquots of 250 μl and 650 μl were collected from the apical and basolateral compartments and stored below –65 °C until analysis. Concentration of Na-F was measured by a Fluostar Optima fluorescent multiplate reader (BMG Labtechnologies, Germany).

2.4.3. BBB permeability calculation

The apparent permeability coefficient (P_{app}) for indolinone and Na-F was calculated in centimeters per second (cm/s) according to the equation [40]:

$$P_{app} \text{ (cm/s)} = \frac{V_R}{A C_{D0}} \times \left(\frac{\Delta C_R}{\Delta t} \right)$$

where V_R is the volume in the receiver compartment, A is the surface area of the filter membrane (0.336 cm² for 24-well inserts, 4.7 cm² for six-well inserts), C_{D0} is the initial concentration in the donor compartment, and $\Delta C_R/\Delta t$ is the change of concentration over time in the receiver compartment.

Recovery for indolinone and Na-F was calculated according to the equation:

$$\text{Recovery (\%)} = \frac{C_{Df} V_D + C_{Rf} V_R}{C_{D0} V_D} \times 100$$

where C_{Df} and C_{Rf} are the final concentrations of the compound in the donor and receiver compartments, respectively, C_{D0} is the initial concentration in the donor compartment, and V_D and V_R are the volumes in the donor and receiver compartments, respectively. All results are expressed as means ± S.E.M.

Low permeability and high efflux can be limiting factors for BBB penetration. A common way of quantifying P-gp interaction *in vitro* is by calculating the efflux ratio (ER) across P-gp expressing cell monolayers, which is defined as [41–45]:

$$\text{ER} = \frac{P_{app B \rightarrow A}}{P_{app A \rightarrow B}}$$

Compounds showing an ER > 2.0 usually indicate P-gp efflux.

To confirm that indolinone and Na-F did not attach to the plastic material and that the diffusion barrier was only provided by the cell monolayer, control experiments were performed using collagen-coated inserts without cells.

2.5. Transporter studies

2.5.1. Calcein-AM uptake in porcine brain capillary endothelial cells (PBCECs)

The calcein-AM uptake assay was performed in primary porcine brain capillary endothelial cells (PBCECs) seeded in 96-well plates (Corning Costar) at a density of 2.5 × 10⁵ cells/cm². Culture medium was Earl's Medium 199 (Biochrom, Berlin, Germany) supplemented with L-glutamine, penicillin, streptomycin, gentamycin, and FBS. After achieving confluence, the cells were used for the calcein assay as previously described [46]. Briefly, cells were washed twice with

pre-warmed Krebs–Ringer Buffer (KRB) and then incubated for 15 min with 100 μ l of 2 μ M calcein-AM in KRB at 37 °C. After this pre-incubation time, 100 μ l of indolinone at increasing concentrations in KRB was added to each well to achieve a final concentration of 5, 50, and 500 μ M indolinone. Stock solution of indolinone was prepared in DMSO. Dilutions were then made with KRB. The final concentration of DMSO on the cells did not exceed 1%. At this concentration, DMSO did not affect the assay [46]. After an incubation time of 30 min at 37 °C, the cells were washed twice with cold (5 °C) KRB and subsequently incubated with 200 μ l 1% Triton-X in KRB for 20 min. Fluorescence was measured in a plate reader (Tecan, Infinite F200 Pro) with an excitation/emission wavelength of 485/520 nm. Intracellular fluorescence was obtained by subtracting background fluorescence of control wells. Calcein uptake was expressed as % of control (KRB).

2.5.2. Cellular uptake assay

The cell uptake assay was also performed with PBCECs. The cells were treated as described above and also seeded in a 96-well plate [47]. Confluent cells were washed twice with KRB, then pre-incubated for 15 min at 37 °C with 200 μ l KRB. After removal of KRB, the cells were incubated with 200 μ l indolinone in KRB (100 and 1000 μ M) at 37 °C for 30 min. The cells were again washed twice with KRB, followed by incubation with 200 μ l 1% Triton-X in KRB for 30 min at 37 °C. Indolinone content was determined by LC–MS/MS as described in Section 2.2. The area of each well was 0.32 cm². Based on the presumption that the cell monolayer had a height of 3 μ m, the total volume of the cells in one well was 0.096 μ l. This volume was taken into consideration when the content of indolinone (in 200 μ l KRB) was calculated.

3. Results and discussion

3.1. Chromatographic performance and method validation

3.1.1. Chromatographic performance

Based on the slow inter-conversion at RT [9,28] of (*E,Z*)-3-(4-hydroxy-3,5-dimethoxybenzylidene)indolin-2-one (indolinone) (Fig. 1A), both *E* and *Z* isomers peak areas were integrated and quantified in RHB (Fig. 1). Since isotope-labeled indolinone was not available, the structurally related (*E,Z*)-3-(benzylidene)indolin-2-one was selected as I.S. (Fig. 1B) [22]. For quantification of analyte and I.S., an identical peak integration of both *E* and *Z* isomers was performed (Fig. 2). The calibration curve ranging from 30.0 to 3000 ng/ml was fitted by least-square quadratic regression, and a weighting factor of $1/X^2$ was applied. The mean coefficient of determination (R^2) was 0.9919 (Supplementary Table 1), and acceptance criteria were fulfilled [2,3] (Supplementary Table 1).

Supplementary table related to this article can be found, in the online version, at <http://dx.doi.org/10.1016/j.jpba.2014.05.026>.

3.1.2. Assessment of carry-over

The mean carry-over was 0.00% (acceptance criteria: below 20%) for indolinone (Fig. 2A) and 0.0839% (below 5%) for I.S. (Fig. 2B). Hence, the carry-over did not impact precision and accuracy of the method (Supplementary Table 2).

Supplementary table related to this article can be found, in the online version, at <http://dx.doi.org/10.1016/j.jpba.2014.05.026>.

3.1.3. Selectivity for indolinone

Selectivity imprecision (CV%) for the six samples at the LLOQ (duplicates, three different RHB batches) was 8.34% (below 20%) and inaccuracy (RE%) was –12.3% (within $\pm 20\%$), indicating that the quantification method was selective for indolinone (Supplementary Table 3).

Supplementary table related to this article can be found, in the online version, at <http://dx.doi.org/10.1016/j.jpba.2014.05.026>.

3.1.4. Specificity for indolinone

The peak areas measured in the blank RHB sample were 0.00% (below 20%), demonstrating that the method was specific for indolinone (data not shown).

3.1.5. Intra-run and inter-run repeatability for indolinone

Intra-run imprecision (CV%) was 6.29% (below 20%) for the LLOQ, and 1.88–5.62% (below 15%) of the nominal value for all the other QCs (Supplementary Table 4). The inaccuracy (RE%) was 6.57% (within $\pm 20\%$) for the LLOQ and –10.1% to 2.33% (within $\pm 15\%$) of the nominal values for the other QC levels (Supplementary Table 4). Inter-run imprecision (CV%) ranged from 1.49% to 5.87% (below 20% for LLOQ, and below 15% for all other QC levels), and the inaccuracy (RE%) was between –9.50% and –0.0589% (below 20% for LLOQ, and below 15% for all other QC levels) (Supplementary Table 4). According to international guidelines [2,3], the method was thus precise and accurate.

Supplementary table related to this article can be found, in the online version, at <http://dx.doi.org/10.1016/j.jpba.2014.05.026>.

3.1.6. Extraction yield

The absolute recovery of indolinone was 81.5% for QCL (90.0 ng/ml), 91.3% for QCM (1500 ng/ml), and 91.8% for QCH (2400 ng/ml) (Supplementary Table 5). For the I.S., an absolute recovery of 83.6% was determined (Supplementary Table 5). Consequently, the extraction yield was proven to be consistent, precise, and reproducible according to FDA guidance [2].

Supplementary table related to this article can be found, in the online version, at <http://dx.doi.org/10.1016/j.jpba.2014.05.026>.

3.1.7. Dilution test

For both QC series, imprecision (CV%) was below 15% (6.36% for dilution factor 100 and 4.48% for dilution factor 10), and inaccuracy (RE%) was within $\pm 15\%$ of the nominal values (–8.62% and 7.27%, respectively) (Supplementary Table 6). Hence, precision and accuracy of the method was not affected by dilution of samples up to 100-fold.

Supplementary table related to this article can be found, in the online version, at <http://dx.doi.org/10.1016/j.jpba.2014.05.026>.

3.1.8. Processed sample stability at autosampler conditions

At both concentration levels (90.0 ng/ml and 2400 ng/ml), imprecision (CV%) was below 15% (5.13% and 3.14%, respectively, data not shown), and inaccuracy (RE%) was within $\pm 15\%$ of the nominal values (–0.191% and –11.5%, respectively) (Supplementary Table 7). Thus, processed samples of indolinone proved to be stable for at least 28 h at autosampler conditions (10 °C, protected from light).

Supplementary table related to this article can be found, in the online version, at <http://dx.doi.org/10.1016/j.jpba.2014.05.026>.

3.1.9. Freeze and thaw cycle stability

Imprecision (CV%) for the six replicates at the QCL (90.0 ng/ml) and the QCH (2400 ng/ml) was below 15% (4.69% and 3.52%, respectively, data not shown), and inaccuracy (RE%) was within $\pm 15\%$ (12.6% and 0.564%, respectively) (Supplementary Table 7), demonstrating that indolinone stored below –65 °C in RHB was stable for at least three freeze and thaw cycles.

3.1.10. Biological samples stability on benchtop at RT

Imprecision (CV%) for the six replicates of QCL (90.0 ng/ml) and QCH (2400 ng/ml) exceeded 15%, and inaccuracy was not within

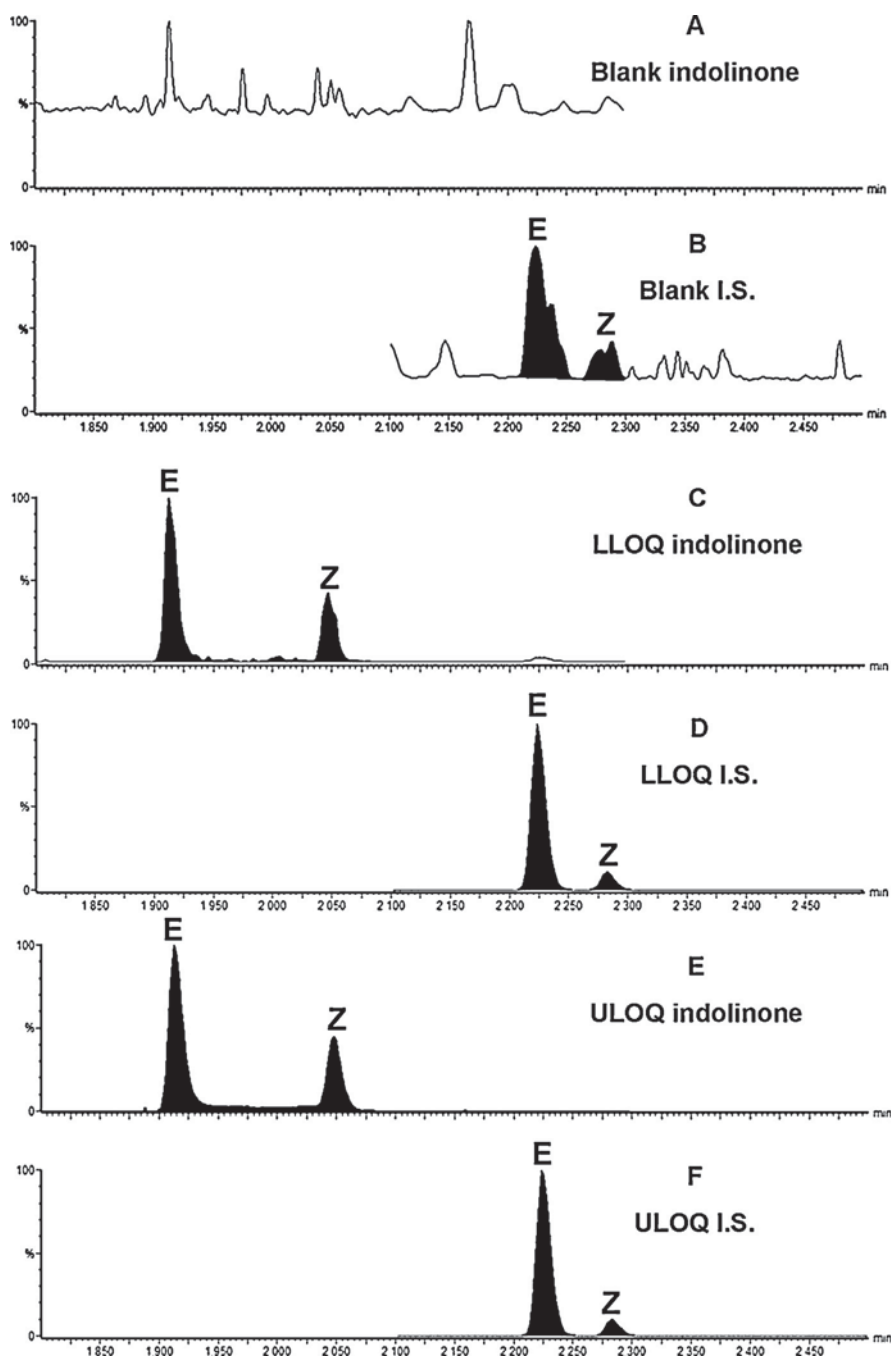


Fig. 2. Typical MRM chromatograms of blank RHB injected after the ULOQ and monitored for indolinone (A) and for I.S. (B), of RHB spiked at 30.0 ng/ml (LLOQ) of indolinone (C), and 1000 ng/ml of I.S. (D), of RHB spiked at 3000 ng/ml (ULOQ) of indolinone (E) and 1000 ng/ml of I.S. (F).

$\pm 15\%$ of the nominal values, indicating that indolinone was not stable when stored for 4 h at RT (data not shown). For this reason, the benchtop stability test was reduced to 3 h. Under these new conditions, imprecision (CV%) for the six replicates at low concentration (90.0 ng/ml) was 3.13%, and for the six replicates at high concentration (2400 ng/ml) it was 2.43% (data not shown). Inaccuracy (RE%) was 5.38% and -4.40% , respectively (Supplementary Table 7). Consequently, samples were shown to be stable for 3 h under benchtop conditions (RT) (Supplementary Table 7).

3.1.11. Biological samples long-term stability below -65°C

As the slope of the calculated linear regression was 0.900 (acceptance criteria: 1 ± 0.15), the stability of the samples stored below -65°C for 16 days could be confirmed (Fig. 3).

3.1.12. Stock solutions stability test

Our previous study demonstrated that stock solutions of indolinone and I.S. stored below -65°C for 190 days and kept for ca. 6 h at RT were stable, since the degradation expressed by the difference percentage (-1.11% and -1.46% for indolinone and I.S., respectively) was below 5% [22].

3.2. *In silico* prediction of blood–brain barrier permeability

In silico methods are nowadays routinely used for a rapid assessment of physico-chemical properties of compounds. Descriptor values averaged over the 18 low energy conformers of (E,Z)-indolinone show no violation of Lipinski's rule of five [21] (MW < 500, cLogP < 5, donorHB < 5, acceptHB < 10; Table 1) along

Table 1
Mean values of the most relevant *in silico* pharmacokinetic descriptors for (*E,Z*)-indolinone.

QikProp descriptors (3D)					Chemaxon Marvin (2D)				
Compound	MW	donorHB	acceptHB	cLogP _{o/w}	cLogBB	Human oral absorption (%)	PSA (Å ²)	cLogP _{o/w}	PSA (Å ²)
(<i>E,Z</i>)-indolin-2-one	297.30	2.00	4.75	2.44	−0.78	93.2	77.8	2.65	67.8

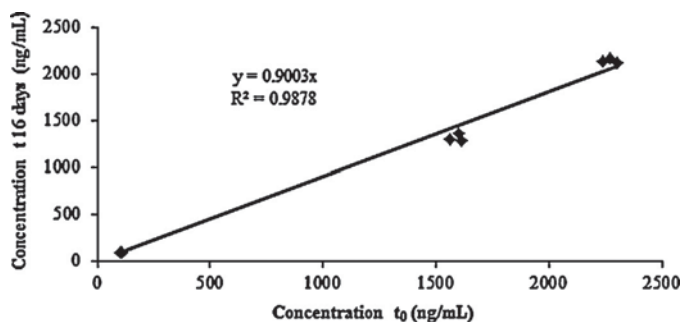


Fig. 3. Long-term stability (LTS) of indolinone in RHB for 16 days below -65°C .

with a high predicted human oral absorption (93.2%). The values of both 2D- and 3D-based PSA descriptor were not only well below the maximum acceptable threshold of 140 \AA^2 for good oral absorption, but also meet the criteria for a passive permeation through the BBB ($\text{PSA} < 90 \text{ \AA}^2$) [48]. Similarly, both predicted $\text{cLogP}_{o/w}$ values were within the range that is favorable for blood–brain transport. On the other hand, the specialized QikProp model for brain/blood partitioning predicted a cLogBB of -0.78 (usual range from -3.0 to 1.2) indicating a slight preference for the blood environment [49].

3.3. Blood–brain barrier screening

3.3.1. Human *in vitro* BBB model

In the *in vitro* BBB model with immortalized human brain capillary endothelial cells (hBMEC cell line) [25], the P_{app} of indolinone for apical to basolateral transport ($P_{\text{app A}\rightarrow\text{B}}$) was $19.2 \pm 0.485 \times 10^{-6} \text{ cm/s}$ (Table 2). Compared to the $P_{\text{app A}\rightarrow\text{B}}$ of the negative control Na-F ($3.20 \pm 0.0295 \times 10^{-6} \text{ cm/s}$), this value was considerably higher and suggested that indolinone may cross the BBB. The P_{app} value for basolateral to apical transport ($P_{\text{app B}\rightarrow\text{A}}$) was $21.7 \pm 0.326 \times 10^{-6} \text{ cm/s}$ (Table 3). The efflux ratio of 1.13 indicated no active efflux mediated transport for indolinone ($\text{ER} < 2.0$) [41–45].

The recovery of indolinone was $\geq 88.9\%$ in all experiments, suggesting that the obtained P_{app} values were reliable. A recovery above 80% is needed for an acceptable approximation of the P_{app} value [50]. After each permeability experiment, TEER values were determined, and they were found to be in the same range ($43.1 \pm 0.431 \Omega \text{ cm}^2$, Fig. 4) as before the assay. This indicated that barrier integrity of the cell monolayers was maintained throughout the experiments, and that indolinone did not affect cell layer integrity.

3.3.2. Animal *in vitro* BBB models

3.3.2.1. Primary co-culture rat/bovine *in vitro* BBB model. The P_{app} of Na-F in the presence of indolinone ($2.28 \pm 0.168 \times 10^{-6} \text{ cm/s}$) (Table 4) was in the same range as that of Na-F alone (data not shown). This result attested the integrity of the cell monolayer during the transport experiment. The $P_{\text{app A}\rightarrow\text{B}}$ ($27.1 \pm 1.67 \times 10^{-6} \text{ cm/s}$) was more than 10-fold higher than that of Na-F and hence, suggested high BBB permeability. Given that $P_{\text{app A}\rightarrow\text{B}}$ of indolinone across membranes with cells and control membranes (*i.e.* without cells) were very close, that data suggested that indolinone is freely diffusing across BBECS.

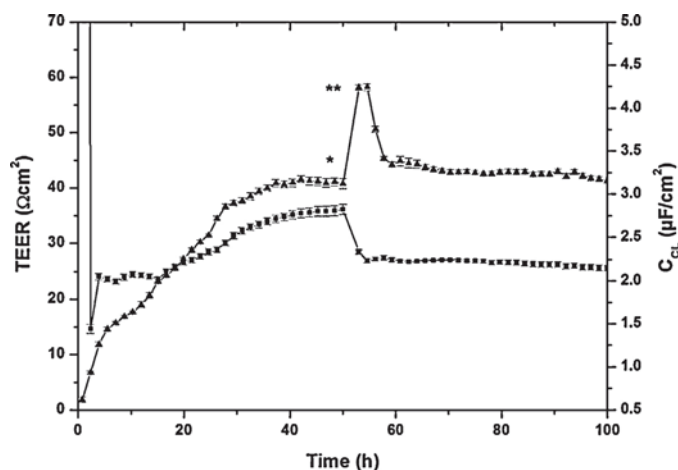


Fig. 4. Mean TEER values (▲) and C_{Cl} values (■) recorded real-time by the CellZscope system of hBMEC cells grown on 24-well tissue culture inserts. (*) Insert transfer to 24-well plate for indolinone permeability assay. (**) Insert transfer to CellZscope (37°C) for barrier integrity control.

3.3.2.2. Primary triple co-culture rat *in vitro* BBB model. The *in vitro* BBB model composed of primary RBECS, rat pericytes, and rat glial cells formed a tight barrier with a TEER value of $427.8 \pm 62.9 \Omega \text{ cm}^2$, and a $P_{\text{app A}\rightarrow\text{B}}$ $0.884 \pm 0.186 \times 10^{-6} \text{ cm/s}$ for Na-F (Table 5). The $P_{\text{app A}\rightarrow\text{B}}$ of indolinone was $56.2 \pm 3.63 \times 10^{-6} \text{ cm/s}$ (Table 5). Compared to the $P_{\text{app A}\rightarrow\text{B}}$ of the paracellular permeability marker Na-F this value was 60 times higher (Table 5) and hence, suggested that indolinone crossed the BBB very effectively. The P_{app} value of indolinone from basolateral to apical was $34.6 \pm 1.41 \times 10^{-6} \text{ cm/s}$ (Table 6). The efflux ratio was below 1 and indicated no active mediated efflux mechanism for indolinone ($\text{ER} < 2.0$) in the triple co-culture model. TEER values recorded after the experiments ($189.1 \pm 8.52 \Omega \text{ cm}^2$) were lower than prior to the assay. This could be explained by cell disturbance due to a switch from cell culture medium to buffer, and to the lack of barrier stabilizing factors from glial cells and culture medium. However, the resistance remained well above the threshold indicative of barrier tightness [39,51]. The Na-F permeability coefficients also indicated a preserved barrier function, and no harmful effect of indolinone on RBECS.

3.4. Transporter studies

3.4.1. Calcein-AM uptake in porcine brain capillary endothelial cells (PBCEC)

In PBCEC, the calcein assay is specific for assessing P-gp transport activity, and the known P-gp inhibitor verapamil (positive control) increased cellular calcein fluorescence by 500% compared to the control (KRB) (Fig. 5). Treatment with indolinone at 5, 50, and $500 \mu\text{M}$ led to no calcein accumulation, indicating that the compound was neither a P-gp substrate nor a P-gp inhibitor (Fig. 5).

3.4.2. Cellular uptake assay

The validated LC–MS/MS method for quantification of indolinone in RHB was used to quantify the content of indolinone in the lysing medium (mixture of KRB and 1% Triton). No analytical interferences were found showing that the RHB quantitative method can be applied to such an assay (data not shown).

Table 2
Screening of indolinone regarding its ability to cross the *in vitro* human BBB model using immortalized human brain capillary endothelial cells (hBMEC cell line) from the apical (A) to the basolateral (B) compartment ($n = 2-3$).

<i>In vitro</i> human BBB model (hBMEC cell line)	Transport direction	Samples	Time of withdrawal (min)	Mean concentration (ng/ml)	Mean amount (ng)	P_{app} of analyte \pm S.E.M. ($\times 10^{-6}$ cm/s)	P_{app} of Na-F \pm S.E.M. ($\times 10^{-6}$ cm/s)	Recovery of analyte (%)
Control inserts (without cells)	A to B	Donor compartment (300 μ l)	60	1272	381	–	–	–
		Receiver compartment (1200 μ l)	60	118	142	71.2	74.0	106 ^a
Inserts with cells	A to B	Donor compartment (300 μ l)	60	1337	401	–	–	–
		Receiver compartment (1200 μ l)	60	31.9	38.3	19.2 \pm 0.485	3.20 \pm 0.0295	88.9 ^a

^a The recovery was assessed with the experimental concentration of the WS (1647 ng/ml).

Table 3
Screening of indolinone regarding its ability to cross the *in vitro* human BBB model using immortalized human brain capillary endothelial cells (hBMEC cell line) from the basolateral (B) to the apical (A) compartment ($n = 2-3$).

<i>In vitro</i> human BBB model (hBMEC)	Transport direction	Samples	Time of withdrawal (min)	Mean concentration (ng/ml)	Mean amount (ng)	P_{app} of analyte \pm S.E.M. ($\times 10^{-6}$ cm/s)	P_{app} of Na-F \pm S.E.M. ($\times 10^{-6}$ cm/s)	Recovery of analyte (%)
Control inserts (without cells)	B to A	Donor compartment (1200 μ l)	60	1647	1976	–	–	–
		Receiver compartment (300 μ l)	60	328	98.5	49.4	50.2	105 ^a
Inserts with cells	B to A	Donor compartment (1200 μ l)	60	1448	1738	–	–	–
		Receiver compartment (300 μ l)	60	144	43.3	21.7 \pm 0.326	3.10 \pm 0.0231	90.1 ^a

^a The recovery was assessed with the experimental concentration of the WS (1647 ng/ml).

Table 4
Screening of indolinone regarding its ability to cross the *in vitro* animal BBB model using primary bovine capillary endothelial cells and primary rat brain glial cells from the apical (A) to the basolateral (B) compartment ($n = 3$).

<i>In vitro</i> primary triple co-culture BBB rat model	Transport direction	Samples	Time of withdrawal (min)	Mean concentration (ng/ml)	Mean amount (ng)	P_{app} of analyte \pm S.E.M. ($\times 10^{-6}$ cm/s)	P_{app} of Na-F \pm S.E.M. ($\times 10^{-6}$ cm/s)	Recovery of analyte (%)
Control inserts (without cells)	A to B	Donor compartment (2500 μ l)	60	1230	1844	–	–	–
		Receiver compartment (2500 μ l)	60	302	755	27.9 ± 1.19	24.2 ± 1.24	105 ^a
Inserts with cells	A to B	Donor compartment (300 μ l)	60	937	1406	–	–	–
		Receiver compartment (700 μ l)	60	303	757	27.1 ± 1.67	2.28 ± 0.168	87.3 ^a

^a The recovery was assessed with the experimental concentration of the WS (1669 ng/ml).

Table 5

Screening of indolinone regarding its ability to cross the *in vitro* animal BBB model using primary rat brain endothelial cells, pericytes and astrocytes from the apical (A) to the basolateral (B) compartment ($n = 3$ for control inserts, $n = 4$ for inserts with cells seeded).

<i>In vitro</i> primary triple co-culture BBB rat model	Transport direction	Samples	Time of withdrawal (min)	Mean concentration (ng/ml)	Mean amount (ng)	P_{app} of analyte \pm S.E.M. ($\times 10^{-6}$ cm/s)	P_{app} of Na-F \pm S.E.M. ($\times 10^{-6}$ cm/s)	Recovery of analyte (%)
Control inserts (without cells)	A to B	Donor compartment (300 μ l)	60	862	259	–	–	–
		Receiver compartment (700 μ l)	60	188	132	71.6 ± 0.813	124 ± 2.63	85.4 ^a
Inserts with cells	A to B	Donor compartment (300 μ l)	60	775	232	–	–	–
		Receiver compartment (700 μ l)	60	148	104	56.2 ± 3.63	0.884 ± 0.186	73.6 ^a

^a The recovery was assessed with the experimental concentration of the WS (1523 ng/ml).

Table 6
Screening of indolinone regarding its ability to cross the *in vitro* animal BBB model using primary rat brain endothelial cells, pericytes, and astrocytes from the basolateral (B) to the apical (A) compartment ($n = 3$ for control inserts, $n = 4$ for inserts with cells seeded).

<i>In vitro</i> primary triple co-culture BBB rat model	Transport direction	Samples	Time of withdrawal (min)	Mean concentration (ng/ml)	Mean amount (ng)	P_{app} of analyte \pm S.E.M. ($\times 10^{-6}$ cm/s)	P_{app} of Na-F \pm S.E.M. ($\times 10^{-6}$ cm/s)	Recovery of analyte (%)
Control inserts (without cells)	B to A	Donor compartment (700 μ l)	60	1068	748	–	–	–
		Receiver compartment (300 μ l)	60	172	51.5	28.0 \pm 2.18	39.2 \pm 7.45	7.05 ^a
Inserts with cells	B to A	Donor compartment (700 μ l)	60	984	689	–	–	–
		Receiver compartment (300 μ l)	60	212	63.6	34.6 \pm 1.41	0.378 \pm 0.115	70.6 ^a

^a The recovery was assessed with the experimental concentration of the WS (1523 ng/ml).

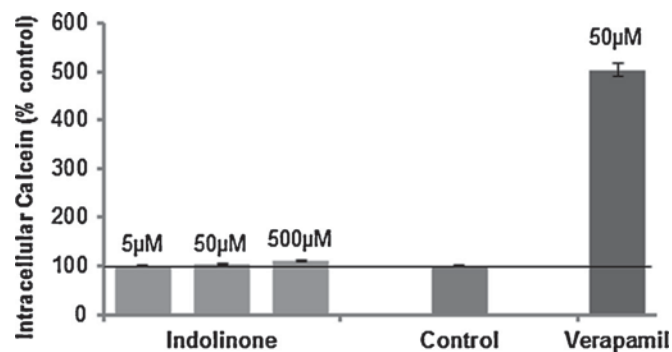


Fig. 5. Calcein-AM uptake assay in primary porcine brain capillary endothelial cells (PBCECs). Indolinone was tested at 5, 50, and 500 μ M in KRB. Pure KRB was used as control. Verapamil (50 μ M, P-gp inhibitor) was used as positive control.

At 100 μ M of indolinone, all measured concentrations were below the LLOQ of the method (30.0 ng/ml), whereas at 1000 μ M of indolinone, the concentration inside the cells was 433.3 μ M after 30 min, demonstrating that indolinone can easily penetrate PBCEC layers.

4. Conclusions

We developed a LC–MS/MS method for (*E,Z*)-3-(4-hydroxy-3,5-dimethoxybenzylidene)indolin-2-one (indolinone) in RHB and validated the assay according to EMA and FDA guidelines [2,3]. (*E,Z*)-3-(Benzylidene)-indolin-2-one, a closely related synthetic compound, was used as I.S. [22]. The standard calibration curve of indolinone in RHB in the range of 30.0–3000 ng/ml was quadratic and a weighting factor of $1/X^2$ was applied. The LLOQ was 30.0 ng/ml. Dilution of samples up to 100-fold did not affect precision and accuracy. The carry-over was within the acceptance criteria. Indolinone was stable for 3 h at RT, and for three successive freeze and thaw cycles. The processed samples could be stored in the autosampler at 10 °C for at least 28 h. Moreover, indolinone was stable for at least 16 days in RHB when stored below –65 °C. These data demonstrated that the method was selective, specific, precise, accurate, and capable of producing reliable results. A comparison of two *in vitro* primary animal BBB models (co-culture bovine/rat BBB model, and triple co-culture rat brain endothelial cells/pericytes/astrocytes BBB model) and an immortalized monoculture human model (hBMEC cell line) as a possible surrogate BBB model were used for screening indolinone regarding its ability to cross the BBB. The data obtained with the two well-established animal *in vitro* BBB models showed good correlation with our human *in vitro* mono-culture model and were indicative of a high BBB permeation potential of indolinone. These findings were corroborated by *in silico* prediction of BBB penetration. Finally, calcein-AM and uptake assays showed that indolinone accumulated in PBCECs and was neither a P-gp inhibitor nor a P-gp substrate. This was confirmed by calculation of the efflux ratio which was found to be lower than 2. The validated LC–MS/MS assays will be used for further bioavailability studies addressing oral bioavailability and pharmacokinetic properties.

Conflict of interest

None declared.

Acknowledgments

We are grateful to Prof. K.S. Kim and Prof. D. Grab (Johns Hopkins University, Baltimore, MD, USA) for provision of the hBMEC

cell line through the Swiss Tropical and Public Health Institute, Basel, Switzerland (Swiss TPH, Prof. R. Brun). Financial support from the Swiss National Science Foundation (project 105320.126888) is gratefully acknowledged. Thanks are due to Dr. Melanie Raith for the synthesis of indolinone and to Orlando Fertig for excellent technical assistance.

References

- [1] S. Kiefer, A.C. Mertz, A. Koryakina, M. Hamburger, P. Küenzi, (E,Z)-3-(3',5'-dimethoxy-4'-hydroxy-benzylidene)-2-indolinone blocks mast cell degranulation, *Eur. J. Pharm. Sci.* 40 (2010) 143–147.
- [2] Guideline on Bioanalytical Method Validation, European Medicines Agency (EMA/CHMP/EWP/192217/2009), London, 21 July 2011.
- [3] Guidance for Industry: Bioanalytical Method Validation, US Food and Drug Administration (FDA), Center for Drug Evaluation and Research, May 2001.
- [4] M. Hamburger, *Isatis tinctoria* – from the rediscovery of an ancient medicinal plant towards a novel anti-inflammatory phytopharmaceutical, *Phytochem. Rev.* 1 (2002) 333–344.
- [5] J.B. Hurry, *The Woad Plant and its Dye*, AM Kelley, 1973.
- [6] Y.P. Zhu, *Chinese Materia Medica: Chemistry, Pharmacology, and Applications*, Harwood Academic Publishers, Amsterdam, 1998.
- [7] M.C. Recio, M. Cerda-Nicolas, O. Potterat, M. Hamburger, L. Rios, Anti-inflammatory and anti-allergic activity in vivo of lipophilic *Isatis tinctoria* extracts and tryptanthrin, *Planta Med.* 72 (2006) 539–546.
- [8] M.C. Recio, M. Cerda-Nicolas, M. Hamburger, L. Rios, Anti-arthritis activity of a lipophilic woad (*Isatis tinctoria*) extract, *Planta Med.* 72 (2006) 715–720.
- [9] G.U. Rüster, B. Hoffmann, M. Hamburger, Inhibitory activity of indolin-2-one derivatives on compound 48/80-induced histamine release from mast cells, *Pharmazie* 59 (2004) 236–237.
- [10] M. Hamburger, G.U. Rüster, M.F. Melzig, HPLC based activity profiling for inhibitors of human neutrophil elastase in *Isatis tinctoria* leaf extracts, *Nat. Prod. Commun.* 1 (2006) 1107–1110.
- [11] T. Kunikata, T. Tatefuji, H. Aga, K. Iwaki, M. Ikeda, M. Kurimoto, Indirubin inhibits inflammatory reactions in delayed-type hypersensitivity, *Eur. J. Pharmacol.* 410 (2000) 93–100.
- [12] T. Ishihara, K. Kohno, S. Ushio, K. Iwaki, M. Ikeda, M. Kurimoto, Tryptanthrin inhibits nitric oxide and prostaglandin E2 synthesis by murine macrophages, *Eur. J. Pharmacol.* 407 (2000) 197–204.
- [13] C. Oberthür, C. Heinemann, P. Elsner, E. Benfeldt, M. Hamburger, A comparative study on the skin penetration of pure tryptanthrin and tryptanthrin in *Isatis tinctoria* extract by dermal microdialysis coupled with isotope dilution ESI-LC-MS, *Planta Med.* 69 (2003) 385–389.
- [14] C. Oberthür, R. Jäggi, M. Hamburger, HPLC based activity profiling for 5-lipoxygenase inhibitory activity in *Isatis tinctoria* leaf extracts, *Fitoterapia* 76 (2005) 324–332.
- [15] H. Danz, D. Baumann, M. Hamburger, Quantitative determination of the dual COX-2/5-LOX inhibitor tryptanthrin in *Isatis tinctoria* by ESI-LC-MS, *Planta Med.* 68 (2002) 152–157.
- [16] H. Danz, S. Stoyanova, O.A.R. Thomet, H.-U. Simon, G. Dannhardt, H. Ulbrich, et al., Inhibitory activity of tryptanthrin on prostaglandin and leukotriene synthesis, *Planta Med.* 68 (2002) 875–880.
- [17] H. Danz, S. Stoyanova, P. Wippich, A. Brattström, M. Hamburger, Identification and isolation of the cyclooxygenase-2 inhibitory principle in *Isatis tinctoria*, *Planta Med.* 67 (2001) 411–416.
- [18] T. Mohn, I. Plitzko, M. Hamburger, A comprehensive metabolite profiling of *Isatis tinctoria* leaf extracts, *Phytochemistry* 70 (2009) 924–934.
- [19] S. Leclerc, M. Garnier, R. Hoessel, D. Marko, J.A. Bibb, G.L. Snyder, et al., Indirubins inhibit glycogen synthase kinase-3 β and CDK5/P25, two protein kinases involved in abnormal tau phosphorylation in Alzheimer's disease, *J. Biol. Chem.* 276 (2001) 251–260.
- [20] C. Heinemann, S. Schliemann-Willers, C. Oberthür, M. Hamburger, P. Elsner, Prevention of experimentally induced irritant contact dermatitis by extracts of *Isatis tinctoria* compared to pure tryptanthrin and its impact on UVB-induced erythema, *Planta Med.* 70 (2004) 385–390.
- [21] C.A. Lipinski, F. Lombardo, B.W. Dominy, P.J. Feeney, Experimental and computational approaches to estimate solubility and permeability in drug discovery and development settings, *Adv. Drug Deliv. Rev.* 46 (2001) 3–26.
- [22] M. Oufir, C. Sampath, V. Butterweck, M. Hamburger, Development and full validation of an UPLC-MS/MS method for the determination of an anti-allergic indolinone derivative in rat plasma, and application to a preliminary pharmacokinetic study, *J. Chromatogr. B* 902 (2012) 27–34.
- [23] K.M.M. Doan, J.E. Humphreys, L.O. Webster, S.A. Wring, L.J. Shampine, C.J. Serabjit-Singh, et al., Passive permeability and P-glycoprotein-mediated efflux differentiate central nervous system (CNS) and non-CNS marketed drugs, *J. Pharmacol. Exp. Ther.* 303 (2002) 1029–1037.
- [24] R. Kikuchi, S.M. de Morais, J.C. Kalvass, In vitro P-glycoprotein efflux ratio can predict the in vivo brain penetration regardless of biopharmaceutics drug disposition classification system class, *Drug Metab. Dispos.* 41 (2013) 2012–2017.
- [25] D.E. Eigenmann, G. Xue, K.S. Kim, A.V. Moses, M. Hamburger, M. Oufir, Comparative study of four immortalized human brain capillary endothelial cell lines, hCMEC/D3, hBMEC, TY10, and BB19, and optimization of culture conditions, for an in vitro blood–brain barrier model for drug permeability studies, *Fluids Barriers CNS* 10 (2013) 33.
- [26] R. Cecchelli, B. Dehouck, L. Descamps, L. Fenart, V. Buée-Scherrer, C. Duhem, et al., In vitro model for evaluating drug transport across the blood–brain barrier, *Adv. Drug Deliv. Rev.* 36 (1999) 165–178.
- [27] S. Nakagawa, M.A. Deli, H. Kawaguchi, T. Shimizudani, T. Shimono, A. Kittel, et al., A new blood–brain barrier model using primary rat brain endothelial cells, pericytes and astrocytes, *Neurochem. Int.* 54 (2009) 253–263.
- [28] L. Sun, N. Tran, F. Tang, H. App, P. Hirth, G. McMahon, et al., Synthesis and biological evaluations of 3-substituted indolin-2-ones: a novel class of tyrosine kinase inhibitors that exhibit selectivity toward particular receptor tyrosine kinases, *J. Med. Chem.* 41 (1998) 2588–2603.
- [29] T. Mohn, O. Potterat, M. Hamburger, Quantification of active principles and pigments in leaf extracts of *Isatis tinctoria* by HPLC/UV/MS, *Planta Med.* 73 (2007) 151–156.
- [30] M.F. Stins, J. Badger, K. Sik Kim, Bacterial invasion and transcytosis in transfected human brain microvascular endothelial cells, *Microb. Pathog.* 30 (2001) 19–28.
- [31] J. Wegener, D. Abrams, W. Willenbrink, H.-J. Galla, A. Janshoff, Automated multi-well device to measure transepithelial electrical resistances under physiological conditions, *Biotechniques* 37 (2004) 590.
- [32] M.-P. Dehouck, S. Méresse, P. Delorme, J.-C. Fruchart, R. Cecchelli, An easier, reproducible, and mass-production method to study the blood–brain barrier in vitro, *J. Neurochem.* 54 (1990) 1798–1801.
- [33] J. Booher, M. Sensenbrenner, Growth and cultivation of dissociated neurons and glial cells from embryonic chick, rat and human brain in flask cultures, *Neurobiology* 2 (1972) 97.
- [34] M. Boveri, V. Berezowski, A. Price, S. Slupek, A.-M. Lenfant, C. Benaud, et al., Induction of blood–brain barrier properties in cultured brain capillary endothelial cells: comparison between primary glial cells and C6 cell line, *Glia* 51 (2005) 187–198.
- [35] S. Veszelka, M. Pásztói, A.E. Farkas, I. Krizbai, N.T.K. Dung, M. Niwa, et al., Pentosan polysulfate protects brain endothelial cells against bacterial lipopolysaccharide-induced damages, *Neurochem. Int.* 50 (2007) 219–228.
- [36] S. Veszelka, A.E. Tóth, F.R. Walter, Z. Datki, E. Mózes, L. Fülöp, et al., Docosahexaenoic acid reduces amyloid- β induced toxicity in cells of the neurovascular unit, *J. Alzheimers Dis.* 36 (2013) 487–501.
- [37] N. Perriere, P.H. Demeuse, E. Garcia, A. Regina, M. Debray, J.-P. Andreux, et al., Puromycin-based purification of rat brain capillary endothelial cell cultures. Effect on the expression of blood–brain barrier-specific properties, *J. Neurochem.* 93 (2005) 279–289.
- [38] S. Nakagawa, M.A. Deli, S. Nakao, M. Honda, K. Hayashi, R. Nakaoka, et al., Pericytes from brain microvessels strengthen the barrier integrity in primary cultures of rat brain endothelial cells, *Cell. Mol. Neurobiol.* 27 (2007) 687–694.
- [39] M.A. Deli, C.S. Ábrahám, Y. Kataoka, M. Niwa, Permeability studies on in vitro blood–brain barrier models: physiology, pathology, and pharmacology, *Cell. Mol. Neurobiol.* 25 (2005) 59–127.
- [40] K.A. Youdim, A. Avdeef, N.J. Abbott, In vitro trans-monomer permeability calculations: often forgotten assumptions, *Drug Discovery Today* 8 (2003) 997–1003.
- [41] E. Kerns, L. Di, *Drug-Like Properties: Concepts, Structure Design and Methods: From ADME to Toxicity Optimization*, Academic Press, 2008.
- [42] N. Sjöstedt, H. Kortejärvi, H. Kidron, K.-S. Vellonen, A. Urtti, M. Yliperttula, Challenges of using in vitro data for modeling P-glycoprotein efflux in the blood–brain barrier, *Pharm. Res.* 31 (2014) 1–19.
- [43] Y. Uchida, S. Ohtsuki, Y. Katsukura, C. Ikeda, T. Suzuki, J. Kamiie, et al., Quantitative targeted absolute proteomics of human blood–brain barrier transporters and receptors, *J. Neurochem.* 117 (2011) 333–345.
- [44] J.W. Polli, S.A. Wring, J.E. Humphreys, L. Huang, J.B. Morgan, L.O. Webster, et al., Rational use of in vitro P-glycoprotein assays in drug discovery, *J. Pharmacol. Exp. Ther.* 299 (2001) 620–628.
- [45] K.M. Giacomini, S.-M. Huang, D.J. Tweedie, L.Z. Benet, K.L. Brouwer, X. Chu, et al., Membrane transporters in drug development, *Nat. Rev. Drug Discov.* 9 (2010) 215–236.
- [46] B. Bauer, D.S. Miller, G. Fricker, Compound profiling for P-glycoprotein at the blood–brain barrier using a microplate screening system, *Pharm. Res.* 20 (2003) 1170–1176.
- [47] M. Ott, M. Huls, M.G. Cornelius, G. Fricker, St John's wort constituents modulate P-glycoprotein transport activity at the blood–brain barrier, *Pharm. Res.* 27 (2010) 811–822.
- [48] D.F. Veber, S.R. Johnson, H.-Y. Cheng, B.R. Smith, K.W. Ward, K.D. Kopple, Molecular properties that influence the oral bioavailability of drug candidates, *J. Med. Chem.* 45 (2002) 2615–2623.
- [49] H. van de Waterbeemd, G. Camenisch, G. Folkers, J.R. Chretien, O.A. Raevsky, Estimation of blood–brain barrier crossing of drugs using molecular size and shape, and H-bonding descriptors, *J. Drug Target.* 6 (1998) 151–165.
- [50] I. Hubatsch, E.G. Ragnarsson, P. Artursson, Determination of drug permeability and prediction of drug absorption in Caco-2 monolayers, *Nat. Protoc.* 2 (2007) 2111–2119.
- [51] P.J. Gaillard, A.G. de Boer, Relationship between permeability status of the blood–brain barrier and in vitro permeability coefficient of a drug, *Eur. J. Pharm. Sci.* 12 (2000) 95–102.

3.2 Pharmacokinetics and *in vitro* blood-brain barrier screening of the plant-derived alkaloid tryptanthrin

Evelyn A. Jähne, Daniela E. Eigenmann, Chethan Sampath, Veronika Butterweck, Maxime Culot, Roméo Cecchelli, Fabien Gosselet, Fruzsina R. Walter, Mária A. Deli, Martin Smieško, Matthias Hamburger, and Mouhssin Oufir

Planta Medica 82 (2016) 1021-1029

DOI: 10.1055/s-0042-105295

In the present study, we evaluated the key pharmacokinetic (PK) properties of the anti-inflammatory alkaloid indolo[2,1-b]quinazoline-6,12-dione (tryptanthrin, **Fig. 2**), isolated from the ancient medicinal plant *Isatis tinctoria* L.. Moreover, we studied the ability of the compound to cross the BBB. For this purpose, UPLC-MS/MS quantification methods in lithium heparinized rat plasma and Ringer HEPES buffer (RHB) were validated according to international guidelines. In the second part of our work, we applied the validated quantification methods to a preliminary PK study in Sprague Dawley male rats (2 mg/kg b.w.) and to three human and animal *in vitro* BBB models. The results obtained from the three different *in vitro* BBB models suggested a high BBB permeation potential of tryptanthrin. From the bidirectional BBB models, an ER below 2 was calculated. Hence, tryptanthrin was not subjected to active mediated transport.

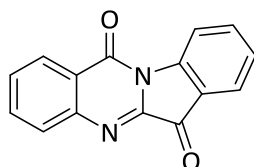


Fig.2: Indolo[2,1-b]quinazoline-6,12-dione (tryptanthrin)

My contributions to this publication: development and validation of the UPLC-MS/MS methods in lithium heparinized rat plasma and RHB, cultivation of human cells (hBMEC cell line), preparation of the immortalized human in vitro BBB model, design and performance of permeability experiments, sample preparation and analysis, PK data analysis using PKSolver, writing the manuscript draft, and preparation of figures and tables.

Evelyn Andrea Jähne

Pharmacokinetics and *In Vitro* Blood-Brain Barrier Screening of the Plant-Derived Alkaloid Tryptanthrin*

Authors

Evelyn A. Jähne¹, Daniela E. Eigenmann¹, Chethan Sampath², Veronika Butterweck^{2,3}, Maxime Culot⁴, Roméo Cecchelli⁴, Fabien Gosselet⁴, Fruzsina R. Walter⁵, Mária A. Deli⁵, Martin Smieško⁶, Matthias Hamburger¹, Mouhssin Oufir¹

Affiliations

The affiliations are listed at the end of the article

Key words

- tryptanthrin
- UPLC-MS/MS
- validation
- pharmacokinetics (PK)
- blood-brain barrier (BBB)

received January 19, 2016

revised March 3, 2016

accepted March 4, 2016

Bibliography

DOI <http://dx.doi.org/10.1055/s-0042-105295>
 Published online April 19, 2016
 Planta Med 2016; 82: 1021–1029 © Georg Thieme Verlag KG Stuttgart · New York · ISSN 0032-0943

Correspondence

Prof. Matthias Hamburger
 Division of Pharmaceutical Biology
 Department of Pharmaceutical Sciences
 University of Basel
 Klingelbergstrasse 50
 CH-4056 Basel
 Switzerland
 Phone: + 41 6 1267 1425
 Fax: + 41 6 1267 1474
matthias.hamburger@unibas.ch

Correspondence

Dr. Mouhssin Oufir
 Division of Pharmaceutical Biology
 Department of Pharmaceutical Sciences
 University of Basel
 Klingelbergstrasse 50
 CH-4056 Basel
 Switzerland
 Phone: + 41 6 1267 1544
 Fax: + 41 6 1267 1474
mouhssin.oufir@unibas.ch

Abstract

▼
 The indolo[2,1-b]quinazoline alkaloid tryptanthrin was previously identified as a potent anti-inflammatory compound with a unique pharmacological profile. It is a potent inhibitor of cyclooxygenase-2, 5-lipoxygenase-catalyzed leukotriene synthesis, and nitric oxide production catalyzed by the inducible nitric oxide synthase. To characterize the pharmacokinetic properties of tryptanthrin, we performed a pilot *in vivo* study in male Sprague-Dawley rats (2 mg/kg bw i.v.). Moreover, the ability of tryptanthrin to cross the blood-brain barrier was evaluated in three *in vitro* human and animal blood-brain barrier models. Bioanalytical UPLC-MS/MS methods used were validated according to current international guidelines. A half-life of 40.63 ± 6.66 min and a clearance of 1.00 ± 0.36 L/h/kg were found in the *in vivo* pharmacokinetic study. *In vitro* data obtained with the two primary animal blood-brain barrier models showed a good correlation with an immortalized human monoculture blood-brain barrier model (hBMEC cell line), and were indicative of a high blood-brain barrier permeation potential of tryptanthrin. These findings were corroborated by the *in silico* prediction of blood-brain barrier penetration. P-glycoprotein interaction of tryptanthrin was assessed by calculation of the efflux ratio in bidirectional permeability assays. An efflux ratio below 2 indicated that tryptanthrin is not subjected to active efflux.

Abbreviations

▼
 A: apical
 AUC: area under the curve
 B: basolateral

BBB: blood-brain barrier
 BBEC: bovine brain capillary endothelial cells
 C₀: concentration at time zero
 C_{Cl}: cell layer capacitance
 CL: clearance
 ER: efflux ratio
 EMA: European Medicines Agency
 FDA: Food and Drug Administration
 hBMEC: human brain microvascular endothelial cell line
 K_e: elimination rate constant
 I.S.: internal standard
 LLOQ: lower limit of quantification
 MRT: mean residence time
 NSAIDs: non-steroidal anti-inflammatory drugs
 P_{app}: apparent permeability coefficient
 PK: pharmacokinetic
 PSA: polar surface area
 QC: quality control
 QCH: quality control high
 QCL: quality control low
 QCM: quality control medium
 RBEC: primary rat brain capillary endothelial cells
 RHB: Ringer HEPES buffer
 SS: stock solution
 t_{1/2}: terminal half life
 TEER: transendothelial electrical resistance
 ULOQ: upper limit of quantification
 V₂: volume of distribution at terminal phase
 WS: working solution

Supporting information available online at <http://www.thieme-connect.de/products>

* Dedicated to Prof. Dr. Dr. h. c. mult. Kurt Hostettmann in recognition of his outstanding contribution to natural product research.

Introduction

We previously identified the indolo[2,1-b]quinazoline alkaloid tryptanthrin (● Fig. 1 A) as a pharmacologically active compound in the ancient anti-inflammatory plant *Isatis tinctoria* L. (Brassicaceae) [1–4]. The compound was found to possess a unique pharmacological profile, since it potently inhibits cyclooxygenase-2 (COX-2), 5-lipoxygenase (5-LOX)-catalyzed leukotriene synthesis *in vitro* and *in vivo* via a not yet clarified mechanism [1,2,5], and inducible nitric oxide synthase (iNOS)-catalyzed nitric oxide (NO) production [6]. Recent findings suggest that the dual inhibition of COX-2 and 5-LOX-catalyzed eicosanoid formation may provide a novel approach for the treatment of age-related neurodegenerative disorders such as Alzheimer's disease, given that the two enzymes are upregulated in the central nervous system in age-related brain pathologies [7]. Epidemiological studies have shown that prolonged use of NSAIDs such as ibuprofen reduces the risk, and delays the onset of Alzheimer's disease in arthritis patients [8]. Some of the current NSAIDs cross the BBB, but NSAIDs only inhibit cyclooxygenases. Thus, the unique pharmacological profile and a scaffold that completely differs from that of current NSAIDs render tryptanthrin a promising starting point for medicinal chemistry efforts. To further evaluate the potential of tryptanthrin as a new drug lead, we performed a pilot PK study in male Sprague-Dawley rats (2 mg/kg bw i.v.). The ability of tryptanthrin to cross the BBB was assessed in human and animal *in vitro* BBB models. For quantification of tryptanthrin in lithium heparinized rat plasma and RHB, UPLC-MS/MS methods were validated according to the guidelines of the FDA and the EMA [9, 10].

Results and Discussion

UPLC-MS/MS methods for tryptanthrin in lithium heparinized rat plasma and RHB were validated with respect to intra-run and inter-run repeatability, carryover, specificity, selectivity, extraction yield, dilution, and short-term/long-term stabilities. To fulfill the acceptance criteria of the FDA and EMA guidelines, imprecision (CV%) should be below 15% for all levels (20% for the LLOQ as the exception) and inaccuracy (RE%) should be within $\pm 15\%$ of the nominal value for all levels ($\pm 20\%$ of the nominal value for the LLOQ). The calibration curves in the range of 10.0–2000 ng/mL (rat plasma) and 20.0–2000 ng/mL (RHB) were fitted by quadratic regression with a $1/X$ weighting factor. The mean coefficients of determinations (R^2) were 0.999 (rat plasma) and 0.997 (RHB) (Tables 1 S and 2 S, Supporting Information). For all rat plasma QCs, the intra-run imprecision (CV%) was between 1.62% and 7.21% of the nominal values (Table 3 S, Supporting Information). Inaccuracy (RE%) was in the range of -13.2% to 9.41% of the nominal values (Table 3 S, Supporting Information). Inter-run imprecision (CV%) ranged from 3.11% to 7.10%, and inaccuracy (RE%) was between -11.8% and 7.74% (Table 3 S, Supporting Information). For the RHB method, intra-run imprecision ranged from 1.10% to 12.8% of the nominal values for all QC levels. The inaccuracy (RE%) was between -12.2% and 2.82% of the nominal values for all QC levels (Table 4 S, Supporting Information). Inter-run imprecision (CV%) ranged from 2.41% to 9.04%, and the inaccuracy (RE%) was between -7.54% and 3.66% (Table 4 S, Supporting Information). After sample extraction from lithium heparinized rat plasma, the mean carryover was 9.91% for tryptanthrin and 0.0696% for I.S. (● Fig. 2 and Table 5 S, Supporting Information).

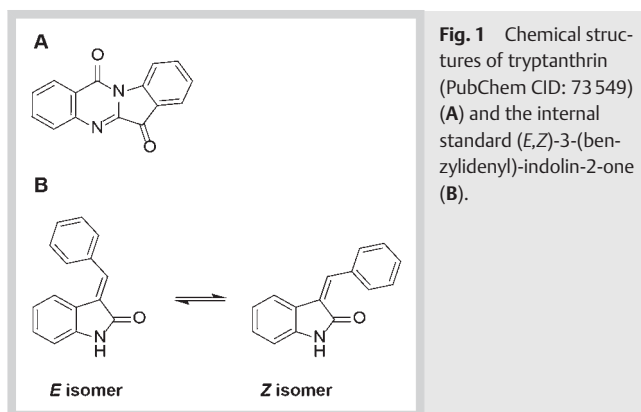


Fig. 1 Chemical structures of tryptanthrin (PubChem CID: 73 549) (A) and the internal standard (E,Z)-3-(benzylidene)-indolin-2-one (B).

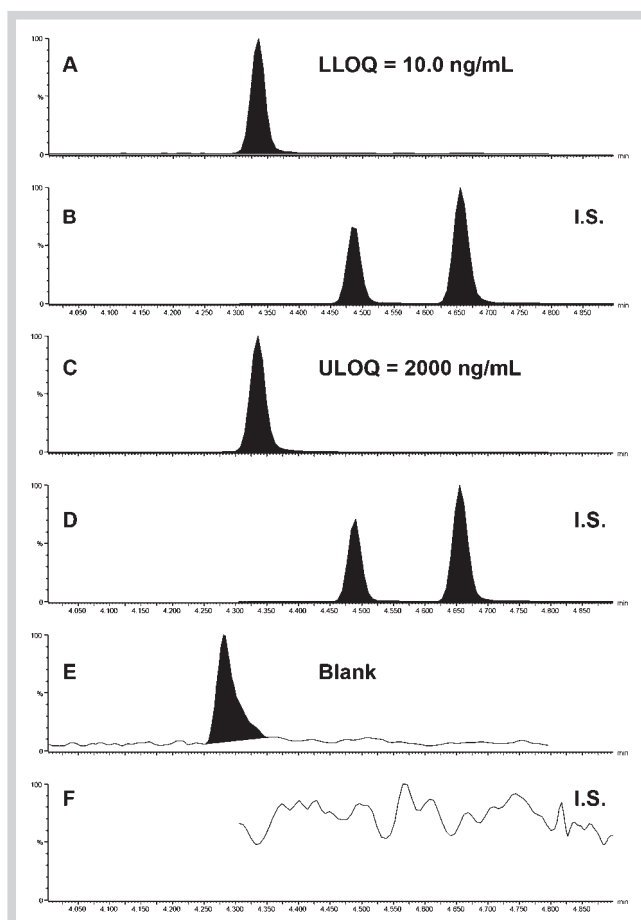


Fig. 2 Typical MRM chromatograms of lithium heparinized rat plasma spiked with 10.0 ng/mL (LLOQ) tryptanthrin (A) and 1000 ng/mL I.S. (B) of lithium heparinized rat plasma spiked with 2000 ng/mL (ULOQ) tryptanthrin (C) and 1000 ng/mL I.S. (D), and of blank lithium heparinized rat plasma injected directly after the ULOQ and monitored for tryptanthrin (E) and for the I.S. (F).

tion). The mean carryover of the RHB samples was 6.71% for tryptanthrin and 0.0793% (below 5%) for I.S. (● Fig. 3 and Table 6 S, Supporting Information). Selectivity imprecision (CV%) for the six rat plasma samples at the LLOQ (duplicates, three different plasma batches) was 7.68% (below 20%) and the inaccuracy (RE%) was 2.99% (within $\pm 20\%$) (Table 7 S, Supporting Information). For the method validation in RHB, selectivity imprecision

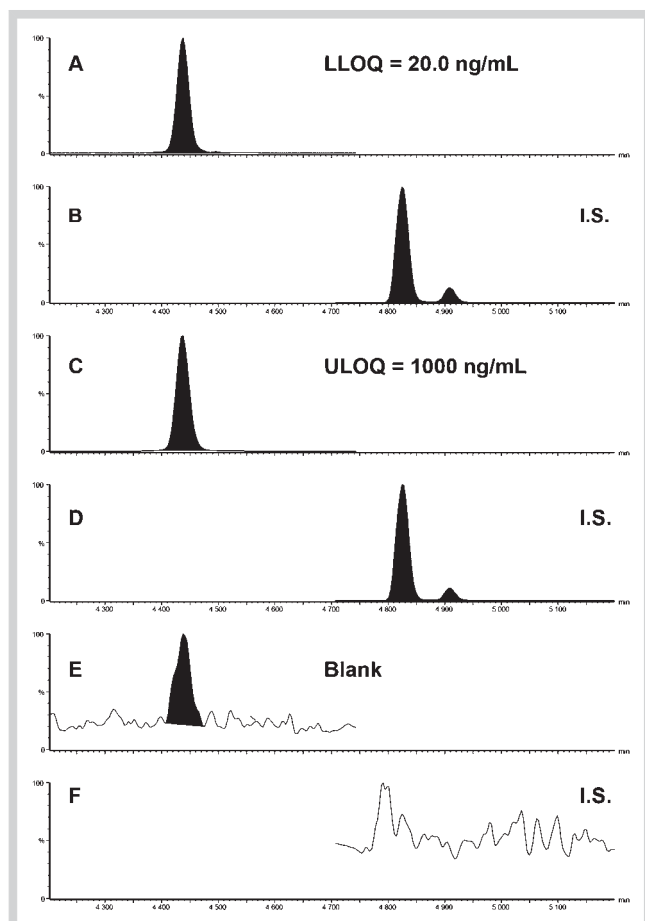


Fig. 3 Typical MRM chromatograms of RHB spiked with 20.0 ng/mL (LLOQ) tryptanthrin (A) and 1000 ng/mL I.S. (B) of RHB spiked with 2000 ng/mL (ULOQ) tryptanthrin (C) and 1000 ng/mL I.S. (D), and of blank RHB injected directly after the ULOQ and monitored for tryptanthrin (E) and for the I.S. (F).

(CV%) for the six samples at the LLOQ (duplicates, three different RHB batches) was 5.37% (below 20%) and the inaccuracy (RE%) was -7.62% (within $\pm 20\%$), demonstrating that the quantification method was selective for tryptanthrin (Table 8 S, Supporting Information).

The peak areas measured in the blank sample were in all plasma batches and all RHB batches less than 8.87% of the LLOQ (below 20%), indicating that the quantitative assay is also specific for tryptanthrin (data not shown). The absolute recovery for tryptanthrin extracted from the rat plasma was 79.4% for QCL (30 ng/mL), 77.5% for QCM (1000 ng/mL), and 77.6% for QCH (1600 ng/mL) (Table 9 S, Supporting Information). The absolute recoveries of the RHB samples were 60.8%, 78.6%, and 88.0% at concentrations of 60, 1000, and 1600 ng/mL, respectively (Table 10 S, Supporting Information). Dilution of samples up to 100-fold did not affect precision and accuracy of the methods (Tables 11 S and 12 S, Supporting Information). Tryptanthrin proved to be stable in the rat plasma and RHB for 4 h at RT and after three successive freeze and thaw cycles (Tables 13 S and 14 S, Supporting Information). Samples extracted from lithium heparinized rat plasma proved to be stable in the autosampler at 10°C up to 36 h when protected from light (Table 13 S, Supporting Information). Samples extracted from RHB could be stored in the autosampler at 10°C during 19 h (Table 14 S, Supporting Informa-

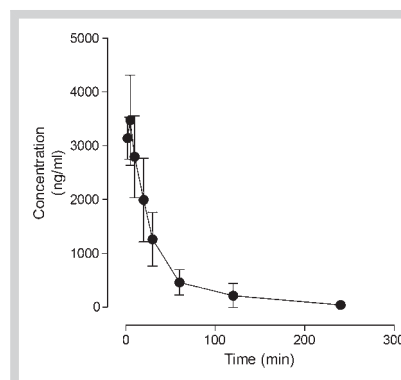


Fig. 4 Mean plasma concentration versus time profile of tryptanthrin in male Sprague-Dawley rats ($n = 4$) following i.v. administration (2 mg/kg bw).

Table 1 PK parameters obtained with a single intravenous dose of 2 mg/kg bw tryptanthrin in rats ($n = 4$). Data were calculated using non-compartmental analysis.

Parameters	Mean	SD
C_0 (ng/mL)	3395	479
$t_{1/2}$ (min)	40.63	6.66
T_{max} (min)	4.25	1.50
C_{max} (ng/mL)	3526	755
AUC_{0-last} (ng \times h/mL)	2082	683
$AUC_{0-\infty}$ (ng \times h/mL)	2228	877
MRT (min)	44.11	6.26
V_z (L/kg)	1.02	0.53
CL (L/h/kg)	1.00	0.36

AUC_{0-last} : AUC from time zero to 240 min; $AUC_{0-\infty}$: AUC with extrapolation to infinity

tion). Tryptanthrin samples in the rat plasma were stable when stored below -65°C up to 90 days (Fig. 1 S, Supporting Information), as the slope of the calculated linear regression was 0.920 (acceptance criteria: 1 ± 0.15). Stability of the RHB samples stored below -65°C could be confirmed up to nine days (Fig. 2 S, Supporting Information), as the slope of the calculated linear regression was 0.858 (acceptance criteria: 1 ± 0.15). Tryptanthrin stock solution (DMSO) was stored below -65°C for 427 days, and kept for 6 h at RT. The results showed that the degradation expressed by the percentage differences (-1.59%) was below 5%, indicating that the DMSO stock solution of tryptanthrin was stable for roughly 14 months when stored below -65°C (Table 15 S, Supporting Information). The DMSO stock solution of I.S. stored below -65°C was stable up to 190 days [11].

The validated method in the lithium heparinized rat plasma was applied to a pilot PK study of tryptanthrin in Sprague-Dawley rats after a single intravenous dose of 2 mg/kg bw ($n = 4$). The main PK parameters of tryptanthrin calculated by non-compartmental analysis are shown in Table 1, and the mean plasma concentration versus time profile after i.v. administration is shown in Fig. 4. The initial concentration (C_0) was 3395 ng/mL, and the AUC calculated on the trapezoidal rule was 2228 ng \times h/mL. The clearance was 1.00 L/h/kg, and the half-life time ($t_{1/2}$) was 40.63 min (Table 1).

In the immortalized human BBB monoculture model (Fig. 5) with the hBMEC cell line, the apparent permeability coefficient from apical to basolateral ($P_{app A \rightarrow B}$), and the P_{app} from basolateral to apical ($P_{app B \rightarrow A}$) were $36.96 \pm 0.43 \times 10^{-6}$ cm/s and $37.16 \pm 0.89 \times 10^{-6}$ cm/s, respectively (Table 2). Compared to the P_{app} coefficients of the negative control Na-F ($P_{app A \rightarrow B} = 3.20 \pm 0.03$; $P_{app B \rightarrow A} = 3.10 \pm 0.02 \times 10^{-6}$ cm/s), the P_{app} values of tryptanthrin

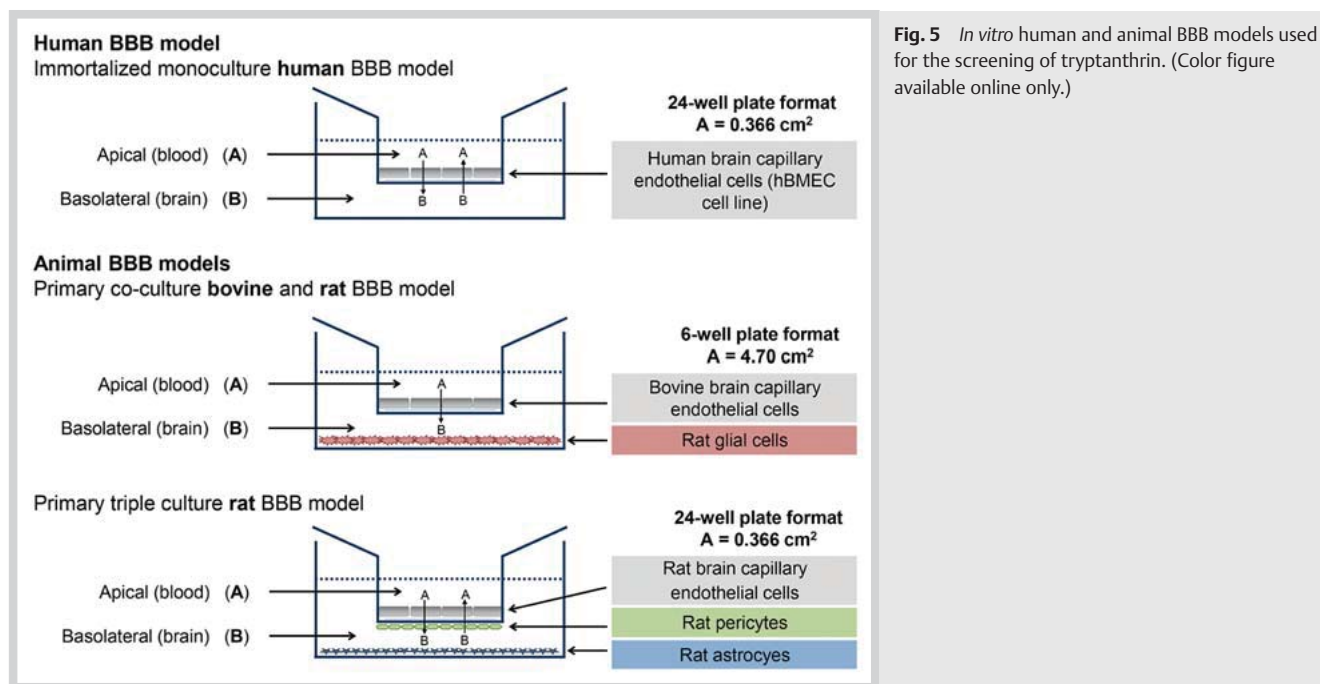


Fig. 5 *In vitro* human and animal BBB models used for the screening of tryptanthrin. (Color figure available online only.)

Table 2 Screening of tryptanthrin in the *in vitro* human BBB model (n = 3).

<i>In vitro</i> human BBB model (hBMVEC cell line)	Transport direction	Samples	Time of withdrawal (min)	Mean concentration (ng/mL)	Mean amount (ng)	Mean P_{app} of analyte \pm SEM ($\times 10^{-6}$ cm/s)	Mean P_{app} of Na-F \pm SEM ($\times 10^{-6}$ cm/s)	Recovery of analyte (%)	Efflux ratio
Inserts with cells	A to B	Donor compartment (300 μ L)	60	1 031	309	–	–	–	–
		Receiver compartment (1200 μ L)	60	44.39	31.07	36.96 ± 0.43	3.20 ± 0.03	102	–
Control inserts (without cells)	A to B	Donor compartment (300 μ L)	60	1 047	314	–	–	–	–
		Receiver compartment (1200 μ L)	60	126	152	105	74.3	130	–
Inserts with cells	B to A	Donor compartment (1200 μ L)	60	1 167	1 401	–	–	–	–
		Receiver compartment (300 μ L)	60	179	53.56	37.16 ± 0.89	3.10 ± 0.02	104	1.01
Control inserts (without cells)	B to A	Donor compartment (1200 μ L)	60	1 361	1 634	–	–	–	–
		Receiver compartment (300 μ L)	60	297	89.18	61.87	50.16	120	–

were more than 10-fold higher, suggesting that tryptanthrin crosses the BBB (Table 2). The ER of 1.01 indicated no active efflux for tryptanthrin (ER < 2.0). Since a low recovery leads to underestimation of P_{app} values, the recovery should be as high as possible [12]. In all experiments, the recovery of tryptanthrin was in the range of 100%, suggesting that the obtained P_{app} values were reliable. After each permeability experiment, TEER values were recorded and found to be in the same range as before the assay (around $25 \Omega \text{ cm}^2$, Fig. 6). This indicated that tryptanthrin did not affect cell layer integrity. Furthermore, C_{CL} values were between $0.50\text{--}5.00 \mu\text{F}/\text{cm}^2$, confirming that the cell monolayer was confluent (Fig. 6) [13].

The primary coculture rat/bovine *in vitro* BBB model (Fig. 5) exhibited TEER values of $350\text{--}400 \Omega \text{ cm}^2$ (data not shown). The mean $P_{app A \rightarrow B}$ ($36.15 \pm 0.90 \times 10^{-6}$ cm/s) (Table 3) of tryptan-

thrin was in the same range as in the immortalized human BBB monoculture model (Table 2). The mean $P_{app A \rightarrow B}$ was more than 10-fold higher than that of Na-F and suggested high BBB permeability. The mean P_{app} of Na-F in the presence of tryptanthrin ($3.17 \pm 0.19 \times 10^{-6}$ cm/s) (Table 3) was in the same range as that of Na-F alone (data not shown), indicating that the integrity of the cell monolayer was maintained during the transport experiment. Since the mean $P_{app A \rightarrow B}$ values of tryptanthrin across membranes with cells ($36.15 \pm 0.90 \times 10^{-6}$ cm/s) and control membranes (i.e., without cells; $36.14 \pm 3.99 \times 10^{-6}$ cm/s) (Table 3) were very close, tryptanthrin appears to freely diffuse across BBECs.

The *in vitro* BBB model composed of primary RBECs, pericytes, and glial cells (Fig. 5) formed a tight barrier with a TEER value of $399 \pm 44.5 \Omega \text{ cm}^2$ (data not shown) and a mean $P_{app A \rightarrow B}$ of

Table 3 Screening of tryptanthrin in the *in vitro* primary coculture rat/bovine BBB model (n = 3).

<i>In vitro</i> primary coculture BBB bovine/rat model	Transport direction	Samples	Time of withdrawal (min)	Mean concentration (ng/mL)	Mean amount (ng)	Mean P_{app} of analyte \pm SEM ($\times 10^{-6}$ cm/s)	Mean P_{app} of Na-F \pm SEM ($\times 10^{-6}$ cm/s)	Recovery of analyte (%)
Inserts with cells	A to B	Donor compartment (1500 μ L)	60	635	953	–	–	–
		Receiver compartment (2500 μ L)	60	237	592	36.15 \pm 0.90	3.17 \pm 0.19	106
Control inserts (without cells)	A to B	Donor compartment (1500 μ L)	60	686	1028	–	–	–
		Receiver compartment (2500 μ L)	60	237	592	36.14 \pm 3.99	24.20 \pm 1.24	112

Table 4 Screening of tryptanthrin in the *in vitro* primary triple coculture rat BBB model (n = 4).

<i>In vitro</i> primary triple coculture BBB rat model	Transport direction	Samples	Time of withdrawal (min)	Mean concentration (ng/mL)	Mean amount (ng)	Mean P_{app} of analyte \pm SEM ($\times 10^{-6}$ cm/s)	Mean P_{app} of Na-F \pm SEM ($\times 10^{-6}$ cm/s)	Recovery of analyte (%)	Efflux ratio
Inserts with cells	A to B	Donor compartment (300 μ L)	60	1193	358	–	–	–	–
		Receiver compartment (700 μ L)	60	189	132	83.40 \pm 4.02	1.14 \pm 0.53	125	–
Control inserts (without cells)	A to B	Donor compartment (300 μ L)	60	1093	328	–	–	–	–
		Receiver compartment (700 μ L)	60	262	183	116 \pm 1.79	153 \pm 11.41	132	–
Inserts with cells	B to A	Donor compartment (700 μ L)	60	1631	1142	–	–	–	–
		Receiver compartment (300 μ L)	60	339	102	64.12 \pm 2.91	0.52 \pm 0.18	136	0.77
Control inserts (without cells)	B to A	Donor compartment (700 μ L)	60	1313	919	–	–	–	–
		Receiver compartment (300 μ L)	60	302	90.54	57.15 \pm 4.28	38.21 \pm 2.89	110	–

1.14 \pm 0.53 $\times 10^{-6}$ cm/s for Na-F (Table 4). The P_{app} A→B of tryptanthrin was 83.40 \pm 4.02 $\times 10^{-6}$ cm/s (Table 4). Compared to the P_{app} A→B of the paracellular permeability marker Na-F (Table 4), this value was more than 70 times higher and hence, suggested that tryptanthrin permeated the cell layer very effectively. The mean P_{app} value of tryptanthrin from basolateral to apical was 64.12 \pm 2.91 $\times 10^{-6}$ cm/s (Table 4). Since the calculated ER in the triple coculture model was below 2 (ER = 0.77; Table 4), tryptanthrin was not involved in an active mediated efflux mechanism. TEER values recorded after the experiments (176 \pm 9.40 Ω cm²; data not shown) were lower than prior to the assay, but still presenting a tight barrier [14, 15]. This was also corroborated by low permeability coefficients for Na-F.

The most relevant *in silico* descriptors for permeability are summarized in Table 16S, Supporting Information. Tryptanthrin fulfilled Lipinski's Rule of five (QikProp: MW = 248 < 500, cLogP = 1.0 < 5.0, donorHB = 0 < 5, acceptHB = 6 < 10), along with a high-predicted human oral absorption (84.4%) [16]. The values of both 3D- and 2D-based PSA descriptors (PSA_{QikProp} = 73 Å² and PSA_{Marvin} = 50 Å²) were not only well below the maximum acceptable threshold of 140 Å² for good oral absorption, but also met the criteria for a passive permeation through the BBB (PSA < 90 Å²) [17]. Similarly, both predicted cLogP_{QikProp} = 1.00 and cLogP_{Marvin} = 2.40 were within the range that is favorable for blood-brain transport. On the other

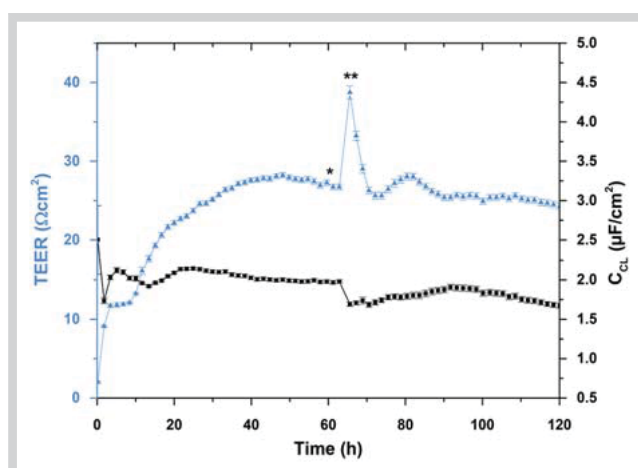


Fig. 6 Mean TEER values (▲) and C_{cl} values (■) for hBMEC cell monolayers, recorded in real-time by the CellZscope system. * Transfer of insert to a 24-well plate for tryptanthrin permeability assays; ** transfer of insert to CellZscope for barrier integrity control. (Color figure available online only.)

hand, the QikProp model for brain/blood partitioning predicted a $c\text{LogBB}$ of -0.450 (usual range from -3.0 to 1.2), indicating a slight preference for the blood environment [18].

In summary, the UPLC-MS/MS methods for tryptanthrin in lithium heparinized rat plasma and RHB were developed and validated according to both EMA and FDA guidelines, and applied to a PK study and three BBB models [9, 10]. The rat plasma method and the PK data from the pilot study will serve for the design of a full PK study addressing oral bioavailability. Moreover, it is planned to determine PK parameters by both non-compartmental and compartmental analysis using WinNonlin software to select the most appropriate body model. For estimation of the *in vivo* absorption of tryptanthrin, *in vitro* experiments with the Caco-2 permeability assay and a method validation in Hanks' balanced salt solution (HBSS) are in progress.

The BBB permeation potential of tryptanthrin was evaluated in two *in vitro* primary animal BBB models [19, 20] and in one *in vitro* human immortalized BBB model [21]. A good correlation was found, and data were indicative of a high BBB penetration of tryptanthrin when compared to Na-F. Furthermore, the data suggested that tryptanthrin crossed the cell monolayers by passive diffusion. These results were consistent with *in silico* BBB permeation modelling. In addition, the efflux ratios determined in the bidirectional *in vitro* BBB models suggested that tryptanthrin was not subjected to active efflux. Considering the unique pharmacological profile of tryptanthrin, the data here indicate that the compound is a promising lead for drug development in the area of neuroinflammatory diseases.

Material and Methods



Chemicals and reagents

Tryptanthrin (PubChem CID: 73 549) (● Fig. 1 A) and the I.S. [(*E,Z*)-3-(benzylidenyl)-indolin-2-one (● Fig. 1 B)] were synthesized according to established procedures [1]. Both compounds showed a purity of $\geq 99\%$ as determined by HPLC and NMR [22]. All solvents were of analytical grade. Methanol was from Lab-Scan, formic acid and trifluoroacetic acid were supplied by BioSolve, and albumin from bovine serum (BSA) and sodium fluorescein (Na-F, $10 \mu\text{g}/\text{mL}$) were purchased from Sigma-Aldrich. Acetonitrile and DMSO were purchased from Scharlau. HPLC grade water was prepared using an EASYpure II (Barnstead, Dubuque, IA, USA) water purification system. Ostro® 96-well plates were provided by Waters Corp. Blank male Sprague-Dawley rat plasma in lithium heparin batches were from Seralab. Tissue culture inserts (transparent polyethylene membrane, $3.0 \mu\text{m}$ pore size) for the 24-well format were from Greiner Bio-one®, and tissue culture inserts (polycarbonate membrane, $0.4 \mu\text{m}$ pore size) used for the 6-well plates were from Corning. Ringer HEPES buffer RHB (150 mM NaCl , 2.2 mM CaCl_2 , 0.2 mM MgCl_2 , 5.2 mM KCl , 2.8 mM glucose , 5 mM HEPES , 6 mM NaHCO_3 , $0.2\% \text{ BSA}$) was prepared in-house, adjusted to pH 7.4, and stored at 4°C .

Instrumentation and UHLC-MS/MS conditions

The UPLC-MS/MS system consisted of an ACQUITY UPLC system (Waters Corp.) and a Waters tandem quadrupole detector (TQD) mass spectrometer. Chromatographic separation was performed on a Waters UPLC HSS T3 column ($100 \text{ mm} \times 2.1 \text{ mm}$; $1.8 \mu\text{m}$ particle size). Column temperature was set at 45°C , and the autosampler was set at 10°C . The mobile phase was delivered at a flow rate of $0.5 \text{ mL}/\text{min}$. Weak and strong wash solvents were

water-methanol ($50:50$, v/v) and acetonitrile-isopropanol-acetone ($40:30:30$, v/v/v) both containing 0.2% trifluoroacetic acid. The seal wash solvent consisted of a water-acetonitrile mixture ($90:10$, v/v). MS detection was performed with electrospray ionization in the positive mode (ESI+). Nitrogen, generated by a nitrogen generator N2-Mistral (Schmidlin AG), was used both as a desolvation and nebulization gas. Argon was used as a collision gas. MS/MS parameters were generated using Waters IntelliStart software followed by manual optimization. Multiple reaction monitoring (MRM) transitions were $248.7 > 129.8$ for tryptanthrin, and $221.8 > 194.0$ for the I.S. [(*E,Z*)-3-(benzylidenyl)-indolin-2-one] (● Figs. 2 and 3). Due to the slow inter-conversion at RT of the I.S., both *E* and *Z* isomer peaks were integrated and quantified (● Figs. 2 and 3) [11, 23]. The capillary voltage was 3.5 kV . The cone voltage was 51 V , and the collision energy was 31 eV for both tryptanthrin and the I.S. The source temperature was set at 150°C , and the desolvation temperature was 400°C . The flow rates for the desolvation gas and cone gas were $900 \text{ L}/\text{h}$ and $10 \text{ L}/\text{h}$, respectively. Data were acquired with MassLynx V4.1 software and quantified with QuanLynx software (Waters, Corp.).

Chromatographic conditions for samples extracted from lithium heparinized rat plasma

The mobile phases consisted of 10 mM ammonium formate + 0.05% formic acid (eluent A) and acetonitrile + 0.05% formic acid (eluent B). The following gradient was used for separation: $0\text{--}1.0 \text{ min}$, 5% of B; $1\text{--}6 \text{ min}$, $5\text{--}100\%$ of B; $6\text{--}7 \text{ min}$, 100% of B; $7\text{--}7.1 \text{ min}$, $100\text{--}5\%$ of B; $7.1\text{--}8 \text{ min}$, 5% of B. The injection solvent consisted of 65% of eluent C (water + 0.1% formic acid) and 35% of eluent D (acetonitrile + 0.1% formic acid). Total run time was 8 min and the dwell time was automatically set at 0.2 sec (● Fig. 2).

Chromatographic conditions for samples extracted from Ringer HEPES Buffer

The mobile phases consisted of water containing 0.1% formic acid (eluent C) and methanol containing 0.1% formic acid (eluent E). The following gradient was used for separation: $0\text{--}1 \text{ min}$, 20% of E; $1\text{--}5 \text{ min}$, $20\text{--}90\%$ of E; $5\text{--}5.1 \text{ min}$, $90\text{--}100\%$ of E; $5.1\text{--}6 \text{ min}$, 100% of E; $6\text{--}6.1 \text{ min}$, $100\text{--}20\%$ of E; $6.1\text{--}7 \text{ min}$, 20% of E. The total run time was 7 min . As an injection solvent, pure methanol was used. The dwell time was automatically set at 0.142 sec (● Fig. 3).

Sample preparation

SS of the analyte and I.S. were prepared in DMSO and stored below -65°C . Working solutions (WS1) of the analyte and I.S. were prepared in methanol by further diluting the corresponding SS to obtain a concentration of $100 \mu\text{g}/\text{mL}$ for tryptanthrin and $10 \mu\text{g}/\text{mL}$ for I.S. WS1 of the I.S. was further diluted with acetonitrile + 1% formic acid (for the rat plasma method) or methanol (for the RHB method) to give a second working solution (WS2) at $1000 \text{ ng}/\text{mL}$. SS and WS1 were stored below -65°C until use. WS2 was prepared daily before each analytical run. Seven calibration samples (calibrators) in the range of $10.0\text{--}2000 \text{ ng}/\text{mL}$ (rat plasma) and $20.0\text{--}2000 \text{ ng}/\text{mL}$ (RHB) were prepared in the corresponding matrices by serial dilution with WS1 of tryptanthrin ($100 \mu\text{g}/\text{mL}$). QCs at low (QCL), middle (QCM), and high (QCH) levels were prepared in lithium heparinized rat plasma at concentrations of 30.0 , 1000 , and $1600 \text{ ng}/\text{mL}$, and in RHB at concentrations of 60.0 , 1000 , and $1600 \text{ ng}/\text{mL}$.

Sample extraction from the lithium heparinized rat plasma was performed as follows: the Ostro® plate was placed onto a 96-deep-well plate (96-DWP) serving as a collection plate. To 50 µL lithium heparinized rat plasma containing tryptanthrin, 150 µL of I.S. at 1000 ng/mL were added. The Ostro® plate/collection plate assembly was mixed for 10 min at RT on an Eppendorf Thermomixer (1000 rpm). After mixing, the plates were placed on a positive pressure processor (Biotage® PRESSURE+, Uppsala, Sweden), and a pressure of 30–40 psi was applied for 10 min. The Ostro® plate was discarded and the filtrate in the collection plate was dried under nitrogen gas (Evaporex EVX-96, Apricot Designs). The dried extract was reconstituted with 200 µL of injection solvent (65% solvent C and 35% D).

For the sample extraction from RHB, aliquots of RHB (200 µL) containing tryptanthrin were subjected to protein precipitation by adding 100 µL of I.S. at 1000 ng/mL, 200 µL of BSA solution (60 g/L), and 1000 µL of ice-cold acetonitrile. The mixture was briefly vortexed, mixed for 10 min at RT on an Eppendorf Thermomixer (1400 rpm), and centrifuged for 20 min at 16 160 g at 10 °C. The supernatant (1300 µL) was transferred into a 96-DWP, dried under nitrogen gas flow, and reconstituted with 200 µL of injection solvent (methanol).

After reconstitution of tryptanthrin with the corresponding injection solvents, sample preparation (for both RHB and rat plasma) was continued as follows: the 96-DWPs were shaken for 45 min at RT on an Eppendorf Mixmate and centrifuged for 2 min at 2060 g (Megafuge, Heraeus Instruments AG). Due to nonspecific adsorption of the I.S. onto the 96-DWP, each sample was transferred into a 300-µL glass insert of an HPLC vial before injection into the UPLC-MS/MS system in full loop mode (5 µL).

Method validation

The UPLC-MS/MS quantification methods for tryptanthrin in lithium heparinized rat plasma and RHB were fully validated according to FDA and EMA guidelines [9, 10]. The calibration curves of tryptanthrin were in the range of 10.0–2000 ng/mL for the rat plasma and 20.0–2000 ng/mL for the RHB. Each calibration curve was validated by QCs at low, medium, and high concentration levels [30.0 (QCL for rat plasma)/60.0 (QCL for RHB), 1000 (QCM), and 1600 ng/mL (QCH)], which were inserted randomly into the analytical run. Calibrators and QCs at all concentration levels were analyzed in duplicate. Carryover was assessed by directly injecting an extracted blank (lithium heparinized rat plasma/RHB) after the upper limit of quantification (ULOQ = 2000 ng/mL). Specificity and selectivity of the methods were evaluated by six blank samples and six QC samples of tryptanthrin at the LLOQ (duplicates, three different batches of lithium heparinized rat plasma or RHB). Intra-run and inter-run repeatability was assessed by injecting six replicates of tryptanthrin at five concentration levels (LLOQ, QCL, QCM, QCH, and ULOQ) on three consecutive days. The absolute recovery of tryptanthrin was determined at three concentration levels [30.0 (rat plasma)/60.0 (RHB), 1000 and 1600 ng/mL] of QC samples by comparing the peak areas of the extracted QC samples with those of the unextracted solutions (= 100% recovery). To extend the upper limit of the calibration curve, a dilution test was performed. For this purpose, a solution of tryptanthrin at 4000 ng/mL in blank rat plasma and RHB was prepared and then further diluted in a ratio of 1 : 10 and 1 : 100. Short-term stabilities were assessed at RT, after cyclic freeze and thaw, and after storage at autosampler conditions (10 °C, light protected). Long-term and stock solution stabilities were determined after storage below –65 °C. For all validation tests, im-

precision was expressed by the coefficient of variation (CV%), and inaccuracy by the relative error (RE%).

Preliminary pharmacokinetic study

All animal experiments were performed according to the policies and guidelines of the Institutional Animal Care and Use Committee (IACUC) of the University of Florida, Gainesville, FL, USA (NIH publication #85–23), study protocol #200 802 291, as previously described [11]. Tryptanthrin was dissolved in DMSO and administered intravenously (i.v.) in a concentration of 2 mg/kg bw (n = 4). Blood samples (300 µL) were collected from the sublingual vein into Vacuette® heparinized tubes at 0 (prior to dosing), 2, 5, 10, 20, and 30 min and 1, 2, 3, 4, 6, 8, and 12 h.

Data analysis

Mean plasma concentrations of tryptanthrin after i.v. administration versus time curves were generated in Graphpad Prism (version 5.01). The PK parameters were determined by non-compartmental analysis using PKSolver [24]. The PK parameters determined were the concentration at time zero (C_0), the terminal elimination half-life ($t_{1/2}$), area under the curve extrapolated to infinity ($AUC_{0-\infty}$), the elimination rate constant (K_e), the MRT, the volume of distribution at terminal phase (V_z), and the CL. $AUC_{0 \rightarrow \text{last}}$ was calculated using a linear/log trapezoidal method from time zero to the last detectable sampling point 240 min after administration.

Blood-brain barrier drug permeability assays

In the human *in vitro* BBB model (● Fig. 5), immortalized human brain microvascular endothelial cells (hBMEC cell line) were seeded at a density of 6.0×10^4 cells/cm² onto collagen-coated 24-well tissue culture inserts. Barrier tightness was assessed by real-time TEER measurements using a CellZscope system (NanoAnalytics) [13]. TEER and cell layer capacitance (C_{CL}) values were recorded every hour. After 60 h, at the maximum mean TEER value of $25.6 \pm 0.0370 \Omega \text{ cm}^2$ (● Fig. 6), the permeability assay for tryptanthrin was carried out. The experiments were performed bidirectionally and in triplicate as previously described [25].

For the primary coculture rat/bovine *in vitro* BBB model, the method of Dehouck et al. (1990) [26] was used with minor modifications. Glial cells were isolated according to Booher and Sensenbrenner (1972) [27] and cultured for 3 weeks at the bottom of 6-well plates. BBECs were isolated from capillary fragments and were seeded onto collagen-coated 6-well tissue culture inserts placed into the wells containing the glial cells (● Fig. 5). After 7 days of coculture, at a mean TEER value of 350–400 $\Omega \text{ cm}^2$ [28], the permeability assay was performed (n = 3).

For the primary triple coculture rat *in vitro* BBB model, RBECs, pericytes, and glial cells were isolated from 3-week-old Wistar rats, similarly as described earlier [29, 30]. Rat glial cells were cultured at the bottom of 24-well plates. Pericytes were seeded onto the bottom side of the inserts, and RBECs were seeded onto the apical side of collagen-coated filter inserts (● Fig. 5). After 4 days of coculture, a mean TEER value of $398.8 \pm 44.5 \Omega \text{ cm}^2$ was measured, and the bidirectional permeability assay was carried out (n = 4).

Tryptanthrin was screened at a concentration of 5 µM together with Na-F as a barrier integrity control marker in RHB. The plates were spiked with the test solution and incubated at 37 °C on a horizontal shaker with moderate speed (100 rpm). Samples were collected from both apical and basolateral compartments after 60 min and stored below –65 °C until analysis. The fluorescent

marker (Na-F) was quantified by a Chameleon microplate reader ($\lambda_{\text{ex}} = 490 \text{ nm}$, $\lambda_{\text{em}} = 514 \text{ nm}$; Hidex), fluorescence counter ($\lambda_{\text{ex}} = 485 \text{ nm}$, $\lambda_{\text{em}} = 528 \text{ nm}$; Synergy H1, Biotek), and Fluostar Optima multiwell plate reader ($\lambda_{\text{ex}} = 480 \text{ nm}$, $\lambda_{\text{em}} = 520 \text{ nm}$; BMG Labtechnologies), and the analyte by UPLC-MS/MS.

Blood-brain barrier permeability parameters

The apparent permeability coefficients (P_{app}) for tryptanthrin and Na-F were calculated with the following equation [31]:

$$P_{\text{app}} = \frac{V_{\text{R}}}{(AC_{\text{D0}})} \times \frac{\Delta C_{\text{R}}}{\Delta t} \text{ (cm/s)}$$

V_{R} = volume in the receiver compartment; A = surface area of the filter membrane (0.336 cm^2 for 24-well inserts, 4.7 cm^2 for 6-well inserts); C_{D0} = initial concentration in the donor compartment; and $\Delta C_{\text{R}}/\Delta t$ = change of concentration over time in the receiver compartment. To evaluate if tryptanthrin was involved in efflux transport, the ER [32] was calculated:

$$\text{ER} = \frac{P_{\text{app B} \rightarrow \text{A}}}{P_{\text{app A} \rightarrow \text{B}}}$$

Active efflux of the compound was concluded if the ER was > 2.0 [33].

To confirm that the diffusion barrier was only provided by the cell monolayer, control experiments were performed using collagen-coated inserts without cells. Compound loss was assessed by calculating the recovery (mass balance) according to the equation:

$$\text{Recovery (\%)} = \frac{C_{\text{Df}}V_{\text{D}} + C_{\text{Rf}}V_{\text{R}}}{C_{\text{D0}}V_{\text{D}}} \times 100$$

C_{Df} = final concentration of the compound in the donor; C_{Rf} = final concentration of the compound in the receiver compartment; C_{D0} = initial concentration in the donor compartment; and V_{D} , V_{R} = volumes in the donor and receiver compartments, respectively. All results are expressed as means \pm SEM.

In silico prediction of blood-brain barrier permeability

A three-dimensional computer model of tryptanthrin was built using the Maestro modeling environment (Maestro, version 9.3, Schrödinger, LLC, 2012). The global minimum geometry was used as an input for the QikProp application (QikProp, version 3.5, Schrödinger, LLC, 2012) to evaluate various descriptors relevant for drug permeability. The PSA and the logarithm of partition coefficient (cLogP) descriptors were calculated using the Calculator plugin of Chemaxon Marvin web-application (<http://www.chemaxon.com/marvin/sketch/index.php>, accessed on February 12, 2014), which requires only the 2D structural formula as an input.

Supporting information

Data of both full method validations and the *in silico* parameters are available as Supporting Information.

Acknowledgments

Thanks are due to Prof. K. S. Kim and Prof. D. Grab (Johns Hopkins University, Baltimore, MD, USA) for provision of the hBMEC cell line. We are grateful to Dr. M. Raith for the synthesis of tryptanthrin, and to O. Fertig for excellent technical support. Financial support from the Swiss National Science Foundation (project 105 320_126 888) is gratefully acknowledged.

Conflict of Interest

None declared.

Affiliations

- 1 Pharmaceutical Biology, Department of Pharmaceutical Sciences, University of Basel, Basel, Switzerland
- 2 Department of Pharmaceutics, College of Pharmacy, University of Florida, Gainesville, Florida, USA
- 3 Institute for Pharma Technology, Muttensz, Switzerland
- 4 Univ. Artois, EA 2465, Laboratoire de la Barrière Hémato-Encéphalique (LBHE), Lens Cedex, France
- 5 Institute of Biophysics, Biological Research Centre, Hungarian Academy of Sciences, Szeged, Hungary
- 6 Molecular Modeling, Department of Pharmaceutical Sciences, University of Basel, Basel, Switzerland

References

- 1 Danz H, Stoyanova S, Thomet OAR, Simon HU, Dannhardt G, Ulbrich H, Hamburger M. Inhibitory activity of tryptanthrin on prostaglandin and leukotriene synthesis. *Planta Med* 2002; 68: 875–880
- 2 Pergola C, Jazzar B, Rossi A, Northoff H, Hamburger M, Sautebin L, Werz O. On the inhibition of 5-lipoxygenase product formation by tryptanthrin: mechanistic studies and efficacy *in vivo*. *Br J Pharmacol* 2012; 165: 765–776
- 3 Recio MC, Cerdá-Nicolás M, Hamburger M, Ríos L. Anti-arthritis activity of a lipophilic woad (*Isatis tinctoria*) extract. *Planta Med* 2006; 72: 715–720
- 4 Recio MC, Cerdá-Nicolás M, Potterat O, Hamburger M, Ríos L. Anti-inflammatory and antiallergic activity *in vivo* of lipophilic *Isatis tinctoria* extracts and tryptanthrin. *Planta Med* 2006; 72: 539–546
- 5 Danz H, Stoyanova S, Wippich P, Brattström A, Hamburger M. Identification and isolation of the cyclooxygenase-2 inhibitory principle in *Isatis tinctoria*. *Planta Med* 2001; 67: 411–416
- 6 Ishihara T, Kohno K, Ushio S, Iwaki K, Ikeda M, Kurimoto M. Tryptanthrin inhibits nitric oxide and prostaglandin E_2 synthesis by murine macrophages. *Eur J Pharmacol* 2000; 407: 197–204
- 7 Bishnoi M, Patil CS, Kumar A, Kulkarni SK. Protective effects of nimesulide (COX inhibitor), AKBA (5-LOX inhibitor), and their combination in aging-associated abnormalities in mice. *Methods Find Exp Clin Pharmacol* 2005; 27: 465–470
- 8 Dokmeci D. Ibuprofen and Alzheimer's disease. *Folia Med (Plovdiv)* 2004; 46: 5–10
- 9 Guidance for Industry: Bioanalytical Method Validation. US Food and Drug Administration (FDA), Center for Drug Evaluation and Research, May 2001 Available at: <http://www.fda.gov/downloads/Drugs/Guidances/ucm070107.pdf>, Accessed 17.07.2015
- 10 Guideline on bioanalytical method validation. European Medicines Agency (EMA/CHMP/EWP/192217/2009). London, 21 July 2011 Available at: http://www.ema.europa.eu/docs/en_GB/document_library/Scientific_guideline/2011/08/WC500109686.pdf, Accessed 16.07.2015
- 11 Oufir M, Sampath C, Butterweck V, Hamburger M. Development and full validation of an UPLC-MS/MS method for the determination of an anti-allergic indolinone derivative in rat plasma, and application to a preliminary pharmacokinetic study. *J Chromatogr B* 2012; 902: 27–34
- 12 Hubatsch I, Ragnarsson EG, Artursson P. Determination of drug permeability and prediction of drug absorption in Caco-2 monolayers. *Nat Protoc* 2007; 2: 2111–2119
- 13 Wegener J, Abrams D, Willenbrink W, Galla HJ, Janshoff A. Automated multi-well device to measure transepithelial electrical resistances under physiological conditions. *Biotechniques* 2004; 37: 590
- 14 Deli MA, Ábrahám CS, Kataoka Y, Niwa M. Permeability studies on *in vitro* blood-brain barrier models: physiology, pathology, and pharmacology. *Cell Mol Neurobiol* 2005; 25: 59–127
- 15 Gaillard PJ, de Boer AG. Relationship between permeability status of the blood-brain barrier and *in vitro* permeability coefficient of a drug. *Eur J Pharm Sci* 2000; 12: 95–102
- 16 Lipinski CA, Lombardo F, Dominy BW, Feeney PJ. Experimental and computational approaches to estimate solubility and permeability in drug discovery and development settings. *Adv Drug Deliv Rev* 2001; 46: 3–26
- 17 Veber DF, Johnson SR, Cheng HY, Smith BR, Ward KW, Kopple KD. Molecular properties that influence the oral bioavailability of drug candidates. *J Med Chem* 2002; 45: 2615–2623

- 18 van de Waterbeemd H, Camenisch G, Folkers G, Chretien JR, Raevsky OA. Estimation of blood-brain barrier crossing of drugs using molecular size and shape, and H-bonding descriptors. *J Drug Target* 1998; 6: 151–165
- 19 Culot M, Lundquist S, Vanuxeem D, Nion S, Landry C, Delplace Y, Dehouck MP, Berezowski V, Fenart L, Cecchelli R. An *in vitro* blood-brain barrier model for high throughput (HTS) toxicological screening. *Toxicol In Vitro* 2008; 22: 799–811
- 20 Nakagawa S, Deli MA, Kawaguchi H, Shimizudani T, Shimono T, Kittel A, Tanaka K, Niwa M. A new blood-brain barrier model using primary rat brain endothelial cells, pericytes and astrocytes. *Neurochem Int* 2009; 54: 253–263
- 21 Eigenmann DE, Xue G, Kim KS, Moses AV, Hamburger M, Oufir M. Comparative study of four immortalized human brain capillary endothelial cell lines, hCMEC/D3, hBMEC, TY10, and BB19, and optimization of culture conditions, for an *in vitro* blood-brain barrier model for drug permeability studies. *Fluids Barriers CNS* 2013; 10: 33
- 22 Mohn T, Potterat O, Hamburger M. Quantification of active principles and pigments in leaf extracts of *Isatis tinctoria* by HPLC/UV/MS. *Planta Med* 2007; 73: 151–156
- 23 Rüster GU, Hoffmann B, Hamburger M. Inhibitory activity of indolin-2-one derivatives on compound 48/80-induced histamine release from mast cells. *Pharmazie* 2004; 59: 236–237
- 24 Zhang Y, Huo M, Zhou J, Xie S. PKSolver: An add-in program for pharmacokinetic and pharmacodynamic data analysis in Microsoft Excel. *Comput Methods Programs Biomed* 2010; 99: 306–314
- 25 Jähne EA, Eigenmann DE, Culot M, Cecchelli R, Walter FR, Deli MA, Tremmel R, Fricker G, Smiesko M, Hamburger M, Oufir M. Development and validation of a LC-MS/MS method for assessment of an anti-inflammatory indolinone derivative by *in vitro* blood-brain barrier models. *J Pharm Biomed Anal* 2014; 98: 235–246
- 26 Dehouck MP, Méresse S, Delorme P, Fruchart JC, Cecchelli R. An easier, reproducible, and mass-production method to study the blood-brain barrier *in vitro*. *J Neurochem* 1990; 54: 1798–1801
- 27 Booher J, Sensenbrenner M. Growth and cultivation of dissociated neurons and glial cells from embryonic chick, rat and human brain in flask cultures. *Neurobiology* 1972; 2: 97–105
- 28 Boveri M, Berezowski V, Price A, Slupek S, Lenfant AM, Benaud C, Hartung T, Cecchelli R, Prieto P, Dehouck MP. Induction of blood-brain barrier properties in cultured brain capillary endothelial cells: Comparison between primary glial cells and C6 cell line. *Glia* 2005; 51: 187–198
- 29 Veszelka S, Tóth AE, Walter FR, Datki Z, Mózes E, Fülöp L, Bozsó Z, Hellinger E, Vastag M, Orsolits B, Környei Z, Penke B, Deli MA. Docosahexaenoic acid reduces amyloid- β induced toxicity in cells of the neurovascular Unit. *J Alzheimers Dis* 2013; 36: 487–501
- 30 Walter FR, Veszelka S, Pásztói M, Péterfi ZA, Tóth A, Rákhely G, Cervenak L, Ábrahám CS, Deli MA. Tesmilifene modifies brain endothelial functions and opens the blood-brain/blood-glioma barrier. *J Neurochem* 2015; 134: 1040–1054
- 31 Youdim KA, Avdeef A, Abbott NJ. *In vitro* trans-monolayer permeability calculations: often forgotten assumptions. *Drug Discov Today* 2003; 8: 997–1003
- 32 Polli JW, Wring SA, Humphreys JE, Huang L, Morgan JB, Webster LO, Serabjit-Singh CS. Rational use of *in vitro* P-glycoprotein assays in drug discovery. *J Pharmacol Exp Ther* 2001; 299: 620–628
- 33 Hellinger É, Veszelka S, Tóth AE, Walter F, Kittel Á, Bakk ML, Tihanyi K, Háda V, Nakagawa S, Duy TD, Niwa M, Deli MA, Vastag M. Comparison of brain capillary endothelial cell-based and epithelial (MDCK-MDR1, Caco-2, and VB-Caco-2) cell-based surrogate blood-brain barrier penetration models. *Eur J Pharm Biopharm* 2012; 82: 340–351

Supporting Information

Planta Medica

Pharmacokinetics and *in vitro* blood-brain barrier screening of the plant-derived alkaloid tryptanthrin

Evelyn A. Jähne¹, Daniela E. Eigenmann¹, Chethan Sampath², Veronika Butterweck^{2,3}, Maxime Culot⁴, Roméo Cecchelli⁴, Fabien Gosselet⁴, Fruzsina R. Walter⁵, Mária A. Deli⁵, Martin Smieško⁶, Matthias Hamburger¹, and Mouhssin Oufir^{1*}

Affiliation

¹Pharmaceutical Biology, Department of Pharmaceutical Sciences, University of Basel, Klingelbergstrasse 50, CH-4056 Basel, Switzerland

²Department of Pharmaceutics, College of Pharmacy, University of Florida, 1345 Gainesville, Florida, USA

³School of Life Sciences Institute for Pharma Technology, Gründenstrasse 40, CH-4132 Muttenz, Switzerland

⁴Univ. Artois, EA 2465, Laboratoire de la Barrière Hémato-Encéphalique (LBHE), F-62300 Lens Cedex, France

⁵Institute of Biophysics, Biological Research Centre, Hungarian Academy of Sciences, Temesvari krt. 62, H-6726 Szeged, Hungary

⁶Molecular Modeling, Department of Pharmaceutical Sciences, University of Basel, Klingelbergstrasse 50, CH-4056 Basel, Switzerland

Correspondence

Dr. Mouhssin Oufir, Division of Pharmaceutical Biology, Department of Pharmaceutical Sciences, University of Basel, Klingelbergstrasse 50, CH-4056 Basel, Switzerland, Phone: +41-61-267-1544
Fax: +41-61-267-1474
E-Mail: mouhssin.oufir@unibas.ch

Figures

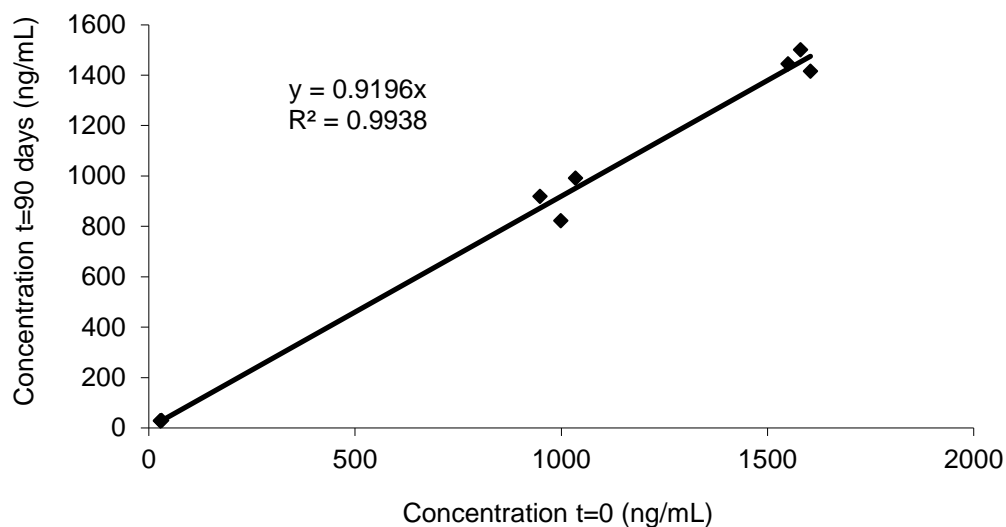


Fig. 1S Long-term stability (LTS) of tryptanthrin in lithium heparinized rat plasma for 90 days below -65°C (N=3).

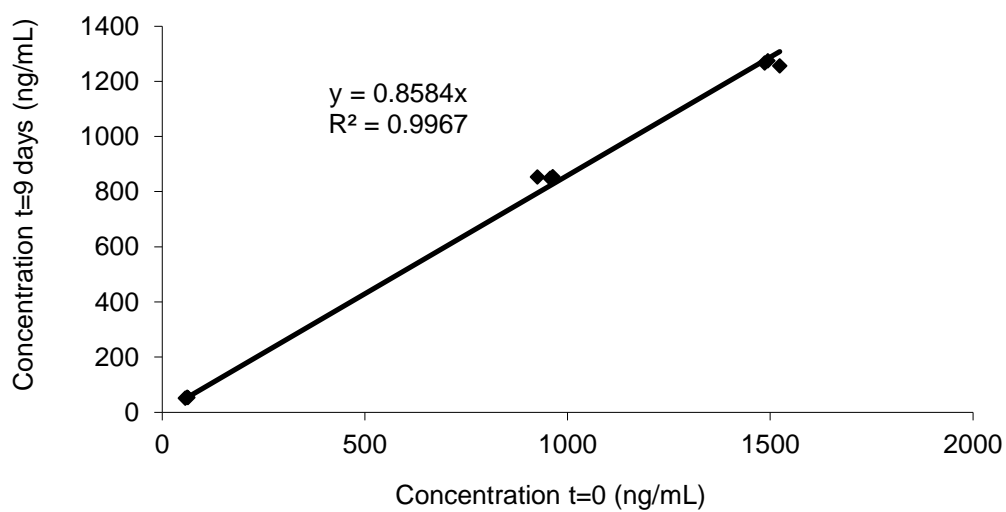


Fig. 2S Long-term stability (LTS) of tryptanthrin in Ringer HEPES buffer for 9 days below -65°C (N=3).

Tables

Table 1S Calibrators and calibration curve parameters for lithium heparinized rat plasma (N=10).

Run number	Nominal level (ng/mL)							Regression parameters			
	10.0	50.0	100	250	500	1000	2000	A	B	C	R ²
1	10.9	49.0	106	251	511	1048	2072	-0.000000100	0.00183	0.00153	0.998
	10.9	43.5	*84.1	*211	471	976	1920				
2	10.0	52.8	108	271	519	981	1933	-0.0000000904	0.00191	0.00283	0.998
	9.88	45.7	108	236	467	927	2184				
3	11.4	47.5	110	263	511	1023	2011	0.0000000198	0.00122	0.00268	0.999
	11.0	50.1	93.7	242	472	989	1986				
4	10.5	53.8	106	269	489	1021	2062	-0.0000000236	0.00239	0.00452	0.999
	9.88	50.2	99.1	254	481	961	1957				
5	10.1	52.5	109	232	507	1021	2035	-0.000000191	0.00221	0.00450	0.999
	10.2	51.4	106	255	494	957	1980				
Mean	10.5	49.6	105	253	492	990	2014	-0.0000000771	0.00191	0.00321	0.999
S.D.	0.544	3.30	5.34	13.7	19.1	37.4	78.7	0.0000000805	0.000450	-	-
CV%	5.19	6.66	5.08	5.41	3.88	3.78	3.91				
RE%	4.84	-0.724	5.19	1.03	-1.54	-0.959	0.705				

$$\text{Response} = A \times \text{Conc.}^2 + B \times \text{Conc.} + C$$

Quadratic regression, 1/X weighting, origin: included

* >15.0% outside acceptance criteria, not used for calculations

Table 2S Calibrators and calibration curve parameters for Ringer HEPES buffer (N=12)

Run number	Nominal level (ng/mL)							Regression parameters			
	20.0	50.0	100	250	500	1000	2000	A	B	C	R ²
1	18.9	43.2	95.2	250	477	939	1873	-0.000000675	0.005543	-0.00485	0.996
	21.9	47.8	107	271	542	*1156	2171				
2	18.0	43.8	99.6	252	469	864	1815	-0.000000797	0.000526	-0.00415	0.993
	20.7	49.8	110	264	566	1038	2299				
3	21.7	44.2	101	256	528	979	2101	-0.00000101	0.000593	-0.0130	0.999
	19.2	45.9	99.9	244	510	974	1932				
4	18.1	46.2	94.8	261	541	925	2224	-0.000000973	0.00487	-0.00805	0.995
	20.8	49.7	96.8	262	557	871	2037				
5	19.3	49.0	102	259	506	1009	2132	-0.000000586	0.000284	-0.00311	0.999
	17.9	49.2	106	262	495	927	1984				
6	18.1	48.9	108	246	522	955	1921	-0.000000349	0.000207	0.000934	0.998
	19.0	52.3	106	256	516	939	2183				
Mean	19.5	47.5	102	257	519	947	2056	-0.000000732	0.00200	-0.00537	0.997
S.D.	1.45	2.83	5.15	7.86	29.9	52.7	152	0.000000250	0.00249	-	-
CV%	7.43	5.97	5.04	3.06	5.76	5.56	7.41				
RE%	-2.64	-5.04	2.14	2.78	3.78	-5.28	2.80				

$$\text{Response} = A \times \text{Conc.}^2 + B \times \text{Conc.} + C$$

Quadratic regression, 1/X weighting, origin: included

* >15.0% outside acceptance criteria, not used for calculations

Table 3S Intra-run (N=6) and inter-run (N=18) imprecision (expressed as CV%) and inaccuracy (expressed as RE%) of lithium heparinized rat plasma QC samples, based on 3 series of 6 replicates for each level.

	LLOQ	QCL	QCM	QCH	ULOQ
Nominal levels (ng/mL)	10.0	30.0	1000	1600	2000
Intra-run Mean	10.9	31.2	963	1464	1736
Intra-run S.D.	0.176	1.97	69.4	38.8	32.4
Intra-run CV%	1.61	6.30	7.21	2.65	1.86
Intra-run RE%	9.41	4.10	-3.73	-8.52	-13.2
Inter-run Mean	10.8	31.2	999	1411	1785
Inter-run S.D.	0.494	2.22	64.9	43.8	68.6
Inter-run CV%	4.59	7.10	6.50	3.11	3.84
Inter-run RE%	7.74	4.05	-0.0702	-11.8	-10.8

Table 4S Intra-run (N=6) and inter-run (N=18) imprecision (expressed as CV%) and inaccuracy (expressed as RE%) of RHB QC samples, based on 3 series of 6 replicates for each level.

	LLOQ	QCL	QCM	QCH	ULOQ
Nominal levels (ng/mL)	20.0	60.0	1000	1600	2000
Intra-run Mean	18.9	61.3	908	1405	2056
Intra-run S.D.	2.42	2.26	25.3	31.4	22.7
Intra-run CV%	12.8	3.68	2.79	2.23	1.10
Intra-run RE%	-5.52	2.18	-9.17	-12.2	2.82
Inter-run Mean	18.5	59.2	1015	1559	2073
Inter-run S.D.	1.67	2.85	25.7	37.6	71.9
Inter-run CV%	9.04	4.82	2.53	2.41	3.47
Inter-run RE%	-7.54	-1.28	1.55	-2.55	3.66

Table 5S Carry-over assessment for tryptanthrin as analyte, and for (*E,Z*)-3-(benzylidenyl)-indolin-2-one as I.S. in lithium heparinized rat plasma (N=10).

Run number	Replicate	Peak response (counts)				Carry-over (%)		Mean Carry-over (%)	
		Blank sample		LLOQ		Analyte	IS	Analyte	IS
		Analyte	IS	Analyte	IS				
1	1	214	*84649	1894	88280	11.3	*-	12.4	*-
	2	229	*75240	1691	78955	13.6	*-		
2	1	256	0.00	2087	94992	12.3	0.00	10.5	0.00
	2	170	0.00	1963	95081	8.67	0.00		
3	1	55.6	0.00	2558	154281	2.17	0.00	2.36	0.0361
	2	49.5	87.0	1936	120559	2.55	0.0722		
4	1	184	0.00	2796	94349	6.60	0.00	5.81	0.00
	2	125	0.00	2488	88433	5.02	0.00		
5	1	438	192	2666	99474	16.4	0.193	18.5	0.242
	2	539	283	2624	97209	20.5	0.291		
Mean						9.91	0.0696		

*Contamination, carry-over of I.S. not calculated

Table 6S Carry-over assessment for tryptanthrin as analyte, and for (*E,Z*)-3-(benzylidenyl)-indolin-2-one as I.S. in Ringer HEPES buffer (N=12).

Run number	Replicate	Peak response (counts)				Carry-over (%)		Mean Carry-over (%)	
		Blank sample		LLOQ		Analyte	IS	Analyte	IS
		Analyte	IS	Analyte	IS				
1	1	847	471	9387	94179	9.02	0.500	8.61	0.465
	2	897	405	10941	94087	8.20	0.431		
2	1	1032	0.00	8137	90033	12.7	0.00	13.2	0.00
	2	1014	0.00	7405	70891	13.7	0.00		
3	1	513	0.00	4783	41605	10.7	0.00	9.66	0.00
	2	382	0.00	4441	44148	8.60	0.00		
4	1	240	0.00	4684	58675	5.12	0.00	5.95	0.00
	2	345	0.00	5098	54825	6.77	0.00		
5	1	159	0.00	6004	116645	2.65	0.00	2.83	0.0104
	2	149	21.6	4935	103819	3.02	0.0210		
6	1	233	0.00	5842	152568	0.00	0.00	0.00	0.00
	2	254	0.00	5397	134481	0.00	0.00		
Mean						6.71	0.0793		

Table 7S: Selectivity test at the LLOQ (10.0 ng/mL) for tryptanthrin, based on three different lithium heparinized rat plasma batches (N=6).

Nominal level (ng/mL)	10.0
Mean	10.4
S.D.	0.365
CV%	3.51
RE%	4.02

Table 8S: Selectivity test at the LLOQ (20.0 ng/mL) for tryptanthrin based on three different Ringer HEPES buffer batches (N=6).

Nominal level (ng/mL)	20.0
Mean	18.5
S.D.	0.993
CV%	5.37
RE%	-7.62

Table 9S: Absolute extraction yields of tryptanthrin and I.S. (*E,Z*)-3-(benzylidenyl)-indolin-2-one for lithium heparinized rat plasma (N=6).

Tryptanthrin nominal levels (ng/mL)	30.0	1000	1600
Absolute recovery (%)	79.4	77.5	77.6
CV%	8.73	4.90	4.80
SD	6.93	3.80	3.72

Internal final level (ng/mL)	750
Absolute recovery (%)	110
CV%	3.98
SD	4.38

Table 10S: Absolute extraction yields of tryptanthrin and I.S. (*E,Z*)-3-(benzylidenyl)-indolin-2-one for Ringer HEPES buffer (N=6).

Tryptanthrin nominal levels (ng/mL)	60.0	1000	1600
Absolute recovery (%)	60.8	78.6	88.0
CV%	3.77	3.26	2.68
SD	2.29	2.56	2.36

Internal final level (ng/mL)	433
Absolute recovery (%)	94.4
CV%	1.81
SD	1.71

Table 11S Dilution test in lithium heparinized rat plasma (N=6).

Nominal level (ng/mL)	4000
Dilution factor	10X
Mean	3833
S.D.	100
CV%	2.62
RE%	-4.19
Dilution factor	100X
Mean	4314
S.D.	104
CV%	2.41
RE%	7.85

Table 12S Dilution test in Ringer HEPES buffer (N=6).

Nominal level (ng/mL)	4000
Dilution factor	10X
Mean	3961
S.D.	130
CV%	3.29
RE%	-0.970
Dilution factor	100X
Mean	4186
S.D.	105
CV%	2.52
RE%	4.66

Table 13S Short-term stabilities in lithium heparinized rat plasma during storage in various conditions (expressed as RE%) (N=6).

Nominal levels (ng/mL)	30.0	1600
Three successive freeze/thaw cycles below -65°C	-1.60	-13.5
Stored rat plasma at RT for 4 h	4.70	-12.5
Processed rat plasma at 10°C for 36 h	-6.58	-12.8

Table 14S Short-term stabilities in Ringer HEPES buffer during storage in various conditions (expressed as RE%) (N=6).

Nominal levels (ng/mL)	60.0	1600
Three successive freeze/thaw cycles below -65°C	9.74	3.24
Stored RHB at RT for 4 h	-1.32	3.27
Processed RHB at 10°C for 19 h	8.12	-2.29

Table 15S Stability of tryptanthrin stock solution in DMSO stored below -65°C for 427 days and 6 hours at RT (N = 6).

Peak area ratios	
Stock solutions tested	New (t=0) SS of tryptanthrin + New SS of I.S.
Mean	4.09
S.D.	0.0716
CV%	1.75
Stock solutions tested	Old (t=427) SS of tryptanthrin + New SS of I.S.
Mean	4.03
S.D.	0.0211
CV%	0.524
Difference %	-1.59

Table 16S Mean values of the most relevant *in silico* descriptors for permeability.

Tryptanthrin (MW: 248.24 g/mol)	
<p><u>QikProp descriptors (3D)</u> donorHB: 0.00 accptHB: 6.00 LogPo/w: 1.01 LogBB: -0.450 Human Oral Absorption [%]: 84.4 PSA [Å²]: 73.1</p>	<p><u>Chemaxon Marvin (2D)</u> LogPo/w: 2.40 LogD7.4: 2.40 PSA [Å²]: 49.7</p>

3.3 Development and full validation of an UPLC-MS/MS method for the quantification of the plant-derived alkaloid indirubin in rat plasma

Evelyn A. Jähne, Chethan Sampath, Veronika Butterweck, Matthias Hamburger, and Mouhssin Oufir

Journal of Pharmaceutical and Biomedical Analysis 128 (2016) 247–252

DOI: 10.1016/j.jpba.2016.05.018

In the present study, we investigated key pharmacokinetic (PK) parameters for the anti-proliferative and anti-inflammatory compound (*Z*)-[2,3'-biindolinylidene]-2',3-dione (indirubin, Fig. 3) from *Isatis tinctoria* L.. Therefore, we developed a UPLC-MS/MS quantification method in lithium heparinized rat plasma and validated it according to current international guidelines. Indirubin was extracted from lithium heparinized rat plasma by using Waters Ostro™ pass-through sample preparation plates. Preliminary PK data were obtained from Sprague Dawley rats after intravenous administration of indirubin (2 mg/kg b.w.) and blood sampling up to 12 hours after i.v. injection. PK parameters were determined by non-compartmental analysis using PKSolver. A half-life ($t_{1/2}$) of around 30 min, and a relatively high clearance (CL) of almost 3 L/h/kg was found for the alkaloid.

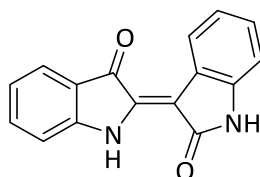


Fig. 3: (*Z*)-[2,3'-biindolinylidene]-2',3-dione

My contributions to this publication: development and validation of the UPLC-MS/MS method in lithium heparinized rat plasma, sample preparation and analysis, PK data analysis using PKSolver, writing the manuscript draft, and preparation of figures and tables.

Evelyn Andrea Jähne



Short communication

Development and full validation of an UPLC-MS/MS method for the quantification of the plant-derived alkaloid indirubin in rat plasma

Evelyn A. Jähne^a, Chethan Sampath^b, Veronika Butterweck^{b,c}, Matthias Hamburger^a, Mouhssin Oufir^{a,*}^a Institute of Pharmaceutical Biology, Department of Pharmaceutical Sciences, University of Basel, Klingelbergstrasse 50, CH-4056 Basel, Switzerland^b Department of Pharmaceutics, College of Pharmacy, University of Florida, 1345 Gainesville, FL, USA^c School of Life Sciences Institute for Pharma Technology, Gründenstrasse 40, CH-4132 Muttenz, Switzerland

ARTICLE INFO

Article history:

Received 19 January 2016

Received in revised form 9 May 2016

Accepted 10 May 2016

Available online 11 May 2016

Keywords:

Indirubin

Pharmacokinetics

Rat plasma

UPLC-MS/MS

Method validation

Phospholipid removal plate

ABSTRACT

An UPLC-MS/MS method for the quantification of indirubin in lithium heparinized rat plasma was developed and validated according to current international guidelines. Indirubin was extracted from rat plasma by using Waters Ostro™ pass-through sample preparation plates. The method was validated with a LLOQ of 5.00 ng/mL and an ULOQ of 500 ng/mL. The calibration curve was fitted by least-square quadratic regression, and a weighting factor of 1/X was applied. Recoveries of indirubin and I.S. were consistent and $\geq 75.5\%$. Stability studies demonstrated that indirubin was stable in lithium heparinized rat plasma for at least 3 freeze/thaw cycles, for 3 h at RT, for 96 h in the autosampler at 10 °C, and for 84 days when stored below -65 °C. Preliminary pharmacokinetic (PK) data were obtained from Sprague Dawley rats after intravenous administration of indirubin (2 mg/kg b.w.) and blood sampling up to 12 h after injection. PK parameters were determined by non-compartmental analysis. Indirubin had a half-life ($t_{1/2}$) of 35 min, and a relatively high clearance (CL) of 2.71 L/h/kg.

© 2016 Elsevier B.V. All rights reserved.

1. Introduction

The bis-indole indirubin is the red isomer of the ancient blue dye indigo. Both indigoids derive from colorless precursors found in various plants including *Baphicacanthus cusia* (Acanthaceae), *Polygonum tinctorium* (Polygonaceae), *Indigofera tinctoria* (Fabaceae) and *Isatis tinctoria* (Brassicaceae), and in some marine mollusks (Muricidae) [1,2]. The clinical interest in the compound was aroused in the early 1980s when indirubin was found to be the active ingredient of Danggui Longhui Wan, a mixture of 11 herbals used in the traditional Chinese medicine to treat chronic myelo-

cytic leukaemia (CML) [1,3]. Indirubin showed potent inhibition of cyclin-dependent kinases (CDKs) via interaction with the ATP-binding site of the kinase [1]. The compound induced a cell cycle arrest mainly in G2 and/or G2/M phase leading to apoptosis of the cell [1,4]. In addition to CDK inhibition, indirubin was shown to block other kinases, such as the glycogen synthase kinase-3 β (GSK-3) and the c-Src kinase [5]. Moreover, the alkaloid was reported to inhibit the cell cycle via activation of the aryl hydrocarbon receptor (AhR) [6,7]. Indirubin was also shown to possess anti-inflammatory properties, via inhibition of interferon γ and interleukin 6 production [8,9]. The compound was found to suppress the NF- κ B signaling pathway, and the expression of NF- κ B regulated-gene products involved in tumorigenesis [9]. Due to the potent anti-proliferative and anti-inflammatory activities, low toxicity, and reasonably drug-like properties indirubin served as a lead for medicinal chemistry efforts [3,10]. Considering the high interest in the compound, it is somewhat surprising that the pharmacokinetic (PK) properties of indirubin and indirubin derivatives have not been evaluated. Up to now, only one bioanalytical method for quantification of indirubin in rat plasma has been published [11]. However, the assay was using HPLC-UV and, therefore, does not meet current requirements for bioanalytical methods in terms of selectivity, specificity, and sensitivity. Therefore, we developed

Abbreviations: AUC, area under the curve; C₀, concentration at time zero; Cal, calibrator; CV%, coefficient of variation; ESI, electrospray ionization; I.S., internal standard; LLOQ, lower limit of quantification; LTS, long-term stability; MRM, multiple reaction monitoring; MRT, mean residence time; PK, pharmacokinetic; QC, quality control; QCH, quality control high; QCL, quality control low; QCM, quality control medium; SS, stock solution; $t_{1/2}$, half-life of elimination; TFA, trifluoroacetic acid; TQD, tandem quadrupole detector; ULOQ, upper limit of quantification; UPLC-MS/MS, ultra-high performance liquid chromatography with tandem mass spectrometric detection; V_d, volume of distribution; WS, working solution.

* Corresponding author.

E-mail addresses: mouhssin.oufir@unibas.ch, moussoufir@yahoo.com (M. Oufir).<http://dx.doi.org/10.1016/j.jpba.2016.05.018>

0731-7085/© 2016 Elsevier B.V. All rights reserved.

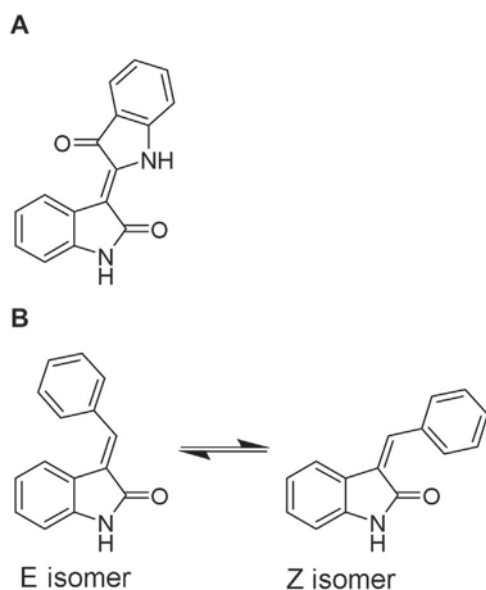


Fig. 1. Chemical structures of (Z)-[2,3'-biindolinylidene]-2',3-dione (indirubin) (A), and internal standard (*E,Z*)-3-(benzylidene)-indolin-2-one (B).

and validated a quantitative UPLC-MS/MS method for indirubin in rat plasma according to the US Food and Drug Administration (FDA) and European Medicines Agency (EMA) guidelines for industry [12,13], and applied it to a pilot PK study with intravenous administration of indirubin in male Sprague Dawley rats.

2. Experimental

2.1. LC-MS/MS analysis

2.1.1. Chemicals and reagents

(Z)-[2,3'-biindolinylidene]-2',3-dione (indirubin) (PubChem CID: 5359405) (Fig. 1A) and the internal standard (I.S.) (*E,Z*)-3-(benzylidene)-indolin-2-one (Fig. 1B) were synthesized according to published procedures [1,14]. Both compounds showed a purity of $\geq 99\%$, as determined by HPLC and NMR [15]. All used solvents were of HPLC grade. Acetonitrile and dimethyl sulfoxide (DMSO) were from Scharlau (Barcelona, Spain). Methanol was supplied by Lab-Scan (Gliwice, Poland). Formic acid and trifluoroacetic acid (TFA) were purchased from BioSolve (Valkenswaard, Netherlands). HPLC grade water was obtained by a Milli-Q (Merck Millipore, Darmstadt, Germany) water purification system. Ostro™ 96-well plates were provided by Waters (Milford, MA, USA), and blank male Sprague Dawley rat plasma in lithium heparin batches were from Seralab (Haywards Heath, UK).

2.1.2. LC-MS/MS instrumentation and chromatographic conditions

Sample analysis was performed on an Acquity UPLC system coupled to an Acquity tandem quadrupole detector (TQD) (all Waters Corp.). Chromatographic separation was performed on a UPLC HSS T3 column (100 mm \times 2.1 mm; 1.8 μ m particle size) (Waters Corp.). Column temperature was set at 45 °C, and autosampler temperature at 20 °C. Mobile phase was delivered at a flow rate of 0.5 mL/min. The mobile phase consisted of water containing 0.1% formic acid (Eluent A) and acetonitrile containing 0.1% formic acid (Eluent B). The following gradient was used: 30% of B (0–1 min); 30–77% of B (1–5 min); 77–100% of B (5–5.01 min); 100% of B (5.01–6 min); 100–30% of B (6–6.01 min); 30% of B (6.01–7 min). Total run time was 7 min. Weak and strong wash solvents were water-acetonitrile (50:50, v/v) containing 0.2% TFA,

and acetonitrile-isopropanol-acetone (40:40:30, v/v/v) containing 0.2% TFA, respectively. The seal wash solvent consisted of a water-acetonitrile mixture (90:10, v/v). Extracted samples were dissolved in DMSO and injected into the UPLC-MS/MS system in full loop mode (2 μ L).

The TQD system was equipped with an electro-spray ionization (ESI) interface, and measurements were performed in positive ion mode (ESI+) with multiple reactions monitoring (MRM). Nitrogen, generated by a nitrogen generator N2-Mistral (Schmidlin AG, Neuheim, Switzerland), was used both as desolvation and nebulization gas. Argon was used as collision gas. Capillary voltage was 4 kV for both analyte and I.S. Source temperature was set at 150 °C, and desolvation temperature was 400 °C. Flow rates for desolvation gas and cone gas were 1000 L/h and 10 L/h, respectively. Data were acquired with MassLynx V4.1 software and quantified by means of QuanLynx software (Waters Corp).

2.1.3. Sample preparation

Stock solutions (SS) of analyte and I.S. were prepared in DMSO. Working solutions (WS1) of analyte (100 μ g/mL) and I.S. (10 μ g/mL) were obtained by further diluting the corresponding SS in methanol. SS and WS1 were stored below –65 °C until use. WS2 of I.S. was prepared freshly before each analytical run by diluting WS1 with acetonitrile + 1% formic acid to a final concentration of 1000 ng/mL. Seven calibration samples (calibrators, cal) in the range of 5.00–500 ng/mL, and quality controls (QCs) at low, medium and high levels (QCL = 15.0 ng/mL, QCM = 250 ng/mL, QCH = 400 ng/mL) were prepared in lithium heparinized rat plasma by serial dilution of WS1 of the analyte. Calibrators and QCs were aliquoted into polypropylene tubes and stored below –65 °C until analysis.

2.1.4. Extraction of plasma samples

Indirubin was extracted from rat plasma using Waters Ostro™ pass-through sample preparation plates. For processing, the Ostro™ plate was placed onto a 96-deep well plate (96-DWP) serving as collection plate. To 50 μ L lithium heparinized rat plasma, 150 μ L of I.S. WS2 at 1000 ng/mL were added. The Ostro™/collection plate assembly was shaken for 10 min at RT on an Eppendorf Thermomixer (1000 rpm). After mixing, the plate assembly was placed onto a positive pressure processor (Biotage® PRESSURE+, Uppsala, Sweden), and a pressure of 30–40 psi was applied for 10 min. The Ostro™ plate was discarded, and the filtrate in the collection plate was dried under nitrogen (Evaporex EVX-96, Apricot Designs, Monrovia, CA, USA). Dried extracts were reconstituted with 200 μ L of DMSO. The 96-DWP was shaken for 45 min at RT on an Eppendorf Mixmate and centrifuged for 2 min at 3000 rpm (Megafuge, Heraeus Instruments AG, Switzerland). Due to adsorption of the I.S. to the polypropylene of 96-DWP, the samples were transferred into 300 μ L glass inserts in HPLC vials, prior to injection in full loop mode (2 μ L).

2.2. Bioanalytical method validation

The method was fully validated according to FDA and EMA guidelines [12,13]. Seven calibrators ranging from 5.00–500 ng/mL were injected at increasing concentrations, after a blank sample (blank rat plasma) and a zero sample (rat plasma only spiked with I.S.). The calibration curve was validated through six QCs (QCL, QCM, and QCH), which were inserted randomly into each analytical run. Calibrators and QCs were analyzed in duplicates. All validation runs were performed as described earlier [16,17]. Imprecision was expressed by the coefficient of variation (CV%), and inaccuracy as the relative error (RE%).

Specificity and selectivity was evaluated by six blank samples and six QC samples of indirubin at the lower limit of quantifica-

tion (LLOQ = 5.00 ng/mL) (duplicates, 3 different batches of lithium heparinized rat plasma), respectively.

Intra-run repeatability and *inter-run reproducibility* of the method were evaluated within one run (intra-run) and within three runs on three consecutive days (inter-run), respectively, by injecting six replicates of indirubin samples at five concentration levels (LLOQ, QCL, QCM, QCH, and ULOQ).

Carry-over was assessed by directly injecting an extracted blank after both replicates of the upper limit of quantification (ULOQ = 500 ng/mL).

Absolute recovery of indirubin was determined at three levels (QCL, QCM, and QCH) by comparing the peak areas of six extracted QC samples with six unextracted samples (= 100% recovery).

Dilution integrity of the samples was tested by spiking blank rat plasma with indirubin at a concentration of 2500 ng/mL, and by further diluting the obtained dilution QC (QC Dil.) with blank rat plasma in a ratio of 1:10 and 1:100. For each concentration level (25.0 and 250 ng/mL), six replicates were analyzed.

Short-term stability was assessed through six replicates at two concentration levels (QCL and QCH) after 3 h at RT, after 3 freeze and thaw cycles, and after 96 h storage under autosampler conditions (20 °C, light protected).

Long-term stability was determined by six replicates at three concentration levels (QCL, QCM, QCH) after 84 days, when stored below –65 °C. Stored samples were analyzed by a freshly prepared calibration curve.

Stock solution stability for indirubin was assessed after storage for 598 days below –65 °C, and for 6 h at RT. For this purpose, a working solution (5 µg/mL) was prepared in injection solvent from the freshly prepared and the stored stock solutions, and injected six times in the UPLC-MS/MS system. Stock solution stability of I.S. after 190 days storage below –65 °C was already described by Oufir et al. [16].

2.3. Preliminary PK study

All animal studies were performed according to the policies and guidelines of the Institutional Animal Care and Use Committee (IACUC) of the University of Florida, Gainesville, USA (NIH publication # 85-23), study protocol # 200802291 as previously described [16]. Indirubin was dissolved in DMSO and administered intravenously in male Sprague Dawley rats (N = 4) at a dose of 2 mg/kg b.w. Blood samples (300 µL) were collected from the sublingual vein into Vacuette® heparinized tubes at times of 0 (prior to dosing), 2, 5, 10, 20, 30 min, 1, 2, 3, 4, 6, 8, and 12 h. Blood samples were centrifuged at 4000 rcf for 15 min at 4 °C. The plasma samples were aliquoted into 1.5 mL tubes and stored below –65 °C until analysis. PK parameters were determined by non-compartmental analysis using PKSolver 2.0 [18].

2.4. Data analysis

Mean plasma concentrations of indirubin after intravenous (i.v.) administration versus time curves were generated in Graphpad Prim (version 5.01, San Diego, CA, USA). PK parameters were determined by non-compartmental analysis using PKSolver 2.0 [18], and included the concentration at time zero (C_0), the terminal elimination half-life ($t_{1/2}$), area under the curve extrapolated to infinity ($AUC_{0-\infty}$), the elimination rate constant (K_e), the mean residence time (MRT), the volume of distribution at terminal phase (V_z), and the clearance (CL). $AUC_{0 \rightarrow \text{last}}$ was calculated using a linear/log trapezoidal method from time zero to the last detectable sampling point 240 min after administration.

Table 1

Intra-run (N = 6) and inter-run (N = 18) imprecision (CV%) and inaccuracy (RE%) of QC samples, based on 3 series of 6 replicates for each level.

	LLOQ	QCL	QCM	QCH	ULOQ
Nominal level (ng/mL)	5.00	15.0	250	400	500
Intra-run Mean	4.97	13.8	238	418	490
Intra-run S.D.	0.304	0.414	5.65	14.3	14.3
Intra-run CV%	6.11	3.01	2.37	3.42	2.92
Intra-run RE%	–0.564	–8.22	–4.73	4.51	–1.95
Inter-run Mean	5.17	13.6	233	412	498
Inter-run S.D.	0.385	0.512	3.70	10.6	13.5
Inter-run CV%	7.44	3.77	1.59	2.57	2.71
Inter-run RE%	3.46	–9.60	–6.66	2.96	–0.487

3. Results and discussion

3.1. LC-MS/MS analysis

MS/MS parameters were generated using Waters IntelliStart software, and manually optimized according to Table S1. Due to the slow inter-conversion at RT of the I.S., both *E* and *Z* isomer peaks were integrated and quantified as previously described [16,17]. Quantification was achieved using MRM transitions at m/z 262.70 > 219.17 (Quantifier) and 262.70 > 190 (Qualifier) for indirubin, and 221.8 > 194.0 for I.S. The fragmentation patterns of indirubin and I.S. are shown in Fig. S3.

3.2. Method validation

The method of indirubin in rat plasma was validated with respect to specificity, selectivity, intra-run and inter-run reproducibility, carry-over, extraction yield, dilution, and short- and long-term stabilities. In accordance with FDA guidance, a run was considered to be valid if at least 75% of the calibrators were used to generate the calibration curve. Moreover, at least one duplicate of the LLOQ (Fig. 2A and B) and the ULOQ (Fig. 2C and D) had to be accepted. Among the six QCs, four replicates in total, and at least one replicate at each level had to be valid. To fulfill the acceptance criteria of FDA and EMA regulatory guidelines [12,13], imprecision (CV%) should be below 15% of the nominal values for all levels (20% for the LLOQ) and inaccuracy (RE%) should be within ±15% of the nominal values for all levels (±20% for the LLOQ). The calibration curve in the range of 5.00–500 ng/mL was fitted by least-square quadratic regression and a weighting factor of 1/X was applied (Table S2). The mean coefficient of determination (R^2) was 0.999 (Table S2).

Selectivity and specificity: The quantification method of indirubin in rat plasma was shown to be selective (CV% = 11.9%, RE% = –0.148%) (Table S3). The peak area of indirubin in the blank rat plasma samples (duplicates, 3 batches) was found to be below 20% (14.8%) of the LLOQ demonstrating that the method was specific (Table S4).

Intra-run repeatability and inter-run reproducibility: Intra-run imprecision (CV%) was in the range of 2.37% and 6.11% (Table 1), and inaccuracy (RE%) was between –8.22% and 4.51% of the nominal values (Table 1). Inter-run imprecision (CV%) ranged from 1.59% to 7.44%, and inaccuracy (RE%) was between –9.60% and 3.46% (Table 1), demonstrating that the acceptance criteria were met (below 15%).

Carry-over: Mean carry-over (Fig. 2E and F) in blank rat plasma samples was 2.60% (below 20%) for indirubin, and 0.00% for I.S. (below 5%), and thus met requirements of the EMA guideline for industry [13] (Table S5).

Extraction yield: The absolute recovery for indirubin was 78.5% for QCL (5.00 ng/mL), 75.5% for QCM (250 ng/mL), and 87.0% for QCH (400 ng/mL) (Table S6). Hence, recovery was consistent (Table S6). For I.S. an absolute recovery of 105% was found (Table S6).

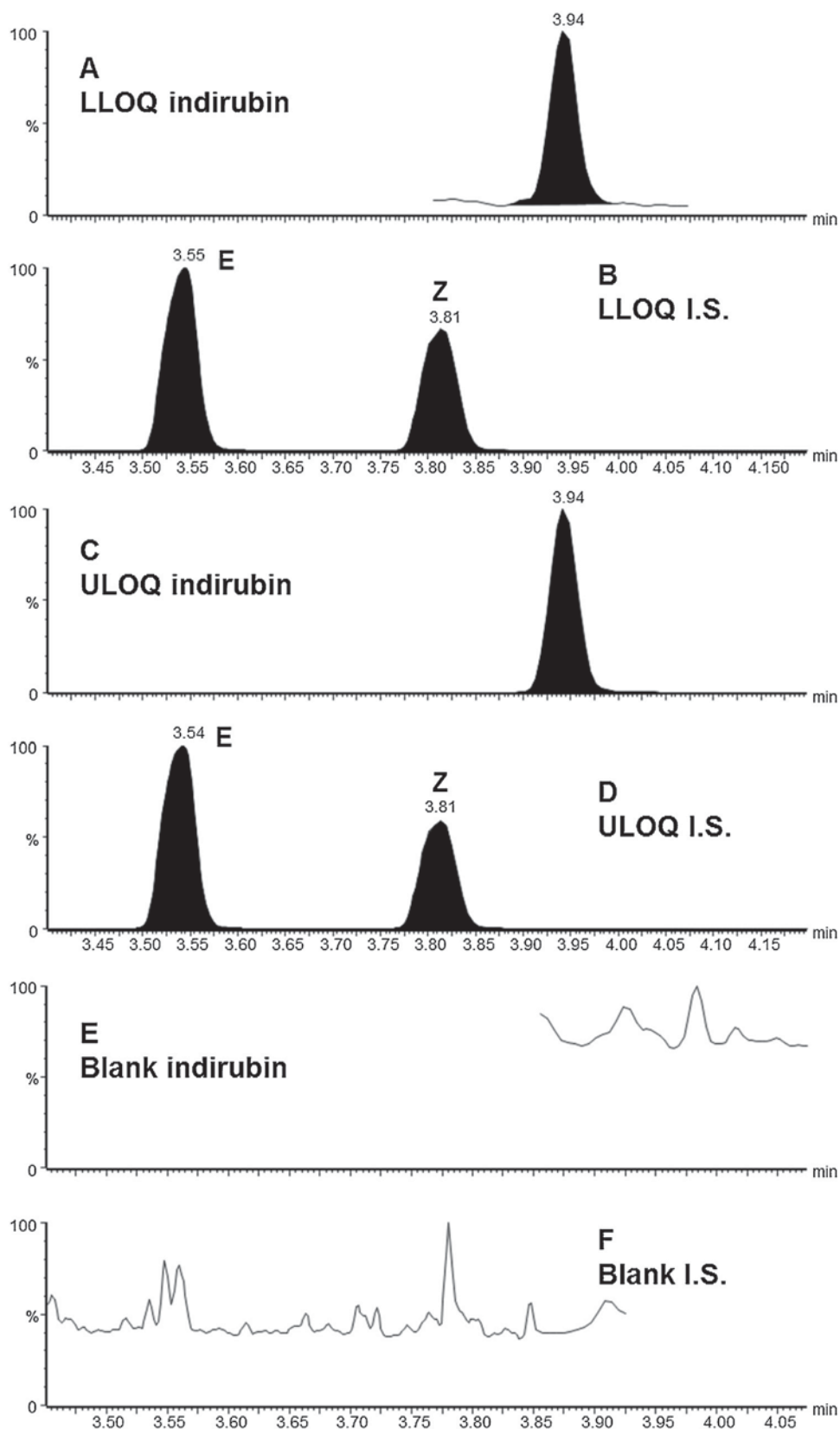


Fig. 2. Typical MRM chromatograms of rat plasma spiked with 5.00 ng/mL (LLOQ) of indirubin (A), with 1000 ng/mL of I.S. (B), with 500 ng/mL (ULOQ) of indirubin (C), with 1000 ng/mL of I.S. (D), of blank rat plasma injected directly after the ULOQ and monitored for indirubin (E), and I.S. (F).

Dilution test: Dilution of samples up to 100-fold did not affect precision and accuracy of the method, as the imprecision (CV%) was below 15% (10× dilution: 3.04%, 100× dilution: 2.67%), and

the inaccuracy (RE%) was within $\pm 15\%$ (10× dilution: -0.177% , 100× dilution: 8.60%) of the nominal value (Table S7).

Short-term stability: Indirubin samples in rat plasma were subjected to 3 freeze and thaw cycles. Imprecision (CV%) for the 6

Table 2

PK parameters after a single intravenous dose of 2 mg/kg bw indirubin in rats (N = 4). Data were calculated by PKSolver using non-compartmental analysis.

Parameter	Mean	SD
C_0 (ng/mL)	1052	329
$t_{1/2}$ (min)	35.0	4.20
T_{max} (min)	5.00	0.00
C_{max} (ng/mL)	811	140
AUC_{0-last} (ng × h/mL)	737	190
$AUC_{0-\infty}$ (ng × h/mL)	763	177
MRT (min)	50.2	8.53
V_z (L/kg)	2.25	0.296
CL (L/h/kg)	2.71	0.520

SD: standard deviation; C_0 : the concentration at time zero; $t_{1/2}$: half-life of elimination; AUC_{0-last} : area under curve from time zero to 240 min; $AUC_{0-\infty}$: area under the curve with extrapolation to infinity; MRT: mean residence time; V_z : volume of distribution at the terminal phase; CL: clearance.

replicates at the QCL (15.0 ng/mL) and the QCH (400 ng/mL) was below 15% (2.39% and 4.38%, respectively, data not shown), and inaccuracy (RE%) was within $\pm 15\%$ (−8.74% and −1.23%, respectively) (Table S8). In addition, indirubin samples were kept for 3 h at RT. Imprecision (CV%) for the 6 replicates at low concentration (15.0 ng/mL) was 3.96%, and 3.62% for the 6 replicates at high concentration (400 ng/mL) (data not shown). Inaccuracy (RE%) was −8.54% for QCL, and −0.207% for QCH (Table S8). Processed samples of indirubin were stored for 96 h under autosampler conditions (20 °C, protected from light). At both concentration levels (15.0 ng/mL and 400 ng/mL), imprecision (CV%) was below 15% (4.14% and 4.67%, respectively, data not shown), and inaccuracy (RE%) was within $\pm 15\%$ of the nominal values (−9.29% and 1.61%, respectively) (Table S8). Hence, according to FDA and EMA guidelines indirubin was stable under the above conditions.

Long-term stability: Stability of indirubin in rat plasma could be confirmed for at least 84 days when stored below −65 °C (Fig. S1), as the slope of the calculated linear regression was 0.944 (acceptance criteria: 1 ± 0.15).

Stock solution stability: Indirubin SS (dissolved in DMSO) was stored below −65 °C for 598 days and kept for 6 h at RT. Analysis showed that the degradation expressed by the percentage differences (−0.142%) was below 5%, indicating that the SS of indirubin was stable after storage below −65 °C for more than 1.5 years (Table S9). The DMSO SS of I.S. stored below −65 °C was stable up to 190 days, as already reported by Oufir et al. [16].

3.3. Preliminary PK study

The validated method was applied to the PK study of indirubin in Sprague Dawley rats after single i.v. dose of 2 mg/kg b.w. (N = 4). Typical MRM chromatograms of rat plasma samples are given in Fig. S2. The main PK parameters of indirubin calculated by non-compartmental analysis using PKSolver [18] are listed in Table 2, and the mean plasma concentration versus time profile is shown in Fig. 3. The initial concentration (C_0) of indirubin was 1052 ng/mL, the clearance was 2.71 L/h/kg, the area under the concentration-time curve (AUC) as calculated with the trapezoidal rule was 737 ng × h/mL, and the half-life ($t_{1/2}$) of indirubin was 35 min (Table 2). Previous PK data reported by Deng et al. obtained from male Wistar rats showed a half-life of 1 h (i.v., 2.8 mg/kg) [11]. The different $t_{1/2}$ found in male Wistar rats (1 h) and Sprague Dawley rats (35 min) may be explained by differing cytochrome P450 isozyme expression in the two strains. Furthermore, Koster et al. [19], reported that different strain suppliers, differences in diet, husbandry, and microflora could additionally influence the variability of isozyme expression [20]. Also, different administered doses (male Sprague Dawley rats: i.v., 2 mg/kg vs. male Wistar rats: i.v., 2.8 mg/kg) and body weight (male Sprague Dawley: 320–350 g

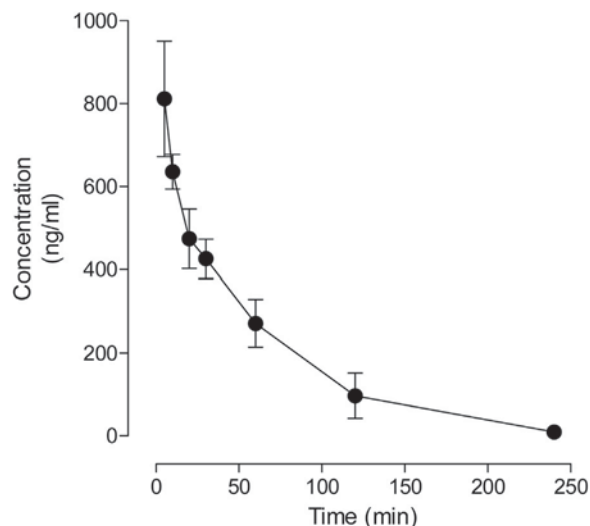


Fig. 3. Mean plasma concentration versus time profile of indirubin in male Sprague Dawley rats (N = 4) after i.v. administration (2 mg/kg b.w.).

vs. male Wistar rats: 280–300 g) might have impacted the excretion of the compound. Independent of that, our data obtained by a fully validated UPLC-MS/MS assay are significantly more reliable than the data in the previous study which were obtained by HPLC-UV analysis [11].

4. Conclusions

A highly selective, rapid and sensitive UPLC-MS/MS assay for quantification of indirubin in lithium heparinized rat plasma was developed and validated according to current regulatory guidelines [12,13]. The calibration curve in the range of 5.00–500 ng/mL was quadratic, with a weighting factor of $1/X$ and $R^2 > 0.999$. The validated method was applied to a pilot PK study in male Sprague Dawley rats after intravenous administration (2 mg/kg b.w.), where a relatively high clearance of 2.71 L/h/kg and a $t_{1/2}$ of 35 min were found. The assay will be subsequently used in a full PK study addressing oral bioavailability in Sprague Dawley rats. Moreover, in vitro metabolism of indirubin will be studied in human hepatocytes and liver microsomes.

Conflict of interest

None declared.

Acknowledgment

Financial support from the Swiss National Science Foundation (grant 05320.126888/1 to MH) is gratefully acknowledged. Thanks go to Orlando Fertig for technical assistance and to Teresa Faleschini and Daniela E. Eigenmann for proofreading of the manuscript.

Appendix A. Supplementary data

Supplementary data associated with this article can be found, in the online version, at <http://dx.doi.org/10.1016/j.jpba.2016.05.018>.

References

- [1] R. Hoessel, S. Leclerc, J.A. Endicott, M.E. Nobel, A. Lawrie, P. Tunnah, Indirubin, the active constituent of a Chinese antileukemia medicine, *Nat. Cell Biol.* 1 (1999) 60–67.

- [2] M. Hamburger, *Isatis tinctoria*—From the rediscovery of an ancient medicinal plant towards a novel anti-inflammatory phytopharmaceutical, *Phytochem. Rev.* 1 (2002) 333–344.
- [3] R. Jautelat, T. Brumby, M. Schäfer, H. Briem, G. Eisenbrand, S. Schwahn, M. Krüger, U. Lücking, O. Prien, G. Siemeister, From the insoluble dye indirubin towards highly active, soluble CDK2-inhibitors, *Chembiochem* 6 (2005) 531–540.
- [4] K.H. Merz, S. Schwahn, F. Hippe, S. Mühlbeyer, S. Jakobs, G. Eisenbrand, Novel indirubin derivatives, promising anti-tumor agents inhibiting cyclin-dependent kinases, *Int. J. Clin. Pharmacol. Ther.* 42 (2004) 656–658.
- [5] S. Leclerc, M. Garnier, R. Hoessel, D. Marko, J.A. Bibb, G.L. Snyder, et al., Indirubins inhibit glycogen synthase kinase-3 β and CDK5/P25, two protein kinases involved in abnormal tau phosphorylation in Alzheimer's disease, *J. Biol. Chem.* 276 (2001) 251–260.
- [6] J. Adachi, Y. Mori, S. Matsui, H. Takigami, J. Fujino, H. Kitagawa, C.A. Miller, T. Kato, K. Saeki, T. Matsuda, Indirubin and indigo are potent aryl hydrocarbon receptor ligands present in human urine, *J. Biol. Chem.* 276 (2001) 31475–31478.
- [7] M. Knockaert, M. Blondel, S. Bach, M. Leost, C. Elbi, G.L. Hager, S.R. Nagy, D. Han, M. Denison, M. Ffrench, Independent actions on cyclin-dependent kinases and aryl hydrocarbon receptor mediate the antiproliferative effects of indirubins, *Oncogene* 23 (2004) 4400–4412.
- [8] T. Kunikata, T. Tatefuji, H. Aga, K. Iwaki, M. Ikeda, M. Kurimoto, Indirubin inhibits inflammatory reactions in delayed-type hypersensitivity, *Eur. J. Pharmacol.* 410 (2000) 93–100.
- [9] G. Sethi, K.S. Ahn, S.K. Sandur, X. Lin, M.M. Chaturvedi, B.B. Aggarwal, Indirubin enhances tumor necrosis factor-induced apoptosis through modulation of nuclear factor- κ B signaling pathway, *J. Biol. Chem.* 281 (2006) 23425–23435.
- [10] P. Polychronopoulos, P. Magiatis, A.-L. Skaltsounis, V. Myrianthopoulos, E. Mikros, A. Tarricone, A. Musacchio, S.M. Roe, L. Pearl, M. Leost, Structural basis for the synthesis of indirubins as potent and selective inhibitors of glycogen synthase kinase-3 and cyclin-dependent kinases, *J. Med. Chem.* 47 (2004) 935–946.
- [11] X.Y. Deng, S.N. Zheng, G.H. Gao, G. Fan, F. Li, Determination and pharmacokinetic study of indirubin in rat plasma by high-performance liquid chromatography, *Phytomedicine* 15 (2008) 277–283.
- [12] Guidance for Industry Bioanalytical Method Validation, in: US Food and Drug Administration (FDA), Center for Drug Evaluation and Research, 2001.
- [13] Guideline on bioanalytical method validation. European Medicines Agency (EMA/CHMP/EWP/192217/2009). London, 2011,21.
- [14] L. Sun, N. Tran, F. Tang, H. App, P. Hirth, G. McMahon, C. Tang, Synthesis and biological evaluations of 3-substituted indolin-2-ones: a novel class of tyrosine kinase inhibitors that exhibit selectivity toward particular receptor tyrosine kinases, *J. Med. Chem.* 41 (1998) 2588–2603.
- [15] T. Mohn, O. Potterat, M. Hamburger, Quantification of active principles and pigments in leaf extracts of *isatis tinctoria* by HPLC/UV/MS, *Planta Med.* 73 (2007) 151–156.
- [16] M. Oufir, C. Sampath, V. Butterweck, M. Hamburger, Development and full validation of an UPLC-MS/MS method for the determination of an anti-allergic indolinone derivative in rat plasma, and application to a preliminary pharmacokinetic study, *J. Chromatogr. B.* 902 (2012) 27–34.
- [17] E.A. Jähne, D.E. Eigenmann, M. Culot, R. Cecchelli, F.R. Walter, M.A. Deli, R. Tremmel, G. Fricker, M. Smiesko, M. Hamburger, Development and validation of a LC-MS/MS method for assessment of an anti-inflammatory indolinone derivative by *in vitro* blood-brain barrier models, *J. Pharm. Biomed. Anal.* 98 (2014) 235–246.
- [18] Y. Zhang, M. Huo, J. Zhou, S. Xie, PKSolver An add-in program for pharmacokinetic and pharmacodynamic data analysis in Microsoft Excel, *Comput. Methods Programs Biomed.* 99 (2010) 306–314.
- [19] A.S. Koster, L. Nieuwenhuis, A.C. Frankhuijzen-Sierevogel, Comparison of microsomal drug-metabolizing enzymes in 14 rat inbred strains, *Biochem. Pharmacol.* 38 (1989) 759–765.
- [20] S. Kacew, Role of rat strain in the differential sensitivity to pharmaceutical agents and naturally occurring substances, *J. Toxicol. Environ. Health A.* 47 (1996) 1–30.

Supporting Information

Journal of Pharmaceutical and Biomedical Analysis

Development and full validation of an UPLC-MS/MS method for the quantification of the plant-derived alkaloid indirubin in rat plasma

Evelyn A. Jähne¹, Chethan Sampath², Veronika Butterweck^{2,3}, Matthias Hamburger¹, and Mouhssin Oufir^{1*}

¹Pharmaceutical Biology, Department of Pharmaceutical Sciences, University of Basel, Klingelbergstrasse 50, CH-4056 Basel, Switzerland

²Department of Pharmaceutics, College of Pharmacy, University of Florida, 1345 Gainesville, Florida, USA

³School of Life Sciences Institute for Pharma Technology, Gründenstrasse 40, CH-4132 Muttenz, Switzerland

*Corresponding author: Dr. Mouhssin Oufir, Institute of Pharmaceutical Biology, Department of Pharmaceutical Sciences, University of Basel, Klingelbergstrasse 50, CH-4056 Basel, Switzerland, Phone: +41 61 267 1544 Fax: +41 61 267 1474
E-Mail: mouhssin.oufir@unibas.ch

Figures

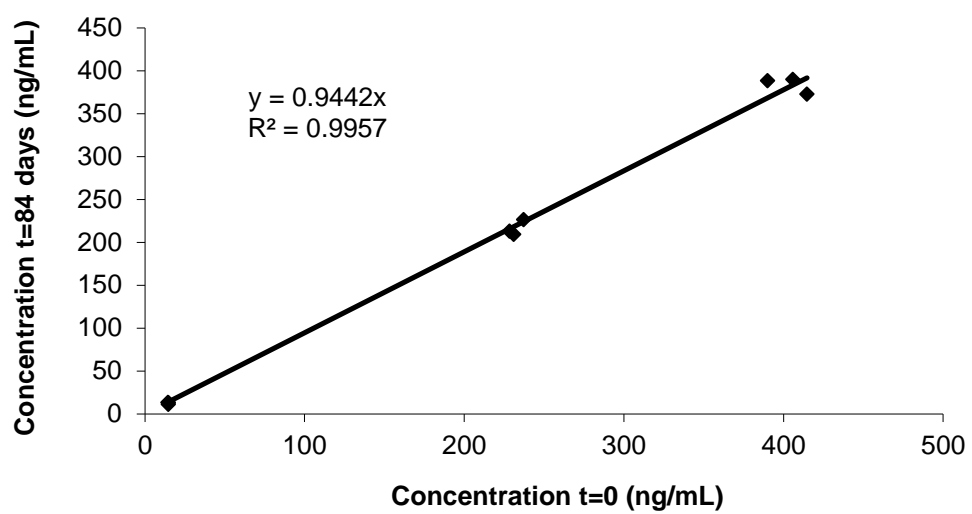


Fig. S1: Long-term stability of indirubin in rat plasma, kept for 84 days below -65°C .

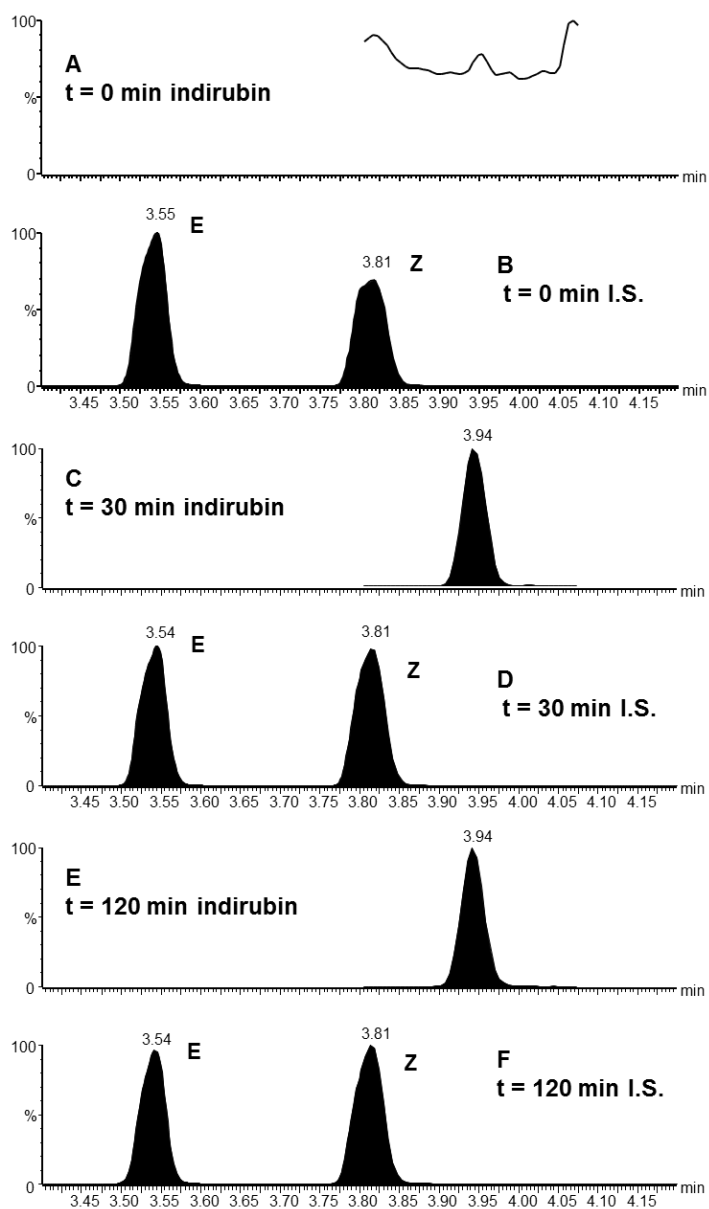


Fig. S2: Typical MRM chromatograms of rat plasma samples at t_0 monitored for indirubin (A) and I.S.(B), of rat plasma samples at 30 min after i.v. injection monitored for indirubin (C) and I.S. (D), and of rat plasma sample at 120 min after i.v. injection monitored for indirubin (E) and I.S. (F).

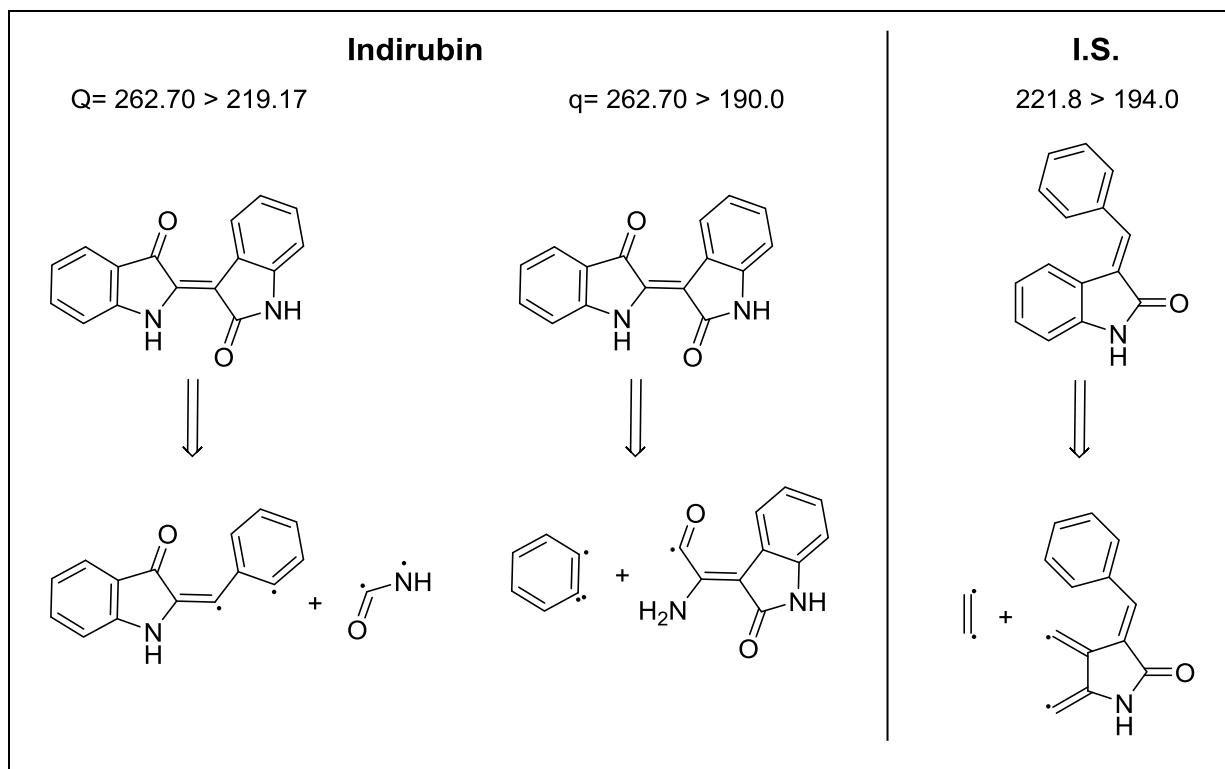


Fig. S3: Fragmentation pattern of indirubin and its I.S.

Tables

Table S1: Optimized MS/MS parameters in ESI positive mode for indirubin as analyte and (*E,Z*)-3-(benzylidene)-indolin-2-one as I.S.

Compounds	MRM transitions	Cone voltage (V)	Collision energy (eV)	Dwell time (ms)
Indirubin	Quan.: 262.70→219.17	58	25	108
	Qual.: 262.70→190	58	38	108
I.S.	221.8→194.0	46	25	108

Table S2: Calibrators and calibration curve parameters (N=8). Response: $A \times \text{Conc.}^2 + B \times \text{Conc.} + C$, Quadratic regression, 1/X weighting, Origin: included

Run number	Nominal level (ng/mL)							Regression parameters			
	5.00	10.0	20.0	50.0	100	250	500	A	B	C	R ²
1	4.45	10.5	19.7	51.3	100	240	500	-0.0000385	0.403	0.224	0.999
	4.95	11.4	21.1	50.7	97.2	257	502				
2	4.92	10.3	19.1	50.5	98.5	241	482	-0.0000612	0.406	0.166	0.999
	5.12	*11.7	21.5	51.3	101	254	520				
3	4.36	10.3	20.5	48.7	97.5	240	483	-0.0000893	0.431	0.145	0.998
	5.42	9.50	20.9	56.1	103	247	524				
4	4.74	10.5	19.7	49.2	94.8	239	501	-0.000107	0.479	0.378	0.999
	4.91	10.5	22.2	54.9	105	249	505				
Mean	4.86	10.4	20.6	51.6	100	246	502	-0.0000741	0.430	0.228	0.999
S.D.	0.342	0.559	1.03	2.61	3.32	6.93	15.0	0.0000304	0.0349	-	-
CV%	7.04	5.37	5.01	5.05	3.33	2.82	2.99				
RE%	-2.82	4.05	2.96	3.14	-0.369	-1.65	0.444				

* >15.0% outside acceptance criteria, not used for calculations

Table S3: Selectivity test at the LLOQ for indirubin (duplicates, 3 different batches of lithium heparinized rat plasma) (N=6).

Nominal level (ng/mL)	5.00
Mean	4.99
S.D.	0.593
CV%	11.9
RE%	-0.148

Table S4: Specificity test of six blank samples (duplicates, 3 different batches of lithium heparinized rat plasma) (N=6).

Matrix number	Peak area	LLOQ%
1	0.00	0.00
	30.7	14.8
2	0.00	0.00
	0.00	0.00
3	25.4	12.3
	0.00	0.00
LLOQ 1	215	
LLOQ 2	201	
Mean	208	

Table S5: Carry-over assessment for indirubin as analyte, and for (*E,Z*)-3-(benzylidene)-indolinone as I.S. (N=8).

Run number	Replicate	Peak response (counts)				Carry-over (%)		Mean Carry-over (%)	
		Blank sample		LLOQ		Analyte	I.S.	Analyte	I.S.
		Analyte	I.S.	Analyte	I.S.				
1	1	0.00	0.00	221	102421	0.00	0.00	0.00	0.00
	2	0.00	0.00	218	97250	0.00	0.00		
2	1	0.00	0.00	221	102421	0.00	0.00	0.00	0.00
	2	0.00	0.00	218	97250	0.00	0.00		
3	1	6.60	0.00	175	86466	3.77	0.00	2.97	0.00
	2	4.61	0.00	213	85771	2.17	0.00		
4	1	46.3	0.00	312	118087	14.8	0.00	7.41	0.00
	2	0.00	0.00	301	110477	0.00	0.00		
Mean						2.60	0.00		

Table S6: Absolute extraction yield of indirubin and I.S. (N=6).

Indirubin nominal level (ng/mL)	15.0	250	400
Absolute recovery (%)	78.5	75.5	87.0
CV%	8.34	5.64	3.46
SD	6.55	4.26	3.01
<hr/>			
I.S. final level (ng/mL)	433		
Absolute recovery (%)	105		
CV%	3.13		
SD	3.29		

Table S7: Dilution integrity test at 250 ng/mL (10X) and 25 ng/mL (100X) (N=6).

Nominal level (ng/mL)	2500	
Dilution factor	10X	100X
Mean	2496	2715
S.D.	75.9	72.6
CV%	3.04	2.67
RE%	-0.177	8.60

Table S8: Short-term stabilities in rat plasma during storage under various conditions (expressed as RE%) (N=6).

Nominal level (ng/mL)	15.0	400
Three successive freeze/thaw cycles below -65°C	-8.74	-1.23
Stored at RT for 3 hours	-8.54	-0.207
Processed plasma samples at 20°C for 96 hours	-9.29	1.61

Table S9: Stability of indirubin stock solution in DMSO stored below -65°C for 598 days, and for 6 hours at RT (N=6)

		Peak area ratios
Stock solutions tested		New (t=0) SS of indirubin + New SS of I.S.
Mean		510
S.D.		4.39
CV%		0.860
Stock solutions tested		Old (t=598 days) SS of indirubin + New SS of I.S.
Mean		509
S.D.		12.1
CV%		2.37
Difference (%)		-0.142

3.4 Caco-2 permeability studies and *in vitro* hERG liability assessment of tryptanthrin and indolinone

Evelyn A. Jähne, Daniela E. Eigenmann, Fahimeh Moradi-Afrapoli, Sheela Verjee, Veronika Butterweck, Simon Hebeisen, Timm Hettich, Götz Schlotterbeck, Martin Smieško, Matthias Hamburger, and Mouhssin Oufir

Planta Medica 82 (2016) 1192-1201

DOI: 10.1055/s-0042-110323

To predict oral absorption of the anti-inflammatory tryptanthrin and indolinone, we screened the two alkaloids in the Caco-2 model. P-glycoprotein (P-gp) interactions were assessed by co-incubation of a P-gp inhibitor (verapamil) and by calculation of the efflux ratio. For exact sample quantification, both compounds were partially validated in Hank's Balanced Salt Solution (HBSS) according to the guidelines of the Food and Drug Administration (FDA) and the European Medicine Agency (EMA). Tryptanthrin displayed a high permeability across the Caco-2 monolayer and its transepithelial transport was dominated by passive diffusion. The efflux ratio below 2 and the unchanged apparent permeability coefficients (P_{app}) in presence of the P-gp inhibitor verapamil (50 μ M) indicated that tryptanthrin was not involved in P-gp interactions. For indolinone, a low recovery was found in the Caco-2 assay. Further analysis using a High-Resolution Mass Spectrometry (HR-MS) system pointed to extensive phase II metabolism of indolinone (sulfonation and glucuronidation). Moreover, to identify potential human ether-a-go-go related gene (hERG) liabilities, the two compounds were screened against hERG channel inhibition by means of the patch-clamp technique. For both compounds, a weak hERG block was observed. *In silico* methods predicted a high oral absorption for tryptanthrin as well as slight inhibition of the hERG potassium channel in the μ M range.

My contributions to this publication: development and partial validation of the UPLC-MS/MS methods in HBSS, cultivation of Caco-2 cells, design of Caco-2 experiments, screening of the compounds in the Caco-2 model, sample preparation and analysis, MetID using MassMetaSite software, writing the manuscript draft, and preparation of figures and tables.

Evelyn Andrea Jähne

Caco-2 Permeability Studies and *In Vitro* hERG Liability Assessment of Tryptanthrin and Indolinone

Authors

Evelyn A. Jähne¹, Daniela E. Eigenmann¹, Fahimeh Moradi-Afrapoli¹, Sheela Verjee², Veronika Butterweck², Simon Hebeisen³, Timm Hettich⁴, Götz Schlotterbeck⁴, Martin Smieško⁵, Matthias Hamburger¹, Mouhssin Oufir¹

Affiliations

The affiliations are listed at the end of the article

Key words

- Caco-2
- metabolism
- U(H)PLC-MS/MS
- validation
- HR-MS
- hERG
- *Isatis tinctoria*

received March 23, 2016

revised May 27, 2016

accepted June 7, 2016

Bibliography

DOI <http://dx.doi.org/10.1055/s-0042-110323>
Published online July 15, 2016
Planta Med 2016; 82: 1192–1201 © Georg Thieme Verlag KG Stuttgart · New York · ISSN 0032-0943

Correspondence

Dr. Mouhssin Oufir
Institute of Pharmaceutical Biology
Department of Pharmaceutical Sciences
University of Basel
Klingelbergstrasse 50
4056 Basel
Switzerland
Phone: + 41 6 12 67 15 44
Fax: + 41 6 12 67 14 74
mouhssin.oufir@unibas.ch

Correspondence

Prof. Matthias Hamburger
Institute of Pharmaceutical Biology
Department of Pharmaceutical Sciences
University of Basel
Klingelbergstrasse 50
4056 Basel
Switzerland
Phone: + 41 6 12 67 15 44
Fax: + 41 6 12 67 14 74
matthias.hamburger@unibas.ch

Abstract

▼
Tryptanthrin and (*E,Z*)-3-(4-hydroxy-3,5-dimethoxybenzylidene)indolinone (indolinone) were recently isolated from *Isatis tinctoria* as potent anti-inflammatory and antiallergic alkaloids, and shown to inhibit COX-2, 5-LOX catalyzed leukotriene synthesis, and mast cell degranulation at low μM to nM concentrations. To assess their suitability for oral administration, we screened the compounds in an *in vitro* intestinal permeability assay using human colonic adenocarcinoma cells. For exact quantification of the compounds, validated UPLC-MS/MS methods were used. Tryptanthrin displayed high permeability (apparent permeability coefficient $> 32.0 \times 10^{-6} \text{ cm/s}$) across the cell monolayer. The efflux ratio below 2 (< 1.12) and unchanged apparent permeability coefficient values in the presence of the P-glycoprotein inhibitor verapamil ($50 \mu\text{M}$) indicated that tryptanthrin was not involved in P-glycoprotein interactions. For indolinone, a low recovery was found in the human colon adenocarcinoma cell assay. High-resolution mass spectrometry pointed to extensive phase II metabolism of indolinone (sulfation and glucuronidation). Possible cardiotoxic liability of the compounds was assessed *in vitro* by measurement of an inhibitory effect on human ether-a-go-go-related gene tail currents in stably transfected HEK 293 cells using the patch clamp technique. Low human ether-a-go-go-related gene inhibition was found for tryptanthrin ($\text{IC}_{50} > 10 \mu\text{M}$) and indolinone (IC_{50} of $24.96 \mu\text{M}$). The analysis of compounds using various *in silico* methods confirmed favorable pharmacokinetic properties, as well as a slight inhibition of the human ether-a-go-go-related gene potassium channel at micromolar concentrations.

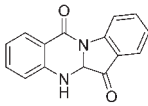
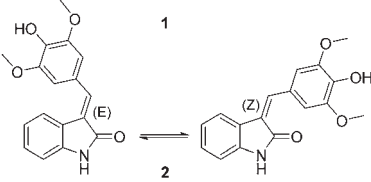
Abbreviations

▼

ADMET:	absorption, distribution, metabolism, excretion, and toxicity
A:	apical
B:	basolateral
BCRP:	breast cancer resistance protein
Caco-2:	human colonic adenocarcinoma cells
Cal:	calibrator
ER:	efflux ratio
HBSS:	Hank's balanced salt solution
hERG:	human ether-a-go-go-related gene
HR-MS:	high-resolution mass spectrometry
I.S.:	internal standard
LLOQ:	lower limit of quantification
MRP:	multi-drug resistance protein
OATP:	organic anion transporting polypeptide
P_{app} :	apparent permeability coefficient
P-gp:	P-glycoprotein
QC:	quality control
QCH:	quality control high
QCL:	quality control low
QCM:	quality control medium
SS:	stock solution
$t_{1/2}$:	terminal half-life
TEER:	transendothelial electrical resistance
U(H)PLC:	ultrahigh performance liquid chromatography
ULOQ:	upper limit of quantification
WS:	working solution

Supporting information available online at <http://www.thieme-connect.de/products>

Introduction

Tryptanthrin (**1**; ) and (*E,Z*)-3-(4-hydroxy-3,5-dimethoxybenzylidene)indolin-2-one (indolinone) (**2**; ) were previously identified as pharmacologically active alkaloids of the ancient anti-inflammatory plant *Isatis tinctoria* L. (Brassicaceae) [1]. Tryptanthrin was found to possess a unique pharmacological profile, since it potently inhibits COX-2, 5-lipoxygenase (5-LOX) catalyzed leukotriene synthesis *in vitro* and *in vivo* via a not yet fully elucidated mechanism [2–4], and iNOS catalyzed nitric oxide (NO) production [5]. Indolinone was found to block IgE-mediated degranulation of sensitized mast cells at nM concentrations without directly interfering with signaling upstream of the histamine-containing granules [6]. To further evaluate the potential of these alkaloids as novel anti-inflammatory and antiallergic leads, an assessment of their ADMET properties was warranted. We already reported on the pharmacokinetic (PK) properties in Sprague-Dawley rats and the *in vitro* blood-brain barrier (BBB) permeation potential of the compounds [7–9].

Presently, little is known about the oral absorption of indolinone and tryptanthrin. For this reason, we assessed the intestinal permeability in the well-established Caco-2 model [10]. As the strongly expressed efflux transporter P-gp in the intestine may substantially affect *in vivo* absorption of a compound due to its broad substrate specificity, we also assessed the P-gp interaction of tryptanthrin and indolinone in the Caco-2 assay. Besides P-gp, the hERG channel is a major anti-target in drug discovery, given that drug-induced hERG inhibition is the most important risk factor leading to fatal cardiac complications, such as arrhythmia [11]. We, therefore, studied possible hERG channel inhibition of tryptanthrin and indolinone by means of a patch clamp assay *in vitro*.

Results and Discussion

A full UPLC-MS/MS method validation for tryptanthrin and indolinone in Ringer HEPES buffer was recently reported [7–9]. Therefore, only a partial validation was performed for the two compounds in HBSS buffer (see Supporting Information). The calibration curves for tryptanthrin (10.0–1000 ng/mL) and indolinone (30.0–3000 ng/mL) were fitted by least-squares quadratic regression, and weighting factors of $1/X$ (for tryptanthrin) or $1/X^2$ (indolinone) were applied. Mean coefficients of determinations (R^2) were 0.997 for tryptanthrin and 0.995 for indolinone (Table S1, Supporting Information). To fulfill the acceptance criteria of the US Food and Drug Administration (FDA) [12] and the European Medicines Agency (EMA) [13], imprecision (CV%) should be below 15% for all levels (20% for the LLOQ as an exception), and inaccuracy (RE%) should be within $\pm 15\%$ of the nominal values for all levels ($\pm 20\%$ for the LLOQ). The mean carryover was 0.598% for tryptanthrin (0.00796% for I.S.) and 0.00% for indolinone (0.484% for I.S.) (Table S2, Supporting Information). The quantification methods of tryptanthrin (CV% = 7.17%, RE% = -5.37%) and indolinone (CV% = 8.15%, RE% = -11.2%) were shown to be selective (Table S3, Supporting Information). Peak areas of tryptanthrin and indolinone samples (duplicates, three batches) were found to be below 20% (0.00%, data not shown) of the LLOQ, demonstrating that both methods were specific. Dilution of samples up to 100-fold did not affect the precision and accuracy of the methods (Table S4, Supporting Information). Absolute recoveries for tryptanthrin were 76.3% for QCL (30.0 ng/mL),

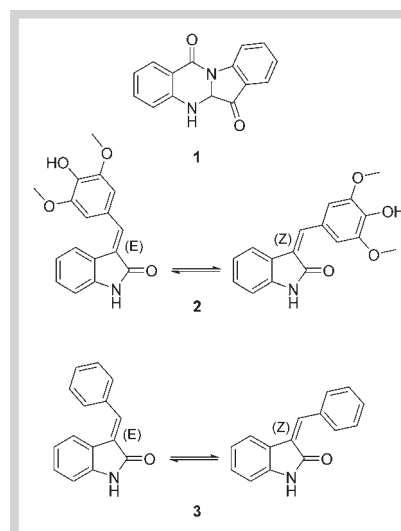


Fig. 1 Chemical structures of tryptanthrin (**1**), *E/Z*-indolinone (**2**), and the I.S. (*E/Z*)-3-(benzylidene)-indolin-2-one (**3**).

72.7% for QCM (500 ng/mL), and 71.3% for QCH (800 ng/mL) (Table S5, Supporting Information). Absolute recoveries of indolinone were 90.2%, 91.1%, and 94.5% at concentrations of 90, 1500, and 2400 ng/mL, respectively (Table S5, Supporting Information). Hence, recoveries were consistent within this concentration range (Table S5, Supporting Information). Tryptanthrin and indolinone were stable in HBSS for 4 h at room temperature, and after three successive freeze/thaw cycles (Table S6, Supporting Information). Moreover, tryptanthrin and indolinone samples in HBSS were stable up to 6 days (Table S7, Supporting Information) when stored below -65°C , as the slope of the calculated linear regressions was 0.8902 for tryptanthrin and 0.9822 for indolinone (acceptance criteria: slope 1 ± 0.15). The validated quantification methods were subsequently applied to an intestinal permeability assay using Caco-2 cells.

To evaluate the cell viability of the Caco-2 cells in the presence of tryptanthrin and indolinone, the 3-(4,5-dimethylthiazol-2-yl)-2,5-di-phenyltetrazoliumbromid (MTT) test was performed. Incubation with different concentrations of the compounds (1.25–20 μM) for 4 h indicated that the cell viability was not affected given that mean cell viabilities of 103% (tryptanthrin) and 94% (indolinone) were found with the highest concentration (data not shown). Test concentrations in the intestinal permeability assay did not exceed 10 μM .

The *in vitro* Caco-2 model formed a tight cellular barrier with mean TEER values of $550 \pm 12.7 \Omega\text{cm}^2$ (data not shown), and a mean P_{app} below $1.76 \pm 1.79 \times 10^{-6} \text{ cm/s}$ for the integrity marker sodium fluorescein (Na-F), which was screened in parallel. Mean TEER values recorded after the experiments ($487 \pm 7.57 \Omega\text{cm}^2$; data not shown) were in a similar range prior to the assay, indicating that the integrity of cell monolayers was maintained during the transport experiment. The mean P_{app} for tryptanthrin (5 μM) from A to B ($P_{\text{app A}\rightarrow\text{B}}$) and the mean P_{app} from B to A ($P_{\text{app B}\rightarrow\text{A}}$) were $32.0 \pm 6.86 \times 10^{-6} \text{ cm/s}$ and $37.2 \pm 0.890 \times 10^{-6} \text{ cm/s}$, respectively (Table 1). Similar results were found when tryptanthrin was tested at a concentration of 10 μM ($P_{\text{app A}\rightarrow\text{B}} = 33.1 \pm 3.36 \times 10^{-6} \text{ cm/s}$, $P_{\text{app B}\rightarrow\text{A}} = 35.0 \pm 2.70 \times 10^{-6} \text{ cm/s}$). Compared to the mean P_{app} values of the negative control Na-F ($< 1.76 \pm 1.79 \times 10^{-6} \text{ cm/s}$), mean P_{app} values of tryptanthrin were considerably higher and demonstrated that tryptanthrin crossed the intestinal barrier. The absorptive $P_{\text{app A}\rightarrow\text{B}}$ and the secretory $P_{\text{app B}\rightarrow\text{A}}$ showed no significant differences at both test concentrations (5

Table 1 Permeability data of tryptanthrin in the Caco-2 model (n = 3)

Concentration (μM)	Transport direction	Δt (min)	Recovery (%) mean \pm S. D.	P_{app} ($\times 10^{-6}$ cm/s) mean \pm S. D.	ER	
5	A \rightarrow B	10	83.4 \pm 17.3	32.0 \pm 6.86	1.12	
		30	84.5 \pm 19.1			
		60	83.7 \pm 19.1			
		120	93.5 \pm 17.8			
		Cell extraction	–			
		Control without cells	78.7 \pm 18.06			31.5 \pm 7.29
		Na-F (10 $\mu\text{g}/\text{mL}$)	90.5 \pm 5.54			0.532 \pm 0.0256
	B \rightarrow A	10	90.0 \pm 4.49	35.8 \pm 3.41		
		30	94.8 \pm 8.92			
		60	93.7 \pm 11.2			
		120	87.4 \pm 4.23			
		Cell extraction	–			
		Control without cells	89.3 \pm 7.75		37.0 \pm 3.78	
		Na-F (10 $\mu\text{g}/\text{mL}$)	98.6 \pm 2.49		0.516 \pm 0.0515	
10	A \rightarrow B	10	82.1 \pm 6.18	33.1 \pm 3.36	0.957	
		30	84.1 \pm 3.06			
		60	84.0 \pm 6.96			
		120	93.1 \pm 5.11			
		Cell extraction	–			
		Control without cells	105.4 \pm 8.74			39.6 \pm 1.56
		Na-F (10 $\mu\text{g}/\text{mL}$)	88.7 \pm 5.70			0.684 \pm 0.0802
	B \rightarrow A	10	90.8 \pm 4.50	35.0 \pm 2.70		
		30	85.4 \pm 2.63			
		60	85.8 \pm 1.97			
		120	83.1 \pm 3.12			
		Cell extraction	–			
		Control without cells	99.4 \pm 5.82		37.9 \pm 1.73	
		Na-F (10 $\mu\text{g}/\text{mL}$)	95.6 \pm 3.57		1.76 \pm 1.79	
5 + Verapamil (50 μM)	A \rightarrow B	10	81.6 \pm 1.50	29.4 \pm 1.45	1.19	
		30	87.0 \pm 3.85			
		60	81.0 \pm 3.88			
		120	91.2 \pm 3.28			
		Na-F (10 $\mu\text{g}/\text{mL}$)	86.1 \pm 5.81			0.676 \pm 0.132
	B \rightarrow A	10	99.4 \pm 1.60	35.1 \pm 0.472		
		30	95.6 \pm 2.24			
		60	90.1 \pm 1.23			
		120	86.0 \pm 0.959			
		Na-F (10 $\mu\text{g}/\text{mL}$)	92.9 \pm 1.99		0.611 \pm 0.0386	

and 10 μM), indicating that the transport of tryptanthrin was concentration-independent in this range (Table 1). To evaluate whether tryptanthrin was a P-gp substrate, the compound was coincubated with the P-gp inhibitor verapamil (50 μM) [14]. The mean P_{app} values of tryptanthrin from A to B and vice versa remained unaffected in the presence of verapamil, demonstrating that tryptanthrin was not subjected to P-gp efflux (Table 1). As the calculated ER ($P_{\text{app B}\rightarrow\text{A}}/P_{\text{app A}\rightarrow\text{B}}$) was around 1 (5 μM : 1.12, 10 μM : 0.957; Table 1), we assumed that tryptanthrin predominantly crossed the Caco-2 monolayer by passive diffusion. These findings could be corroborated by results obtained from control experiments. Mean P_{app} values of tryptanthrin across membranes with a Caco-2 cell monolayer were $32.0 \pm 6.86 \times 10^{-6}$ cm/s and $31.5 \pm 7.29 \times 10^{-6}$ cm/s for control membranes without cells, indicating that tryptanthrin crossed the cell monolayer by passive diffusion (Table 1). Similar observations for tryptanthrin have already been made in human and animal *in vitro* BBB models, where comparable mean P_{app} values of approx. 36×10^{-6} cm/s were found in experiments with a cell monolayer and control [9]. Moreover, the high permeability of tryptanthrin,

combined with its high lipophilicity, may explain the rather fast elimination ($t_{1/2}$ of approx. 40 min) found in the pilot PK study with Sprague-Dawley rats [9].

A previous study by Zhu et al. [15] on the transport characteristics of tryptanthrin confirmed the high permeability and its transepithelial transport by passive diffusion of tryptanthrin in the Caco-2 model. However, their P_{app} values were significantly (factor 2) higher than the P_{app} values obtained in our permeability studies, even though Caco-2 cells from the same origin were used (ATCC). Moreover, the ER in this study was 0.77 (vs. our ERs of 0.957–1.12), suggesting greater permeability in the absorptive directions. These differences might be explained by the Caco-2 comparison study of Hayeshi et al. demonstrating that besides cell source, passage number and culture conditions can also impact the transporter expression and thus the inter-laboratory variability in permeability data [16]. In the previous study on tryptanthrin, lower passage (31–40 vs. 60–65) and lower cell density (5×10^4 cells/cm² vs. 1.14×10^5 cells/cm²) were used for the transport experiments in the transwell system. Moreover, it should be noted that HPLC-UV analysis was used in that study,

Table 2 Permeability data of indolinone in the Caco-2 model (n = 3). *Due to the low recovery, no reliable P_{app} and ER calculations were possible.

Concentration (μM)	Transport direction	Δt (min)	Recovery (%) mean \pm S. D.	P_{app} ($\times 10^{-6}$ cm/s) mean \pm S. D.	ER
5	A \rightarrow B	10	67.1 \pm 12.6	*	*
		30	40.5 \pm 4.78		
		60	17.8 \pm 4.07		
		120	12.8 \pm 0.708		
		Cell extraction	0.527 \pm 0.129		
		Control without cells	110.0 \pm 20.2	42.0 \pm 2.05	
		Na-F (10 $\mu\text{g}/\text{mL}$)	82.1 \pm 3.60	0.357 \pm 0.0411	
	B \rightarrow A	10	102.1 \pm 3.75	*	
		30	87.9 \pm 3.35		
		60	69.3 \pm 5.08		
		120	36.3 \pm 4.64		
		Cell extraction	1.23 \pm 0.171		
		Control without cells	83.3 \pm 9.09	34.0 \pm 2.04	
		Na-F (10 $\mu\text{g}/\text{mL}$)	124.2 \pm 14.0	0.356 \pm 0.0758	
10	A \rightarrow B	10	38.6 \pm 5.28	*	*
		30	31.4 \pm 0.731		
		60	19.0 \pm 2.53		
		120	12.3 \pm 1.51		
		Cell extraction	0.363 \pm 0.0228		
		Control without cells	113.8 \pm 18.85	40.8 \pm 3.96	
		Na-F (10 $\mu\text{g}/\text{mL}$)	74.1 \pm 16.6	1.01 \pm 0.0293	
	B \rightarrow A	10	65.5 \pm 5.18	*	
		30	53.4 \pm 5.76		
		60	45.9 \pm 3.19		
		120	27.4 \pm 1.07		
		Cell extraction	1.12 \pm 0.257		
		Control without cells	117.0 \pm 4.62	47.8 \pm 2.10	
		Na-F (10 $\mu\text{g}/\text{mL}$)	122.4 \pm 11.9	0.227 \pm 0.0115	
5 + Verapamil (50 μM)	A \rightarrow B	10	37.3 \pm 4.34	*	*
		30	28.1 \pm 3.66		
		60	29.1 \pm 2.11		
		120	37.0 \pm 1.29		
		Na-F (10 $\mu\text{g}/\text{mL}$)	82.7 \pm 9.17	0.283 \pm 0.155	
	B \rightarrow A	10	68.5 \pm 3.62	*	
		30	53.7 \pm 4.10		
		60	51.1 \pm 2.54		
		120	29.6 \pm 2.60		
		Na-F (10 $\mu\text{g}/\text{mL}$)	90.8 \pm 11.7	0.285 \pm 0.124	

which does not meet current requirements for bioanalytical analysis in terms of selectivity, specificity, and sensitivity.

For an acceptable estimation of the P_{app} value, recovery should be at least 80% [10, 17]. Incomplete recovery might be due to adsorption of analytes to the transwell plate, metabolism, or compound retention within the cells [18, 19]. In all experiments, the mean recoveries of tryptanthrin were in the range of 81.0 \pm 3.88% to 99.4 \pm 1.60%, suggesting that the obtained P_{app} values were reliable.

For indolinone, calculation of the P_{app} values and ER was not possible due to a continued and significant loss of the compound over time (i.e., after 120 min, a recovery < 36.3% was determined; **Table 2**). Binding of the compound to the plate could be excluded, as mean recoveries in the control experiments (without cells) were all > 83% (**Table 2**). Cell extraction showed that compound loss due to retention in the cells was also minimal, since $\leq 1.23\%$ of indolinone was recovered after lysis (**Table 2**).

In Caco-2 cells, the expression levels of cytochrome P-450 metabolizing enzymes are relatively low [20, 21]. However, they express phase II enzymes such as UDP-glucuronosyltransferases (UGTs), sulfotransferases (SULTs), and glutathione-S-transferases (GSTs)

[22], and we therefore assessed a possible phase II metabolism of indolinone. For both isomers of the compound, UPLC-MS/MS analysis showed a time-dependent decline of peak intensity. However, a new peak that increased over the incubation time in the Caco-2 assay appeared between those of the *E*- and *Z*-isomers of indolinone (data not shown). This observation was made in samples taken from both the A and B compartments, while this peak was not observed in the Caco-2 cell lysate. High-resolution MS analysis with a UHPLC Q-TOF system and extracted ion chromatogram (EIC) at the mass-to-charge ratio (m/z) of 298.1074 ($[M + H]^+$ indolinone) indicated the formation of four metabolites (**Fig. 2**). Metabolite identification (Met-ID) using the Mass-MetaSite software proposed the formation of two sulfate and two glucuronide conjugates (ions at 378.0642 and 474.1395 m/z , respectively) (**Table 3**). Sulfate and glucuronide conjugates were excreted in comparable amounts to the A and B compartments (data not shown). Phase II metabolism in the Caco-2 assay has already been reported for various phenolic compounds, such as apigenin (UGT and SULT) [23], curcumin (GST) [24], and emodin (UGT) [25]. For those examples, the compounds were first metabolized in the cells, prior to active-mediated efflux.

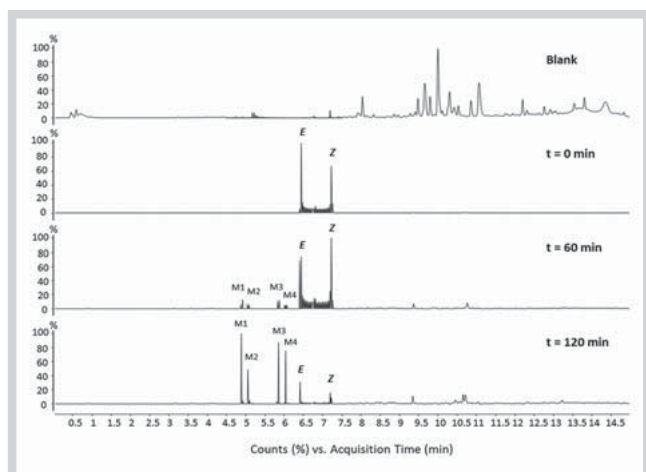


Fig. 2 QTOF EIC at 298.1074 m/z mass window \pm 20 ppm (*E/Z*-indolinone) at $t = 0, 60,$ and 120 , demonstrating a decrease of indolinone and the appearance of four metabolites.

UGTs are capable of forming O-, N-, S-, or C-linked glucuronides [26], while SULTs catalyze conjugation with O-, N-, and S- acceptor groups of a molecule. However, conjugation at a hydroxyl moiety is the dominant reaction for both enzymes [26,27]. Besides glucuronide conjugates M1 and M3 found at 474.1 m/z , sodium adducts ($[C_{23}H_{23}NO_{10} + Na]^+$) at a mass of 496.1214 m/z were also detected (► Figs. 3 and 4). MS/MS experiments at two collision energies (20 and 40 eV) were performed to locate the conjugation site on the chemical structure (► Fig. 5). However, the low concentrations of metabolites, intense adduct ions, and a fragmentation at the glycosidic linkage precluded a distinction between O- or N-conjugation. Given the slow *E/Z* isomerization of indolinone at room temperature, an assignment of the metabolite peaks to the respective *E* or *Z* isomer was not possible [28].

The middle peak that appeared between those of the *E* and *Z* isomers of indolinone by UPLC-MS/MS analysis after an incubation time of 120 min was not observed when indolinone was coincubated with the P-gp inhibitor verapamil. Thus, we conclude that one or more metabolites were involved in P-gp efflux. However, we were not able to identify which of the four metabolites identified by HR-MS/MS coeluted in the UPLC-MS/MS assay. As P-gp is only expressed on the A side in the Caco-2 assay and metabolites were identified on both sides of the compartment, we conclude that the indolinone conjugates were not only involved in

P-gp efflux. According to the literature, it is also possible that multi-drug resistance proteins (MRPs, expressed on the apical and basolateral side), the breast cancer resistance protein (BCRP, expressed on the apical side), and organic anion transporting polypeptides (OATPs, expressed on the apical side) are responsible for their efflux [29,30]. However, synthesis of the metabolites and further experiments with the corresponding transport inhibitors would be required to fully understand the transport mechanism of the indolinone conjugates.

We previously reported on the high BBB permeation potential of indolinone in three human and animal *in vitro* BBB models. Surprisingly, no metabolism was observed for indolinone in these cell-based assays [8]. This finding was in agreement with a recent study analyzing the expression pattern of phase II enzymes in freshly isolated human brain microvessels, where only one isoform of SULTs and no UGTs could be detected [31,32]. Overall, indolinone underwent extensive phase II metabolism, which in turn may explain the fast elimination of indolinone found in the previous PK study in rats ($t_{1/2}$ of approx. 4 min) [7]. However, incubations with hepatocytes and microsomes are needed to assess the metabolic stability of the compound in more detail.

A possible cardiotoxic liability of tryptanthrin and indolinone was assessed *in vitro* by measurement of an inhibitory effect on hERG tail currents in stably transfected HEK 293 cells (► Table 4). A total of 6 experiments was used for data analysis (► Fig. 6). Representative current traces recorded for tryptanthrin and indolinone are given in ► Table 4. For tryptanthrin, concentrations of 0.3, 3, and 10 μ M were tested. At the highest concentration (10 μ M), an inhibition of $36.0 \pm 3.57\%$ ($n = 3$) was found. Poor solubility of the compound precluded testing at higher concentrations. The estimated IC_{50} was $> 10 \mu$ M. Compared to strong hERG blockers (e.g., E-4031, IC_{50} of 7.7 nM) [33], the IC_{50} of tryptanthrin was relatively high. *In silico* predictions proposed a plasma protein binding of 91% for tryptanthrin (Table S8, Supporting Information). Therefore, a low free plasma concentration is expected, which most probably results in a safety margin of ($IC_{50, hERG}/\text{free plasma concentration}$) > 30 . Compounds with such safety margins are assumed not to cause arrhythmias [34]. Moreover, according to the ICH (International Conference on Harmonization) safety guideline S7B [35], further nonclinical data (e.g., effect on sodium/calcium channels) are required to ensure cardiac safety in humans. Previous studies in the functional *Xenopus* oocyte assay (voltage clamp technique) proposed no I_{hERG} inhibition (0.00%) for tryptanthrin when tested at 100 μ M [36]. However, the potency of the compounds tested in the oocyte model is usually decreased three- to tenfold compared to mammalian cells (e.

Table 3 Met ID by using Mass-MetaSite. The software proposed the presence of two glucuronides and two sulfates with masses of 474.1391 and 378.0641 m/z , respectively.

Name	Retention time (min)	z	m/z measured	m/z shift	Ion	m/z calculated	m/z Diff. (ppm)
M1 + 176 (glucuronide)	4.88	1	474.1391	+ 176.0321	$[C_{23}H_{23}NO_{10} + H]^+$	474.1395	0.71
M2 + 80 (sulfonic acid)	5.06	1	378.0641	+ 79.9568	$[C_{17}H_{15}NO_7S + H]^+$	378.0642	0.31
M3 + 176 (glucuronide)	5.85	1	474.1391	+ 176.0321	$[C_{23}H_{23}NO_{10} + H]^+$	474.1395	0.24
M4 + 80 (sulfonic acid)	6.04	1	378.0641	+ 79.9568	$[C_{17}H_{15}NO_7S + H]^+$	378.0642	0.36
<i>E</i> -Indolinone (parent)	6.41	1	298.1073	0	$[C_{17}H_{15}NO_4 + H]^+$	298.1074	0.41

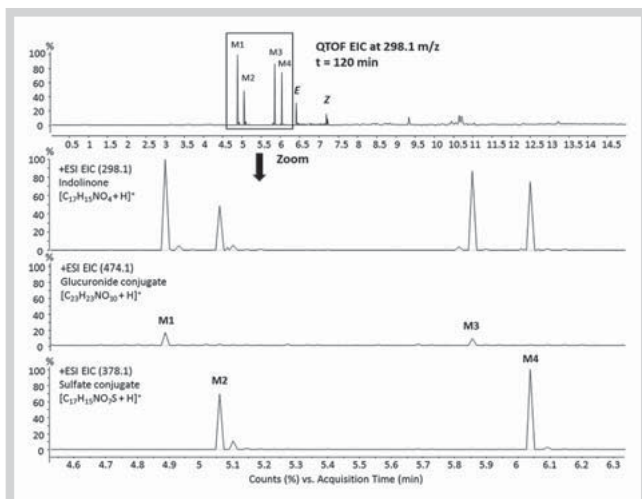


Fig. 3 Zoom of the QTOF EIC after 120 min at 298.1 m/z (*E/Z*-indolinone), 378.1 m/z (sulfate conjugates), and 474.1 m/z (glucuronide conjugates).

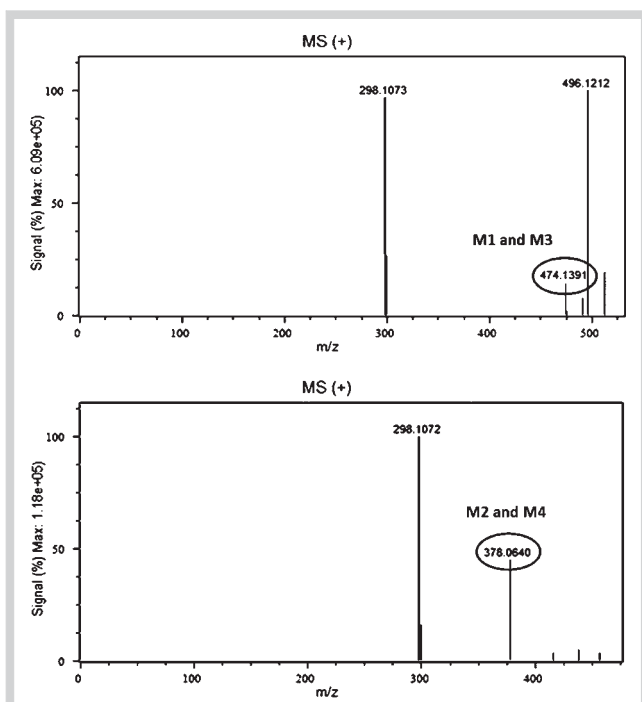


Fig. 4 Mass spectra of glucuronide conjugates (474.1391 m/z, M1 and M3) and sulfate conjugates (378.0640 m/z, M2 and M4).

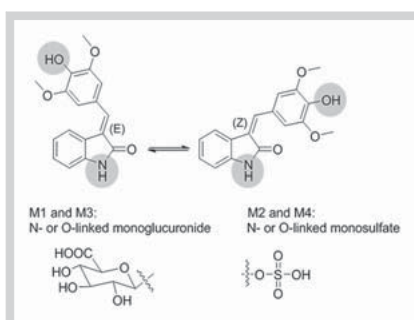


Fig. 5 Proposed phase II metabolites of indolinone.

g., HEK 293) [37, 38]. For indolinone, four concentrations (1.0, 10, 30, and 100 μM) were tested, and an IC_{50} of 24.9 μM (Hill coefficient: 1.44) was found (Table 4). However, given the high plasma protein binding (95%, predicted *in silico*, Table S8, Supporting Information), the high metabolic instability (*in vitro* Caco-2 assay), and the fast clearance (*in vivo* PK study) [7] of indolinone, a hERG block under physiological conditions appears rather unlikely.

In vitro data obtained from the Caco-2 and hERG assays were corroborated by *in silico* predictions using Percepta Profiler, Schrodinger Qik Prop, and the VirtualTox Lab. Along with no violations of Lipinski's rule of five, the ACD Percepta Profiler proposed a high permeability in the Caco-2 assay, a 100% absorption in the human intestinal models, and a relatively low probability (0.35) for P-gp interaction (Table S8, Supporting Information). *In silico* predictions for indolinone indicated high permeability in the Caco-2 assay, 100% absorption in the human intestinal model, and a moderate probability (0.43) for P-gp interaction (Table S8, Supporting Information). Additionally, good oral absorption (>84%) and Caco-2 permeability ($P_{\text{app}} > 60 \times 10^{-6} \text{ cm/s}$) in the QikProp application. For both compounds, inhibition of the hERG potassium channel at low micromolar concentrations ($\text{IC}_{50 \text{ hERG}}$ and $K_{\text{d hERG}}$, respectively) was predicted with two conceptually different *in silico* techniques (QSAR in QikProp, and molecular docking and scoring in the VirtualToxLab). The predictions were thus in excellent agreement with experimental data (Table S9, Supporting Information).

Materials and Methods

Chemicals and reagents

Tryptanthrin (**1**; Fig. 1), indolinone (**2**; Fig. 1), and the I.S. (*E,Z*)-3-(benzylidene)-indolin-2-one (**3**; Fig. 1) were synthesized according to established procedures [39,40]. Purity of the compounds was $\geq 99\%$, as determined by HPLC and NMR [41]. All reagents were obtained from Sigma-Aldrich unless otherwise indicated. All solvents were of analytical grade. Methanol was from Lab-Scan. Formic acid (FA) and trifluoroacetic acid (TFA) were supplied by BioSolve. Acetonitrile and dimethyl sulfoxide (DMSO) were purchased from Scharlau. Tween 20 was provided by Fluka. FBS "Gold" was from PAA Laboratories. MEM nonessential amino acids solution (NEAA) (100X) was supplied by Gibco. HPLC grade water was obtained from a Milli-Q water purification system (Millipore Merck). Tissue culture flasks were from BD Biosciences, and 6-well plates and inserts were from Corning Costar.

Sample preparation

SS of tryptanthrin, indolinone, and I.S. were prepared in DMSO and stored below -65°C . Working solutions (WS1) of analytes (100 $\mu\text{g/mL}$) and I.S. (10 $\mu\text{g/mL}$) were prepared in methanol by further diluting the corresponding SS. For analytes, calibration samples (Cals) and QCs at low, middle, and high levels were prepared in HBSS (without phenol red) by serial dilution of the corresponding WS1 (range: 10.0–1000 ng/mL for tryptanthrin; 30.0–3000 ng/mL for indolinone). All Cals and QCs were aliquoted into polypropylene tubes and stored below -65°C . Due to the adsorption of tryptanthrin to the container surface, all tubes were pretreated with 0.2% Tween 20. For the I.S., a second WS at a concentration of 1000 ng/mL was prepared daily by fur-

Table 4 Representative hERG current traces mean values of relative tail current inhibition, IC₅₀, and Hill values for tryptanthrin (A, n = 3), indolinone (B, n = 3), E-4031 (C, positive control, n = 4), and DMSO (D, negative control, n = 4).

Compound	IC ₅₀ value (μM)	Hill coefficient
Tryptanthrin	> 10	0.73
Concentration (μM)	Rel. tail current (%)	Mean ± SEM
0.3	99.85, 96.28, 92.78	96.30 ± 2.04%
1.0	91.69, 88.28, 90.48	90.15 ± 1.00%
10.0	67.85, 56.84, 67.20	63.96 ± 3.57%
Indolinone	24.96	1.44
Concentration (μM)	Rel. tail current (%)	Mean ± SEM
1.0	99.78, 90.96, 101.9	97.55 ± 3.35%
10.0	82.38, 73.49, 86.08	80.65 ± 3.74%
30.0	40.97, 41.42, 41.77	41.39 ± 0.23%
100	14.03, 12.35, 15.61	14.00 ± 0.94%
E-4031	0.01 163	1.20
Concentration (nM)	Rel. tail current (%)	Mean ± SEM
1.0	93.05, 98.47, 83.29, 92.57	91.85 ± 3.15%
3.0	83.93, 85.83, 78.10, 78.27	81.53 ± 1.97%
10	61.97, 65.57, 57.36, 49.75	58.66 ± 3.41%
30	21.69, 20.93, 22.86, 18.69	21.04 ± 0.88%
DMSO	–	–
Concentration (nM)	Rel. tail current (%)	Mean ± SEM
0.3	96.35, 96.84, 97.58, 101.18	97.99 ± 1.09%
Bath solution	0.3% DMSO perfused for > 12 min	

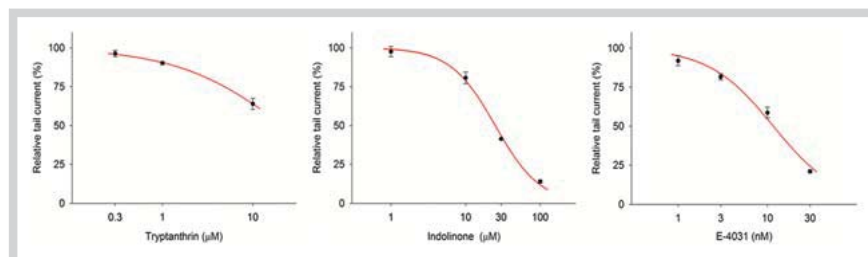


Fig. 6 Dose-response curves for the inhibition of the hERG tail current by tryptanthrin, indolinone, and the positive control E-4031. (Color figure available online only.)

ther diluting WS1 in methanol. HBSS samples were extracted as previously described by protein precipitation using acetonitrile [7–9]. Due to nonspecific binding of the I.S. onto the 96-DWP, each sample was transferred into a 300-μL glass insert of an HPLC vial prior to analysis.

UPLC-MS/MS settings

Method validation was performed on a Waters Acquity UPLC system coupled to a Waters Acquity tandem quadrupole detector. Chromatographic separation was performed on a Waters UPLC HSS T3 column (100 mm × 2.1 mm; 1.8 μm particle size). Mobile phase was delivered at a flow rate of 0.5 mL/min (Table S10, Supporting Information). Weak and strong wash solvents were water-acetonitrile (50:50, v/v) and acetonitrile-isopropanol-acetone (40:30:30, v/v/v) containing 0.2% TFA. The seal wash solvent consisted of a water-acetonitrile mixture (90:10, v/v). Samples were injected into the UPLC-MS/MS system in full loop mode (Table S10, Supporting Information). Mass spectrometric detection was in the positive ionization mode (ESI+). Nitrogen was generated by a nitrogen generator N2-Mistral (Schmidlin AG)

and used both as a desolvation and nebulization gas. Argon was used as the collision gas. MS/MS parameters were generated using Waters IntelliStart software, followed by manual optimization (Table S11, Supporting Information). The capillary voltage was 3.5 kV, the source temperature was set at 150 °C, and the desolvation temperature was 400 °C. Flow rates for the desolvation gas and cone gas were 900 L/h and 10 L/h, respectively. Data were acquired with MassLynx V4.1 software and quantified by means of QuanLynx software (Waters, Corp.).

Cell viability assays

Cytotoxicity of analytes in Caco-2 cells was determined with the MTT assay in a 96-well format [42,43]. A suspension of the cell line was seeded into a 96-well flat bottom tissue culture plate at a density of 5×10^3 cells/well, and incubated in an incubator (37 °C, 5% CO₂) for 48 h. Cells were treated with 200 μL of test samples, dissolved in culture medium at final concentrations of 1.25–20 μM, and incubated for 48 h. Afterwards, 20 μL of MTT reagent (5 mg/mL, dissolved in PBS) were added to each well. The plate was kept on an orbital shaker at 100 rpm and 37 °C for 4 h. Finally,

the medium was removed, 150 μL of DMSO were added, and the plate was agitated on an orbital shaker for 15 min. Absorbance was measured at 570 nm on a microplate reader with a reference filter of 620 nm. A set of wells with no test sample, treated with the highest concentration of DMSO (1%), served as controls. Betulinic acid was used as a positive control. Cell viability was calculated according to the following equation:

$$\text{Cell viability (\%)} = \frac{\text{Absorbance of test well}}{\text{Absorbance of control}} \times 100$$

Caco-2 experiments

The human colon adenocarcinoma cell line Caco-2 was a gift of Prof. H.P. Hauri, Biocenter, University of Basel, and originated from the ATCC. Caco-2 cells were maintained at 37 °C in a humidified atmosphere with 5% CO_2 , and passaged at a confluence of 70–90%. Cells were cultured in Dulbecco's modified Eagle medium (DMEM) supplemented with FBS (10%), L-glutamine (200 mM), and nonessential amino acids (1%). For the permeability assay, Caco-2 cells of passages 60 to 65 were seeded at a density of 3.58×10^5 cells/ cm^2 in 6-well Transwell inserts (translucent polycarbonate membrane, 0.4 μm pore size, 1.0×10^8 pores/ cm^2). Permeability experiments were performed 19–21 days after seeding. Monolayer integrity was assessed by measuring the TEER (before and after the experiment) with an epithelial voltohmmeter (EVOM, World Precision Instruments). Permeability experiments were performed when TEER values of 400–600 Ωcm^2 were reached.

Tryptanthrin and indolinone were screened at concentrations of 5 and 10 μM , together with sodium fluorescein (Na-F, 10 $\mu\text{g}/\text{mL}$) as a paracellular barrier integrity marker. To evaluate whether indolinone and tryptanthrin were P-gp substrates, they were coin-cubated (5 μM) with the P-gp inhibitor verapamil (50 μM). Transport experiments were performed in triplicate, and in a bidirectional way. Therefore, 1.6 mL test solution (5 or 10 μM dissolved in HBSS + 0.2% BSA) were added either to the A (1.6 mL, $P_{\text{app}}^{\text{A} \rightarrow \text{B}}$) or the B side (2.8 mL, $P_{\text{app}}^{\text{B} \rightarrow \text{A}}$). The receiver compartment was spiked with HBSS + 0.2% BSA alone. After incubation at 37 °C on an orbital shaker at 100 rpm, sample aliquots (220 μL) were collected from both A and B compartments after 10, 30, 60, and 120 min, and stored below –65 °C until analysis. The fluorescent marker (Na-F) was quantified by a Chameleon microplate reader ($\lambda_{\text{ex}} = 490$ nm, $\lambda_{\text{em}} = 514$ nm; Hidex), and the analytes by UPLC-MS/MS. The P_{app} for analytes and Na-F were calculated according to the following equation [44]:

$$P_{\text{app}} = \frac{V_{\text{R}}}{(AC_{\text{D0}})} * \frac{\Delta C_{\text{R}}}{\Delta t} \text{ (cm/s)}$$

V_{R} = volume in the receiver compartment; A = surface area of the filter membrane (4.7 cm^2 for 6-well inserts); C_{D0} = initial concentration in the donor compartment; $\Delta C_{\text{R}}/\Delta t$ = change of concentration over time in the receiver compartment. The ER [44] was calculated as follows:

$$\text{ER} = \frac{P_{\text{app}}^{\text{B} \rightarrow \text{A}}}{P_{\text{app}}^{\text{A} \rightarrow \text{B}}}$$

An ER > 2.0 was considered as an indication for active efflux [35]. To ensure that the diffusion barrier was only provided by the cell monolayer, control experiments were performed using inserts without cells. Compound loss was assessed by calculating the recovery (mass balance) according to the following equation:

$$\text{Recovery (\%)} = \frac{C_{\text{Df}}V_{\text{D}} + C_{\text{Rf}}V_{\text{R}}}{C_{\text{D0}}V_{\text{D}}} \times 100$$

C_{Df} = final concentration of the compound in the donor; C_{Rf} = final concentration of the compound in the receiver compartment; C_{D0} = initial concentration in the donor compartment; V_{D} , V_{R} = volumes in the donor and receiver compartments, respectively. All results are expressed as means \pm S.D.

Cell extraction

Cell extraction was performed according to a published protocol [45], with minor modifications. After the experiment, inserts were washed with ice-cold DPBS (without $\text{Ca}^{2+}/\text{Mg}^{2+}$) and transferred into a petri dish (22.1 cm^2). Subsequently, 750 μL of Triton™ X-100 solution (1% in HBSS) were added to the A side, and dishes were shaken on an orbital shaker at 100 rpm for 15 min at 37 °C. Cells were scraped off the membrane using a cell scraper, transferred into a 1.5-mL tube, and stored below –65 °C. Frozen cell suspensions were thawed at 37 °C under shaking at 1400 rpm (Thermomixer comfort, Eppendorf AG). To precipitate proteins and extract indolinone, 750 μL of acetonitrile were added to the cell suspension (750 μL). Samples were vortexed, mixed for 10 min on a thermomixer (37 °C, 1400 rpm), and centrifuged for 5 min at 16 100 g. Supernatants of the first extraction were transferred into a fresh 1.5-mL tube and stored at 4 °C. After adding 750 μL of acetonitrile to the pellet, the pellet was homogenized with six pulses of an ultrasonic disintegrator (Branson Sonifier 250, Branson Ultrasonic Corporation; settings: output control 2, duty cycle 30%), followed by 10 min of extraction (37 °C, 1400 rpm) and 5 min of centrifugation (16 100 g). The extraction was repeated, and all supernatants (of the first, second, and third extraction) were combined in a 96-DWP and evaporated to dryness under nitrogen flow. Dried samples were reconstituted with 200 μL of injection solvent (Table S10, Supporting Information) containing I.S., and transferred into 300 μL glass inserts of HPLC vials prior to UPLC-MS/MS analysis. Recovery was calculated by multiplying the measured concentration with the reconstituted volume.

Identification of metabolites

The metabolite search of indolinone was performed in a transwell system equally, as described for the Caco-2 transporter experiments. To identify metabolites of indolinone in the Caco-2 assay, 7 μL of extracted HBSS samples were injected into the Agilent 1290 Infinity UHPLC system consisting of a degasser, a binary pump, an autosampler, a thermostat, and a column oven (Agilent Series 1290, Agilent Technologies). The UHPLC system was connected to an HR mass spectrometer (Agilent Series 6540 Q-TOF, Agilent Technologies) operating in the positive mode, using an Agilent Jet Stream electrospray ion source (AJS). Chromatographic separation was achieved at 45 °C on an HSS T3 column (C_{18}) (100 mm \times 2.1 mm; 1.8 μm particle size; Waters Corp.). The mobile phase was delivered at a flow rate of 0.5 mL/min (Table S10, Supporting Information), and the total run time was 20 min. ESI source parameters were as follows: nebulizer pressure 40 psi, nozzle voltage 1500 V, sheath gas flow of 11 L/min, sheath gas temperature 300 °C, drying gas flow of 7 L/min, and drying gas temperature of 300 °C. Capillary and fragmentor voltages were set to 3500 V and 187 V, respectively. The Q-TOF system was running at 2 GHz in instrument mode at a resolving power of 30 000 (measured at m/z 1521). Acquired MS spectra were automatically recalibrated with two internal references

(121.0509 *m/z* and 922.0098 *m/z*). Data acquisition was performed in targeted MS/MS mode, MS scan 100–1000, *m/z* at 1.5 Hz, and MS/MS 50–480 *m/z* at 3 Hz. Precursor ions were isolated based on retention time and accurate mass with a width of 1.3 *m/z* in Q1. Samples were fragmented with two collision energies of 20 and 40 eV. The system was operated under the software MassHunter Acquisition and Qualitative Analysis version B.06.00 (Agilent Technologies), and data were analyzed using the software Mass-MetaSite (Molecular Discovery).

hERG screening

hERG currents were recorded in HEK 293 cells stably expressing the hERG channel. The patch-clamp experiments were performed as previously described by Hebeisen et al. 2015 [46]. Electrophysiological measurements were carried out 24–72 h after seeding. After formation of a Gigaohm seal between the patch electrodes and the individual HEK 293 cell (pipette resistance range: 2.0–7.0 MΩ; seal resistance >1 GΩ), the cell membrane across the pipette tip was ruptured to assure electrical access to the cell interior (whole-cell patch configuration). Once a stable seal was established, hERG outward tail currents were measured upon depolarization of the cell membrane to –40 mV for 3 s after activation of the channels at +20 mV for 2 s. The holding potential was –80 mV and the pulse frequency was 0.1 Hz. Tryptanthrin and indolinone were screened at concentrations of 0.3, 1.0, and 10 μM, and 1.0, 10, 30, and 100 μM, respectively (n = 3). Data acquisition and processing were performed using PatchMaster (HEKA electronics) and SigmaPlot 11.0 (Systat Software). Concentration response curves were fitted with a sigmoidal two-parameter equation:

$$\text{current}_{\text{peak,relative}} = \frac{100}{1 + \left(\frac{X}{IC_{50}}\right)^H}$$

X = compound concentration, IC₅₀ = concentration of the drug at half maximal inhibition, H = Hill coefficient.

Culture medium consisted of a 1:1 mixture of DMEM and nutrient mixture F-12 with L-glutamate supplemented with 10% FBS and 1.0% penicillin/streptomycin solution. For electrophysiological measurements, cells were seeded onto 35 mm sterile culture dishes containing 2 mL of medium without antibiotics. During the entire experiment, cells were continuously perfused with an extracellular bath solution (137 mM NaCl, 1.8 mM CaCl₂, 1 mM MgCl₂, 4 mM KCl, 10 mM D-glucose, 10 mM HEPES, adjusted to pH 7.4 [NaOH]). Micropipettes were filled with an intracellular pipette solution (130 mM KCl, 1 mM MgCl₂, 5 mM Mg-ATP, 10 mM 4-(2-hydroxyethyl)-1-piperazineethanesulfonic acid [HEPES], 5 mM ethylene glycol tetraacetic acid [EGTA], pH 7.2 [KOH]). As a negative control, four additional experiments were conducted with bath solution containing 0.3% DMSO (Table 4). As a positive control, a dose-response curve of E-4031 was recorded [33]. Concentrations of 1 nM, 3 nM, 10 nM, and 30 nM were tested (n = 4) (Table 4 and Fig. 6).

In silico prediction

In silico predictions of Caco-2 permeability and hERG inhibition for tryptanthrin and indolinone were performed with Percepta (ACD/Labs, ACD/Percepta Platform, version 12.01), Schrodinger Qik Prop (QikProp, version 4.1, Schrödinger, LLC, 2014), and the VirtualTox Lab (version 5.8) [47]. While Percepta and QikProp rely on calculating physicochemical descriptors (according to, e.g., Lipinski's rule of five) and determining pharmacologically rele-

vant properties (e.g., plasma protein binding, Caco-2 cell permeability, ion channel inhibition) using trained QSAR models, the VirtualToxLab *in silico* technology represents a fully 3D/4D-based approach, estimating the binding potential of a compound toward a given macromolecular target employing flexible molecular docking, followed by quantification of the energy change associated with the transfer of the docked compound from an aqueous environment into the protein binding site.

Supporting information

Data of both full method validations and the *in silico* parameters are available as Supporting Information.

Acknowledgments

Financial support from the Swiss National Science Foundation (project 105320_126888) is gratefully acknowledged. Further thanks go to Orlando Fertig for technical assistance and to Teresa Faleschini for proofreading the manuscript.

Conflict of Interest

The authors declare no conflict of interest.

Affiliations

- 1 Pharmaceutical Biology, Department of Pharmaceutical Sciences, University of Basel, Basel, Switzerland
- 2 Institute for Pharma Technology, School of Life Sciences, University of Applied Sciences Northwestern Switzerland, Muttenz, Switzerland
- 3 B'SYS GmbH, The Ionchannel Company, Witterswil, Switzerland
- 4 Institute for Chemistry and Bioanalytics, School of Life Sciences, University of Applied Sciences, Northwestern Switzerland, Muttenz, Switzerland
- 5 Molecular Modeling, Department of Pharmaceutical Sciences, University of Basel, Basel, Switzerland

References

- 1 Hamburger M. *Isatis tinctoria*—From the rediscovery of an ancient medicinal plant towards a novel anti-inflammatory phytopharmaceutical. *Phytochem Rev* 2002; 1: 333–344
- 2 Danz H, Stoyanova S, Thomet OA, Simon HU, Dannhardt G, Ulbrich H, Hamburger M. Inhibitory activity of tryptanthrin on prostaglandin and leukotriene synthesis. *Planta Med* 2002; 68: 875–880
- 3 Pergola C, Jazzar B, Rossi A, Northoff H, Hamburger M, Sautebin L, Wertz O. On the inhibition of 5-lipoxygenase product formation by tryptanthrin: mechanistic studies and efficacy *in vivo*. *Br J Pharmacol* 2012; 165: 765–776
- 4 Recio MC, Cerda-Nicolas M, Potterat O, Hamburger M, Rios L. Anti-inflammatory and antiallergic activity *in vivo* of lipophilic *Isatis tinctoria* extracts and tryptanthrin. *Planta Med* 2006; 72: 539–546
- 5 Ishihara T, Kohno K, Ushio S, Iwaki K, Ikeda M, Kurimoto M. Tryptanthrin inhibits nitric oxide and prostaglandin E2 synthesis by murine macrophages. *Eur J Pharmacol* 2000; 407: 197–204
- 6 Kiefer S, Mertz AC, Koryakina A, Hamburger M, Küenzi P. (E,Z)-3-(3',5'-Dimethoxy-4'-hydroxy-benzylidene)-2-indolinone blocks mast cell degranulation. *Eur J Pharm Sci* 2010; 40: 143–147
- 7 Oufir M, Sampath C, Butterweck V, Hamburger M. Development and full validation of an UPLC-MS/MS method for the determination of an anti-allergic indolinone derivative in rat plasma, and application to a preliminary pharmacokinetic study. *J Chromatogr B* 2012; 902: 27–34
- 8 Jähne EA, Eigenmann DE, Culot M, Cecchelli R, Walter FR, Deli MA, Tremmel R, Fricker G, Smiesko M, Hamburger M, Oufir M. Development and validation of a LC-MS/MS method for assessment of an anti-inflammatory indolinone derivative by *in vitro* blood-brain barrier models. *J Pharm Biomed Anal* 2014; 98: 235–246
- 9 Jähne EA, Eigenmann DE, Sampath C, Butterweck V, Culot M, Cecchelli R, Gosselet F, Walter FR, Deli MA, Smiesko M, Hamburger M, Oufir M. Pharmacokinetics and *in vitro* blood-brain barrier screening of the plant-

- derived alkaloid tryptanthrin. *Planta Med* 2016; DOI: 10.1055/s-0042-105295
- 10 Hubatsch I, Ragnarsson EG, Artursson P. Determination of drug permeability and prediction of drug absorption in Caco-2 monolayers. *Nat Protoc* 2007; 2: 2111–2119
 - 11 Laverty HG, Benson C, Cartwright EJ, Cross MJ, Garland C, Hammond T, Holloway C, McMahon N, Milligan J, Park BK, Primohamed M, Pollard C, Radford J, Roome N, Sager P, Singh S, Suter T, Suter W, Trafford A, Volders PGA, Wallis R, Weaver R, York M, Valentin JP. How can we improve our understanding of cardiovascular safety liabilities to develop safer medicines? *Br J Pharmacol* 2011; 163: 675–693
 - 12 FDA. Guidance for industry: bioanalytical method validation. US Department of Health and Human Services, Food and Drug Administration (CDER and CVM), May 2001. Available at <http://www.fda.gov/downloads/Drugs/Guidances/ucm070107.pdf>. Accessed February 15, 2016
 - 13 European Medicines Agency E. Guideline on bioanalytical method validation, EMEA/CHMP/EWP/192217/2009, Committee for Medicinal Products for Human Use (CHMP), London, 21 July 2011. Available at http://www.ema.europa.eu/docs/en_GB/document_library/Scientific_guideline/2011/08/WC500109686.pdf. Accessed February 15, 2016
 - 14 Wang Z, Hop CE, Leung KH, Pang J. Determination of *in vitro* permeability of drug candidates through a caco-2 cell monolayer by liquid chromatography/tandem mass spectrometry. *J Mass Spectrom* 2000; 35: 71–76
 - 15 Zhu X, Zhang X, Ma G, Yan J, Wang H, Yang Q. Transport characteristics of tryptanthrin and its inhibitory effect on P-gp and MRP2 in Caco-2 cells. *J Pharm Pharm Sci* 2011; 14: 325–335
 - 16 Hayeshi R, Hilgendorf C, Artursson P, Augustijns P, Brodin B, Dehertogh P, Fisher K, Fossati L, Hovenkamp E, Korjamo T, Masungi C, Maubon N, Mols R, Müllertz A, Mönkkönen J, O'Driscoll C, Oppers-Tiemissen HM, Ragnarsson EGE, Rooseboom M, Ungell AL. Comparison of drug transporter gene expression and functionality in Caco-2 cells from 10 different laboratories. *Eur J Pharm Sci* 2008; 35: 383–396
 - 17 Broeders JJ, Van Eijkeren JC, Blaauboer BJ, Hermens JL. Transport of chlorpromazine in the Caco-2 cell permeability assay: a kinetic study. *Chem Res Toxicol* 2012; 25: 1442–1451
 - 18 Heikkinen AT, Mönkkönen J, Korjamo T. Kinetics of cellular retention during Caco-2 permeation experiments: role of lysosomal sequestration and impact on permeability estimates. *J Pharmacol Exp Ther* 2009; 328: 882–892
 - 19 Palmgren JJ, Monkkonen J, Korjamo T, Hassinen A, Auriola S. Drug adsorption to plastic containers and retention of drugs in cultured cells under *in vitro* conditions. *Eur J Pharm Biopharm* 2006; 64: 369–378
 - 20 Engman HA, Lennernas H, Taipalensuu J, Otter C, Leidvik B, Artursson P. CYP3A4, CYP3A5, and MDRI in human small and large intestinal cell lines suitable for drug transport studies. *J Pharm Sci* 2001; 90: 1736–1751
 - 21 Korjamo T, Mönkkönen J, Uusitalo J, Turpeinen M, Pelkonen O, Honkakoski P. Metabolic and efflux properties of Caco-2 cells stably transfected with nuclear receptors. *Pharm Res* 2006; 23: 1991–2001
 - 22 Meunier V, Bourrie M, Berger Y, Fabre G. The human intestinal epithelial cell line Caco-2; pharmacological and pharmacokinetic applications. *Cell Biol Toxicol* 1995; 11: 187–194
 - 23 Chen J, Lin H, Hu M. Metabolism of flavonoids via enteric recycling: role of intestinal disposition. *J Pharmacol Exp Ther* 2003; 304: 1228–1235
 - 24 Usta M, Wortelboer HM, Vervoort J, Boersma MG, Rietjens IM, Van Bladeren PJ, Cnubben NH. Human glutathione S-transferase-mediated glutathione conjugation of curcumin and efflux of these conjugates in Caco-2 cells. *Chem Res Toxicol* 2007; 20: 1895–1902
 - 25 Liu W, Feng Q, Li Y, Ye L, Hu M, Liu Z. Coupling of UDP-glucuronosyltransferases and multidrug resistance-associated proteins is responsible for the intestinal disposition and poor bioavailability of emodin. *Toxicol Appl Pharmacol* 2012; 265: 316–324
 - 26 Jancova P, Anzenbacher P, Anzenbacherova E. Phase II drug metabolizing enzymes. *Biomed Pap Med Fac Univ Palacký Olomouc Czechoslov* 2010; 154: 103–116
 - 27 Tukey RH, Strassburg CP. Human UDP-glucuronosyltransferases: metabolism, expression, and disease. *Annu Rev Pharmacol Toxicol* 2000; 40: 581–616
 - 28 Rüster GU, Hoffmann B, Hamburger M. Inhibitory activity of indolin-2-one derivatives on compound 48/80-induced histamine release from mast cells. *Pharmazie* 2004; 59: 236–237
 - 29 Lee JK, Abe K, Bridges AS, Patel NJ, Raub TJ, Pollack GM, Brouwer KL. Sex-dependent disposition of acetaminophen sulfate and glucuronide in the *in situ* perfused mouse liver. *Drug Metab Dispos* 2009; 37: 1916–1921
 - 30 Jiang W, Xu B, Wu B, Yu R, Hu M. UDP-glucuronosyltransferase (UGT) 1A9-overexpressing HeLa cells is an appropriate tool to delineate the kinetic interplay between breast cancer resistance protein (BCRP) and UGT and to rapidly identify the glucuronide substrates of BCRP. *Drug Metab Dispos* 2012; 40: 336–345
 - 31 Shawahna R, Uchida Y, Declèves X, Ohtsuki S, Yousif S, Dauchy S, Jacob A, Chassoux F, Daumas-Duport F, Couraud PO, Terasaki T, Scherrmann JM. Transcriptomic and quantitative proteomic analysis of transporters and drug metabolizing enzymes in freshly isolated human brain microvessels. *Mol Pharm* 2011; 8: 1332–1341
 - 32 Shawahna R, Declèves X, Scherrmann JM. Hurdles with using *in vitro* models to predict human blood-brain barrier drug permeability: a special focus on transporters and metabolizing enzymes. *Curr Drug Metab* 2013; 14: 120–136
 - 33 Zhou Z, Gong Q, Ye B, Fan Z, Makielski JC, Robertson GA, January CT. Properties of HERG channels stably expressed in HEK 293 cells studied at physiological temperature. *Biophys J* 1998; 74: 230–241
 - 34 Redfern WS, Carlsson L, Davis AS, Lynch WG, MacKenzie I, Palethorpe S, Siegl PKS, Strang I, Sullivan AT, Wallis R. Relationships between preclinical cardiac electrophysiology, clinical QT interval prolongation and torsade de pointes for a broad range of drugs: evidence for a provisional safety margin in drug development. *Cardiovasc Res* 2003; 58: 32–45
 - 35 Food and Drug Administration. Guidance for industry: S7B nonclinical evaluation of the potential for delayed ventricular repolarization (QT interval prolongation) by human pharmaceuticals, 2005. Available at www.fda.gov/. Accessed February 15, 2016
 - 36 Schramm A, Saxena P, Chlebek J, Cahliková L, Baburin I, Hering S, Hamburger M. Natural products as potential human ether-a-go-go-related gene channel inhibitors—screening of plant-derived alkaloids. *Planta Med* 2014; 80: 740–746
 - 37 Witchel HJ, Milnes JT, Mitcheson JS, Hancox JC. Troubleshooting problems with *in vitro* screening of drugs for QT interval prolongation using HERG K⁺ channels expressed in mammalian cell lines and *Xenopus* oocytes. *J Pharmacol Toxicol Methods* 2002; 48: 65–80
 - 38 Po SS, Wang DW, Yang ICH, Johnson JP, Nie L, Bennett PB. Modulation of HERG potassium channels by extracellular magnesium and quinidine. *J Cardiovasc Pharmacol* 1999; 33: 181–185
 - 39 Sun L, Tran N, Tang F, App H, Hirth P, McMahon G, Tang C. Synthesis and biological evaluations of 3-substituted indolin-2-ones: a novel class of tyrosine kinase inhibitors that exhibit selectivity toward particular receptor tyrosine kinases. *J Med Chem* 1998; 41: 2588–2603
 - 40 Friedländer P, Roschdestwenski N. Über ein Oxidationsprodukt des Indigoblaus. *Ber Dtsch Chem Ges* 1915; 48: 1841–1847
 - 41 Mohn T, Potterat O, Hamburger M. Quantification of active principles and pigments in leaf extracts of *Isatis tinctoria* by HPLC/UV/MS. *Planta Med* 2007; 73: 151–156
 - 42 Gerlier D, Thomasset N. Use of MTT colorimetric assay to measure cell activation. *J Immunol Methods* 1986; 94: 57–63
 - 43 Tofighi Z, Asgharian P, Goodarzi S, Hadjiakhoondi A, Ostad SN, Yassa N. Potent cytotoxic flavonoids from Iranian *Securigera securidaca*. *Med Chem Res* 2014; 23: 1718–1724
 - 44 Youdim KA, Avdeef A, Abbott NJ. *In vitro* trans-monolayer permeability calculations: often forgotten assumptions. *Drug Discov Today* 2003; 8: 997–1003
 - 45 Verjee S, Brügger D, Abdel-Aziz H, Butterweck V. Permeation characteristics of hypericin across Caco-2 monolayers in the absence or presence of quercitrin – a mass balance study. *Planta Med* 2015; 81: 1111–1120
 - 46 Hebeisen S, Pires N, Loureiro AI, Bonifácio MJ, Palma N, Whyment A, Spanswick D, Soares-da-Silva P. Eslicarbazepine and the enhancement of slow inactivation of voltage-gated sodium channels: a comparison with carbamazepine, oxcarbazepine and lacosamide. *Neuropharmacology* 2015; 89: 122–135
 - 47 Vedani A, Dobler M, Hu Z, Smieško M. OpenVirtualToxLab – a platform for generating and exchanging *in silico* toxicity data. *Toxicol Lett* 2015; 232: 519–532

Supporting Information

Planta Medica

Caco-2 permeability studies and *in vitro* hERG liability assessment of tryptanthrin and indolinone

Evelyn A. Jähne¹, Daniela E. Eigenmann¹, Fahimeh Moradi-Afrapoli¹, Sheela Verjee², Veronika Butterweck², Simon Hebeisen³, Timm Hettich⁴, Götz Schlotterbeck⁴, Martin Smieško⁵, Matthias Hamburger^{1*}, and Mouhssin Oufir^{1*}

¹Pharmaceutical Biology, Department of Pharmaceutical Sciences, University of Basel, Klingelbergstrasse 50, CH-4056 Basel, Switzerland

²Institute for Pharma Technology, School of Life Sciences, University of Applied Sciences Northwestern Switzerland, Gründenstrasse 40, CH-4132 Muttenz, Switzerland

³B'SYS GmbH, The Ionchannel Company, Benkenstrasse 254, CH-4108 Witterswil, Switzerland

⁴Institute for Chemistry and Bioanalytics, School of Life Sciences, University of Applied Sciences, Northwestern Switzerland, , Gründenstrasse 40, CH-4132 Muttenz, Switzerland

⁵Molecular Modeling, Department of Pharmaceutical Sciences, University of Basel, Klingelbergstrasse 50, CH-4056 Basel, Switzerland

*Corresponding authors: Prof. Matthias Hamburger and Dr. Mouhssin Oufir, Institute of Pharmaceutical Biology, Department of Pharmaceutical Sciences, University of Basel, Klingelbergstrasse 50, CH-4056 Basel, Switzerland, Phone: +41 61 267 1544 Fax: +41 61 267 1474
E-Mail: matthias.hamburger@unibas.ch, mouhssin.oufir@unibas.ch

Method validation

UPLC-MS/MS method validation was performed according to US Food and Drug Administration (FDA) and European Medicines Agency (EMA) guidelines. Seven calibrators ranging from 10.00 – 1000 ng/mL (tryptanthrin), and 30.0 – 3000 ng/mL (indolinone) were injected at increasing concentrations, after a blank sample (blank HBSS) and a zero sample (HBSS only spiked with I.S.). Calibration curves were validated through six QCs (QCL, QCM, and QCH), which were inserted randomly into each analytical run. Calibrators and QCs were analyzed in duplicates. Carry-over was assessed by directly injecting an extracted blank after both replicates of the upper limit of quantification (ULOQ). Specificity and selectivity were evaluated by six blank samples and six QC samples at the LLOQ (duplicates, 3 different batches of HBSS), respectively. Intra-run repeatability of the methods was evaluated by injecting six replicates at five concentration levels (LLOQ, QCL, QCM, QCH, and ULOQ). To assess dilution integrity, a solution of analyte (4000 ng/mL tryptanthrin, or 15000 ng/mL indolinone) in HBSS was prepared and then further diluted ten- and hundred-fold. Absolute recovery was determined at three concentration levels (QCL, QCM, and QCH) by comparing the peak areas of six extracted QC samples with six unextracted samples (= 100% recovery). Short-term stabilities were assessed with six replicates at two concentration levels (QCL and QCH), after 3 hours at RT, and after 3 freeze and thaw cycles. Long-term stability was determined by three replicates at the same concentration levels (QCL, QCM, and QCH). After storage of minimum 6 days (below -65°C) samples were analyzed by a freshly prepared calibration curve.

Figures

Fig. S1 Typical MRM chromatograms of blank HBSS injected after the ULOQ and monitored for tryptanthrin (A), for I.S. (B), of HBSS spiked at 10.0 ng/mL (LLOQ) of tryptanthrin (C), and 1000 ng/mL of I.S. (D), of HBSS spiked at 1000 ng/mL (ULOQ) of tryptanthrin (E), and 1000 ng/mL of I.S. (F).

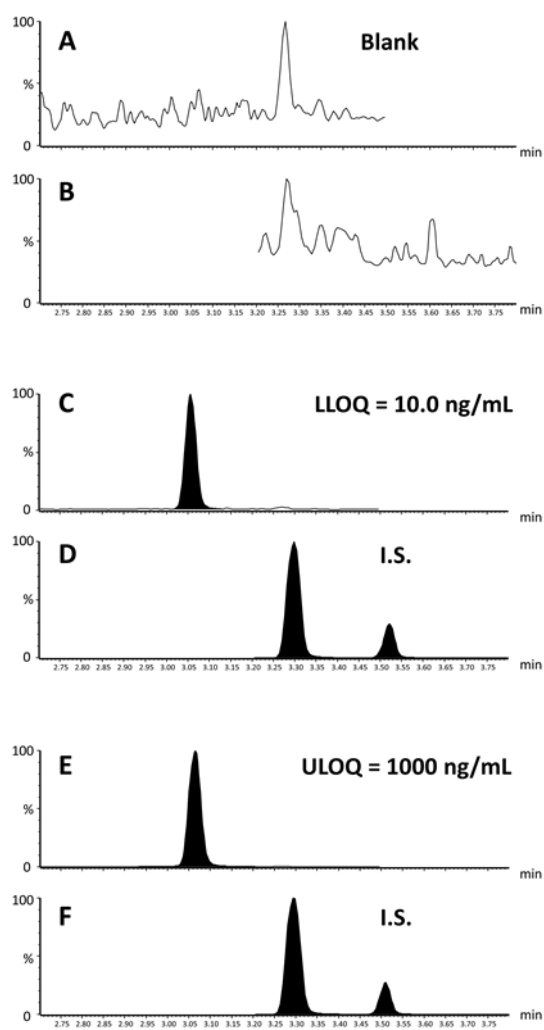
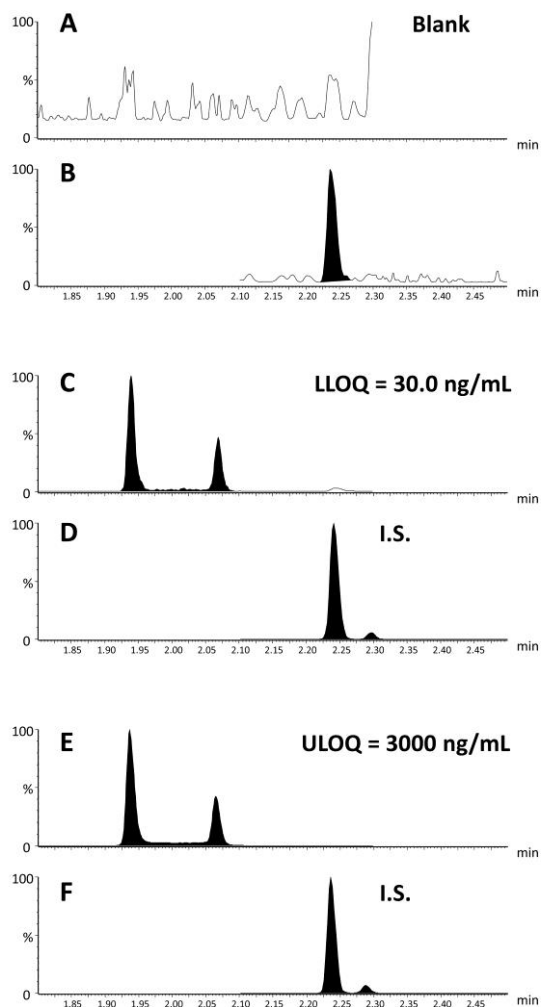


Fig. S2 Typical MRM chromatograms of blank HBSS injected after the ULOQ and monitored for indolinone (A), for I.S. (B), of HBSS spiked at 30.0 ng/mL (LLOQ) of indolinone (C), and 1000 ng/mL of I.S. (D), of HBSS spiked at 3000 ng/mL (ULOQ) of indolinone (E), and 1000 ng/mL of I.S. (F).



Tables

Table S1 Calibrators and calibration curve parameters for analytes. Response = A x Conc.² + B x Conc. + C, quadratic regression, weighting factor 1/X (tryptanthrin) and 1/X² (indolinone), origin: included (tryptanthrin), excluded (indolinone) (n = 6-10)

Compound	Nominal level (ng/mL)										Regression parameters			
	10.0	40.0	80.0	160	320	500	1000	A	B	C	R ²			
Tryptanthrin														
Mean	9.84	39.2	80.0	166	311	503	1002	-0.000634	3.15	0.236	0.997			
S.D.	0.504	4.52	5.63	8.02	20.4	29.6	42.2	0.0000761	0.261	-	-			
CV%	5.12	11.5	7.04	4.83	6.58	5.88	4.22							
RE%	-1.57	-1.91	-0.0290	3.70	-2.83	0.588	0.176							
Indolinone														
Mean	30.3	95.8	254	512	1012	1957	3026	-0.00000000566	0.000193	-0.000492	0.995			
S.D.	1.70	6.33	16.9	29.0	72.1	106	199	0.00000000759	0.0000134	-	-			
CV%	5.62	6.61	6.65	5.67	7.12	5.43	6.57							
RE%	1.16	-4.22	1.43	2.38	1.24	-2.15	0.862							

Table S2 Carry-over assessment for both analytes and I.S. (n = 6-10)

Compound	Mean carry-over (%)
Tryptanthrin	0.598
I.S.	0.00796
Indolinone	0.00
I.S.	0.484

Table S3 Selectivity test at the LLOQ, based on 3 different HBSS batches (n = 6)

Compound	Nominal level (ng/mL)	10.0
Tryptanthrin	Mean	9.46
	S.D.	0.678
	CV%	7.17
	RE%	-5.37
Compound	Nominal level (ng/mL)	30.0
Indolinone	Mean	26.7
	S.D.	2.17
	CV%	8.15
	RE%	-11.2

Table S4 Dilution test (n = 6)

Compound	Nominal level (ng/mL)	4000	
	Dilution factor	10X	100X
Tryptanthrin	Mean	3768	3788
	S.D.	163	266
	CV%	4.33	7.01
	RE%	-5.79	-5.29
Compound	Nominal level (ng/mL)	15000	
	Dilution factor	10X	100X
Indolinone	Mean	14305	15443
	S.D.	894	332
	CV%	6.25	2.15
	RE%	-4.63	2.96

Table S5 Absolute extraction yield of analytes and I.S. (n = 6)

Compound	Nominal level (ng/mL)	30.0	500	800
Tryptanthrin	Absolute recovery %	76.3	72.7	71.3
	CV%	8.15	7.18	4.39
	RE%	6.22	5.22	3.13
	Nominal level (ng/mL)	433		
I.S.	Absolute recovery %	79.9		
	CV%	4.62		
	RE%	3.69		
	Nominal level (ng/mL)	90.0	1500	2400
Indolinone	Absolute recovery %	90.2	91.1	94.5
	CV%	12.8	7.23	3.66
	RE%	11.6	6.58	3.46
	Nominal level (ng/mL)	444		
I.S.	Absolute recovery %	83.1		
	CV%	6.49		
	RE%	5.40		

Table S6 Short-term stabilities during storage at various conditions expressed as CV% and RE% (n = 6)

Compound	Nominal level (ng/mL)	CV%		RE%	
		30.0	800	30.0	800
Tryptanthrin	3 successive F/T cycles below -65°C	6.13	8.04	-3.80	-12.0
	Stored samples at RT for 4h	10.9	5.98	-5.15	-10.4
Indolinone	Nominal level (ng/mL)	90.0	2400	90.0	2400
	3 successive F/T cycles below -65°C	5.41	4.94	-4.36	-0.388
	Stored samples at RT for 4h	3.31	3.91	7.22	4.30

Table S7 Long-term stabilities expressed as difference (%) between t=0 and t=storage time (n = 3)

Compound	Nominal level (ng/mL)	30.0	500	800	Slope
Tryptanthrin	Stored samples below -65°C for 7 days	4.64	-12.1	-10.6	0.890
Compound	Nominal level (ng/mL)	90.0	1500	2400	Slope
Indolinone	Stored samples below -65°C for 6 days	-8.71	-11.4	2.53	0.982

Table S8 *In silico* parameters determined by ACD/Labs Percepta

PhysChem profiling		
Compound	Tryptanthrin	Indolinone
LogP	2.44	2.47
MW	248.24	297.31
H-donors	0	2
H-acceptors	4	5
Rot. bonds	0	3
Rings	4	3
Lipinski	0 violations	0 violations
Lead-like	0 violations	0 violations
Solubility	0.0008 mg/mL	0.009 mg/mL
ADME profiling		
Caco-2	Pe=23.4 x 10 ⁻⁶ cm/s (highly permeable)	Pe=17.2 x 10 ⁻⁶ cm/s (highly permeable)
Plasma protein binding	91%	95%
Central nervous system	Score = -2.90 (penetrant)	Score = -2.90 (penetrant)
Human intestinal model	100% (highly absorbed)	100% (highly absorbed)
Metabolic stability	0.65	0.55
Drug Safety Profiling		
P-gp substrates	0.35	0.43

Table S9 *In silico* parameters calculated by QikProp (Schrödinger software suite) and VirtualToxLab (3D based)

Compound	QikProp			VirtualToxLab
	Human oral absorption (%)	QPPCaco-2 (x 10 ⁻⁶ cm/s) ^a	QP logHERG ^b	Kd hERG (μM)
Tryptanthrin	84.0	76.5	-5.1 (7.9 μM)	4.40
Indolinone ^c	91.0	62.8	-5.0 (10 μM)	1.80

^a Caco-2 permeability (x 10⁻⁶ cm.s⁻¹): score below 2.5 = poor, above 50 = great

^b Values below -5 (i.e. IC₅₀ below 10 μM; in brackets) should be of concern

^c Average values calculated over two (*E*- and *Z*-) isomers

Table S10 Optimized UPLC parameters for tryptanthrin and indolinone.

Eluents: A1: high purity water + 0.1% FA; B1: acetonitrile + 0.1% FA, B2: methanol + 0.1% formic acid.

Optimized UHPLC parameters							
Compounds	Total run time (min)	Eluent	Gradient	Injection solvent	Injection vol. (μL)	Column temp. (°C)	Autosampler temp. (°C)
Tryptanthrin (MS/MS)	6	A1 + B1	30-100% B1 in 5 min	DMSO	2	45	20
Indolinone (MS/MS)	4	A1 + B1	2-100% B1 in 2.5 min	35% A1 + 65% B2	5	45	10
Indolinone (HR-MS)	15	A1 + B1	2-100 % B1 in 13 min	35% A1 + 65% B2	7	45	10

Table S11 Optimized MS/MS parameters in ESI positive mode for tryptanthrin and indolinone as analyte, and (*E,Z*)-3-(benzylidenyl)-indolin-2-one as I.S..

Optimized MS/MS parameters			
Compounds	MRM transitions	Cone voltage (V)	Collision energy (eV)
Tryptanthrin	248.7 → 129.8	51	31
Indolinone	297.7 → 265.0	46	38
I.S.	221.8 → 194.0	46	21

4 Conclusions and outlook

For the three anti-inflammatory alkaloids tryptanthrin, indolinone, and indirubin, UPLC-MS/MS quantification methods in three different matrices (rat plasma, RHB, HBSS) were validated according to current international guidelines for industry¹⁻³. The methods were successfully applied to an *in vivo* pilot PK study in Sprague Dawley rats (i.v. administration) and two *in vitro* permeability assays (Caco-2 and BBB models). Furthermore, hERG liabilities were determined by measuring the *in vitro* effect of the compounds on the cardiac hERG potassium channel by means of the patch-clamp technique. Data obtained from the *in vitro* assays were corroborated by various *in silico* methods.

For tryptanthrin, a clearance of 1 L/h/kg and a relatively short $t_{1/2}$ of around 40 min were determined in the pilot PK study. In the Caco-2 model, tryptanthrin displayed in both directions (A→B and B→A) high mean P_{app} values in the range of 35×10^{-6} cm/s, demonstrating that the compound crosses the Caco-2 monolayer very efficiently, and in a concentration independent manner in the tested range of 5-10 μ M. The calculated efflux ratio ($ER = P_{app\ B \rightarrow A} / P_{app\ A \rightarrow B}$) for tryptanthrin was around 1, which pointed to a predominantly passive diffusion across the Caco-2 monolayer. In addition, mean P_{app} values of tryptanthrin across the Caco-2 cells monolayer (32.0×10^{-6} cm/s) were very close to mean P_{app} values of the control experiments (without cells: 31.5×10^{-6} cm/s), confirming that tryptanthrin freely diffused across the cell monolayer. Moreover, mean P_{app} values of tryptanthrin from apical to basolateral and vice versa remained unaffected in the presence of the P-gp inhibitor verapamil. This observation demonstrated that tryptanthrin was not subjected to P-gp efflux. In addition, the ER below 2 showed that the compound was not involved in active-mediated efflux. Similar findings regarding permeability and P-gp interaction of tryptanthrin were previously reported⁴. However, it should be noted that HPLC-UV analysis was used in these studies, which does not meet current requirements for bioanalytical quantitation in terms of selectivity, specificity, and sensitivity.

Data obtained with our recently validated human *in vitro* BBB model^{5,6} using immortalized human brain microvascular endothelial cells (hBMEC cell line) demonstrated that tryptanthrin crosses the BBB very efficiently. Mean P_{app} values for the compound in the human BBB model were in a similar range (around 36×10^{-6} cm/s) as the mean P_{app} values in the well-characterized animal *in vitro* BBB model using primary bovine brain capillary endothelial cells (BBECs) co-cultured with primary glial cells⁷. Mean P_{app} values of tryptanthrin across the membrane with cells and without cells were very close (36×10^{-6} cm/s). Hence, the transport of the compound across the BBB was dominated by passive diffusion. For the primary triple co-culture rat *in vitro* BBB model using primary rat brain capillary endothelial cells (RBECs), pericytes, and glial cells, mean P_{app} values were roughly twice as high as the permeability coefficients obtained in the human BBB model⁸. TEER values in the primary co-cultured BBB models (mean TEER values: 350 - 400 Ω cm²) were significantly higher than those observed in the immortalized BBB model (mean TEER values: 25 Ω cm²). However, the P_{app} values of the paracellular integrity marker Na-F in the human BBB model ($3.10 - 3.20 \times 10^{-6}$ cm/s) were in a similar range as those obtained in the primary BBB models ($0.520 - 3.17 \times 10^{-6}$ cm/s), indicating that a

reasonably tight barrier was formed by the hBMEC cells. Overall, data from the three *in vitro* BBB models showed good correlation and were indicative of a high BBB permeation potential of tryptanthrin.

In the hERG safety assay, tryptanthrin was shown to slightly inhibit the hERG channel (IC_{50} of 22 μ M). Compared to strong hERG blockers (e.g. E-4031, IC_{50} of 7.7 nM)⁹, the IC_{50} of tryptanthrin was relatively high. *In silico* predictions proposed a plasma protein binding of 91% for the compound. Therefore, we would expect a low free plasma concentration, which most probably results in a safety margin ($IC_{50 \text{ hERG}} / \text{free plasma concentration}$) of > 30 . Substances with such a safety margin are presumed not to cause arrhythmias¹⁰. Previous studies in the functional *Xenopus* oocyte assay (voltage clamp technique) proposed no I_{hERG} inhibition (0.00%) for tryptanthrin when tested at 100 μ M¹¹. However, it should be noted that the potency of compounds tested in oocytes is usually three- to tenfold decreased compared to mammalian cells (e.g. HEK 293), as the lipophilic yolk can adsorb the compound and thus decreases the free fraction¹².

Along with no violations of Lipinski's rule of five, the *in silico* methods predicted a high permeability for tryptanthrin in the Caco-2 assay, good oral absorption ($> 84\%$), and a relatively low probability for P-gp interaction (0.35). The calculated polar surface area (PSA) of 73 \AA^2 (PSA_{QikProp}) was not only well below the maximum acceptable threshold of 140 \AA^2 for good oral absorption, but also met the criteria for a passive permeation through the BBB ($PSA < 90 \text{\AA}^2$). In addition, the predicted *in silico* inhibition of the hERG potassium channel in the low μ M range ($IC_{50 \text{ hERG}}$) was in very good agreement with the experimental data.

Overall, numerous favorable drug-like properties (such as high permeability, good oral absorption, no P-gp interaction) were found for tryptanthrin. However, one major drawback of the compound was its high lipophilicity resulting in a relatively fast elimination of the compound ($t_{1/2}$ around 40 min). A technical challenge which we encountered during sample preparation was the non-specific binding of tryptanthrin in aqueous buffer to various surfaces (e.g. the polypropylene tubes). This major issue could be solved by pre-treating the plastic tubes with 0.2% Tween 20. However, it clearly demonstrated the importance of method development and validation prior to sample analysis.

For indolinone, a recovery of $< 36\%$ was determined after 2 hours of incubation in the Caco-2 assay. To avoid an underestimation of the P_{app} values, a recovery above 80% is needed^{13,14}. Incomplete recovery is usually ascribed to adsorption to the Transwell plate, metabolism, or compound retention within the cells/in the cell membrane^{15,16}. Binding of indolinone to the plastic could be excluded, as the mean recoveries of the control experiments (without cells) were all above 83%. Cell extraction demonstrated that indolinone was not trapped within the cells, as less than 1.23% of the compound was recovered after cell lysis. In contrast to the intestine, cytochrome P-450 (CYPs) metabolizing enzymes are poorly expressed in Caco-2 cells^{17,18}. However, these cells express phase II enzymes,

such as UDP-glucuronosyltransferases (UGTs), sulfotransferases (SULTs), and glutathione-S-transferases (GSTs)¹⁹. High resolution MS analysis with a UHPLC Q-TOF system indicated the formation of two sulfate conjugates and two glucuronide conjugates with molecular masses of 378.1 and 474.1 m/z, respectively. Approximately similar amounts of both metabolites were found in the apical and basolateral compartments, while no significant levels of phase II metabolites could be detected in the Caco-2 cell lysate.

Intestinal transport of glucuronide and sulfate conjugates are poorly described in literature, but it seems to be likely that MRPs (expressed on the apical and basolateral side), BCRP (apical) and OATP (apical) are responsible for their efflux, because these conjugates are transported this way in the liver^{21,22}. It is generally believed that the main site of drug metabolism is the liver. But for some compounds, experimental evidence exists that they also undergo extensive intestinal conjugation and excretion²³. Various polyphenolic compounds such as apigenin (UGT and SULT)²⁴, curcumin (GST)²⁵, and emodin (UGT)²⁶ have been shown to undergo phase II metabolism in the Caco-2 assay. Besides natural products (particularly dietary flavonoids)²⁴, only few studies reported on sulfation and glucuronidation of synthetic drugs (e.g. raloxifene²⁷ and methyldopa²⁸) in the Caco-2 monolayer, followed by efflux of the metabolites.

UGTs catalyze the addition of a glucuronic acid moiety to substrate molecules containing an O-, N-, S- or C- acceptor group²⁹, while SULTs are capable of catalyzing the formation of O-, N- or S-linked conjugates³⁰. However, conjugation at a hydroxyl moiety is the dominant reaction for both enzymes. Given the structure of indolinone, we assume that either O-linked (phenol) or N-linked (amide) glucuronide/sulfate conjugates were formed. To locate the exact conjugation site on the chemical structure, targeted MS/MS experiments (50-480 m/z at 3 Hz) in parallel with MS scan (100-1000 m/z at 1.5 Hz) were performed at two collision energies (20 and 40 eV). However, the low concentrations of metabolites, the intense sodium adduct ions, and the fragmentation pattern of the metabolites (loss of sulfate or glucuronide residues) precluded a differentiation between O- or N-conjugation. Due to the slow *E/Z* isomerization of indolinone at room temperature³¹, an assignment of the metabolite peaks to the respective *E* or *Z* isomer was also not possible.

Previous studies reported on the metabolism of the indolinone derivative sunitinib (Sutent, Pfizer) after i.v./oral administrations of [¹⁴C] sunitinib in rats, monkeys, and humans. Sunitinib was found to be extensively metabolized in all species. But only minor sulfate and glucuronide metabolites could be detected in the feces and urine of rats and monkeys³². Fragment ions of the sunitinib glucuronide indicated that the glucuronidation occurred on the nitrogen atom of the indolyldene/demethylpyrrole moiety, while sulfation was observed at the O-atom after hydroxylation (phase I reaction) of the parent compound³².

Overall, indolinone underwent extensive phase II metabolism in the Caco-2 assay, which in turn may explain the fast elimination of indolinone found in the previous PK study in rats ($t_{1/2}$ of approx. 4 min)³³. However, incubations with hepatocytes, microsomes, S9 fractions or isolated enzymes would be needed to assess the metabolic stability of the compound in more detail. An additional approach to determine the exact conjugation site would be the synthesis of the proposed metabolites. By comparing the retention time (RT) of the synthesized metabolites with the RT (in the HR-MS assay) of the metabolites obtained from the Caco-2 assay, metabolite identification could be possible.

In the human and animal *in vitro* BBB models, indolinone was shown to cross the BBB³⁴. However, due to its fast metabolism, it appears rather unlikely that the compound reaches the brain in a sufficiently high amount. Surprisingly, no metabolism was observed for indolinone in the cell-based BBB models. Publications on the presence of phase II enzymes at the BBB are conflicting since most of the data refer to brain homogenates instead of isolated brain microvessels^{35,36}. A recent study³⁶ analyzing the expression pattern of phase II enzymes of freshly isolated human brain microvessels revealed that only one isoform of SULTs (SLUT1A1) is present in the BBB, while UGTs are completely absent from the human brain^{36,37}.

For indolinone, a hERG inhibition of approx. 86% was found when tested at 100 μ M (IC_{50} of around 25 μ M). But given the high plasma protein binding (95%, predicted *in silico*), the high metabolic instability (*in vitro* Caco-2 assay), and the fast clearance (*in vivo* PK study)³³ of indolinone, a hERG block under physiological conditions appears rather unlikely for the compound.

In silico predictions for indolinone indicated no violation of Lipinski's rule of five, a high human oral absorption (93.2%), and a moderate probability (0.43) for P-gp interaction. However, as the compound was extensively metabolized (Caco-2 assay) and thus quickly eliminated (PK studies), indolinone clearly needs to be chemically modified towards a metabolically more stable compound without losing its inhibitory activity on Fc ϵ RI-receptor dependent mast cell degranulation.

For indirubin, a short $t_{1/2}$ of around 35 min and a relatively high clearance of almost 3 L/h/kg were determined in the preliminary PK study in Sprague Dawley rats. Previous PK data reported by Deng et al. obtained from male Wistar rats showed a $t_{1/2}$ of 1 hour (i.v., 2.8 mg/kg)³⁸. The different $t_{1/2}$ found in male Wistar rats (1 hour) and Sprague Dawley rats (35 min) might be explained by differing cytochrome P450 isozyme expression in the two strains. Also, different administered doses (male Sprague Dawley rats: i.v., 2 mg/kg bw vs. male Wistar rats: i.v., 2.8 mg/kg bw) and body weight (male Sprague Dawley: 320 - 350 g vs. male Wistar rats: 280 - 300 g) may have impacted the excretion of the compound. Independent of that, our data were obtained by a fully validated UPLC-MS/MS bioanalytical method and are, therefore, significantly more reliable and robust than the data of the previous study obtained by only HPLC-UV analysis³⁸.

In the *in vitro* permeability studies, indirubin precipitated even at low concentrations on the filter inserts of the Transwell systems. The software program EPI suite (ImageWare Systems, version 3.20) estimated a water solubility of indirubin of about 188 mg/L at room temperature. However, thermodynamic solubility studies investigating the saturated solution of indirubin in equilibrium demonstrated that indirubin is completely insoluble in aqueous buffer (RHB, HBSS). Addition of various solubilizing agents such as 0.2% Cremophor EL, 5 mg/mL Poloxamer 188, or 1% DMSO could not improve the solubility issue of indirubin in the transporter buffers (RHB, HBSS)³⁹. Indirubin was also tested in the hERG assay at concentrations up to 3 μ M. But again, the compound precipitated in the bath solution and precluded reliable predictions. For this reason, we decided to stop working on the compound in aqueous buffers, as structural modifications towards more soluble derivate and/or more complex formulations (e.g. liposomes or lipid-based formulations) are required. Schering AG already reported on the synthesis of more soluble indirubin (aryl-substituted and sulfur-containing) analogs^{40,41}, while other research groups improved the bioavailability of indirubin by a nanoparticle formulation⁴².

In summary, we were able to determine first key PK parameters in rats and a selection of physicochemical properties (such as permeability, solubility, metabolic stability) in *in vitro* assays for tryptanthrin, indolinone, and indirubin. However, to fully assess the drug-likeness of a compound, additional *in vitro* tests such as human microsomal/hepatocyte stability, cytochrome P450 inhibition, and plasma protein binding are needed. To identify which UGT/SULT isoforms are responsible for the metabolism of indolinone in the Caco-2 assay, further *in vitro* studies with recombinant enzymes would be required³. The PK parameters obtained from Sprague Dawley rats after i.v. administration provided a preliminary insight about the *in vivo* performance of the compounds. All three compounds were rapidly eliminated ($t_{1/2}$ 4 – 40 min) and thus need to be chemically modified towards more soluble/metabolically stable compounds without losing their activity. Furthermore, to estimate the oral bioavailability of the compounds, oral administrations in Sprague Dawley rats would be required. Additionally, a new validated bioanalytical method including the four phase II metabolites of indolinone would be mandatory. The Caco-2 assay already gave preliminary information about the oral bioavailability of the compounds. According to the drug interaction guidelines from the FDA³, EMA⁴³, and Japanese MHLW⁴⁴, assessment of P-gp and BCRP interactions are recommended for new molecular entities. Tryptanthrin was already shown not to be a P-gp substrate. To investigate whether tryptanthrin is a P-gp inhibitor, co-incubation with a P-gp substrate (e.g. digoxin) would be needed⁴⁵. In addition, further experiments on BCRP (substrate/inhibitor identification) would be reasonable. As we assumed that indolinone conjugates are actively excreted in the apical and basolateral compartment of the Caco-2 assay, it would also be interesting to see whether the efflux changes in presence of a BCRP (e.g. Ko143)⁴⁶, MRP (such as MK-571 and leukotriene C₄)²⁴, or OAT (e.g. estrone sulfate)²⁴ inhibitor. Such experiments would enable us to identify which transporters are involved in the efflux of the indolinone conjugates.

In addition, bioavailability of poorly water soluble compounds can be increased by food, and by the presence of micelles of bile salts, phospholipids, and lipolysis products⁴⁷. To simulate the intestinal fluid in the fasted (FaSSIF-TM) and the fed state (FeSSIF-TM), several attempts have been made to develop biorelevant transport media for the Caco-2 model^{48,49}. As these media can essentially influence the drug solubility/stability and, therefore, the absorption of a compound, it would be worthwhile to study the effect of these biorelevant media on our alkaloids in the Caco-2 assay. In the *in vitro* hERG assay, indolinone and tryptanthrin displayed a weak hERG block. Besides the hERG potassium channel, sodium and calcium ion channels contribute to the cardiac action potential. Therefore, the ICH (International Conference on Harmonization) safety guideline S7B⁵⁰ recommends further testing on sodium/calcium channels before moving into clinical trials⁵⁰.

Historically, natural products are the major source of new structural leads in drug discovery. But it should be emphasized that nowadays isolated natural products typically do not serve as new drug substances by themselves. Numerous natural products (such as β -lactams⁵¹ or paclitaxel^{52,53}) with poor physicochemical properties (chemical/enzymatic instability or low permeability/solubility) have later become blockbuster drugs by means of adequate structural modifications (e.g. derivatization, addition of clavulanic acid) or formulations (albumin-bound formulation of paclitaxel, Abraxane[®]). Thus, given the novelty of the pharmacological profile of tryptanthrin and indolinone, we believe that structural modifications and further preclinical testing (including bioactivity) of these compounds would be worthwhile.

References

1. FDA, U. Guidance for industry: bioanalytical method validation (draft guidance). *US FDA* (2013).
2. Guideline on bioanalytical method validation. European Medicines Agency (EMA/CHMP/EWP/192217/2009). London, 21 July 2011.
3. Administration, F. and D. Draft guidance for industry—drug interaction studies, study design, data analysis, implications for dosing, and labeling recommendations. *Food and Drug Administration* (2012).
4. Zhu, X. *et al.* Transport characteristics of tryptanthrin and its inhibitory effect on P-gp and MRP2 in Caco-2 cells. *J. Pharm. Pharmaceut. Sci.* **14**, 325–335 (2011).
5. Eigenmann, D. E. *et al.* Comparative study of four immortalized human brain capillary endothelial cell lines, hCMEC/D3, hBMEC, TY10, and BB19, and optimization of culture conditions, for an *in vitro* blood–brain barrier model for drug permeability studies. *Fluids Barriers CNS* **10**, 33 (2013).
6. Eigenmann, D. E., Jähne, E. A., Smieško, M., Hamburger, M. & Oufir, M. Validation of an immortalized human (hBMEC) *in vitro* blood–brain barrier model. *Anal. Bioanal. Chem.* 1–13 (2016).
7. Culot, M. *et al.* An *in vitro* blood–brain barrier model for high throughput (HTS) toxicological screening. *Toxicol. In Vitro* **22**, 799–811 (2008).
8. Nakagawa, S. *et al.* A new blood–brain barrier model using primary rat brain endothelial cells, pericytes and astrocytes. *Neurochem. Int.* **54**, 253–263 (2009).
9. Zhou, Z. *et al.* Properties of HERG channels stably expressed in HEK 293 cells studied at physiological temperature. *Biophys. J.* **74**, 230–241 (1998).

10. Redfern, W. S. *et al.* Relationships between preclinical cardiac electrophysiology, clinical QT interval prolongation and torsade de pointes for a broad range of drugs: evidence for a provisional safety margin in drug development. *Cardiovasc. Res.* **58**, 32–45 (2003).
11. Schramm, A., Jähne, E. A., Baburin, I., Hering, S. & Hamburger, M. Natural Products as Potential Human Ether-a-Go-Go-Related Gene Channel Inhibitors – Outcomes from a Screening of Widely Used Herbal Medicines and Edible Plants. *Planta Med.* **80**, 1045–1050 (2014).
12. Witchel, H. J., Milnes, J. T., Mitcheson, J. S. & Hancox, J. C. Troubleshooting problems with in vitro screening of drugs for QT interval prolongation using HERG K⁺ channels expressed in mammalian cell lines and *Xenopus* oocytes. *J. Pharmacol. Toxicol. Meth.* **48**, 65–80 (2002).
13. Broeders, J., van Eijkeren, J., Blaauboer, B., J. & Hermens, J., L. Transport of chlorpromazine in the Caco-2 cell permeability assay: a kinetic study. *Chem. Res. Toxicol.* **25**, 1442–1451 (2012).
14. Hubatsch, I., Ragnarsson, E. G. & Artursson, P. Determination of drug permeability and prediction of drug absorption in Caco-2 monolayers. *Nat. Protoc.* **2**, 2111–2119 (2007).
15. Heikkinen, A. T., Mönkkönen, J. & Korjamo, T. Kinetics of cellular retention during Caco-2 permeation experiments: role of lysosomal sequestration and impact on permeability estimates. *J. Pharmacol. Exp. Therap.* **328**, 882–892 (2009).
16. Palmgren, J., Monkkonen, J., Korjamo, T., Hassinen, A. & Auriola, S. Drug adsorption to plastic containers and retention of drugs in cultured cells under in vitro conditions. *Eur. J. Pharm. Biopharm.* **64**, 369–378 (2006).
17. Engman, H., *et al.* CYP3A4, CYP3A5, and MDR1 in human small and large intestinal cell lines suitable for drug transport studies. *J. Pharm. Sci.* **90**, 1736–1751 (2001).
18. Korjamo, T. *et al.* Metabolic and efflux properties of Caco-2 cells stably transfected with nuclear receptors. *Pharm. Res.* **23**, 1991–2001 (2006).
19. Meunier, V., Bourrie, M., Berger, Y. & Fabre, G. The human intestinal epithelial cell line Caco-2; pharmacological and pharmacokinetic applications. *Cell Biol. Tox.* **11**, 187–194 (1995).
20. Tukey, R. H. & Strassburg, C. P. Human UDP-glucuronosyltransferases: Metabolism, expression, and disease. *Ann. Rev. Pharm. Tox.* **40**, 581–616 (2000).
21. Lee, J. K. *et al.* Sex-dependent disposition of acetaminophen sulfate and glucuronide in the in situ perfused mouse liver. *Drug Metab. Dispos.* **37**, 1916–1921 (2009).
22. Jiang, W., Xu, B., Wu, B., Yu, R. & Hu, M. UDP-glucuronosyltransferase (UGT) 1A9-overexpressing HeLa cells is an appropriate tool to delineate the kinetic interplay between breast cancer resistance protein (BCRP) and UGT and to rapidly identify the glucuronide substrates of BCRP. *Drug Metab. Dispos.* **40**, 336–345 (2012).
23. Kurzer, M. S. & Xu, X. Dietary phytoestrogens. *Ann. Rev. Nutr.* **17**, 353–381 (1997).
24. Hu, M., Chen, J. & Lin, H. Metabolism of flavonoids via enteric recycling: Mechanistic studies of disposition of apigenin in the Caco-2 cell culture model. *J. Pharmacol. Exp. Ther.* **307**, 314–321 (2003).
25. Usta, M. *et al.* Human glutathione S-transferase-mediated glutathione conjugation of curcumin and efflux of these conjugates in Caco-2 cells. *Chem. Res. Toxicol.* **20**, 1895–1902 (2007).
26. Liu, W. *et al.* Coupling of UDP-glucuronosyltransferases and multidrug resistance-associated proteins is responsible for the intestinal disposition and poor bioavailability of emodin. *Toxicol. Appl. Pharmacol.* **265**, 316–324 (2012).
27. Jeong, E. J., Lin, H. & Hu, M. Disposition mechanisms of raloxifene in the human intestinal Caco-2 model. *J. Pharmacol. Exp. Therap.* **310**, 376–385 (2004).
28. Chikhale, P. J. & Borchardt, R. T. Metabolism of L-alpha-methyldopa in cultured human intestinal epithelial (Caco-2) cell monolayers. Comparison with metabolism in vivo. *Drug Metab. Dispos.* **22**, 592–600 (1994).
29. Guillemette, C. Pharmacogenomics of human UDP-glucuronosyltransferase enzymes. *Pharmacogenomics J.* **3**, 136–158 (2003).
30. Jancova, P., Anzenbacher, P. & Anzenbacherova, E. Phase II drug metabolizing enzymes. *Biomed. Pap. Med. Fac. Univ. Palacky. Olomouc. Czech. Repub.* **154**, 103–116 (2010).
31. Ruster, G. U., Hoffmann, B. & Hamburger, M. Inhibitory activity of indolin-2-one derivatives on compound 48/80-induced histamine release from mast cells. *Pharmazie* **59**, 236–7. (2004).
32. Speed, B. *et al.* Pharmacokinetics, Distribution, and Metabolism of [14C]Sunitinib in Rats, Monkeys, and Humans. *Drug Metab. Dispos.* **40**, 539–555 (2012).
33. Oufir, M., Sampath, C., Butterweck, V. & Hamburger, M. Development and full validation of an UPLC-MS/MS method for the determination of an anti-allergic indolinone derivative in rat plasma, and application to a preliminary pharmacokinetic study. *J. Chromator. B* **902**, 27–34 (2012).

34. Jähne, E. A. *et al.* Development and validation of a LC-MS/MS method for assessment of an anti-inflammatory indolinone derivative by *in vitro* blood-brain barrier models. *J. Pharm. Biomed. Anal.* **98**, 235–246 (2014).
35. Shang, W. *et al.* Expressions of glutathione S-transferase alpha, mu, and pi in brains of medically intractable epileptic patients. *BMC Neurosci.* **9**, 1 (2008).
36. Shawahna, R. *et al.* Transcriptomic and Quantitative Proteomic Analysis of Transporters and Drug Metabolizing Enzymes in Freshly Isolated Human Brain Microvessels. *Mol. Pharmaceutics* **8**, 1332–1341 (2011).
37. Shawahna, R., Declèves, X. & Scherrmann, J.-M. Hurdles with using *in vitro* models to predict human blood-brain barrier drug permeability: a special focus on transporters and metabolizing enzymes. *Curr. Drug Metab.* **14**, 120–136 (2013).
38. Deng, X. Y., Zheng, S. N., Gao, G. H., Fan, G. & Li, F. Determination and pharmacokinetic study of indirubin in rat plasma by high-performance liquid chromatography. *Phytomedicine* **15**, 277–283 (2008).
39. Buckley, S. T., Fischer, S. M., Fricker, G. & Brandl, M. *In vitro* models to evaluate the permeability of poorly soluble drug entities: challenges and perspectives. *Eur. J. Pharm. Sci.* **45**, 235–250 (2012).
40. Prien, O., Steinmeyer, A., Siemeister, G. & Jautelat, R. Aryl-substituted indirubin derivatives, their production and use. (Patents, 2001).
41. Prien, O., Steinmeyer, A., Siemeister, G. & Jautelat, R. Sulfur-containing indirubin derivatives, their production and use. (Patents, 2001).
42. Wu, B. Nanoparticles of indirubin, derivatives thereof and methods of making and using same. (Patents, 2015).
43. Agency, E. M. Guideline on the investigation of drug interactions. (European Medicines Agency Canary Wharf, London, UK, 2012).
44. Japanese Ministry of Health, Labour and Welfare (JMHLW) Guideline on drug-drug interactions (2014).
45. Giacomini, K. M. *et al.* Membrane transporters in drug development. *Nat. Rev. Drug Discov.* **9**, 215–236 (2010).
46. Pick, A., Klinkhammer, W. & Wiese, M. Specific inhibitors of the breast cancer resistance protein (BCRP). *Chem. Med. Chem.* **5**, 1498–1505 (2010).
47. Administration, F. and D. Guidance for industry: food-effect bioavailability and fed bioequivalence studies. *Food and Drug Administration, Rockville, MD* (2002).
48. Markopoulos, C. *et al.* Biorelevant media for transport experiments in the Caco-2 model to evaluate drug absorption in the fasted and the fed state and their usefulness. *Eur. J. Pharmaceut. Biopharm.* **86**, 438–448 (2014).
49. Vertzoni, M. *et al.* Dissolution media simulating the intraluminal composition of the small intestine: physiological issues and practical aspects. *J. Pharm. Pharmacol.* **56**, 453–462 (2004).
50. Cavero, I. & Crumb, W. ICH S7B draft guideline on the non-clinical strategy for testing delayed cardiac repolarisation risk of drugs: a critical analysis. *Expert Opin. Drug Saf.* **4**, 509–530 (2005).
51. Deshpande, A. D., Baheti, K. G. & Chatterjee, N. R. Degradation of b-lactam antibiotics. *Curr. Sci.* **87**, 1684–1695 (2004).
52. Singla, A. K., Garg, A. & Aggarwal, D. Paclitaxel and its formulations. *Int. J. Pharm.* **235**, 179–192 (2002).
53. Desai, N. *et al.* Increased antitumor activity, intratumor paclitaxel concentrations, and endothelial cell transport of cremophor-free, albumin-bound paclitaxel, ABI-007, compared with cremophor-based paclitaxel. *Clin. Cancer Res.* **12**, 1317–1324 (2006).

Acknowledgments

An erster Stelle möchte ich mich bei meinem Doktorvater Herrn Prof. Dr. Matthias Hamburger, für die Möglichkeit an diesem interessanten Projekt zu arbeiten, für die gewährte Freiheit bei der Durchführung dieser Arbeit und für das entgegengebrachte Vertrauen bedanken. Seine fachlichen Ratschläge und Diskussionen waren für mich stets sehr inspirierend und wertvoll.

Des Weiteren möchte ich mich bei Herrn Prof. Dr. Jürgen Drewe bedanken, der sich netterweise dazu bereit erklärt hat das Korreferat zu übernehmen. Ein grosses Dankeschön geht auch an Herrn Prof. Dr. Kurt E. Hersberger für die Übernahme des Vorsitzes. Vielen Dank auch für die schöne Zeit (Samstage) in der Apotheke Hersberger.

I also would like to thank my direct supervisor Dr. Mouhssin Oufir for his enthusiasm and support during my PhD. He always gave me the freedom to develop my own ideas (“ok, let’s be crazy”), even though the solution was not always “easy and quick”. Without him, this work would not have been possible.

I acknowledge Prof. Dr. Veronika Butterweck, Sheela Verjee, Dr. Ursula Thormann, Dr. Simon Hebeisen, Timm Hettich, Dr. Martin Smieško, Prof. Dr. Maxime Culot, Prof. Dr. Romeo Cecchelli, Fruzsina Walter, and Prof. Dr. Mária A. Deli for their scientific input, and their pleasant and fruitful collaboration.

Ganz besonders möchte ich mich bei Frau Dr. Daniela E. Eigenmann für die wunderbare Kompanie und die Unterstützung während meines Doktorats bedanken. In dieser Zeit ist für mich eine tiefe Freundschaft entstanden, die wohl nicht nur auf ihren Berner Charme zurückzuführen ist. Further thanks go to Teresa Faleschini and Dr. Claudia Keller for proof-reading my thesis with extraordinary patience and perception, and for just being such good friends. Ein besonderer Dank gilt Orlando Fertig für seine technische Unterstützung, seinen Ordnungssinn und seine aufmunternden Gesten, die mich immer wieder zum Lachen gebracht haben. Des Weiteren möchte ich mich bei Manuela Rogalski für ihr ambitioniertes „Management“ unserer Gruppe bedanken. Für die angenehme Zusammenarbeit in den Praktika danke ich insbesondere Herrn Dr. Olivier Potterat, Stephan Winzap, Justine Ramseyer, Dr. Daniela E. Eigenmann, Jakob Reinhardt and Frau Dr. Eliane Garo.

Warm thanks go also to my other current and former fellow colleagues in the lab: Alen, Anja, Christian, Clizia, Diana, Elisabetta, Fahimeh, Karin, Maria, Mike, Niels, Olga, Samad, Sara, Steffi, Tasquiah, and Yoshie. Thank you for creating this pleasant and friendly working atmosphere!

Zudem danke ich meiner Familie für ihre Liebe, ihre Unterstützung, ihr Vertrauen und dafür, dass sie mir stets die Freiheit gelassen haben meinen Interessen zu folgen, um meinen eigenen Weg zu gehen.

Evelyn Andrea Jähne

Curriculum vitae

PERSONAL DATA

Name: Jähne
First Name: Evelyn Andrea
E-mail: evelyn.jaehne@hotmail.com
Mobile phone: +41 (0)77 415 39 21
Date of birth: 17.07.1983
Nationality: Swiss

EDUCATION

09/2012 – 06/2016 **PhD Thesis, Division of Pharmaceutical Biology, Department of Pharmaceutical Sciences, University of Basel, Switzerland**
Title: Early ADMET profiling of anti-inflammatory alkaloids using validated LC-MS/MS methods

09/2009 – 09/2011 Master of Science (MSc) in Pharmacy (University of Basel)
09/2010 – 07/2011 Assistant pharmacist at Apotheke Hersberger (Basel)
01/2010 – 07/2010 Master thesis (Department of Pharmacology and Toxicology, University of Vienna, Austria), Title: Screening for natural-derived modulators of ligand- and voltage- gated ion channels

02/2008 – 01/2010 Bachelor of Science (BSc) in Pharmaceutical Sciences (University of Basel)

10/2004 – 01/2008 Bachelor of Science (BSc) in Molecular Biology (University of Basel)

WORK EXPERIENCE

02/2013 – 06/2016 Teaching assistant (University of Basel)
Systematics of medicinal and toxic plants: Assistance during practical course, guiding tours in the botanical garden Brüglingen (Basel)
Pharmaceutical Biology: Practical course in microscopy

12/2011 – 02/2016 Pharmacist at Apotheke Hersberger (part-time circa 5-10%)

01/2012 – 08/2012 Scientific associate at B'Sys GmbH, Biological Monitoring Systems, Ion Channel Research (Witterswil, Switzerland)

01/07/ – 01/09/2010 Student assistant at B'Sys GmbH (Witterswil, Switzerland)

26/01/ – 13/02/2009 Internship at Bosnalijek, Pharmaceutical and Chemical Industry (Sarajevo, Bosnia & Herzegovina, under supervision of PD Dr. G. Betz)

29/08/ – 04/09/2008 Hostess at the 68th World Congress of Pharmacy and Pharmaceutical Sciences organized by the International Pharmaceutical Federation (FIP) (Basel)

10/2006 – 02/2007 Student assistant at the Division of Pharmaceutical Biology (University of Basel)

ADDITIONAL QUALIFICATIONS

23 – 26/08/2015	Novartis International Biotechnology Leadership Camp (BioCamp)
Since 08/2015	Active member at Pharmaciens Sans Frontières (PSF, Schweiz)
Crisis interventions training for humanitarian aid workers organized by Pharmaciens Sans Frontières (PSF, Apotheker ohne Grenzen Deutschland e.V.):	
18 – 20/07/2014	Basics in humanitarian work for pharmacists I (Wilhelmsthal, Germany)
12 – 14/06/2015	Basics in humanitarian work for pharmacists II (Schweinfurt, Germany)
26/04/2015	Refresher course (Berlin, Germany)
03/2015	Pharmacokinetic/Pharmacodynamic Modelling in Drug Development and Research, 20-hour workshop (Bonn International Graduate School “Drug Sciences”, Germany)
09/2015	1-week Summer School Biopharmacy at the University of Applied Sciences Northwestern Switzerland School of Life Sciences (FHNW, Muttenz, Switzerland)
01/2010 – 07/2010	Leonardo Da Vinci Grant Financial support during MSc project at University of Vienna (Austria)

LANGUAGES

German	Native language
English	Fluent
Spanish	Fluent
Latinum	

PUBLICATIONS, SHORT LECTURES, AND POSTER PRESENTATIONS (SELECTION)

Publications

Doktorandenporträt Artikel in *ChemieXtra*

Frisch ab Labor, Phytopharmazie sucht nach besser verträglichen Wirkstoffen, Naturstoff mit neuem Wirkmechanismus, Ausgabe 03/16, p. 8-10

EA Jähne, DE Eigenmann, F Moradi-Afrapoli, S Verjee, V Butterweck, S Hebeisen, T Hettich, G Schlotterbeck, M Smieško, M Hamburger, M Oufir; Caco-2 permeability studies and *in vitro* hERG liability assessment of tryptanthrin and indolinone. *Planta Med* 2016, 82:1192-1201

EA Jähne, C Sampath, V Butterweck, M Hamburger, M Oufir; Development and full validation of an UPLC-MS/MS method for the quantification of the plant-derived alkaloid indirubin in rat plasma. *J Pharm Biomed Anal* 2016, 128:247-252

EA Jähne, DE Eigenmann, C Sampath, V Butterweck, M Culot, R Cecchelli, F Gosselet, FR Walter, MA Deli, M Smieško, M Hamburger, M Oufir; Pharmacokinetics and *in vitro* blood-brain barrier screening of the plant-derived alkaloid tryptanthrin. *Planta Med* 2016, 82:1021-1029

EA Jähne, DE Eigenmann, M Culot, R Cecchelli, FR Walter, MA Deli, R Tremmel, G Fricker, M Smiesko, M Hamburger, M Oufir; Development and validation of a LC-MS/MS method for assessment of an anti-inflammatory indolinone derivative by *in vitro* blood-brain barrier models. *J Pharm Biomed Anal* 2014, 98:235-246

DE Eigenmann, **EA Jähne**, M Smieško, M Hamburger, M Oufir; Validation of an immortalized human (hBMEC) *in vitro* blood-brain barrier model. *Anal Bioanal Chem* 2016, 408:2095-2107

A Schramm, **EA Jähne**, I Baburin, S Hering, M Hamburger; Natural products as potential hERG channel inhibitor- outcomes from a screening of widely used herbal medicines and edible plants. *Planta Med* 2014, 80:1045-1050

DE Eigenmann, C Dürig, **EA Jähne**, M Smiesko, M Culot, F Gosselet, HC Cederberg Helms, B Brodin, L Wimmer, MD Mihovilovic, M Hamburger, M Oufir; *In vitro* blood-brain barrier permeability predictions for GABA_A receptor modulating piperine analogs. *Eur J Pharm Biopharm* 2016, 108:118-126

DC Rueda, A Schöffmann, M de Mieri, M Raith, **EA Jähne**, S Hering, M Hamburger; Identification of dihydrostilbenes in *Pholidota chinensis* as a new scaffold for GABA_A receptor modulators, *Bioorg Med Chem* 2014, 22:1276-1284

C Guccione, M Oufir, V Piazzini, DE Eigenmann, **EA Jähne**, V Zabela, MC Bergonzi, M Smiesko, M Hamburger, AR Bilia; Preparation and analysis of nanovectors for brain delivery of andrographolide as neuroprotective agent. Submitted in: *J Mater Chem B* 2016

Short Lecture

08/2014 8th Young Researchers Workshop of the Society for Medicinal Plant and Natural Product Research, Guimarães (Portugal)

Poster presentations

09/2015 1st World Conference on ADMET and DMPK, Red Island (Croatia)
08/2014 62nd International Congress and Annual Meeting of the Society for Medicinal Plant and Natural Product Research, Guimarães (Portugal)
06/2014 International Congress of Phytotherapy, Winterthur (Switzerland)
2013 – 2015 Swiss Pharma Science Day, Bern (Switzerland)

